Thermal ageing of polydicyclopentadiene

Jing Huang

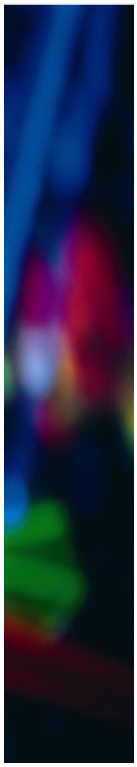

2019-ENAM-0050

École doctorale n° 432 : Sciences des Métiers de l'ingénieur

Doctorat

T H È S E

pour obtenir le grade de docteur délivré par

l'École Nationale Supérieure d'Arts et Métiers

Spécialité " Mécanique et Matériaux "

présentée et soutenue publiquement par

Jing HUANG

le 6 Décembre 2019

Thermal ageing of polydicyclopentadiene

Directeur de thèse : **Emmanuel RICHAUD**
Co-encadrement de la thèse : **Pierre-Yves LE GAC**

Jury

M. Jean-Luc GARDETTE, Professeur, Institut de Chimie de Clermont-Ferrand	Président
Mme Christa FITTSCHEN, Directeur de Recherche EPST, Université de Lille	Rapporteur
M. Riccardo AMORATI, Professeur, Université de Bologne	Rapporteur
Mme Véronique MONTEMBAULT, Professeur, Université du Mans	Examinateur
Mme Renata DROZDZAK-MATUSIAK, Ingénieur de recherche, Telene SAS	Examinateur
M. Emmanuel RICHAUD, Professeur, PIMM, Arts et métiers ParisTech	Examinateur
M. Pierre-Yves LE GAC, Ingénieur de recherche, IFREMER, Brest	Examinateur

T H È S E

Arts et Métiers - Campus de Paris
Laboratoire de Procédés et Ingénierie en Mécanique et Matériaux

Remerciements

Ce travail de thèse a été réalisé au laboratoire Procédés et Ingénierie en Mécanique et Matériaux pendant trois ans. Je remercie toutes les personnes qui ont contribué au bon déroulement de cette étude et à la rédaction de cette thèse.

Tout d'abord, j'adresse mes remerciements et ma respectueuse gratitude à mon directeur de thèse, Pr Emmanuel Richaud, pour votre disponibilité, votre efficacité, votre patience, votre confiance et vos judicieux conseils qui ont contribué à alimenter ma réflexion.

Je tiens également à remercier M. Pierre Yves Le Gac, qui a encadré cette thèse à IFREMER Brest, pour vos participations aux discussions des résultats, vos suggestions précieuses qui ont fortement fait avancer ce projet et surtout pour m'avoir encouragé à continuer à la fin de cette thèse.

Ces travaux ont été évalué par un jury composé de Jean-Luc Gardette qui a accepté d'examiner mon travail et de présider le jury, Riccardo Amorati, Christa Fittschen, Véronique Montembault et Renata Drozdzak. Mes sincères remerciements à mes rapporteurs, Riccardo Amorati et Christa Fittschen pour leur lecture attentive du manuscrit ce qui a permis une discussion riche lors de la soutenance. Je tiens à tous vous remercier pour le temps que vous avez passé à évaluer ce travail et pour la pertinence de vos questions et remarques qui me feront avancer pour la suite.

Ensuite, je tiens à remercier très chaleureusement, tous les membres de ce projet et notamment Gille Recher, Laurent Fontaine, Adelina David et Clémence Nicolas. Merci pour votre présence, votre confiance, vos connaissances et aussi tous ces moments agréables passés ensemble en réunion. Et je remercie Wendy Minne pour avoir réalisé les préparations des échantillons initiaux. Je remercie également mon stagiaire Christiano Rodrigues pour son aide technique lors de ces derniers mois de thèse.

Je remercie ici toute l'équipe de laboratoire PIMM, pour leur accueil, en particulier

Guillaume Miquelard-Garnier, Sylvie Girault, Ilias Iliopoulos et Bruno Fayolle. Merci pour ses précieux conseils et ses aides.

Je souhaite remercier toutes les personnes que j'ai connues pendant ces trois ans. Je remercie en particulier mes collègues de bureau : Justine et Yan et tous les docteurs/doctorants Maxime, Clément, Fatima, Armando, Romain, Camille …

Finalement, un grand merci à mes parents et mes amis de m'avoir toujours soutenue durant mes études.

Contents

Introduction

The Nobel Prize in chemistry 2005 was awarded to Yves Chauvin, Robert H. Grubbs and Richard R. Schrock for the development of the metathesis method in organic synthesis. After its discovery in 70's, the olefin metathesis reaction was widely developed and used in the pharmaceutical and polymer industries. Polydicyclopentadiene (PDCPD) is one of the most industrially used polymers obtained by Ring Opening Metathesis Polymerisation (ROMP). It displays particularly interesting properties from a technical and an economic point of view: high toughness, density close to 1, good chemical resistance to acids and bases due to its hydrocarbon structure, short processing time (less than 5 minutes). The new generation of metallic catalysts is insensitive to oxygen and water and allows the polymerization to be easily realized in ambient conditions.

This polymer can be hence envisaged for application in severe environments in particular in the marine environment for deep-sea oil extraction. A challenging problem which arises in this domain is that the lifetime of this material remains unknown. The high concentration in remaining double bonds in the polymer and the use of a high catalyst concentration for ROMP which makes a fast polymerization possible are expected to enhance the chemical instability compared to other hydrocarbon polymers. To our knowledge, few studies tackled the lifetime of thermosets obtained by ROMP. Moreover, little attention has been paid to the lifetime of polymer in a marine environment which is a complex subject. This thesis was thus performed in the frame of the "Vieillissement de Réseaux POlymérisés par Métathèse" VRPOM project granted by French National Research Agency (ANR) and bringing together Institut des Molécules et Matériaux du Mans (expert in metathesis), IFREMER (expert in marine ageing of polymers), TELENE SAS company (expert in PDCPD manufacturing) and Process and engIneering in Mechanics and Materials lab at Arts et Métiers ParisTech (expert in polymer ageing and lifetime prediction). The lifetime prediction approach always bases on performing accelerated ageing tests, which must be later extrapolated to service condition. Given the poor reliability of existing empirical approaches, we decided to use a more scientific approach based on the understanding of degradation mechanisms and kinetics.

In the first chapter of this thesis, a general presentation of this polymer will be made in terms of its polymerization mechanism, catalysts used in ROMP, and manufacturing process. The existing ageing studies of PDCPD will be presented including mechanical properties changes

which are related to crosslinking created due to thermal oxidation. Besides, the structure-property relationships will be detailed to further support this explanation. The non-empirical kinetic model which is adopted in this work will be described in this chapter, together with the mechanistic study of thermal oxidation which is the cornerstone of this methodology. The approach for describing the effect of oxygen pressure, antioxidants and diffusion of oxygen will be described to establish a proper strategy for investigating the oxidative stability of this material in service conditions.

The second chapter will present the materials and experimental methods used in this study. The different exposure conditions will be detailed, with the characterization methods for chemical and mechanical changes during thermal oxidation.

The investigation in the following chapter (chapter 3) starts from the simplest case i.e. additive-free PDCPD. The objective of this part is to identify the main oxidation products, propose a degradation mechanism and establish a structure-property relationship in line with embrittlement. The results will be used to establish a kinetic model for additive-free PDCPD and determine some kinetic parameters. The model will be tested and validated from comparison with ageing experiments in a wide range of experimental conditions varying by oxygen pressure (to isolate some rate constants) and temperatures (to perform extrapolations). The final part in this chapter will address the effect of diffusion limited of oxygen for additive-free PDCPD, which will be studied and modeled by the kinetic model to predict the behavior of bulk material.

Then, chapter 4 will focus on the development of a more complete kinetic model which integrates the effect of antioxidants. PDCPD stabilized by two families of antioxidants (phenolic and hindered amine) differing by their action mechanisms (sacrificial vs regenerative), molar mass (with effect on physical performances such as limitation of evaporation) will be studied, and their efficiency for slowing down the oxidation rate will be compared. The stabilization reactions will be described by new rate constants, which will be determined from the experimental results and literature. With all these results, the difference efficiency between these different stabilizers will be explained. Those results will help us to choose stabilizers suitable for ROMP polymerization and improve the lifetime.

In the last chapter, the effect of thermal oxidation of PDCPD on water sorption behavior will be investigated to address the case of thermal oxidation in the marine environment. For that purpose, we will compare the water permeation properties and mechanisms (solubility and diffusion) in virgin PDCPD (which is apolar in essence and thus hydrophobic) and in thermally aged ones. We will tentatively derive some relationships describing the coupling between thermal and water ageing.

A conclusion will summarized the main results of this thesis and propose possible future works.

Chapter 1 Bibliographical review

1. Introduction

This first chapter is related to a bibliographic review of polydicyclopentadiene (PDCPD) behavior and thermal oxidation of polymer with the aim to introduce the scientific strategy implemented in this study. Firstly, a general presentation of the context will be made considering a rapid description of the material, manufacturing process and applications. In the second part, existing knowledge on thermal oxidation of PDCPD will be discussed as well as the methodology for lifetime prediction; this part will show how the mechanistic approach is useful for reliable prediction. Then, the mechanistic approach will be detailed considering all specificities of PDCPD. And finally, we will propose a strategy of work to model thermal oxidation in PDCPD.

2. Context of the study

2.1 Background about PDCPD

Polydicyclopentadiene (PDCPD) is a cross-linked polymer which is obtained by Ring Opening Metathesis Polymerisation (ROMP) of the dicyclopentadiene (DCPD) monomer [1].

The mechanism of metathesis was discovered in 1971 by Yves Chauvin and co-workers [2]. Schrock and Grubbs later improved the existing catalysts and introduced molybdenum and ruthenium based catalysts. The three researchers were awarded the Nobel Prize in Chemistry in 2005 [3]. ROMP, as an application of the metathesis of olefins (Figure1.1), has emerged as an effective and powerful method for the synthesis of macromolecular materials [4].

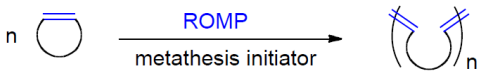

Figure 1.1: Schematic representation of a ring-opening metathesis polymerization (ROMP) reaction.

The metathesis of olefins involves a redistribution reaction of the carbon skeleton between unsaturated double bonds in the presence of a metal catalyst [5], namely the scission and regeneration of carbon-carbon double bonds. The monomers used in the ROMP are highly strained cyclic olefins such as norbornene and cyclopentene, because the driving force of ROMP is the release of strain enthalpy in cyclic olefins [6]. A major feature of this reaction is

that the unsaturated double bond in the monomer can remain in the carbon skeleton compared to any other form of polymerization [4].

Dicyclopentadiene (DCPD) is the monomer of PDCPD which is used for ROMP reaction under a series of different catalytic systems. The structure of the synthesized polymer depends on the type and composition of the catalyst and the polymerization method, ranging from a highly cross-linked insoluble polymer to a linear and completely soluble one [7]. The currently accepted DCPD polymerization mechanism based on Chauvin's original proposal [8] is described below (Figure 1.2a).

Firstly, an initiator (a transition metal alkylidene complex) reacts with a double bond in DCPD to form metallacyclobutane intermediate. Then a cycloreversion reaction occurs on the intermediate to afford a new metal alkylidene (M*). Hence, the reaction continues by repeating these steps until polymerization stops [4]. The ROMP reaction, which is very fast and exothermic, is assumed to occur firstly in norbornene ring due to its larger cycle strain to form a linear PDCPD. As the reaction continues, the double bonds of the cyclopentene olefin are also partially opened and undergo the subsequent metathesis, thereby producing a crosslinked structure [9].

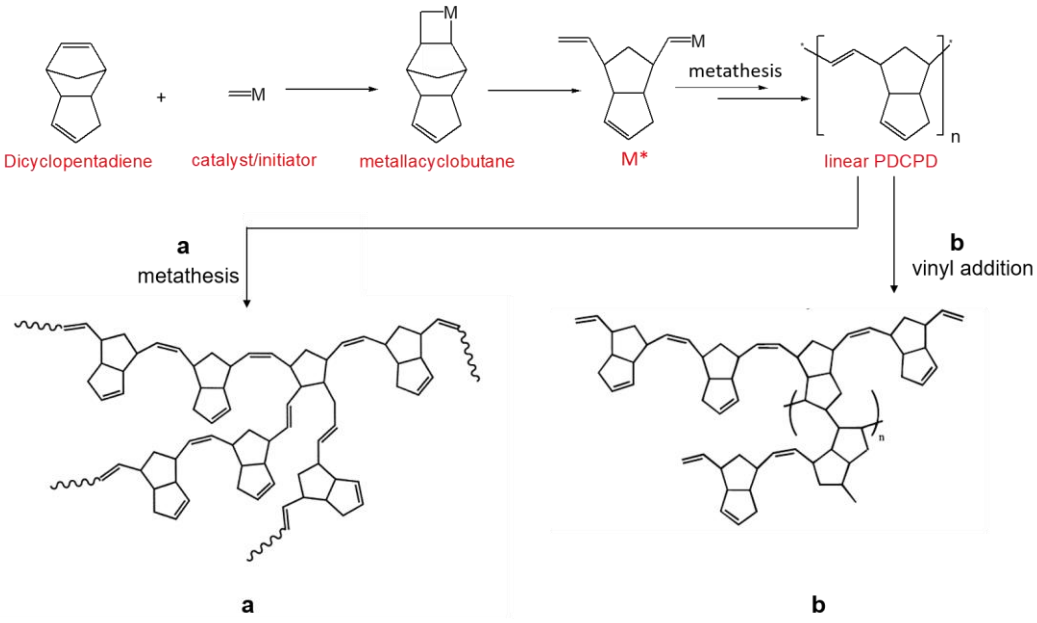

Figure 1.2: Currently accepted mechanism for the polymerization of dicyclopentadiene (a); Two mechanisms proposed by Davidson et al. [7] (b).

Davidson et al. [7], [9] have demonstrated another possibility about the polymerization of DCPD. Two polymerization mechanisms (metathesis of norbornene ring and olefin addition) are operating simultaneously to form crosslinked PDCPD [7], among which olefin addition is the contribution of crosslinking (Figure 1.2b). The proportion of the two pathways remains unclear. This grey area complicates the full understanding of the crosslinked structure of PDCPD. The remaining concentration in double bonds (after polymerization) must hence be carefully determined before discussing the ageing mechanism.

2.2 Catalyst

The catalyst of ROMP is the key to the preparation of PDCPD materials. A broad range of functionalized [4], [10]–[13] cyclic olefins can now be polymerized by ROMP owing to the booming development of well-defined catalysts, which overcomes the main shortcomings of the "undefined" catalytic system ($TiCl_4/Et_3Al$, $MoCl_5/Et_3Al$, etc.).

This section will only deal with the most relevant and commercially available catalysts used for olefin metathesis i.e. metal alkylidenes catalyst systems. Such catalyst systems are usually divided into two families: Schrock catalysts and Grubbs catalysts.

Schrock et al. [14] have introduced well-defined Mo-based alkylidenes (Figure 1.3a), which is a significant advance of the development of highly active olefin metathesis catalysts. However, handling of Schrock catalysts is more demanding, due to its high sensibility to air and moisture, compared to the competing Grubbs catalysts [15].

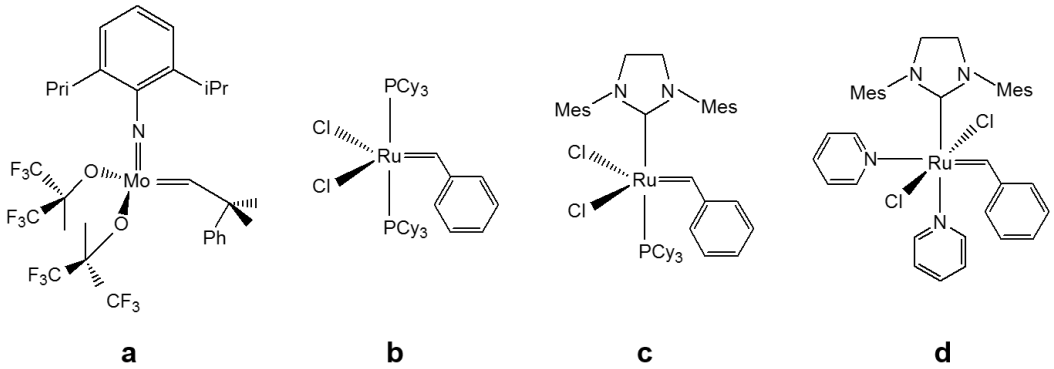

Figure 1.3: Different catalyst system for ROMP reaction.

Grubbs catalysts are ruthenium-bases alkylidenes complexes. A feature of ruthenium is the low oxophilicity, which limits its contamination [4]. The well-known first generation Grubbs catalysts (Figure 1.3b) (ruthenium benzylidene catalyst) system was developed in 1995 [16], [17]. Then the second generation Grubbs catalysts (Figure 1.3c) [18] was created by optimizing the ligand environment of the Ru center (Ru with an N-heterocyclic carbine ligand) with a better catalytic activity [19]. The synthesis of the second generation ruthenium benzylidene catalyst (Figure 1.3c) established a milestone in the history of olefin metathesis and laid the foundation for the further development of related complexes bearing an N-heterocyclic carbene ligand. Choi and Grubbs [20] found a faster initiation rate system by replacing phosphine ligand with more labile pyridine ligands. They have demonstrated that the third generation Grubbs catalyst (Figure 1.3d) could be a good initiator for living ROMP reactions, owing to low polydispersity of resulting polymers [20].

With several generations of development, Grubbs catalysts present many advantages in ROMP reactions: tolerance of many functional groups in the alkene substrates, stability towards air and moisture [21]. Nowadays, Grubbs catalysts are commonly used in olefin metathesis and compete with the most active Schrock catalysts in catalytic activity. A continuous survey across the catalysts structures has led to the development of stable ruthenium catalysts for polymer technology, so-called “latent” catalysts [21] exhibiting decreased initiation rates which can allow for longer handling of a monomer-catalyst mixture before the polymerization starts. The issue of the influence of catalysts and their by-products on long-term stability remains an open question. The catalyst actually may affect the decomposition of hydroperoxides [22], [23] which will be detailed in the next section. The choose of antioxidants is influenced by the catalyst used, because the interaction between antioxidants and the catalyst can occur possibly leading to lower catalytic performances and/or decreasing protection of polymer. Therefore, it is desirable to investigate the influence of different catalyst systems used in the polymerization of DCPD.

2.3 Process

Today’s commercial DCPD resin formulations are usually processed using Reaction Injection Molding (RIM), because ROMP of PDCPD generally meets exactly most demands of a RIM

process: low viscosity of DCPD, fast polymerization with a suitable catalyst, no gaseous by-products [24]. In the RIM process, two components (component A: DCPD + catalyst, component B: DCPD + co-catalyst) are simultaneously injected into a mold through a mixing head where the reaction can start (Figure 1.4). Polymerization launches once these two components are in contact. Hence, inside the mold, the mixture undergoes a ROMP reaction to product PDCPD. This process is releasing heat and completes in a matter of a few minutes (typically 5 min).

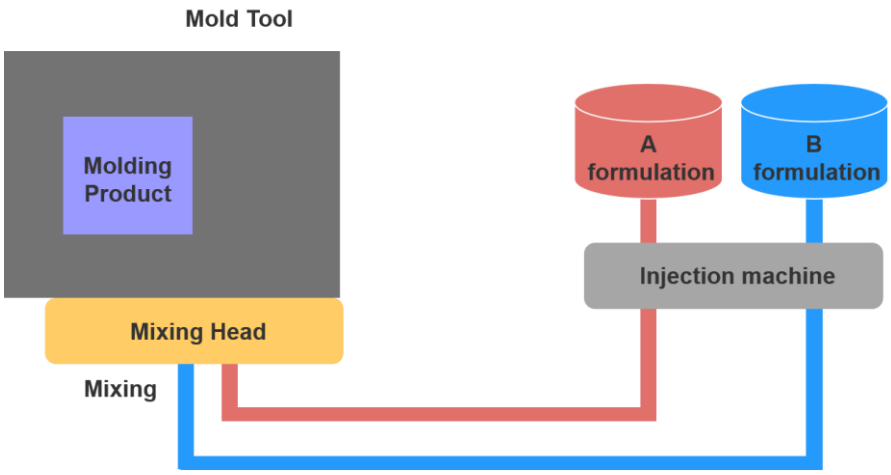

Figure 1.4: Schematic representation of RIM process.

Because of the low viscosity of the monomer streams, the injection pressure is relatively low allowing for lower cost mold materials such as aluminium alloys or nickel shell. The RIM process is especially suitable for the production of large plastic parts.

2.4 Applications

Compared to other thermosets, PDCPD has good impact resistance (See Table 1.1), good chemical resistance in presence of chemicals (acids or bases for instance), very low water absorption (0.09% weight increase after 24 h in water) [25]. PDCPD areas of applications include large to very large parts, possibly used in hostile environments. Some examples include body panels for agricultural and construction equipment, trucks and buses where PDCPD brings great design freedom, high impact resistance even at -40°C, a high heat deflection temperature (typically > 100°C). Furthermore, compact water waste units are also one of the PDCPD applications where the high resistance against acid and base is crucial.

Property	unit	Average values
Density	g/cm^3	1.03
Flexural Strength	MPa	70
Flexural Modulus	MPa	1800-1900
Impact Strength (notched Izod))	kJ/m^2	30

Table 1.1: Physical properties on PDCPD [25].

In this thesis, PDCPD is considered as a candidate for the field joint application to replace substitute polyurethane (PU) (having limited durability at high temperatures in water) and polypropylene (PP) (needing a longer process time) in the offshore oil industry (Figure 1.5).

Deep offshore oil exploitation requires the use of steel pipelines to transport oil to the Floating Production Storage and Offloading unit (FPSO). Production facilities are subject to high hydrostatic pressures (up to 30 MPa) and a large temperature difference between the inside (100°C or more) and the outside (4°C to 3000 m depth). In order to limit the heat losses in the fluid, it is necessary to maintain suitable thermal insulation around the pipelines. Since coated steel pipelines are joined by welding during the installation of offshore pipelines, it is essential to apply a coating at the welding locations (Field Joint) to ensure the continuity of the thermal insulation (Figure 1.5).

The coating material on the Field Joint must be a polymer with good thermal insulation and it must have good durability under specific environmental conditions such as high temperature, high pressure, and seawater. The required service life for this Field Joint coating is 20 years. The question of the durability of PDCPD in an offshore environment has to be assessed.

After a brief general description of the polymer and its applications, we propose to focus now on existing knowledge about thermal oxidation of PDCDP at the macroscopic scale.

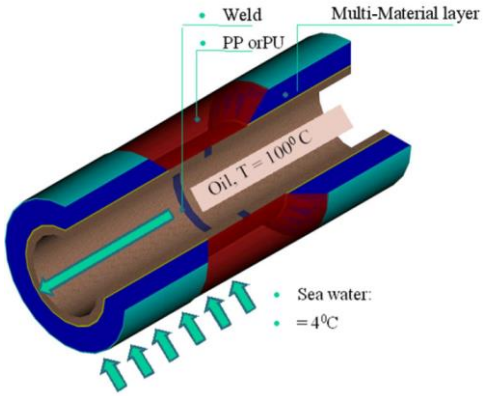

Figure 1.5: Schematic representation of a field joint [26].

3. Thermal degradation of PDCPD at macroscopic scale

3.1 Change of mechanical properties in thermally aged PDCPD

Many authors [26], [27] have emphasized that thermal oxidation induces an increase in thermos-mechanical properties (e.g. T_g, rubbery modulus, tensile properties). In particular, a previous study [26] has illustrated the mechanical properties characterizations of aged PDCPD in seawater at different temperatures (90°C-180°C). Such physical changes could originate from an increase in crosslinking, since this latter triggers the mechanical properties of thermosets [28].

Several studies on elastomers have illustrated the effect of crosslinking on rubbery modulus [29]. One of the originalities of this study will be hence to investigate the effect of ageing induced crosslinking on mechanical properties of a polymer in the glassy state.

Firstly, based on tensile test results (Figure 1.6a), a change in stress at yield has been reported [26]. This property increases during ageing for all temperatures. Nevertheless, Young's modulus is not largely affected by the oxidation. It was also elucidated that the oxidation induces changes from a ductile to a fragile behavior after ageing, and thus it is more likely to cause polymer fracture.

After surface removal, the tensile behavior of an aged sample (14 months at 120°C) is

returnable (Figure 1.6b), which shows the oxidation of PDCPD is confined on the sample surface. This result is owing to the phenomenon of diffusion limited oxidation (DLO) [30]. That means the oxidation only occurs at the surface of the sample, which will be interpreted in the section 5.5.

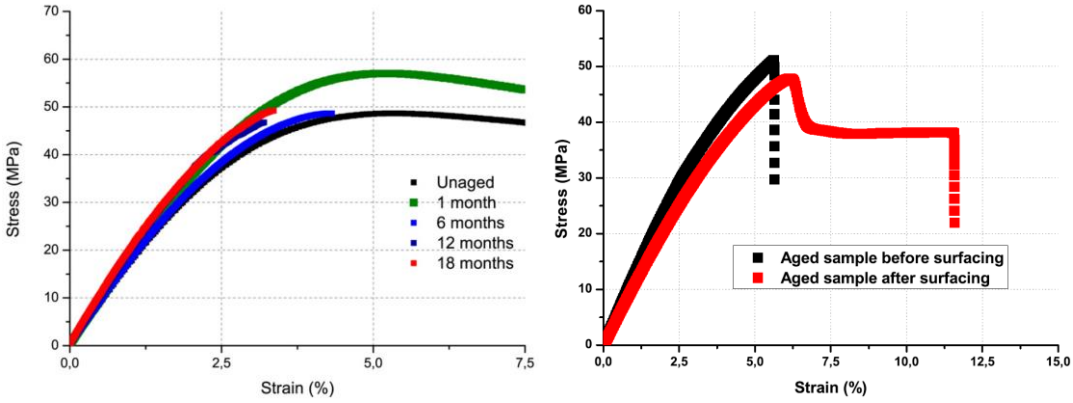

(a) **(b)**

Figure 1.6: Tensile behavior evolution during ageing at 90°C.

- Yield and fracture in glassy state

Yield and fracture properties are crucial criteria for assessing material reliability. These two aspects can be linked by considering the ductile-brittle transition temperature T_B, below which fracture happens before plastic deformation can occur at a given strain rate and above which plastic deformation occurs before fracture (ductile regime) (Figure 1.7). The presence of a possible ductile-brittle transition, which will be affected by the modification of the chain structure during oxidation, should be considered.

It is been shown that for most amorphous polymers, this transition corresponds to the activation of the β-transition, (i.e. $T_B = T_\beta$). In the case of amorphous polymers with large bulky side groups (e.g. PS), the ductile-brittle transition is consistent with the α-transition (i.e. $T_B = T_g$) [31]. As for PDCPD, since the β transition is not always evidenced, it seems that the ductile-brittle transition coincides with the glass transition.

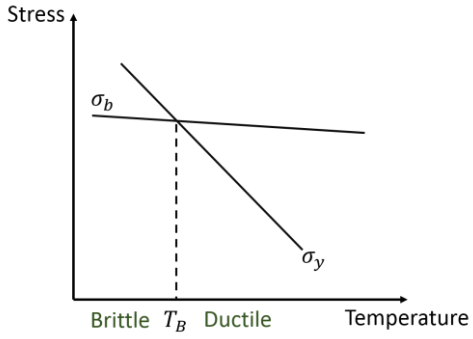

Figure 1.7: Illustration of ductile-brittle transition. σ_b: stress at break; σ_y: yield stress.

There is abundant literature involving the effects of network structure on yielding or on fracture. Most of the experimental results [32]–[34] revealed that the yield stress could be largely affected by network structure and in particular crosslinking density through its influence on T_g. In fact, Kambour's relation [35] shows that stress at yield is directly related to T_g (at a constant strain rate), which has been checked experimentally on different polymers [32]–[34]:

$$\sigma_y = C(T_g - T) \qquad \textit{Equation 1.1}$$

Where σ_y is the yield stress (MPa), C is a constant that depends on strain rate, T_g (K) is the glass temperature transition and T (K) is the absolute temperature. Thus, it is clear that crosslinking induced by oxidation leads to both yield stress and T_g increase.

A linear relationship between the critical stress intensity factor (K_{IC}) and the crosslink density (Figure 1.8) has been stated for PU [32] and epoxy networks [36]. The increase of crosslink density increased both yield stress and T_g and result in a corresponding decrease in K_{IC}.

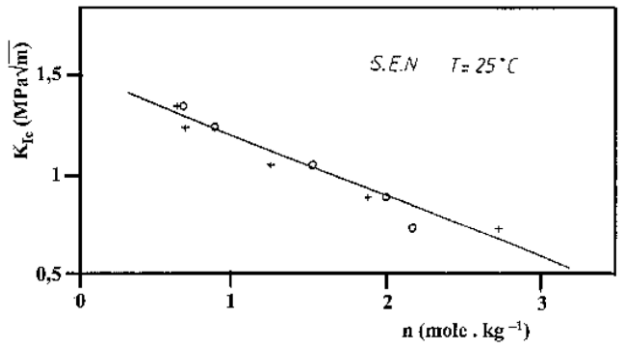

Figure 1.8: Change of K_{IC} at 25°C versus crosslink density for ideal epoxy networks. (+): theoretical; (o): experimental.

- Elastic properties in glassy state

It is well established [35] that the modulus in the glassy state of thermoset polymers mainly depends on cohesion and segmental mobility (i.e. β transition). There is no evidence for the existence of β transition in the case of PDCPD so that Young's modulus is not expected to be largely affected by the oxidation contrary to epoxies where a strong antiplastification phenomenon occurs [37]. However, the cohesive properties can change during oxidation due to the appearance of new chemical groups (e.g. ketones and carboxylic acids). According to Fig. 1.6a, it seems that those effects are quite limited.

With the help of dynamic mechanical analysis, it was pointed out that there are almost no changes in the modulus (Figure 1.9a). However, the oxidation induces a clear increase of the rubbery modulus, which is another evidence of an oxidation-induced crosslinking. This phenomenon can be explained by a large increase in the network density due to the reaction involving the double bonds (Figure 1.10) induced by oxidation of PDCPD.

Figure 1.9b confirms that after surfacing, the aged sample presents the same properties as the unaged one. Especially, they pointed out that for ageing at 90°C, this increase is limited to 0.25 mm from the external surface for ageing.

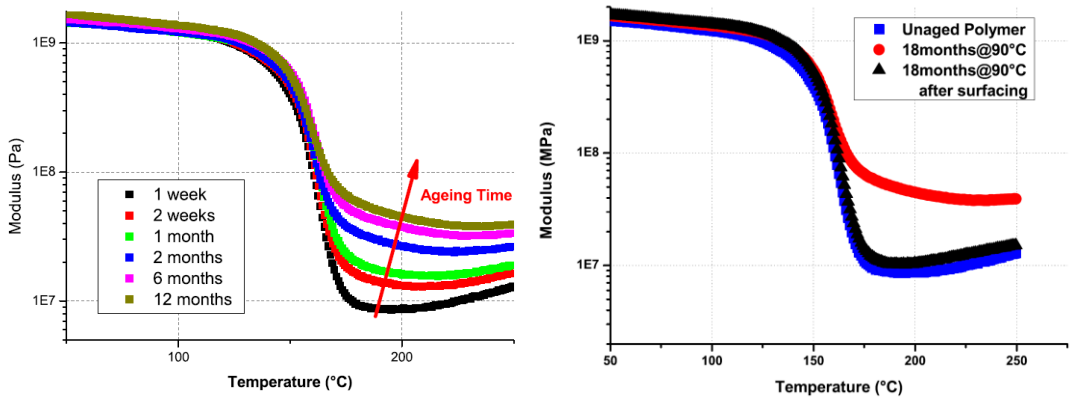

(a) **(b)**

Figure 1.9: The modulus changes with temperature for different ageing times at 90°C in seawater.

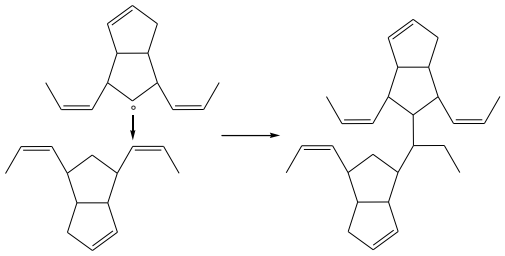

Figure 1.10: Possible reaction of radicals on double bond during oxidation to form crosslinking.

- Glass transition temperature

The network structure in the polymer structure directly influences the T_g. For the ideal networks (i.e. without dangling chains), the relationship between structures and the T_g depends on two main factors: the crosslink density and the chain stiffness [38]. A simplified approach to describe the effect of the crosslink density on the T_g is proposed by Fox and Loshaek [39]:

$$T_g = T_{gl} + K_{FL} v_e \qquad \textit{Equation 1.2}$$

Where T_{gl} (K) is the glass transition temperature of the linear polymer, K_{FL} (K kg mol^{-1}) is a constant that depends on structural consideration and v_e (mol kg^{-1}) is the concentration of elastically active chains.

In the case of oxidation induced crosslinking in an ideal tetra-functional network:

$$\upsilon_e = \upsilon_{e0} + 2x \qquad \textit{Equation 1.3}$$

Where υ_e and υ_{e0} are respectively the number of elastically active network chains before and after aging, x is the crosslinking concentration. By combining this relationship with the above equation 1.2, the change of T_g can be connected to the concentration of crosslinking:

$$T_g = T_{g0} + 2K_{FL}x \qquad \textit{Equation 1.4}$$

with

$$T_{g0} = T_{gl} + K_{FL}\upsilon_{e0} \qquad \textit{Equation 1.5}$$

- Elastic properties in rubbery state

The mechanical properties of crosslink in the rubbery states can be related to the equilibrium entropic elasticity and the relaxation kinetics (segmental mobility). In the case where the polymer is in the rubbery state (temperature is above T_g), the Young's modulus is straight connected with the crosslink density as described by following equation [35]:

$$E = 3\rho RT\upsilon_e \qquad \textit{Equation 1.6}$$

Where E is the Young's modulus (Pa), ρ is the density of polymer (kg m^{-3}), R is gas constant (J K^{-1} mol^{-1}), T is absolute temperature (K) and υ_e is the crosslink density (mol m^{-3}). Since the service temperature of PDCPD is below its T_g, so this equation will be useful for its characterization of network architecture.

In conclusion, oxidation induced crosslinking can explain the observed increase of glass transition temperature, yield stress and rubbery modulus and decrease in toughness. Elastic modulus in the glassy state might increase because of the creation of new polar products. Then a kinetic model, which will be detailed in the next part, shall predict the changes in chemical structure and the concentration of crosslinking so as to later predict the changes in mechanicals proprieties.

In the following section, the DLO effect will be presented to elucidate the confined oxidation layer of the PDCPD sample (Fig. 1.6b and 1.9b).

3.2 Effect of sample thickness

As mentioned above, the thermal oxidation of PDCPD is only confined on the surface, because the oxygen diffusing from the external environment barely reaches in the bulk of the sample. This is a common phenomenon of thermal oxidation which typically leads to heterogeneous oxidation in thickness [40].

Hu et al. [27] have investigated the DLO phenomenon of PDCPD by microscopical observations of the color changes (Figure 1.11). They observed that the sample aged in air at 100°C exhibits a distinct dark surface layer. They justified that after long term ageing, the TOL reaches a "constant" value (Figure 1.12). Therefore, they concluded that the oxidation of PDCPD is limited to a thin surface layer (100 µm at 100°C).

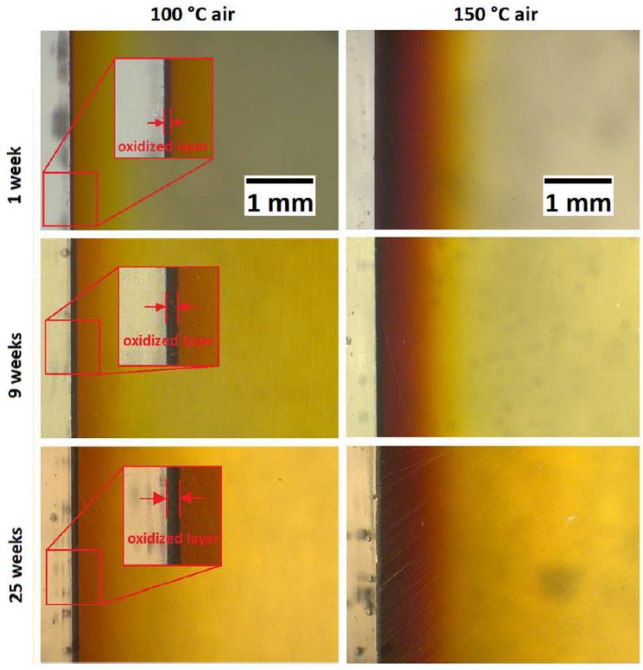

Figure 1.11: Polished sections of PDCPD samples aged in different environments [27].

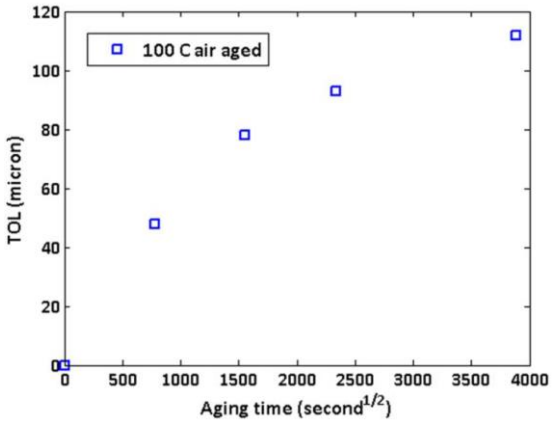

Figure 1.12: Thickness of oxidized layer of PDCPD at 100°C in air [27].

Considering the data exposed above, it clearly appears that thermal oxidation is one of the major degradation pathways for PDCPD polymers. It must be now understood how this degradation can be predicted with time and space which is the aim of the next section.

4. Service lifetime prediction

In practical conditions, the degradation of hydrocarbons polymers such as PDCPD is essentially caused by thermal oxidation reactions, which will further produce a loss of mechanical properties. At a given temperature, the lifetime t_F is defined by the exposure time after which the mechanical property P reaches a critical value (P_F) called the end of life criterion. Among the several existing methods for service lifetime prediction, the empirical method and the less empirical one are presented and compared below.

4.1 Empirical method: Arrhenius modelling

The Arrhenius law is commonly used in the industry to predict the lifetime of thermally aged materials [41]. This empirical approach is based on the hypothesis that lifetime t_F obeys the Arrhenius law:

$$t_F = t_{F0}.exp\frac{E}{RT} \qquad \textit{Equation 1.7}$$

where t_{F0} is the pre-exponential coefficient, E is the activation energy (J mol^{-1}), R is the ideal gas constant (8.314 J mol^{-1} K^{-1}) and T is the exposure temperature (K).

The principle of this method (Figure 1.13) is to perform accelerated ageing experiments at temperatures (T_1, T_2, T_3, T_4) above the operating one, and to determine the corresponding lifetime values (t_{F1}, t_{F2}, t_{F3}, t_{F4}) for the key physical property (e.g. toughness, stress yield). By extrapolating the available data to the operating temperature, it is possible to estimate the lifetime.

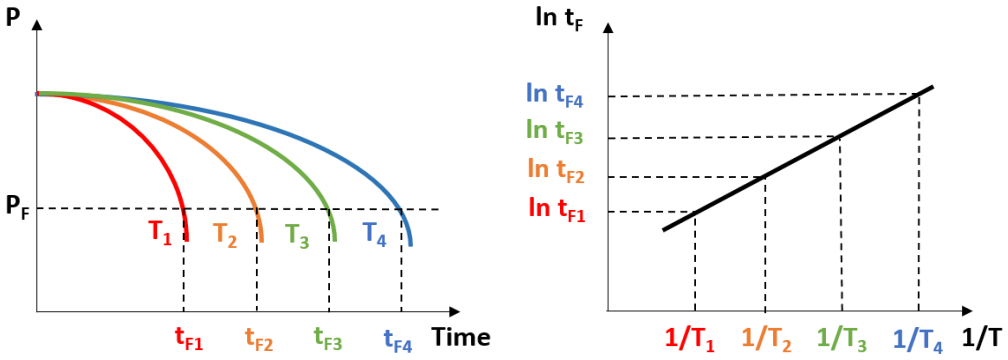

Figure 1.13: Schematic representation of the principle of Arrhenius extrapolation.

Nevertheless, many authors have raised questions about the continuous validity of the "Arrhenius" method and they have demonstrated a non-Arrhenian behavior in the case of thermal oxidation. For example, for unstabilized polypropylene PP and polyethylene PE, a discontinuity at 70 to 80°C has been observed in the Arrhenian plot of the oxidation induction time [42], [43], [44] which is attributed to the changes of the degradation mechanism with temperature [43]. Figure 1.14 displays an Arrhenius plot of literature data on the oxidation of unstabilized polybutadiene PB [45] that shows a remarkable break in terms of oxidation induction time.

Such deviation causes loss of accuracy in polymer lifetime prediction. That is the reason why another prediction method needs to be developed instead of forcing the extrapolation of the Arrhenius plot.

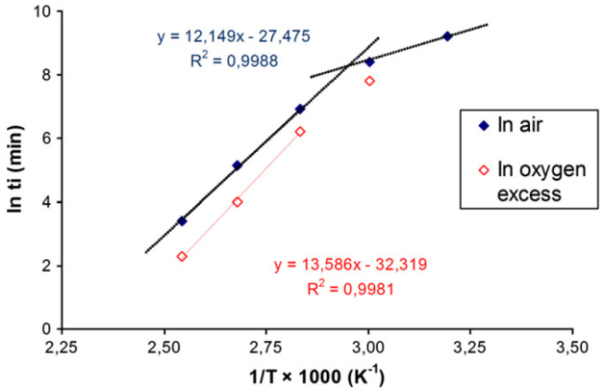

Figure 1.14: Arrhenius plot of oxidation induction time for unstabilized PB [45].

4.2 Multi-scale method

A non-empirical approach is developed and takes into account structural changes at several scales (molecular, macromolecular, morphological, and macroscopic), hence permitting a reliable lifetime prediction possible [46]. This multi-scale approach is based on the knowledge of the mechanisms and the kinetics of degradation. The principle of this method is illustrated below [47]:

- The mechanisms of chemical degradation at the molecular scale should be figured out and converted into a mechanistic scheme which consists of elementary reactions. By applying chemical kinetics, a kinetic model composed of a system of differential equations is established. Its numerical solution gives access to the changes in chemical composition.

- In the case of thick industrial materials, the chemical modifications causing the variations in mechanical properties are dependent on the diffusion of oxygen, which requires the use of a coupling diffusion-reaction in this kinetic model. As a result, this kinetic model is able to predict the thickness of degraded layers.

- Changes at the molecular scale have significant consequences on the macromolecular scale at which this kinetic model also enables the prediction of chain scissions numbers and crosslinking actions.

- Finally, the changes at the molecular scale of the polymer would reflect on the physical properties at the macroscopic scale. Thus, the relationship between macromolecular architectures and properties makes it possible to predict the mechanical behavior changes during the degradation of the material.

This work mainly focuses on the first step of the multi-scale method, namely study about the thermal oxidation at the molecular scale. Since the kinetic model is based on the mechanistic scheme of thermal oxidation of PDCPD, the next section will address the mechanistic aspects in detail.

5. Mechanistic aspects of thermal oxidation of PDCPD

Bolland and Gee [48], [49] firstly proposed a general kinetic model for hydrocarbon polymers. Audouin et al [50] have developed a close loop mechanistic scheme used for kinetic modeling, which can be adapted for several polymers to simulate properly their structural changes during aging. For example, polyolefins (polyethylene (PE) [51], [52], polypropylene (PP) [53],) unsaturated elastomers (polybutadiene (PB) [54], polyisoprene (PI) [55], polychloroprene (CR) [56]) in the rubbery state, and epoxy resin [57] at the temperature below T_g but with some chain mobility $(T > T_\beta)$.

Due to the structural complexity of PDCPD, it is necessary to understand the mechanism of thermal oxidation of unsaturated polymers that is closer to our case. Thus, the thermal oxidation mechanism of unsaturated polymers (PB, PI and CR) are chosen as references for PDCPD studies. The presence of double bonds must be taken into account, which can induce additional reactions in the oxidation mechanism.

5.1 Oxidation mechanisms of unsaturated polymers

Thermal oxidation is an in chain process involving initiation, propagation, termination steps as detailed below.

5.1.1 Initiation

The initiation process is defined as a chemical reaction creating a radical species within the polymer from non-radical species [58]. It is considered that oxidation is initiated by structural defects. Despite they can be present in low quantity in virgin polymer, the hydroperoxides are considered as the key species of the initiation mechanisms. Compared with the dissociation energy of a C-C bond (350 kJ mol^{-1}) and a C-H bond (390 kJ mol^{-1}), the lower dissociation energy of a O-O bond (150 kJ mol^{-1}) makes the decomposition of POOH becoming the main source of formation of radicals (except at high temperature) [47]. For the initiation step, the unsaturated polymers present a combination of uni- and bimolecular decomposition of hydroperoxides (Figure 1.15).

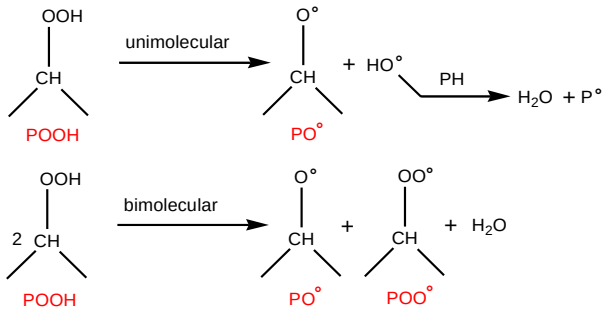

Figure 1.15: Mechanism of unimolecular and bimolecular decomposition of POOH.

The common product of the unimolecular and bimolecular decomposition of POOH is the alkoxyl radical PO°. This one is very unstable and can break to give a carbonyl group (ketone or aldehyde functions) or react rapidly with the substrate to give an alcohol function (Figure 1.16).

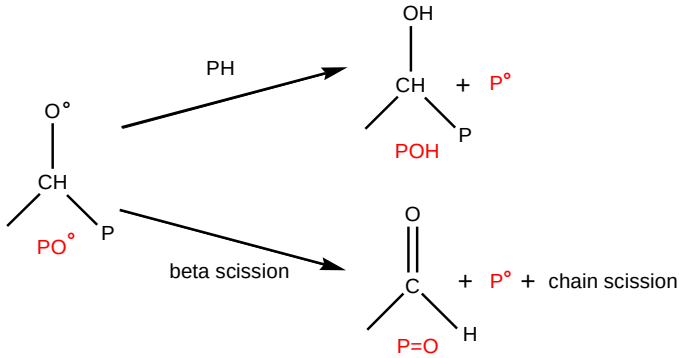

Figure 1.16: Mechanism of rearrangement of radicals PO°.

It has been shown [47] that the mechanistic schemes for the two initiation mechanisms can be schematized as below:

$$POOH \rightarrow 2P^{\circ} + \gamma P{=}O + (1-\gamma)s + \text{inactive products}$$
$$POOH + POOH \rightarrow POO^{\circ} + PO^{\circ} + \gamma P{=}O + (1-\gamma)s + \text{inactive products}$$

Where POOH is hydroperoxide, POO° is peroxyl radical, PO° is alkoxyl radical, γ is carbonyl yield and s expresses a chain scission.

In the case of PB, PI and CR, these decompositions of hydroperoxides bring about the stable oxidation products – carbonyls, which can be characterized by FTIR at 1721 cm^{-1} [45], [54], PI [55] at 1740-1710 cm^{-1} and CR [56] at about 1725 cm^{-1}.

In PDCDP, the exact mechanism for the initiation process is unclear since we don't know if the unimolecular reaction is the main one or bimolecular or if the two coexist. This point needs to be addressed to set up a kinetic model.

5.1.2 Propagation

The propagation step is defined as a chemical reaction that creates new free radicals from radicals species [58]. These reactions are discussed below:

i) First, it was shown that, in the case of PB [54], PI [55] and CR [56], the oxidation takes place mainly on the allyl carbons, because the C-H bond of an allylic C-H is the less stable, according to the following order of C-H bond energy:

	allyl CH	tertiary CH	secondary CH	primary CH
E_d (kJ mol^{-1})	351	380	395	412

Table 1.2: C-H bond energy comparison.

That means the allylic hydrogens are easily abstracted during thermal oxidation. Actually, during the propagation step of the thermal oxidation, the macroradical alkyl P° reacts rapidly with oxygen to give a peroxyl macroradical POO°. Secondly, an allylic hydrogen atom is

abstracted by the POO° peroxyl macroradical, resulting in a new alkyl macroradical P° and a hydroperoxide POOH (Figure 1.16).

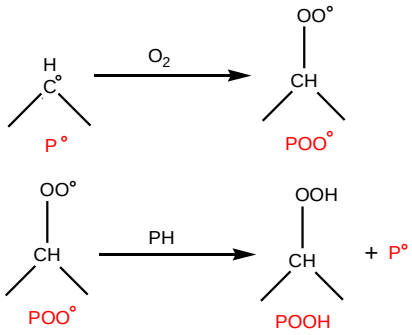

Figure 1.17: Mechanism of propagation step.

ii) The double bonds existing in the structure induce an extra propagation step i.e. the radical addition to double bonds resulting in crosslinking, which is considered in both PB [54], PI [55] and CR [56]. The authors showed that a significant decrease in double bond bands at 967 and 911 cm^{-1} for PB [45], at 836 cm^{-1} for PI [55], and at 1500-2000 cm^{-1} in the case of CR [56]. An example of addition to double bonds has been shown in the case of PB (Figure 1.18) [54]. It is worth noting that during the addition, two oxidizable sites disappear and one crosslink node is created (Figure 1.18).

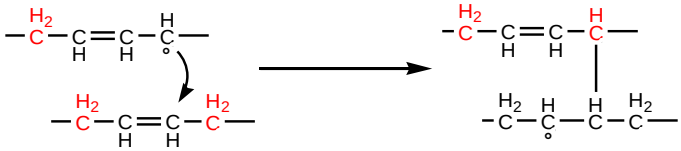

Figure 1.18: Addition reaction of P° to double bonds.

iii) The double bonds can also react with peroxyl (Figure 1.19). However, the resulting crosslink bridges would not be stable and yield epoxides (qualified by FTIR) [59].

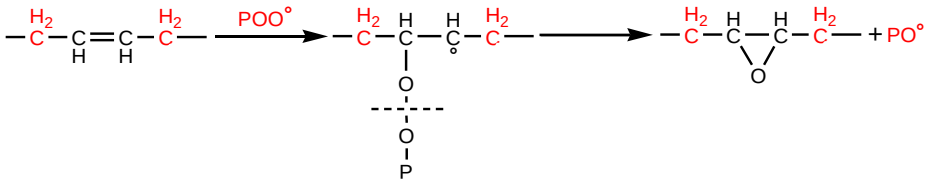

Figure 1.19: Formation of epoxides by the decomposition of a peroxide resulting from the addition of a peroxyl radical to a double bond [59].

The production of epoxides was for example only involved in the mechanistic scheme of PB [60] where the corresponding concentration is not negligible.

In the case of PDCPD, two main propagation steps must be considered: hydrogen abstraction and double bond consumption. The double bond consumption in this polymer has not been characterized yet during thermal oxidation; this point has to be considered in detail during this work.

5.1.3 Termination

The termination step is defined as a chemical reaction of two free radical species to form a stable, non-radical species [58]. In the case of thermal oxidation of polymer, termination reactions involve both $P°$ and $POO°$ depending on external oxygen pressure. Under excess oxygen, a non-terminating bimolecular combination of $POO°$ has been reported in the case of PB [54], PI [55] and CR [56]. This recombination follows the reactions below [44]:

$$POO° + POO° \rightarrow POOOOP \rightarrow [PO° + PO°]_{cage} + O_2$$
$$[PO° + PO°]_{cage} \rightarrow POOP$$
$$[PO° + PO°]_{cage} \rightarrow P = O + POH$$
$$[PO° + PO°]_{cage} \rightarrow 2PO° \rightarrow 2P° + 2P = O$$

Firstly, this recombination generates an unstable tetroxide $POOOOP$, which immediately transforms into alkoxy radicals $PO°$ in the cage. Then, three different reactions are possible for these caged radicals: coupling to form dialkyl peroxide $POOP$; disproportionation by Russell [61], [62] mechanism to generate one carbonyl and one alcohol; diffusion out of the cage of alkoxy radicals $PO°$ following a β scission. The mechanistic scheme of the termination step varies in the case of PB [54], PI [55] and CR [56] according to their respective understanding of the oxidation mechanism.

Based on the description of the three oxidation steps (i.e. initiation, propagation, termination), it is possible to set up an oxidation kinetic model which is the aim of the next section.

5.2 Proposal of kinetic model

A preliminary study about the kinetic modeling of thermal oxidation of PDCPD has been done by Richaud et al. [63]. They have performed the thermal oxidation experiments in air at the temperature ranging from 30°C to 120°C on additive-free PDCPD. They proposed a kinetic model for describing the changes of hydroperoxides and carbonyls which increase with ageing time due to the oxidation reactions of PDCPD:

(1u)	$POOH \rightarrow 2P^{\circ} + \gamma_{CO}P = O$	k_{1u}
(1b)	$POOH \ + POOH \rightarrow P^{\circ} + POO^{\circ} + \gamma_{CO}P = O$	k_{1b}
(2)	$P^{\circ} + O_2 \rightarrow POO^{\circ}$	k_2
(3)	$POO^{\circ} + PH \rightarrow POOH + P^{\circ}$	k_3
(4)	$P^{\circ} + P^{\circ} \rightarrow$ inactive products	k_4
(5)	$P^{\circ} + POO^{\circ} \rightarrow$ inactive products	k_5
(6)	$POO^{\circ} + POO^{\circ} \rightarrow$ inactive products	k_6

Generally, the kinetic parameters are partly obtained from the literature and partly numerically determined by solving the inverse problem [64], namely the values of the kinetic parameters are determined by best simulating the experimental curves of accelerated ageing.

The orders of magnitudes of the rate constants (e.g. $k_1=10^{-4}$ at 90°C) provided a reference for this work. These results bring a lot of inspiration for further study of PDCPD. Based on this scheme, several supplements can be added in accord with the complexity of the PDCPD in particular the effect of double bonds.

However, in order to propose a reliable tool for PDCPD lifetime prediction in industrial applications, it remains to complete this simple model together with a better validation of its lifetime predictions.

On account of the principle of the kinetic model presented in Figure 1.20. Several influence factors will be considered. From the material side, the effects of antioxidants, catalysts and thickness should be involved in our research. One the other side, the oxygen concentration, the

varying temperatures also influence our kinetic model. In the next part, these effects will be described in detail.

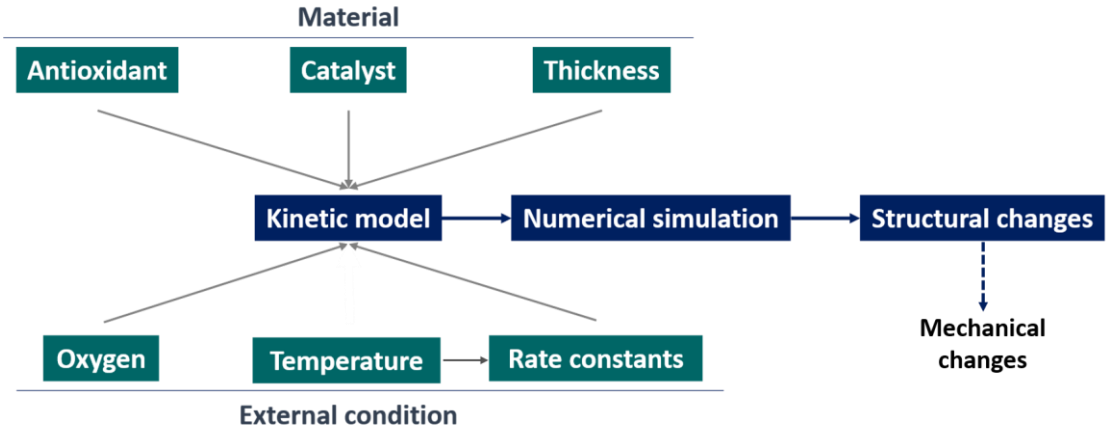

Figure 1.20: Principe of kinetic model.

5.3 Effect of oxygen pressures

Oxygen pressure is a key experimental parameter to assess some kinetic parameters of the model. In fact, the typical inverse method makes it possible to determine the kinetic parameters from the fitting of experimental kinetic curves. However, among the numerous solutions obtained by the inverse method, it would be hard to choose the true one [65]. Studying oxidation under several oxygen pressures can be a solution for selecting the "real" rate constants. Actually, the radicals P° convert rapidly into POO° in the very elevated oxygen regime. So in this condition, the termination process (6) dominates, process whereas (4) and (5) reactions can be neglected. The following strategy can hence be tested:

- Firstly, oxidation is studied in the oxygen excess regime. In this regime, it is possible to determine the termination rate constants k_6 ($POO° + POO° \rightarrow$ inactives products).

- Secondly, oxidation is investigated in the low oxygen pressure (air) to determine the rest rate constants of the termination step: k_4 ($P° + P° \rightarrow$ inactives products) and k_5 ($P° + POO° \rightarrow$ inactives products).

The approach was successfully implemented in the case of PP [65] or PB [54] for example but

remain to be performed in PDCPD for precising the values of termination rate constants.

5.4 Effect of antioxidants

Adding stabilizers play an important role in the prevention of polymer degradation. Two methods of stabilization can be proposed.

One is the one of hydroperoxide reducer (e.g. phosphites, sulphides) which can decompose the hydroperoxides into alcohols and consequently decrease the initiation rate. The other method is to trap radicals using:

- Phenolic antioxidants, which capture POO° radicals in a sacrificial way.
- Hindered Amine Light Stabilizers (called HALS or HAS), which react with the radicals P° and POO° in a regenerative way.

5.4.1 Phenolic antioxidants

The addition of antioxidants bearing the phenol group is a conventional way to prevent polyolefin from degradation. The molecules based on 2,6-di-tert-butylphenol are commonly used.

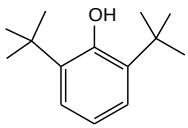

Figure 1.21: Chemical structure of 2,6-Di-tert-butylphenol.

The action mechanism is that the labile hydrogen atom of phenolic antioxidants firstly captured by POO°, which competes with the reaction of POO° to PH:

$$POO^{\circ} + AH \rightarrow POOH + A^{\circ} \qquad k_{s1}$$

Pospíšil [66]–[68] has reported several possible mechanisms of A°, which would continue to react to give inactive products:

- Disproportionation

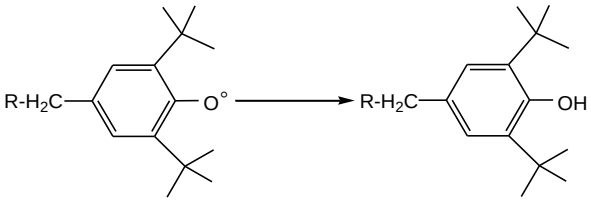

Figure 1.22: Possible disproportionation reaction of A°.

- Inter/ intramolecular radical recombination

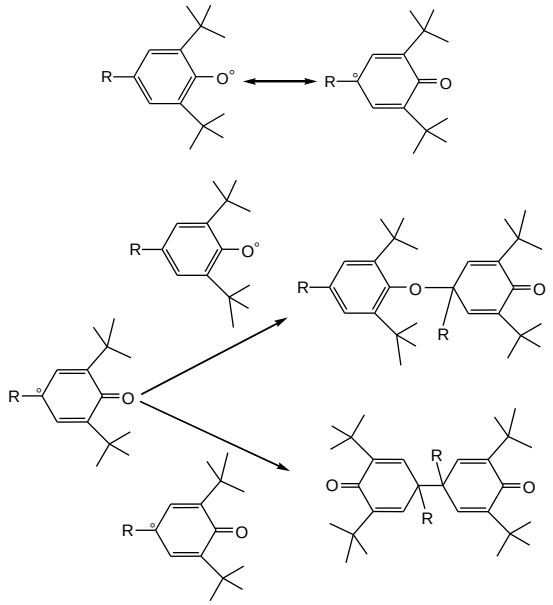

Figure 1.23: Possible inter/intramolecular radical recombinations of A°.

- Radical recombination with POO° or P°

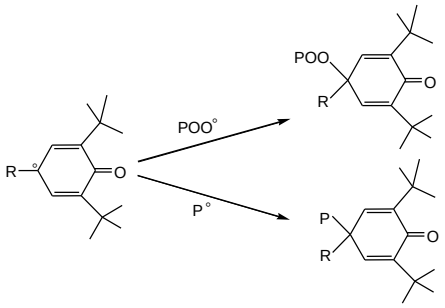

Figure 1.24: Possible radical recombination reactions.

All these processes are competitive depending on temperatures, the concentration of stabilizers, reactivity of POO° [66] so that the authors did not actually reach a consensus in terms of the mechanism. In other words, describing finely the reaction of phenols will be challenging.

5.4.2 Hindered Amine Light Stabilisers

It is been shown that the HALS are outstanding candidates for the prevention of thermal oxidation [69], [70]. The success story of HALS began with the preparation of a stable 2,2,6,6-tetramethylpiperidine-N-oxyl radical (Fig. 1.25).

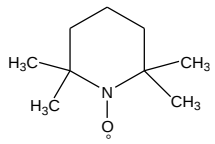

Figure 1.25: 2,2,6,6-tetramethylpiperidine-N-oxyl radical.

The most commonly used HALS are based on tetramethylpiperidinyl group. According to the difference in physical properties, we can distinguish two types of HALS: monomeric HALS and oligomeric ones having lower volatility. The action of HALS is initiated by oxidizing the amine group N-H into nitroxyl group NO° which are the main stabilizing species. Besides, it exists that HALS carrying directly nitroxyl group in their structure (i.e. HALS with group NO-R), which are interesting in our case in comparison with HALS with group NH because they can lead to different interactions with Grubbs catalyst. As will be seen in the following, HALS NO-R displays a more simple mechanism scheme (i.e. with less rate constants) than NH ones, which will help for the calculations of rate constants of the kinetic model.

Identically to phenolic antioxidants, many action mechanisms of HAS are proposed by different authors but they are still uncertain. We can divide the reaction mechanism into two categories: formation of nitroxide and regeneration of nitroxide [71].

Several possible mechanisms are proposed for the nitroxide formation:

- Reaction of the amine with peracid [72] (Figure 1.26).

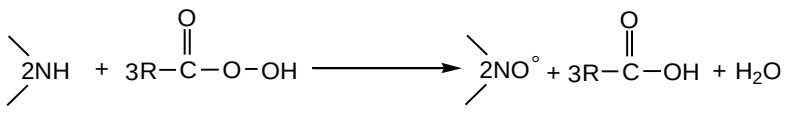

Figure 1.26: Possible reactions of an amine with a peracid forming a nitroxide.

- Amine reacts with the peroxy radical POO° [73] (Figure 1.27).

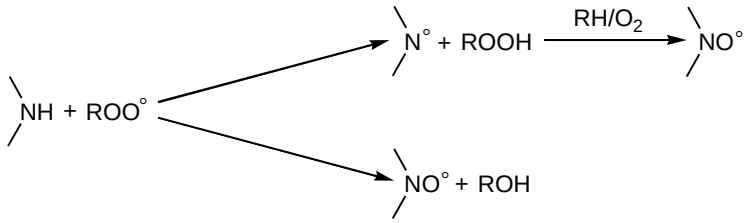

Figure 1.27: Possible reactions of an amine with a peroxy radical forming a nitroxide.

- Amine reacts with the POOH (Figure 1.28) that is pointed out by Sedlar et al. [74].

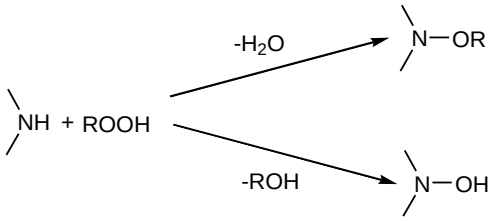

Figure 1.28: Possible reactions of an amine with a hydroperoxide forming a nitroxide.

- Excited charge transfer complex of the amine with oxygen O_2 which was recently proposed by Gijsman [75] (Figure 1.29).

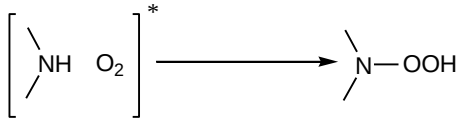

Figure 1.29: Possible reactions of charge transfer complex of the amine leading to a nitroxide.

The efficient action of the HALS is ascribed to the nitroxide regeneration cycle that keeps a high concentration of the main active species for a long time as presented in Figure 1.30. Compared to phenolic antioxidants, HALS makes it possible to convert more active radicals (P° and POO°) into inactive forms by the regeneration of NO°.

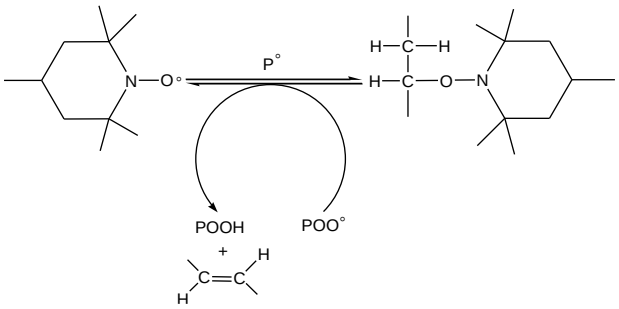

Figure 1.30: Cycle mechanism for nitroxide regeneration [76].

The corresponding part of the mechanistic scheme involving the regeneration of nitroxide has been proposed [76]:

$R-NH+POO^{\circ} \rightarrow R-N^{\circ}+POOH$	k_{NH}
$R-NH+O_2 \rightarrow R-N^{\circ}+\text{inactive products}$	k_{O2}
$R-N^{\circ}+O_2 \rightarrow R-NOO^{\circ}$	k_{N}
$2R-NOO^{\circ} \rightarrow 2R-NO^{\circ}+O_2$	k_{NOO}
$R-NO^{\circ}+P^{\circ} \rightarrow R-NOP^{\circ}$	k_{NO}
$R-NOP+POO^{\circ} \rightarrow R-NO^{\circ}+C=C+POOH$	k_{NOP}

For the HALS of the NO-R type, the mechanistic scheme only concerns the last two steps. Similarly, temperature, concentration and reactivity of all the reagents play a decisive role in the possibility of these reactions. The actions of phenol and HALS involved in the mechanistic scheme for kinetic modeling will be discussed in the result section.

5.5 Diffusion Limited Oxidation (DLO)

According to Figure 1.11 and 1.12, The oxidation controlled by the phenomenon of diffusion of oxygen should be taken into account in the prediction of the lifetime [77]. If the oxygen diffusion in the material is faster than the oxygen consumption (resulting from polymer oxidation), the oxidation rate and oxygen concentration are homogeneous throughout the sample thickness. On the contrary, if oxygen reacts very fast on the surface or diffuses slowly, there will be no oxygen in the bulk of the sample, because the oxidation occurs only at the surface of the sample. The competition between the oxygen diffusion rate and the oxygen

consumption rate can be described by the following relationship [77]:

$$\frac{\partial[O_2]}{\partial t} = D_{O_2} \times \frac{\partial^2[O_2]}{\partial x^2} - r_{ox} \qquad \textit{Equation 1.8}$$

Where $[O_2]$ is oxygen concentration, D_{O_2} is oxygen diffusion coefficient, x is depth of penetration of oxygen, t is time, r_{ox} oxygen consumption rate.

Thus the thickness of the oxidized layer (TOL) can be approximated by the following equation [77]:

$$TOL^2 = \frac{D_{O_2} \times [O_2]}{r_{ox}} \qquad \textit{Equation 1.9}$$

This phenomenon can be clearly observed by the characterization of oxidation products (i.e. carbonyls) [78], [79] (Figure 1.31).

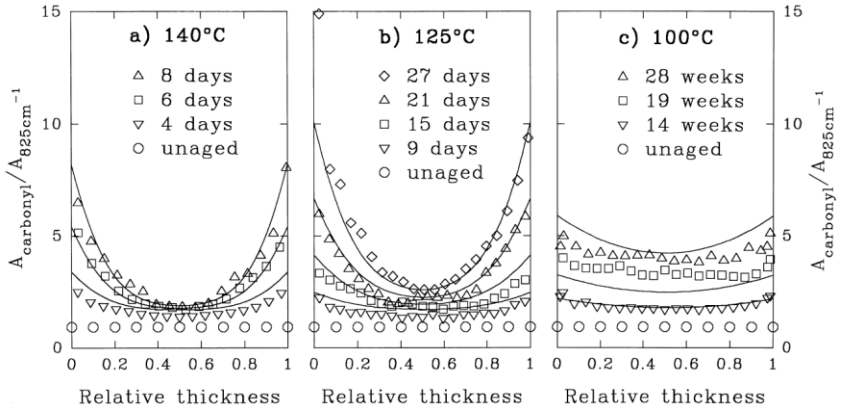

Figure 1.31: Carbonyl profile of neoprene rubber aged at different temperatures.

As we can see in Figure 1.31, the TOL strongly depends on temperature because activation energy of oxygen diffusivity is actually lower than the activation energy for oxidation rate (20 - 50 kJ mol^{-1} [80], [81] versus 50 - 100 kJ mol^{-1} [81], [82]). Among the literature [83], [84], the optical microscopy, the modulus profile, and the microindentation hardness testing are often applied to study the DLO phenomenon and measure the TOL of a polymer.

DLO occurs in the case of PDCDP since the changes of mechanical properties due to thermal ageing only occur on the external surface [26] (section 2.1); the color changes observed by optical microscopy surface [27] (section 2.2). A preliminary study about the oxygen diffusivity

measurements at several temperatures has been performed for unstabilized PDCPD. It has been shown that the thickness of the oxidized layer is observed to be lower than 10 µm at 150°C [81] but few data are reported at lower temperatures. Data presented in Figure 1.11 are obtained for a commercial PDCPD material and the values actually depend on antioxidants concentration. Thus, the effect of DLO is very important and should be considered in our study with a comparison between DLO in pure PDCPD and stabilized one.

5.6 Effect of catalysts

Because of catalysts used during ROMP reaction, the stability of the polymer would be modified by the interaction between metals or metallic compounds and polymer. This influence on PDCPD may be serious, because during the metathesis polymerization, the organometallic catalysts used are in relatively high concentration (typically 100-1000 ppm [85]) compared to the case of polyolefins [86] or elastomers.

There are several possible mechanisms about the effects of metallic compounds on polymer degradation [87]. Acceleration of hydroperoxide decomposition is one of the principal roles of a metallic compound. The corresponding mechanisms in the simple case of unimolecular decomposition of POOH are presented below [88]:

$$POOH + M^{n+} \rightarrow PO^{\circ} + M^{(n+1)+} + OH^{-} \qquad k_{c1}$$

$$POOH + M^{(n+1)+} \rightarrow POOH + M^{n+} + H^{+} \qquad k_{c2}$$

The effect of the catalyst on the decomposition of hydroperoxides is verified in many researches [89]–[93]. Gijsman et al. [23] have verified experimentally the effects of residues of polymerization catalyst on the oxidation rate of PP. They found that the concentration of POOH measured after the oxygen uptake of 1800 mmol/kg varies with the concentration of catalyst residues and the temperature (Figure 1.32). The POOH amounts are higher with a lower Ti concentration, which is explained by the POOH decomposition is catalyzed by the catalyst residues.

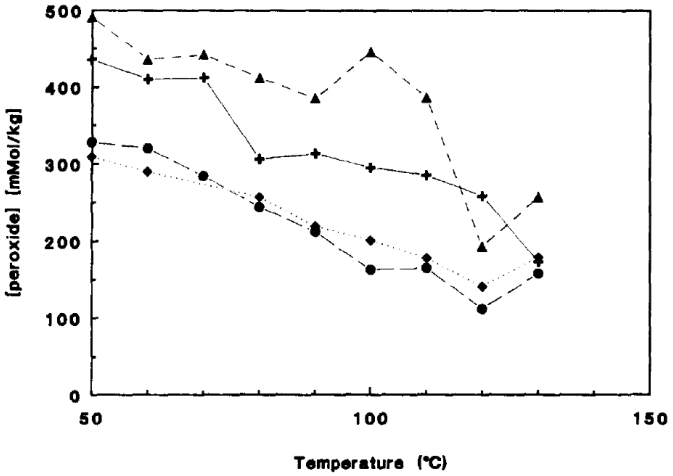

Figure 1.32: The concentration of POOH as a function of temperature, for polypropylene containing: <2 ppm Ti (+), 8 ppm Ti (▲), 64 ppm Ti (●) and 180 ppm Ti (♦) [23].

6. Conclusions et strategy

PDCPD is one of the youngest members of the thermoset family with interesting impact performance and superior chemical resistance. So they are used in many practical applications, including body panels for agricultural and construction equipment, trucks and buses. PDCPD is synthesized from Ring Opening Metathesis Polymerization (ROMP) of dicyclopentadiene in the presence of the catalyst and produced by reaction injection molding process (RIM) with the advantage of very short processing times (typically 5 minutes). PDCPD have attracted extensive interest for field joints in deep offshore application because of these advantages. However, it is facing the challenge of high sensibility to thermal oxidation.

It has been shown that empirical methods are not suitable for predicting the long-term behavior of PDCPD. In order to predict the lifetime of PDCPD in various kinds of ageing conditions (e.g. in submarine conditions), the multi-scale method kinetic modeling will be preferred in this research. Because PDCPD is in a complex degradation environment in the offshore field joint application, its lifetime prediction will be divided into two parts to be studied: thermal oxidation and link with engineering properties (mechanical, interaction with water). The oxidation mechanism at the molecular scale, which is a cornerstone of kinetic modeling, will be emphasized in this thesis.

The following strategy will be chosen:

1. Set up of a kinetic model for thermal oxidation of additive-free PDCPD without DLO

It clearly appears that two remaining scientific questions have to be addressed in order to be able to set up a suitable kinetic model for thermal oxidation of PDCPD.

Firstly, considering the initiation process, how hydroperoxides species decompose in PDCPD. To address this question, an original experimental study will be used with an in situ measurement of hydroperoxides concentration within the polymer during both oxidation and thermolysis. Then, double bonds consumption in PDCPD during the propagation step of the thermal oxidation will be investigated in detail based on chemical measurements during degradation (by FTIR and NMR).

Once the mechanistic scheme for the oxidation of additive-free PDCDP is set up, kinetic parameters will be determined using extensive data-based considering oxidation in a wide range of temperatures (from 20°C to 120°C and oxygen pressure). This kinetic model will allow the prediction of oxidation at the chemical scale for unstabilized PDCDP.

2. Study of the action of stabilizers on PDCPD without DLO

Because PDCPD undergoes fast oxidation compared to other polymers, the use of stabilizers is probably the main route to improve the lifetime of PDCPD. The action of different stabilizers will be added to the mechanistic scheme. The behavior of different stabilizers will be investigated at several ageing temperatures and their efficiency will be compared. With the complete kinetic model, the rate constants of the stabilization reactions will also be evaluated by the inverse method.

3. Study of the oxidation profiles

The experiments for identification of the oxidation profile will be carried out. Meanwhile, the oxidation profile will be simulated with the complete kinetic model.

4. Study of the influence of thermal oxidation on water absorption behavior

The water absorption behavior of PDCPD can be combined with the study of thermal oxidation. Since the ageing of thermal oxidation leads to the formation of hydrophilic products (hydroperoxides, alcohols or carbonyl derivatives), which influence the resistance in aqueous media. Therefore, water absorption will be performed for virgin samples and the aged one.

The final aim is to establish a complete kinetic model with the accurate values of kinetic parameters. The activation energy of each elementary reactions. Extrapolations to other temperatures will allow simulating the changes of the chemical structure and estimate the lifetime for which a critical level of mechanical properties is reached (i.e. the material becomes brittle).

7. References

[1] J. D. Rule and J. S. Moore, "ROMP Reactivity of endo- and exo-Dicyclopentadiene," *Macromolecules*, vol. 35, no. 21, pp. 7878–7882, Oct. 2002.

[2] K. J. Ivin and J. C. Mol, "1 - Introduction," in *Olefin Metathesis and Metathesis Polymerization (Second Edition)*, K. J. Ivin and J. C. Mol, Eds. London: Academic Press, 1997, pp. 1–11.

[3] C. P. Casey, "2005 Nobel Prize in Chemistry. Development of the Olefin Metathesis Method in Organic Synthesis," *J. Chem. Educ.*, vol. 83, no. 2, p. 192, Feb. 2006.

[4] C. W. Bielawski and R. H. Grubbs, "Living ring-opening metathesis polymerization," *Progress in Polymer Science*, vol. 32, no. 1, pp. 1–29, Jan. 2007.

[5] N. Calderon, "Olefin metathesis reaction," *Acc. Chem. Res.*, vol. 5, no. 4, pp. 127–132, Apr. 1972.

[6] O. Nuyken and S. Pask, "Ring-opening polymerization—an introductory review," *Polymers*, vol. 5, no. 2, pp. 361–403, 2013.

[7] T. Davidson, K. Wagener, and D. Priddy, "Polymerization of dicyclopentadiene: a tale of two mechanisms," *Macromolecules*, vol. 29, no. 2, pp. 786–788, 1996.

[8] P. J.-L. Hérisson and Y. Chauvin, "Catalyse de transformation des oléfines par les complexes du tungstène. II. Télomérisation des oléfines cycliques en présence d'oléfines acycliques," *Die Makromolekulare Chemie*, vol. 141, no. 1, pp. 161–176, 1971.

[9] T. Davidson and K. Wagener, "The polymerization of dicyclopentadiene: an investigation of mechanism," *Journal of Molecular Catalysis A: Chemical*, vol. 133, no. 1–2, pp. 67–74, 1998.

[10] S. Hilf and A. F. M. Kilbinger, "Functional end groups for polymers prepared using ring-opening metathesis polymerization," *Nature Chemistry*, vol. 1, no. 7, pp. 537–546, Oct. 2009.

[11] A. Leitgeb, J. Wappel, and C. Slugovc, "The ROMP toolbox upgraded," *Polymer*, vol. 51, no. 14, pp. 2927–2946, Jun. 2010.

[12] S. Sutthasupa, M. Shiotsuki, and F. Sanda, "Recent advances in ring-opening metathesis polymerization and application to synthesis of functional materials," *Polymer Journal*, vol. 42, no. 12, pp. 905–915, Dec. 2010.

[13] W. R. Gutekunst and C. J. Hawker, "A General Approach to Sequence-Controlled

Polymers Using Macrocyclic Ring Opening Metathesis Polymerization," *J. Am. Chem. Soc.*, vol. 137, no. 25, pp. 8038–8041, Jul. 2015.

[14] R. R. Schrock, J. S. Murdzek, G. C. Bazan, J. Robbins, M. DiMare, and M. O'Regan, "Synthesis of molybdenum imido alkylidene complexes and some reactions involving acyclic olefins," *Journal of the American Chemical Society*, vol. 112, no. 10, pp. 3875–3886, May 1990.

[15] J. Heppekausen and A. Fürstner, "Rendering Schrock-type Molybdenum Alkylidene Complexes Air Stable: User-Friendly Precatalysts for Alkene Metathesis," *Angewandte Chemie International Edition*, vol. 50, no. 34, pp. 7829–7832, 2011.

[16] P. Schwab, M. B. France, J. W. Ziller, and R. H. Grubbs, "A Series of Well-Defined Metathesis Catalysts–Synthesis of [RuCl2 (=CHR′)(PR3) 2] and Its Reactions," *Angewandte Chemie International Edition in English*, vol. 34, no. 18, pp. 2039–2041, 1995.

[17] P. Schwab, R. H. Grubbs, and J. W. Ziller, "Synthesis and Applications of RuCl2(CHR')(PR3)2: The Influence of the Alkylidene Moiety on Metathesis Activity," *J. Am. Chem. Soc.*, vol. 118, no. 1, pp. 100–110, Jan. 1996.

[18] M. Scholl, S. Ding, C. W. Lee, and R. H. Grubbs, "Synthesis and activity of a new generation of ruthenium-based olefin metathesis catalysts coordinated with 1, 3-dimesityl-4, 5-dihydroimidazol-2-ylidene ligands," *Organic Letters*, vol. 1, no. 6, pp. 953–956, 1999.

[19] B. F. Straub, "Origin of the High Activity of Second-Generation Grubbs Catalysts," *Angewandte Chemie International Edition*, vol. 44, no. 37, pp. 5974–5978, 2005.

[20] T.-L. Choi and R. H. Grubbs, "Controlled Living Ring-Opening-Metathesis Polymerization by a Fast-Initiating Ruthenium Catalyst," *Angewandte Chemie*, vol. 115, no. 15, pp. 1785–1788, 2003.

[21] S. Monsaert, A. L. Vila, R. Drozdzak, P. V. D. Voort, and F. Verpoort, "Latent olefin metathesis catalysts," *Chemical Society Reviews*, vol. 38, no. 12, pp. 3360–3372, 2009.

[22] E. M. Hoàng, N. S. Allen, C. M. Liauw, E. Fontán, and P. Lafuente, "The thermo-oxidative degradation of metallocene polyethylenes. Part 1: long-term thermal oxidation in the solid state," *Polymer degradation and stability*, vol. 91, no. 6, pp. 1356–1362, 2006.

[23] P. Gijsman, J. Hennekens, and J. Vincent, "The influence of temperature and catalyst residues on the degradation of unstabilized polypropylene," *Polymer Degradation and*

Stability, vol. 39, no. 3, pp. 271–277, Jan. 1993.

[24] J. Asrar, "Reaction injection molding (RIM) system based on metathesis," *Journal of Applied Polymer Science*, vol. 47, no. 2, pp. 289–293, 1993.

[25] C. Slugovc, "Industrial applications of olefin metathesis polymerization," *Olefin Metathesis: Theory and Practice*, pp. 329–333, 2014.

[26] P. Y. Le Gac, D. Choqueuse, M. Paris, G. Recher, C. Zimmer, and D. Melot, "Durability of polydicyclopentadiene under high temperature, high pressure and seawater (offshore oil production conditions)," *Polymer Degradation and Stability*, vol. 98, no. 3, pp. 809–817, Mar. 2013.

[27] Y. Hu, Y. Zhang, and S. Nutt, "Thermal oxidation aging of polydicyclopentadiene and composites," *Polymer Composites*, vol. 39, no. 5, pp. 1742–1751, 2018.

[28] T. R. Long *et al.*, "Influence of molecular weight between crosslinks on the mechanical properties of polymers formed via ring-opening metathesis," *Soft matter*, vol. 14, no. 17, pp. 3344–3360, 2018.

[29] P. Y. Le Gac, V. Le Saux, M. Paris, and Y. Marco, "Ageing mechanism and mechanical degradation behaviour of polychloroprene rubber in a marine environment: Comparison of accelerated ageing and long term exposure," *Polymer Degradation and Stability*, vol. 97, no. 3, pp. 288–296, Mar. 2012.

[30] K. T. Gillen and R. L. Clough, "Rigorous experimental confirmation of a theoretical model for diffusion-limited oxidation," *Polymer*, vol. 33, no. 20, pp. 4358–4365, Jan. 1992.

[31] S. Wu, "Secondary relaxation, brittle–ductile transition temperature, and chain structure," *Journal of Applied Polymer Science*, vol. 46, no. 4, pp. 619–624, 1992.

[32] H. L. Bos and J. J. H. Nusselder, "Toughness of model polymeric networks in the glassy state: effect of crosslink density," *Polymer*, vol. 35, no. 13, pp. 2793–2799, Jun. 1994.

[33] W. D. Cook, A. E. Mayr, and G. H. Edward, "Yielding behaviour in model epoxy thermosets — II. Temperature dependence," *Polymer*, vol. 39, no. 16, pp. 3725–3733, Jun. 1998.

[34] E. D. Crawford and A. J. Lesser, "Brittle to ductile: Fracture toughness mapping on controlled epoxy networks," *Polymer Engineering & Science*, vol. 39, no. 2, pp. 385–392, 1999.

[35] J.-P. Pascault, H. Sautereau, J. Verdu, and R. J. Williams, *Thermosetting polymers*, vol.

477. Marcel Dekker New York, 2002.

[36] E. Espuche, J. Galy, J.-F. Gérard, J.-P. Pascault, and H. Sautereau, "Influence of crosslink density and chain flexibility on mechanical properties of model epoxy networks," *Macromolecular Symposia*, vol. 93, no. 1, pp. 107–115, 1995.

[37] N. Rasoldier *et al.*, "Model systems for thermo-oxidised epoxy composite matrices," *Composites Part A: Applied Science and Manufacturing*, vol. 39, no. 9, pp. 1522–1529, Sep. 2008.

[38] E. A. DiMarzio, "On the second-order transition of a rubber," *Journal of Research of the National Bureau of Standards Section A: Physics and Chemistry*, vol. 68A, no. 6, p. 611, Nov. 1964.

[39] T. G. Fox and S. Loshaek, "Influence of molecular weight and degree of crosslinking on the specific volume and glass temperature of polymers," *Journal of Polymer Science*, vol. 15, no. 80, pp. 371–390, 1955.

[40] M. C. Celina, "Review of polymer oxidation and its relationship with materials performance and lifetime prediction," *Polymer Degradation and Stability*, vol. 98, no. 12, pp. 2419–2429, 2013.

[41] R. M. Koerner, A. E. Lord, and Y. H. Hsuan, "Arrhenius modeling to predict geosynthetic degradation," *Geotextiles and Geomembranes*, vol. 11, no. 2, pp. 151–183, Jan. 1992.

[42] P. Richters, "Initiation process in the oxidation of polypropylene," *Macromolecules*, vol. 3, no. 2, pp. 262–264, 1970.

[43] L. Achimsky, L. Audouin, and J. Verdu, "Kinetic study of the thermal oxidation of polypropylene," *Polymer Degradation and Stability*, vol. 57, no. 3, pp. 231–240, Sep. 1997.

[44] N. Khelidj, X. Colin, L. Audouin, J. Verdu, C. Monchy-Leroy, and V. Prunier, "Oxidation of polyethylene under irradiation at low temperature and low dose rate. Part II. Low temperature thermal oxidation," *Polymer Degradation and Stability*, vol. 91, no. 7, pp. 1598–1605, Jul. 2006.

[45] M. Coquillat, J. Verdu, X. Colin, L. Audouin, and R. Nevière, "Thermal oxidation of polybutadiene. Part 1: Effect of temperature, oxygen pressure and sample thickness on the thermal oxidation of hydroxyl-terminated polybutadiene," *Polymer Degradation and Stability*, vol. 92, no. 7, pp. 1326–1333, Jul. 2007.

[46] X. Colin and J. Verdu, "Strategy for studying thermal oxidation of organic matrix

composites," *Composites Science and Technology*, vol. 65, no. 3–4, pp. 411–419, Mar. 2005.

[47] E. Richaud, "Durabilité des Géotextiles en Polypropylène."

[48] J. Bolland and G. Gee, "Kinetic studies in the chemistry of rubber and related materials. II. The kinetics of oxidation of unconjugated olefins," *Transactions of the Faraday Society*, vol. 42, pp. 236–243, 1946.

[49] J. Bolland and G. Gee, "Kinetic studies in the chemistry of rubber and related materials. III. Thermochemistry and mechanisms of olefin oxidation," *Transactions of the Faraday Society*, vol. 42, pp. 244–252, 1946.

[50] L. Audouin, V. Gueguen, A. Tcharkhtchi, and J. Verdu, "'Close loop' mechanistic schemes for hydrocarbon polymer oxidation," *Journal of Polymer Science Part A: Polymer Chemistry*, vol. 33, no. 6, pp. 921–927, Apr. 1995.

[51] X. Colin, B. Fayolle, L. Audouin, and J. Verdu, "About a quasi-universal character of unstabilised polyethylene thermal oxidation kinetics," *Polymer Degradation and Stability*, vol. 80, no. 1, pp. 67–74, Jan. 2003.

[52] X. Colin *et al.*, "Aging of polyethylene pipes transporting drinking water disinfected by chlorine dioxide. I. Chemical aspects," *Polymer Engineering & Science*, vol. 49, no. 7, pp. 1429–1437, 2009.

[53] A. François-Heude, E. Richaud, E. Desnoux, and X. Colin, "A general kinetic model for the photothermal oxidation of polypropylene," *Journal of Photochemistry and Photobiology A: Chemistry*, vol. 296, pp. 48–65, Jan. 2015.

[54] M. Coquillat, J. Verdu, X. Colin, L. Audouin, and R. Nevière, "Thermal oxidation of polybutadiene. Part 2: Mechanistic and kinetic schemes for additive-free non-crosslinked polybutadiene," *Polymer Degradation and Stability*, vol. 92, no. 7, pp. 1334–1342, Jul. 2007.

[55] X. Colin, L. Audouin, and J. Verdu, "Kinetic modelling of the thermal oxidation of polyisoprene elastomers. Part 1: Unvulcanized unstabilized polyisoprene," *Polymer Degradation and Stability*, vol. 92, no. 5, pp. 886–897, May 2007.

[56] P. Y. Le Gac, G. Roux, J. Verdu, P. Davies, and B. Fayolle, "Oxidation of unvulcanized, unstabilized polychloroprene: A kinetic study," *Polymer Degradation and Stability*, vol. 109, pp. 175–183, Nov. 2014.

[57] E. Ernault, E. Richaud, and B. Fayolle, "Thermal oxidation of epoxies: Influence of

diamine hardener," *Polymer Degradation and Stability*, vol. 134, pp. 76–86, 2016.

[58] D. C. Nonhebel, D. C. Nonhebel, J. Walton, and J. C. Walton, *Free-radical chemistry: structure and mechanism*. CUP Archive, 1974.

[59] M. Coquillat, "Vieillissement des propergols à matrice polybutadiène: modélisation cinétique de l'oxydation," 2007.

[60] M. Guyader, L. Audouin, X. Colin, J. Verdu, and S. Chevalier, "Epoxides in the thermal oxidation of polybutadiene," *Polymer Degradation and Stability*, vol. 91, no. 11, pp. 2813–2815, Nov. 2006.

[61] G. A. Russell, "Deuterium-isotope Effects in the Autoxidation of Aralkyl Hydrocarbons. Mechanism of the Interaction of PEroxy Radicals [1]," *Journal of the American Chemical Society*, vol. 79, no. 14, pp. 3871–3877, Jul. 1957.

[62] J. A. Howard and K. U. Ingold, "Self-reaction of sec-butylperoxy radicals. Confirmation of the Russell mechanism," *Journal of the American Chemical Society*, vol. 90, no. 4, pp. 1056–1058, Feb. 1968.

[63] E. Richaud, P. Y. Le Gac, and J. Verdu, "Thermooxidative aging of polydicyclopentadiene in glassy state," *Polymer Degradation and Stability*, vol. 102, pp. 95–104, Apr. 2014.

[64] X. Colin, L. Audouin, and J. Verdu, "Determination of thermal oxidation rate constants by an inverse method. Application to polyethylene," *Polymer Degradation and Stability*, vol. 86, no. 2, pp. 309–321, Nov. 2004.

[65] E. Richaud, F. Farcas, P. Bartoloméo, B. Fayolle, L. Audouin, and J. Verdu, "Effect of oxygen pressure on the oxidation kinetics of unstabilised polypropylene," *Polymer Degradation and Stability*, vol. 91, no. 2, pp. 398–405, Feb. 2006.

[66] J. Pospíšil, "Chemical and photochemical behaviour of phenolic antioxidants in polymer stabilization—a state of the art report, Part I," *Polymer Degradation and Stability*, vol. 40, no. 2, pp. 217–232, Jan. 1993.

[67] J. Pospíšil, "Chemical and photochemical behaviour of phenolic antioxidants in polymer stabilization: A state of the art report, part II," *Polymer Degradation and Stability*, vol. 39, no. 1, pp. 103–115, Jan. 1993.

[68] J. Pospíšil, "Mechanistic action of phenolic antioxidants in polymers—A review," *Polymer Degradation and Stability*, vol. 20, no. 3–4, pp. 181–202, Jan. 1988.

[69] P. Gijsman and M. Gitton, "Hindered amine stabilisers as long-term heat stabilisers for polypropylene," *Polymer Degradation and Stability*, vol. 66, no. 3, pp. 365–371, Dec.

1999.

[70] F. L. Gugumus, “Polyolefin stabilization: from single stabilizers to complex systems,” *Environmental Science And Pollution Control series*, pp. 1–38, 2000.

[71] P. Gijsman, “A review on the mechanism of action and applicability of Hindered Amine Stabilizers,” *Polymer Degradation and Stability*, vol. 145, pp. 2–10, 2017.

[72] T. Toda, E. Mori, and K. Murayama, “Studies on Stable Free Radicals. IX. Peroxy Acid Oxidation of Hindered Secondary Amines to Nitroxide Radicals,” *Bulletin of the chemical society of Japan*, vol. 45, no. 6, pp. 1904–1908, 1972.

[73] D. J. Carlsson, K. H. Chan, and D. M. Wiles, “Polypropylene Photostabilization by Tetramethylpiperidine Species,” in *Photodegradation and Photostabilization of Coatings*, vol. 151, 0 vols., American Chemical Society, 1981, pp. 51–63.

[74] J. Sedlář, J. Petrůj, J. Pác, and M. Navrátil, “Polymer photostabilization by HALS derivatives: the role of piperidine-hydroperoxide association,” *Polymer*, vol. 21, no. 1, pp. 5–7, Jan. 1980.

[75] P. Gijsman, “New synergists for hindered amine light stabilizers,” *Polymer*, vol. 43, no. 5, pp. 1573–1579, Mar. 2002.

[76] E. Richaud, X. Colin, C. Monchy-Leroy, L. Audouin, and J. Verdu, “Polyethylene stabilization against thermal oxidation by a trimethylquinoleine oligomer,” *Polymer Degradation and Stability*, vol. 94, no. 3, pp. 410–420, Mar. 2009.

[77] L. Audouin, V. Langlois, J. Verdu, and J. C. M. de Bruijn, “Role of oxygen diffusion in polymer ageing: kinetic and mechanical aspects,” *Journal of Materials Science*, vol. 29, no. 3, pp. 569–583, Jan. 1994.

[78] M. Celina, J. Wise, D. K. Ottesen, K. T. Gillen, and R. L. Clough, “Oxidation profiles of thermally aged nitrile rubber,” *Polymer Degradation and Stability*, vol. 60, no. 2–3, pp. 493–504, Jan. 1998.

[79] M. Celina, J. Wise, D. K. Ottesen, K. T. Gillen, and R. L. Clough, “Correlation of chemical and mechanical property changes during oxidative degradation of neoprene,” *Polymer Degradation and Stability*, vol. 68, no. 2, pp. 171–184, Apr. 2000.

[80] M. C. Celina and A. Quintana, “Oxygen diffusivity and permeation through polymers at elevated temperature,” *Polymer*, vol. 150, pp. 326–342, Aug. 2018.

[81] V. Defauchy *et al.*, “Kinetic analysis of polydicyclopentadiene oxidation,” *Polymer Degradation and Stability*, vol. 142, pp. 169–177, Aug. 2017.

[82] M. C. Celina, A. R. Dayile, and A. Quintana, “A perspective on the inherent oxidation sensitivity of epoxy materials,” *Polymer*, vol. 54, no. 13, pp. 3290–3296, Jun. 2013.

[83] J. S. Arrieta, E. Richaud, B. Fayolle, and F. Nizeyimana, “Thermal oxidation of vinyl ester and unsaturated polyester resins,” *Polymer degradation and stability*, vol. 129, pp. 142–155, 2016.

[84] E. Courvoisier, Y. Bicaba, and X. Colin, “Multi-scale and multi-technique analysis of the thermal degradation of poly (ether ether ketone),” *Polymer degradation and stability*, vol. 151, pp. 65–79, 2018.

[85] M. R. Kessler and S. R. White, “Cure kinetics of the ring-opening metathesis polymerization of dicyclopentadiene,” *Journal of Polymer Science Part A: Polymer Chemistry*, vol. 40, no. 14, pp. 2373–2383, 2002.

[86] J. Huang and G. Rempel, “Ziegler-Natta catalysts for olefin polymerization: mechanistic insights from metallocene systems,” *Progress in Polymer Science*, vol. 20, no. 3, pp. 459–526, 1995.

[87] Z. Osawa, “Role of metals and metal-deactivators in polymer degradation,” *Polymer Degradation and Stability*, vol. 20, no. 3–4, pp. 203–236, 1988.

[88] F. Haber and J. Weiss, “On the catalysis of hydroperoxide,” *Naturwissenschaften*, vol. 20, no. 51, pp. 948–50, 1932.

[89] Z. Osawa, T. Shibamiya, and T. Kawamata, “Catalytic action of metallic salts in autoxidation and polymerization. IV. Polymerization of methyl methacrylate by cobalt(II) or (III) acetylacetonate–tert-butyl hydroperoxide or dioxane hydroperoxide,” *Journal of Polymer Science Part A-1: Polymer Chemistry*, vol. 8, no. 10, pp. 2957–2969, 1970.

[90] J. Bartoň and V. Horanská, “Radical reactions initiated by chelate complexes of transition metals. VII. Effect of some copper chelates on the decomposition of cumene hydroperoxide in benzene,” *Die Makromolekulare Chemie*, vol. 157, no. 1, pp. 87–101, 1972.

[91] X.-R. Li and H. Koseki, “Thermal decomposition kinetic of liquid organic peroxides,” *Journal of Loss Prevention in the Process Industries*, vol. 18, no. 4–6, pp. 460–464, Jul. 2005.

[92] S. Skounas, C. Methenitis, G. Pneumatikakis, and M. Morcellet, “Kinetic studies and mechanism of hydrogen peroxide catalytic decomposition by Cu (II) complexes with polyelectrolytes derived from l-alanine and glycylglycine,” *Bioinorganic chemistry and*

applications, vol. 2010, 2010.

[93] I. Ben Talouba, L. Balland, N. Mouhab, and M. A. Abdelghani-Idrissi, "Kinetic parameter estimation for decomposition of organic peroxides by means of DSC measurements," *Journal of Loss Prevention in the Process Industries*, vol. 24, no. 4, pp. 391–396, Jul. 2011.

Chapter 2 Materials and experimental methods

1. Introduction

The methodology adopted for studying the thermal degradation of PDCPD is illustrated in Figure 2.1.

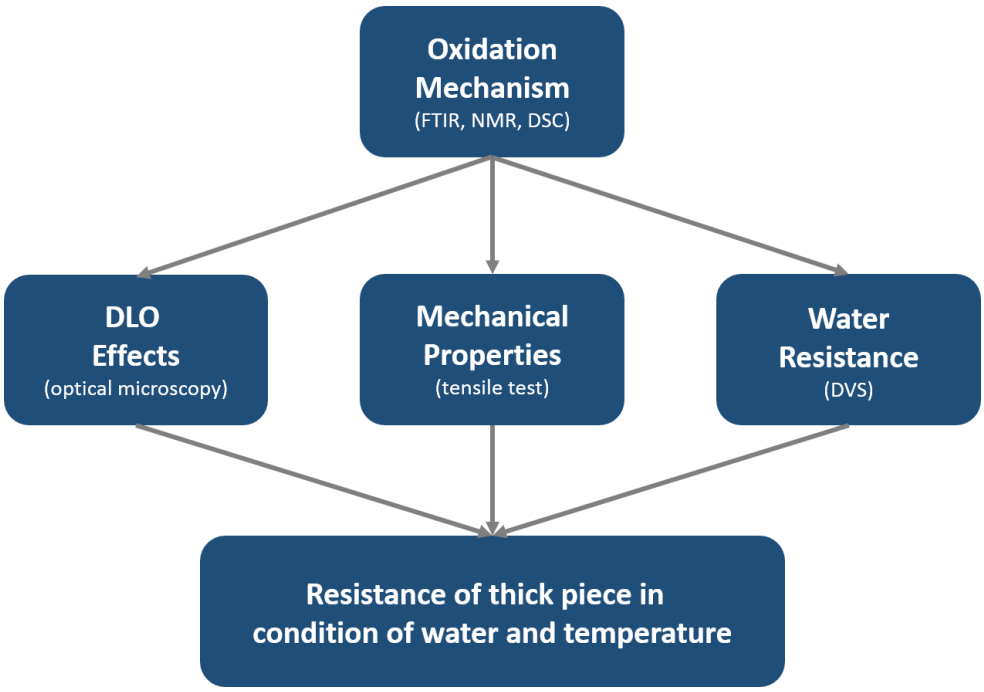

Figure 2.1: Multi-scale approach for lifetime prediction of PDCPD and the main associated experimental techniques.

This multi-scale method will be divided into the following steps:

1. Identification of the oxidation mechanism by characterization of additive-free and stabilized samples in the form of thin films using FTIR, NMR, DSC.

2. Investigation of catalyst effect on thermal oxidation kinetics: Characterization additive-free samples with different catalyst concentrations in the form of thin films with FTIR, DSC.

3. Study of thermal oxidation effect on the water absorption: Characterization additive-free samples in the form of thin films with DVS.

4. Study of the oxidation profile to predict the oxidation in bulk material: Observation of the thickness of the oxidation layer with the optical microscope and/or gravimetric study using additive-free and stabilized bulk materials, confirmation by the kinetic model.

5. Build-up a kinetic model that is able to predict the lifetime corresponding to a loss of plasticity studied by tensile tests.

This chapter presents the investigated materials as well as the thermal and wet exposure environment where the accelerated ageing takes place. Besides, the various analytical techniques used during this thesis to follow the thermal oxidation are also presented.

2. Materials

2.1 PDCPD materials

The PDCPD materials, which were prepared by RIM process at room temperature, used in this study are summarized in Table 2.1. The structures of stabilizers are represented in Figure 2.2.

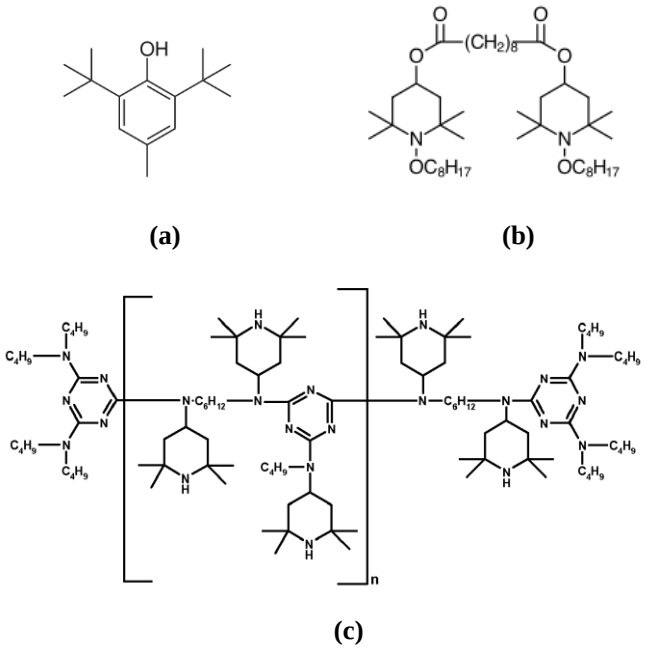

Figure 2.2: Chemical structures of stabilizers used in this work.

Material	Catalyst	Concentration of functional group of antioxidant (mol l^{-1})	Purification	Objectives
M*-PDCPD	2.52 10^{-4} mol.kg^{-1} Ru1	9.09 10^{-2} BHT	Yes	Step 1 and 3: FTIR, NMR, DSC, DVS (thin films 7-15 µm) Step 5 : tensile tests (films 60 µm)
L-PDCPD	1.18 10^{-4} mol.kg^{-1} Ru2	/	No	Step 2: FTIR, DSC (thin films 15 µm) Step 4: optical microscope and gravimetric study (bulky material 2 cm × 1 cm × 1 cm)
H-PDCPD	3.53 10^{-4} mol.kg^{-1} Ru2	/	No	
PDCPD	2.62 10^{-4} mol.kg^{-1} Ru2	2.27 10^{-3} 4.55 10^{-3} 9.09 10^{-3} 2.27 10^{-2} 4.55 10^{-2} BHT	No	Step 1: FTIR (thin films 15 µm) Step 4: optical microscope (bulky material 2 cm × 1 cm × 1 cm)
		2.27 10^{-3} 4.55 10^{-3} 9.09 10^{-3} 2.27 10^{-2} 4.55 10^{-2} Tinuvin 123		
		2.27 10^{-3} 4.55 10^{-3} 9.09 10^{-3} 2.27 10^{-2} 4.55 10^{-2} Chimassorb 2020		

Table 2.1: Investigated PDCPD material details. NB: Ru1 and Ru2 are ruthenium-based Grubbs catalysts.

2.2 Model systems

The model (macro)molecules are used for identification the double bond concentration which is crucial in the kinetic model. 96% Cyclopentene (ref 344508 96 %, Sigma-Aldrich), cis-1,4-

polybutadiene (ref 181374 Sigma-Aldrich) and polybutadiene (ref 181382 Sigma-Aldrich) were used as model (macro)molecules. The cis-1,4,trans-1,4, and vinyl-1,2 unit contents of both homopolymers of polybutadiene (from supplier data) are provided in Table 2.2.

Sample	Microstructure (%)		
	cis-1,4	trans-1,4	vinyl-1,2
PB1	98	/	2
PB2	36	55	9

Table 2.2: The microstructure of the polybutadiene homopolymers.

3. Sample preparation

By cutting the bulk material with a microtome (RM 2255 Leica), films having a thickness lower than 15 µm were obtained. They were then purified by refluxing in CH_2Cl_2 (ref 270997 $\geqslant$ 99.8 %, Sigma-Aldrich) overnight. It is important to note that this thickness is low enough to avoid the Diffusion-Limited Oxidation effects [1]. Unstabilized samples were stored at -20°C before ageing.

4. Exposure conditions

4.1 Thermal ageing

4.1.1 Ventilated oven

Samples were exposed in ventilated ovens at atmospheric pressure at various temperatures (30°C, 50°C, 70°C, 90°C and 120°C). Exposures at 20°C and 25°C were performed in the air-conditioned room of the lab.

4.1.2 Autoclave

The autoclaves were thermally equilibrated for 24 h at 20°C, 30°C, 50°C and 70°C prior to exposure. Then samples were exposed in autoclaves at different pressures from 0.2 to 1 MPa of pure oxygen.

4.1.3 Water ageing

The water ageing was measured in air at 0.1 MPa with fixed water partial pressures in a dynamic vapor sorption apparatus DVS-1000 (Surface Measurement Systems). The additive-free samples were thermal aged at 25°C, 50°C and 70°C for a series of different times. About 1.5 mg virgin and aged samples were tested in DVS at 25°C, 50°C and 70°C under varying water vapor partial pressures (0, 5,10, 15, 20, 30, 40, 50, 60, 70, 80 and 90%) with two cycles of sorption-desorption and 150 minutes steps at each partial pressure. The mass variations of the samples are recorded continuously, which makes it possible to obtain the sorption and desorption curves directly.

The results obtained by DVS shows that the plateaus for change in mass of water are absent for water activity beyond 0.5. So the mass of water for the one without plateau will be taken at the end of each step.

5. Experimental techniques for ageing monitoring

5.1 At molecular scale

5.1.1 Structural changes by Fourier Transform InfraRed Spectroscopy

The FTIR spectra were collected on a Frontier spectrometer (PerkinElmer), as the average of 4 scans performed over a spectral range from 400 to 4000 cm^{-1} with a resolution of 4 cm^{-1}. Spectra were then analyzed with Spectrum™ software. The absorbances of the oxidation products are defined as the maximum height of the peak relative to a defined baseline. The concentrations of the oxidation products and double bonds were calculated using the Beer-Lambert equation:

$$A = \varepsilon \times l \times c \qquad \textit{Equation 2.1}$$

Where A is the peak absorbance, l is the thickness of the film in cm, c is the concentration in mol l^{-1}, and ε the molar absorptivity in l mol^{-1} cm^{-1}.

The concentration in carbonyls (that are the main oxidation products) is calculated with a molar

absorptivity of 300 mol l^{-1} cm^{-1} [2] at 1710 cm^{-1}.

The method for identification and calculation of double bond concentration will be detailed later. To better assess the double bond concentration, some comparisons were made with:
- Cyclopentene: a few drops were placed on a KBr window with an optical path of 0.05 mm (ref 1921supplied by Eurolabo) to verify the assignment of the absorption bands from the carbon-carbon double bonds and to calculate their molar absorptivities.

- Polybutadienes: cast on a KBr disk from a chloroform solution. The analyses, performed after complete solvent evaporation, aimed at verifying the assignment of the absorption bands from the carbon-carbon double bonds.

5.1.2 Solid-state NMR

^{1}H solid-state NMR spectroscopy was used to determine the carbon-carbon double bond concentration. The NMR measurements were performed on a Bruker Avance III NMR spectrometer operating at a ^{1}H Larmor frequency of 700.14 MHz, equipped with an ultrafast MAS 1.3 mm double-resonance ^{1}H-X probe spinning up to 67 kHz. ^{1}H one-pulse experiments were carried out with a 90°(^{1}H) pulse length of 2.0 µs and the recycle delay was varied between 20 s and 120 s, depending on the $T_1(^{1}H)$ relaxation. The ^{1}H chemical shift values were referenced using adamantane as an external reference (1.91 ppm with respect to TMS).

5.1.3 POOH titration by Differential Scanning Calorimetry

The hydroperoxide concentration was measured using a Q10 DSC calorimeter (TA Instrument) driven by Q Series Explorer™ software [2], [3]. Temperature and enthalpy calibrations were first calibrated with an indium standard. Approximately 0.3 mg of virgin or oxidized samples were heated from 20 to 300°C, at a heating rate of 10°C min^{-1}, in a sealed aluminium pan. This heating procedure was performed under an inert atmosphere obtained using nitrogen as a purge gas at a flow rate of 50 ml min^{-1}. Results were processed using the TA Analysis software. The values of exotherms ascribed to hydroperoxides were converted into concentrations using $\triangle H$ = 440 $kJ.mol^{-1}$ [4].

5.1.4 SO_2 and DMS treatments

Sulphur dioxide treatments were used to verify the appearance of hydroperoxides, which transforms POOH into sulphates by the following reactions [5], [6]:

$$POOH + SO_2 \rightarrow PO - SO_2 - OH$$
$$PO - SO_2 - OH + POOH \rightarrow POOP + H_2SO_4$$

Dimethyl sulfide treatments were also conducted to confirm the appearance of hydroperoxides:

$$CH_3 - S - CH_3 + P(=O) - OOH \xrightarrow{fast} CH_3 - S(=O) - CH_3 + P(=O) - OH$$
$$CH_3 - S - CH_3 + POOH \xrightarrow{slow} CH_3 - S(=O) - CH_3 + POH$$

Degraded samples (5 mg) were placed in closed vessels and immersed either in solutions of 5 mg of Na_2SO_3 (ref 71988 Sigma Aldrich) in 10 ml HCl (ref 40253 Sigma Aldrich, 37 wt % in H_2O) in which SO_2 was generated in situ, or in 10 ml DMS (ref 274380 Sigma Aldrich) for 24 hours at room temperature. The effect of both DMS and SO_2 on the exothermal signal measured by DSC will permit a discussion on the nature of peroxide species.

5.1.5 NH_3 treatment

NH_3 treatment was used to identify the nature of oxidation products. Ammonia was generated from an equi-molar solution of NH_4Cl (13.4 g) and NaOH (10 g) in 100 ml of water. Samples were put in a closed vessel where ammonia was generated from an equimolar solution of NH_4Cl (13.4 g) and NaOH (10 g) in 100 ml of water. The treatments were performed at room temperature for 24 hours. The relevant reaction is shown below:

$$NH_4Cl + NaOH \rightarrow NH_3 + H_2O + NaCl$$

The comparison of FTIR spectra before and after NH_3 treatment will help us to discuss the nature of carbonyls detected by FTIR.

5.2 At macroscopic scale

5.2.1 Optical microscopy

Thick samples (L-PDCPD and PDCPD with different stabilizes) with substantially the same shape (2 cm × 1 cm × 1 cm), which were already thermal aged at different temperatures (50°C, 70°C and 120°C), were polished for further observation. Then a Zeiss Axio Imager 2 optical microscope was used to measure the thickness of the oxidized layer.

5.2.2 Gravimetric study

PDCPD samples with different thickness ranging from 10µm to 100µm (prepared with a microtome (RM 2255 Leica)) were aged at 50°C in ventilated oven. Then the corresponding mass uptakes induced by the grafting of oxygen to the polymer were measured by balance (Mettler Toledo).

5.2.3 Tensile Tests

Tensile tests were performed using 60 µm thick samples in order to obtain homogeneous oxidation through the sample thickness. Samples were cut in a dogbone shape with an initial working length of 10 mm. They were tested after several ageing durations at 80°C in air using an Instron test machine with a 50 N load cell. For each condition, at least 8 samples were characterized in order to ensure the reliability of results.

6. References

[1] V. Defauchy *et al.*, "Kinetic analysis of polydicyclopentadiene oxidation," *Polymer Degradation and Stability*, vol. 142, pp. 169–177, Aug. 2017.

[2] E. Richaud, F. Farcas, B. Fayolle, L. Audouin, and J. Verdu, "Hydroperoxide titration by DSC in thermally oxidized polypropylene," *Polymer Testing*, vol. 25, no. 6, pp. 829–838, Sep. 2006.

[3] Y. Ouldmetidji, L. Gonon, S. Commereuc, and V. Verney, "A differential scanning calorimetry method to study polymer photoperoxidation," *Polymer Testing*, vol. 20, no. 7, pp. 765–768, Jan. 2001.

[4] E. Richaud, P. Y. Le Gac, and J. Verdu, "Thermooxidative aging of polydicyclopentadiene in glassy state," *Polymer Degradation and Stability*, vol. 102, pp. 95–104, Apr. 2014.

[5] D. J. Carlsson, R. Brousseau, and D. M. Wiles, "Reactions of sulfur dioxide with oxidized polyolefins," *Polymer Degradation and Stability*, vol. 15, no. 1, pp. 67–79, Jan. 1986.

[6] J. Scheirs, D. Carlsson, and S. Bigger, "A review of the methods for detecting and characterizing hydroperoxide groups in oxidized polyolefins," *Polymer-Plastics Technology and Engineering*, vol. 34, no. 1, pp. 97–116, 1995.

Chapter 3 Thermal oxidation of additive-free PDCPD

1. Introduction

The study of thermal-oxidation should start from the most simple case, which is the additive-free PDCPD thin samples. Then the created kinetic model for this one will be adapted for thick and stabilized PDCPD. A recent study [1] addressed the case of thermal oxidation of PDCPD. This latter was shown to induce an increase in T_g and yield stress, which was linked to a predominant crosslinking mechanism. The relative fast PDCPD oxidation (compared with other unsaturated substrates) was first modeled using higher initiation rate constants (i.e. rate of radical creation) possibly because of the metallic catalyst [2], and low termination rate constants that could be due to lower segmental mobility of POO° in the glassy state [2]. It is however noteworthy that the model proposed in [2] omitted the role of double bonds which is instrumental to predict the crosslinking.

This chapter will be mainly aimed at proposing a more complete model, with a better validation of its kinetic parameters. For that propose, we will focus on the stability of hydroperoxides to estimate initiation rate constants, on the consumption of double bonds (in line with the crosslinking process) and on the build-up of stable products (mainly carbonyls) under several oxygen pressures to access the termination rate constants. Prior to those investigations, a brief study of mechanical properties will be given to answer the structure-properties relationships associated with end-of-life criterion.

2. Mechanical properties

Tensile behaviors of 60 µm thick films aged at 80°C are represented in Figure 3.1 for several concentrations of carbonyls and double bonds (the method for concentration calculation will be detailed in section 3 for double bonds and section 4.1 for carbonyls). For unaged material, the “elastic domain” where stress increases linearly with strain, is followed by the “plastic domain” where sample can undergo large deformation without breaking. Strain at break is hence a marker of toughness of polymers. It clearly appears that oxidation leads to a decrease in strain at break as well as an increase in yield stress (Figure 3.1). Moreover, the decrease in maximal strain can be related to concentration of remaining double bonds and formed carbonyls.

As mentioned in chapter 1 (section 3.1), the toughness (here associated with strain at break) is related to crosslinking density in the structure. However, the decrease of double bonds concentration is due to participation of double bonds to form crosslinking (Figure 1.10). Such specific feature creates a link between changes in chemical structure and changes in mechanical properties. This means that using a kinetic model is able to predict chemical changes during oxidation, then the kinetic model would allow predicting the lifetime from a mechanical point of view.

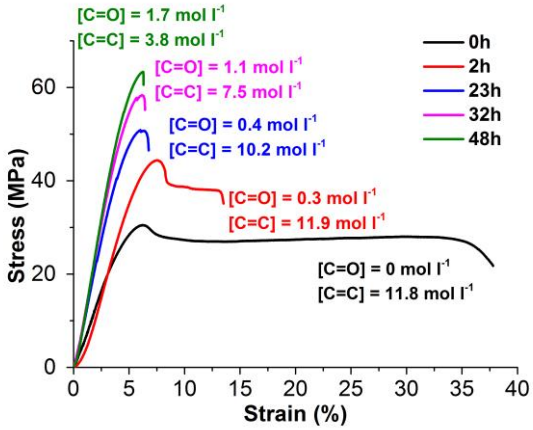

Figure 3.1: Tensile curves for PDPCD samples with varying exposure times at 80°C under air. NB: Concentrations were obtained by using a correction corresponding to $\left(\frac{A_{CH2}}{e}\right)$ *differences in samples tested for tensile tests and ageing tests monitored by FTIR.*

In particular, it seems clear that PDCPD becomes brittle when [C=O] > 0.2 mol l^{-1} which corresponds more or less to $\varepsilon_b = 1/2\varepsilon_{b0}$. In the same time, the increase in σ_y is clearly related to the depletion in double bonds concentrations.

3. Double bonds consumption and termination

A reliable lifetime prediction of PDCPD thus requires an accurate description of crosslink density during oxidation. In this contribution, we aim to monitor the chemical modifications involved in PDCPD crosslinking during its thermal oxidation. Such information will allow a better understanding of the interplay with the variations of the mechanical behavior observed for aged polymers. For this purpose, we will complete the previously established kinetic model

[2] by considering reactions involving the PDCPD double bonds and determining their rate constants. Since crosslinking and double bond consumption can originate from reactions with either P° or POO° species, our strategy relies on the comparison of the ageing behavior under air and under different oxygen pressures [3], [4] (which is a way to isolate the specific contribution of some rate constants) following a similar approach to the one used previously for polybutadiene (PB) [5] and polychloroprene (CR) [6]. Such an experimental approach should help achieve a better separation of the contributions from these two types of reactions.

3.1 Concentration of double bonds in virgin PDCPD

Since the concentration of double bonds in the unaged PDCPD is needed in order to propose a kinetic model, FTIR experiments were firstly used to determine its quantity. The assignment of characteristic absorption bands for double bonds, reported in Figure 3.4a and 3.4b, has been verified using model molecules (cyclopentene and polybutadiene homopolymers, Figure 3.2) and was found to be in agreement with the literature.

More precisely, the peak at 3049 cm^{-1} (Fig. 3.4a) is attributed to ω(=C-H) for cyclic cis double bonds, as confirmed by the FTIR spectrum of cyclopentene (Fig. 3.2a) [7], [8].

The peak at 973 cm^{-1} is related to ω(=C-H) for acyclic trans double bonds, as also observed for a polybutadiene homopolymer with 55 % of trans-1,4 units (Fig. 3.2b) [7], [9], [10].

The cis =C-H wagging bands for cis dialkyl ethylenes are usually located in the 720–680 cm^{-1} region [10]. Two peaks may be observed on the FTIR spectrum of PDCPD near this range at 733 and 709 cm^{-1} (Fig. 3.2c). Nava and al. [9] proved that polybutadienes differing by their 1,2 vinyl, 1,4 cis and 1,4 trans content always display a medium-strong band in the 728-750 cm^{-1} region corresponding to cis ω(=C-H) so that the band at 733 cm^{-1} is attributed to acyclic cis double bonds [10].

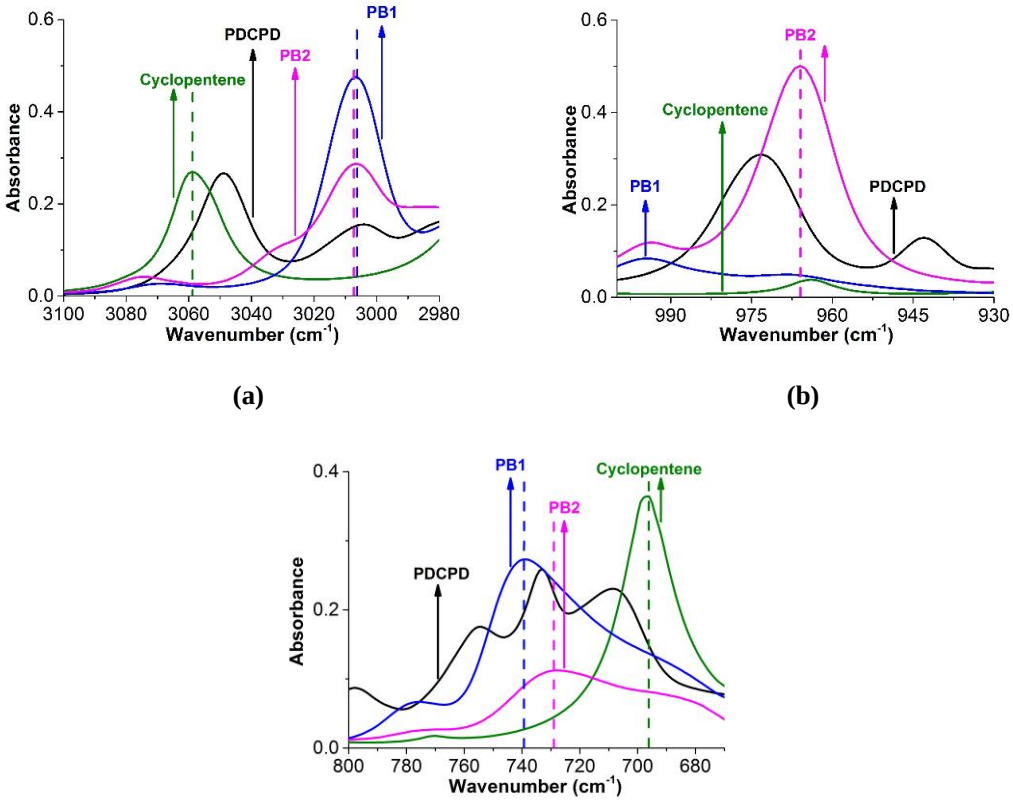

Figure 3.2: Comparison of the FTIR spectra of purified, unaged PDCPD (in black) and model systems: cyclopentene (in green), PB1 (in blue) and PB2 (in magenta).

The total double bond concentration within PDCPD is the sum of three contributions corresponding to cyclic cis -HC=CH- bonds, acyclic cis -HC=CH- bonds and acyclic trans -HC=CH- bonds :

$$[C=C] = [C=C]_{cyclic\ cis\ double\ bond} + [C=C]_{acyclic\ cis\ double\ bond} + [C=C]_{acyclic\ trans\ double\ bond} \qquad \textit{Equation 3.1}$$

Using values of molar absorptivity equal to 19 l mol^{-1} cm^{-1} for cyclic cis -H=C (determined in this work), 60 l mol^{-1} cm^{-1} for cis vinylene units (R-CH=CH-R') [11], and 100 l mol^{-1} cm^{-1} for trans vinylene units (R-CH=CH-R') [12], this concentration can be expressed as:

$$[C=C] = \frac{[=C-H]_{3049}}{2} + \frac{[=C-H]_{973}}{2} + \frac{[=C-H]_{733}}{2}$$
$$= \frac{1}{2} \times \frac{1}{l} \times \left(\frac{A_{3049}}{\varepsilon_{3049}} + \frac{A_{733}}{\varepsilon_{733}} + \frac{A_{973}}{\varepsilon_{973}}\right) \qquad \textit{Equation 3.2}$$

As a result, the double bond concentration of purified, unaged PDCPD is found to be about 10-13 mol l^{-1}. It must be acknowledged that the relative concentration of acyclic and cyclic double bonds does not match well with expected values (their concentration should theoretically be the same) but this has a very limited consequence on the following of our work since we only will model the overall double bond decay.

At room temperature, PDCPD is in the glassy state and the low extent of molecular mobility results in an inefficient motional averaging of the ^1H-^1H dipolar couplings and thus, in a significant broadening of the ^1H NMR peaks. Such a situation renders the contribution from chemically-distinct protons difficult to resolve on the ^1H NMR spectrum of bulk PDCPD. For this reason, ^1H solid-state NMR experiments on PDCPD were performed at high magnetic field (^1H Larmor frequency ν_0 of 700 MHz) in order to improve the separation between the contributions from the different kinds of protons involved in unaged PDCPD. In addition, the ^1H one-pulse experiments were performed under sample rotation at an ultra-fast spinning frequency (ν_r = 50 kHz).

The combination of both experimental conditions led to a clear separation of the peaks related to -CH= and saturated CH / CH_2 protons, as shown in Figure 3.3, and thus enables a rather accurate quantification of the amount of double bonds. The peak at 5.6 ppm is assigned to the -CH= protons whereas the one at 2.7 ppm corresponds to the overlapping of the contributions from the saturated CH and CH_2 protons. The deconvolution of the ^1H NMR spectrum of unaged PDCPD (Figure 3.3), recorded under quantitative conditions, was performed using two components with a Voigt line shape. The ratio between the areas of these components was found to be 1.99, i.e. very close to the value expected by considering the chemical structure of PDCPD. From these solid-state NMR results, the double bond concentration for unaged PDCPD was estimated to be 13 mol l^{-1}, which is in good agreement with the value deduced from FTIR experiments and also consistent with the theoretical value $2\times\rho/M_m$ (ρ is the density = 1045 g l^{-}

[1] and M_m the molar mass of the monomer) expected to be about 15 mol l^{-1} having in mind that a part of double bonds can disappear during curing process and given the uncertainties on molar absortivities. It is possible that the strong heat release during PDCPD polymerization induces a very high crosslinking level (consistently with the higher density value than in Ref. [13]]) and the disappearance of hexahydropentalene groups. This would explain why β transition (associated to hexahydropentalene groups [14]) is absent in our case and why double bond concentration is lower than 15 mol l^{-1}.

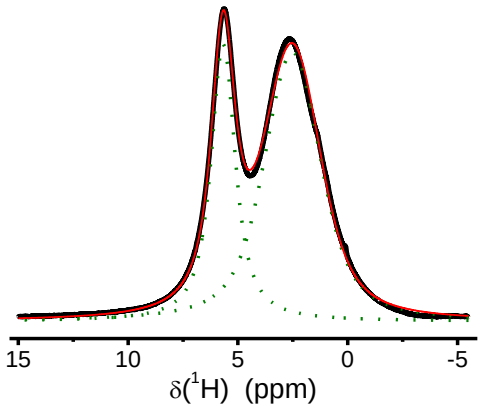

Figure 3.3: One-pulse 1H MAS NMR spectrum of purified, unaged PDCDP, recorded at a 1H Larmor frequency ν_0 of 700 MHz and a MAS frequency ν_r of 50 kHz. The deconvolution of the spectrum (red solid line) using Voigt line shapes (green dotted lines) is also included.

3.2 Concentration of double bonds in oxidized PDCPD

The comparison of the IR spectra obtained on virgin PDCPD and PDCPD thermally oxidized at 50°C under air (Fig. 3.4a and Fig. 3.4b) shows a decrease of the concentration of all types of double bonds, which indicates reactions between double bonds and radicals (Fig. 3.5).

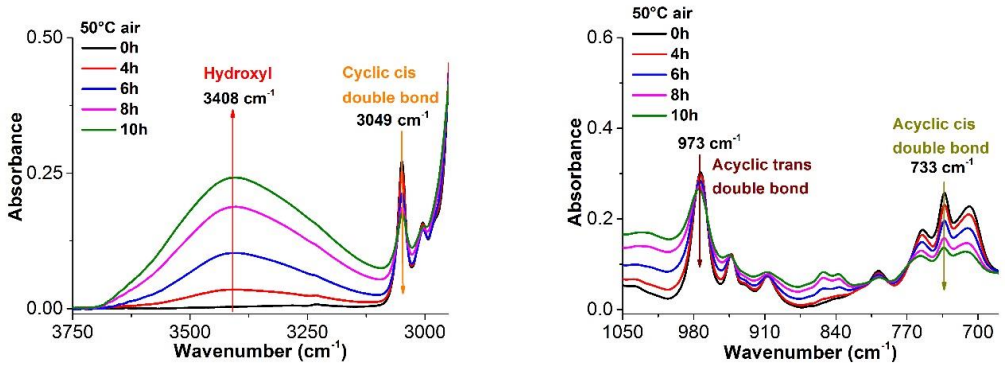

(a) **(b)**

Figure 3.4: Changes in the FTIR spectra of M-PDCPD exposed at 50 °C in air.*

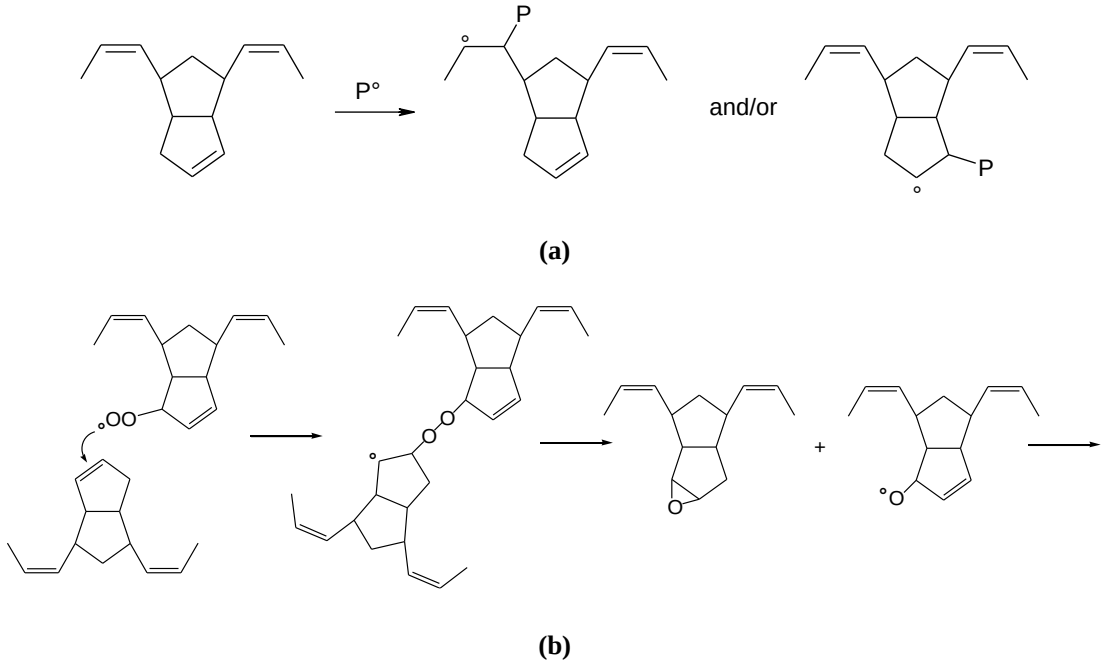

(a)

(b)

Figure 3.5: Propagation step: addition reaction of P° and POO° to double bonds. NB1: radicals can add on each side of the double bond, NB2: Intramolecular addition is not considered in the case of PDCPD due to its structural hindrance.

Addition reactions of alkyl radicals (Fig. 3.5a) could be a possible way of PDCPD crosslinking. This situation differs from the addition of peroxyl radicals (Fig. 3.5b) which would not lead to crosslinking, due to the formation of epoxide products. The occurrence of the reactions depicted in Fig. 3.5b during the thermo-oxidation of PDCPD at 50 °C is evidenced, from an experimental point of view, by the FTIR measurements which indicate the formation of epoxides, as it will be shown later.

Figure 3.6a shows the changes in the concentration of each kind of double bond as a function of the exposure time at 50°C. The corresponding consumption rates, determined as the maximal slope in Figure 3.6b, are compared in Table 3.2. Conformational effects could explain a difference in reactivity limited to the value of bond dissociation energy with each kind of double bond. In a first approach, we considered that the values for each kind of double bond are almost the same, so that we will assume in the following that the reactivity of each of them is ruled by the same set of rate constants (NB: this hypothesis also allows to avoid mistakes due to uncertainties due to molar absorptivity).

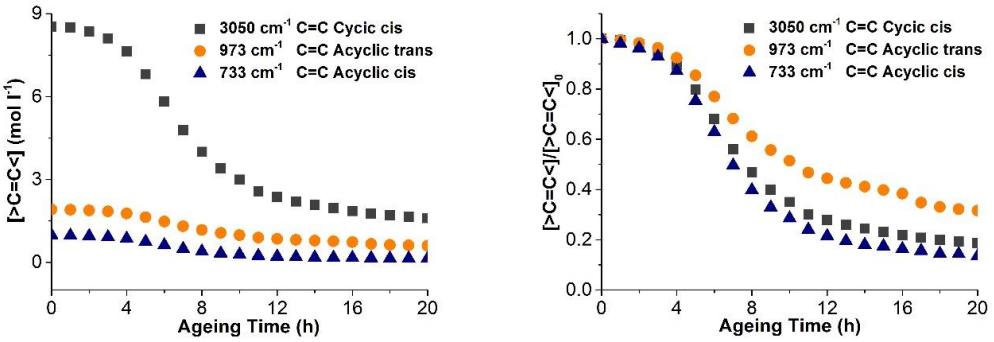

(a) **(b)**

Figure 3.6: Variation of the absolute (a) and relative (b) concentrations of cyclic cis double bonds (band at 3050 cm^{-1} ■), acyclic trans double bonds (band at 973 cm^{-1} ●), and acyclic cis double bonds (band at 733 cm^{-1} ▲) during an exposure under air at 50°C. The relative concentration values in (b) were obtained using a normalization by the corresponding concentrations of the unaged PDCPD.

	$[C=C]_0$ (mol l^{-1})	r_F (mol l^{-1} s^{-1})	Relative r_F (s^{-1})
Acyclic trans: 973 cm^{-1}	1.91	4.24 10^{-5}	2.22 10^{-5}
Acyclic cis: 733 cm^{-1}	0.99	3.43 10^{-5}	3.47 10^{-5}
Cyclic cis: 3050 cm^{-1}	8.53	2.44 10^{-4}	2.86 10^{-5}

Table 3.1: Initial concentration consumption rate (v_F) and relative consumption rate (relative $r_F = r_F/[C=C]_0$) of the different kinds of double bonds in PDCPD.

The same experiments in air were performed at other ageing temperatures (20°C, 30°C, 50°C and 70°C). Decreases in double bonds within the aged PDCPD are reported in Figure 3.7a. The results obtained at a given temperature (30°C) under different oxygen pressures are shown in

Figure 3.7b. Figure 3.7c depicts the variation of the double bond concentration with the exposure time, when the ageing is performed at different temperatures under 1 MPa oxygen pressure. All these data indicate that the double bond consumption rate increases with temperature and oxygen pressure. Besides, the double bond consumption rates are almost the same for ageing under 0.2 MPa and 1 MPa. This feature leads us to consider oxidation under 1 MPa as "representative" of the "oxygen excess conditions" in which P° is almost instantaneously converted into POO°, which will permit to propose a simplified theoretical treatment to extract the rate constants of the reaction POO°+C=C from experimental results.

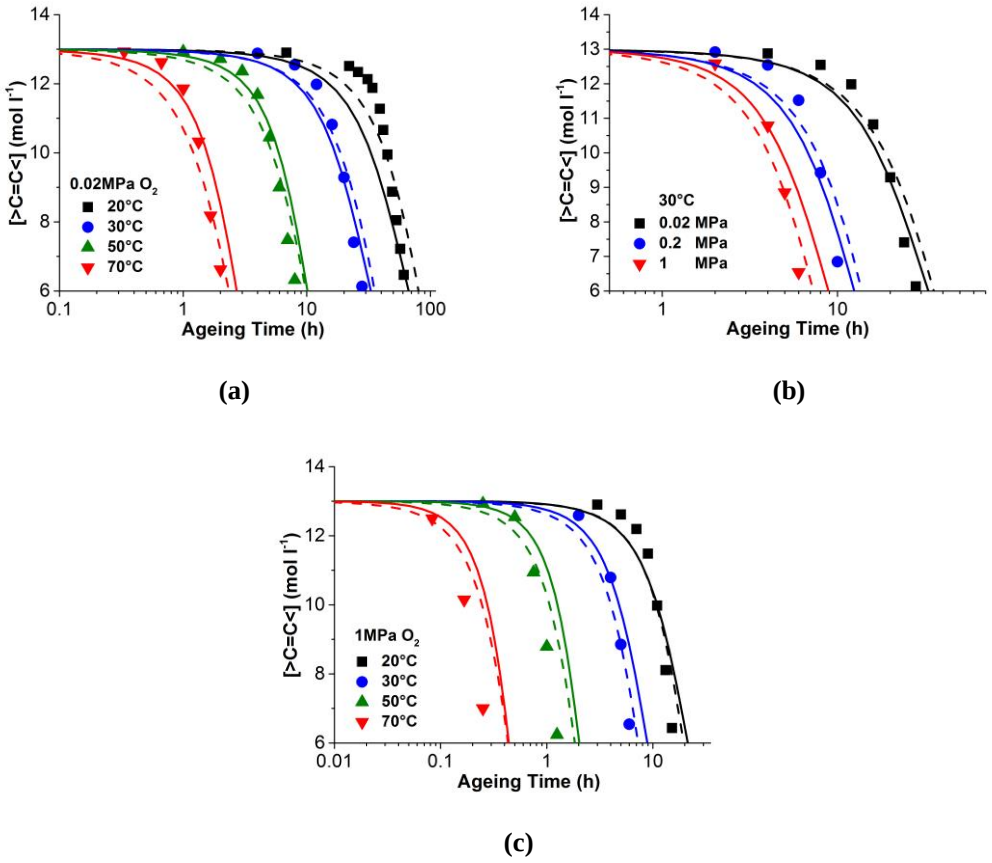

Figure 3.7: Double bond consumption under various ageing conditions: in air at different temperatures (a); Double bonds consumption at 30°C under different oxygen pressures (b); Double bonds consumption under 1 MPa oxygen pressure at different temperatures (c). NB: Dashed lines: simulation curves with the rate constants of set 1 (Table 3.4). Solid lines: simulation curves with the rate constants of set 2 (Table 3.4).

Figure 3.8 shows ^{1}H NMR spectrum of PDCPD after various aging time values (4 h, 7 h and 25 h) at 50°C under air. After 4 h, the ^{1}H NMR spectrum remains qualitatively similar to the

one of the unaged PDCPD (Fig. 3.8). The main difference stands in the presence of a peak of weak amplitude at 2.1 ppm. This contribution, which becomes again more significant after 7 h at 50°C, may be assigned to protons from CH, CH_2 or CH_3 covalently linked to C=O groups. This result is in agreement with the reactions proposed in Fig. 3.11 and 3.12, as well as with the carbonyl build-up derived from FTIR measurements (Fig. 3.10): as the CH_n-C=O protons detected by solid-state NMR, the fraction of carbonyl groups is rather low, but detectable, after 4 h at 50°C, that is to say just above the induction period. After 7 h, the concentration of these species (CH_n-C=O (NMR) and C=O (FTIR)) becomes significant. Interestingly, after 7 h, another change induced by thermal oxidation may be observed on the ^1H NMR spectrum. An additional contribution between the two peaks of unaged PDCPD (2.7 ppm and 5.6 ppm) can also be observed after 7 h, as a shoulder around 4.0 ppm, in the high-frequency side of the peak at 2.7 ppm. After exposure for 25 h at 50°C, the amplitude of this contribution gets higher and is now detected as a well-resolved peak at 4.5 ppm, corresponding to the proton(s) from O-CH or O-CH_2 groups.

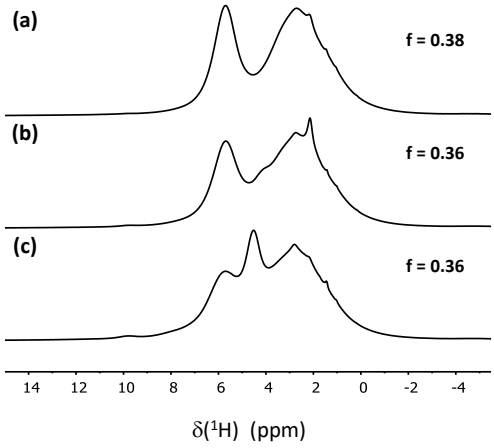

Figure 3.8: Changes of the one-pulse 1H MAS NMR spectrum of PDCDP thermo-oxidized at 50°C under air, as a function of the exposure time: (a) 4 h, (b) 7 h and (c) 25 h. The experiments were carried out at a 1H Larmor frequency ν_0 of 700 MHz and a MAS frequency ν_r of 50 kHz. The fraction f of protons from the double bonds within aged PDCPD is also included and should be compared to f = 0.43, obtained for unaged PDCPD.

Let us now consider the variation of the double bond concentration with the aging time at 50°C. As can be seen in Figure 3.8, the relative amplitude of the peak at 5.6 ppm with respect to the

one at 2.7 ppm decreases during aging while it also displays a significant broadening. Due to the chemical modification of the PDCPD matrix, a distribution of the local region surrounding the =CH- protons, inducing a distribution of the ^{1}H chemical shift value, occurs. The area under the peak at 5.6 ppm should thus be considered, in order to investigate the decrease in double bond concentration with the exposure time at 50°C. The deconvolution performed in the case of the unaged PDCPD was not used because above 7 h of thermal aging, at least four contributions, with a significant overlap for some of them, are involved in the ^{1}H NMR spectrum. The interplay between the different fitting parameters would then lead to a significant inaccuracy on the fraction f of protons involved in double bonds within aged PDCPD. To circumvent this difficulty, f was determined using half of the peak area $A_{-CH=}$, integrating from the high frequency side down to the peak maximum frequency. f may indeed be estimated by calculating $2\times A_{-CH=}/A_{total}$, A_{total} denoting the total area under the ^{1}H NMR spectrum.

It is interesting to note that the NMR and FTIR methods give almost the same trend for samples aged for 0, 4 and 7 h. At very high oxidation levels (i.e. 25 h and more), which is out of the scope, a discrepancy can be observed between NMR and FTIR. It could be possible that conjugated structures are formed and display shifted absorptions for vinyl C-H. In other words, NMR detects the total amount of residual double bonds whereas FTIR detects the unreacted ones (which is the "fuel" of the oxidation process). We however acknowledge that this argument cannot be verified in the present study so that the mechanism of degradation at the high conversion degree remains an open issue. Our approach, which considers mainly low degradation levels, is supported by the fact that the mechanical behavior of PDCPD is largely affected by low levels of oxidation (see section 2).

Lastly, one should also note that a peak at 9.7 ppm characterized by a weak, but increasing amplitude is observed on the ^{1}H NMR spectra of the aged PDCPD (Fig. 3.9). These protons may be related to carboxylic acid protons or aldehydic protons, this latter assignment being in agreement with the reactions proposed in Fig. 3.11.

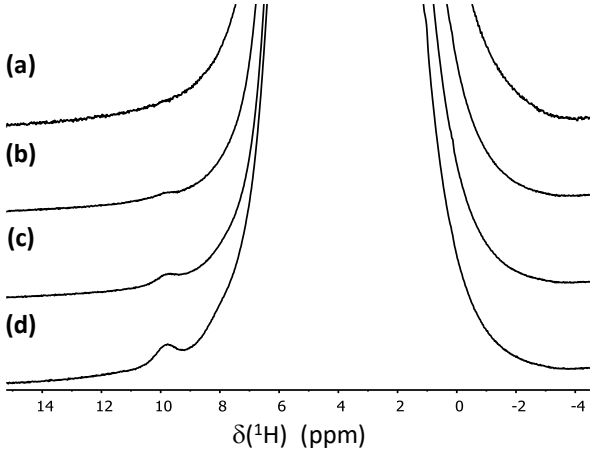

Figure 3.9: Zoom of the one-pulse 1H MAS NMR spectra of purified, unaged and aged PDCDP, recorded at a 1H Larmor frequency ν_0 of 700 MHz and a MAS frequency ν_r of 50 kHz. Ageing was carried out at 50°C, under air, for: (a) 0 h, (b) 4 h, (c) 7 h and (d) 25 h.

4. Formation of stable products

4.1 Formation of carbonyls

The FTIR measurements show the formation of a band at ca 1710 cm^{-1} corresponding to carbonyl functions (Figure 3.10).

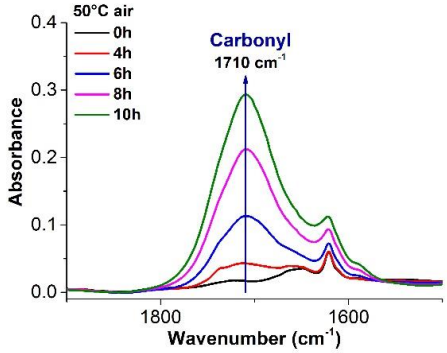

Figure 3.10: Changes in the FTIR spectra of M-PDCPD exposed at 50 °C in air.*

As can be seen in Figure 3.13a, the shapes of the carbonyl band are similar under different oxidation conditions (temperature, oxygen pressure) which means that the corresponding

oxidation products of PDCPD involve the same kind of carbonyl groups. They originate from alkoxy radicals formed during:

① the initiation step during which unimolecular and bimolecular hydroperoxide decomposition can occur (Figure 3.11) :

$$POOH \rightarrow PO^{\circ} + {}^{\circ}OH$$

$$POOH + POOH \rightarrow POO^{\circ} + PO^{\circ} + H_2O$$

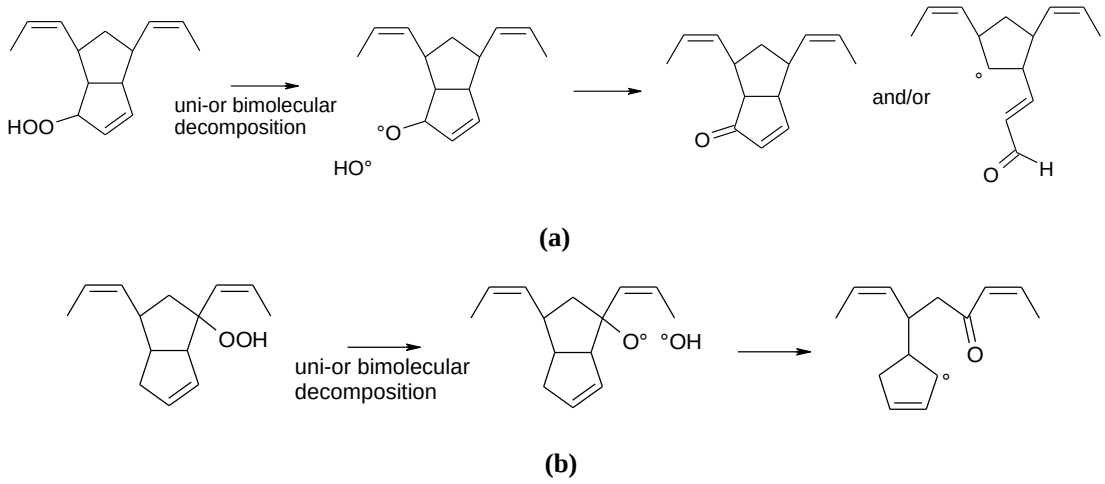

Figure 3.11: Initiation step: hydroperoxide decomposition.

② the termination step by disproportionation by a Russell mechanism [15], [16] (Figure 3.12):

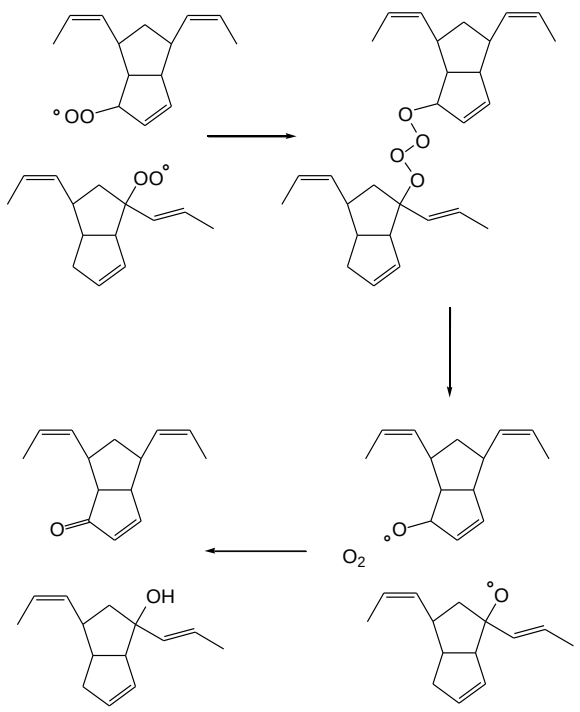

Figure 3.12: Termination step by Russell disproportionation of PO°.

③ the decomposition of POOP° (Fig. 3.5b) that rearrange into PO° which continues to turn into carbonyl functions.

The concentration in carbonyl increases with ageing time accompanied a period of induction (Figure 3.13b) corresponding to the intersect between the maximal tangent for C=O build-up and the x axis. It is worth nothing that induction time corresponds well to [C=O] = 0.2 mol l^{-1} i.e. the time for embrittlement. Meanwhile, the double bond concentration decreases as a function of ageing time with a period of induction. The kinetics of carbonyl build up under several conditions are shown in Figures 3.14.

For all conditions considered here, carbonyl formation over ageing time follows the same behavior. First, an induction period is observed where carbonyl concentration remains very low, and then a classic self-acceleration occurs. It appears, as expected, that an increase in temperature leads to a decrease of the induction period and an increase in oxidation rate. The

oxidation process can also be accelerated by increasing oxygen pressure between 0.02 MPa and 0.5 MPa (Figure 3.14b). Above 0.5 MPa, the oxidation process is not affected by oxygen pressure anymore showing that 0.5 MPa can be considered as the critical pressure. This behavior is observed for all ageing temperatures. The carbonyl build-up obtained under 1 MPa oxygen pressure at different temperatures ranging between 20 °C and 70 °C (Figure 3.14c) also display the self-accelerated shape mentioned above.

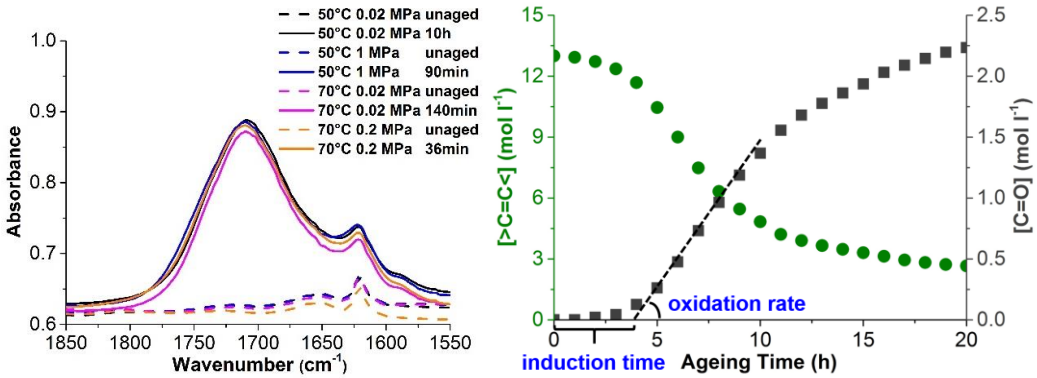

(a) **(b)**

Figure 3.13: Infrared absorption bands of the carbonyl groups resulting from the ageing of PDCPD under various conditions (temperature, oxygen pressure) (a). Changes in the concentration of carbonyls (■) and double bonds (●) during ageing at 50 °C under air (b).

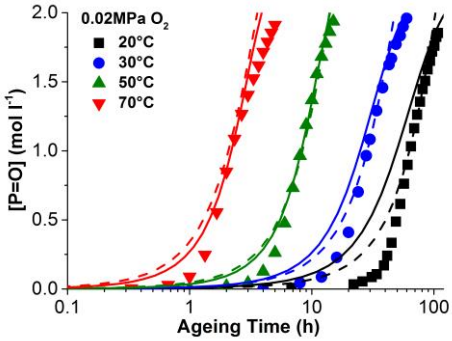

(a)

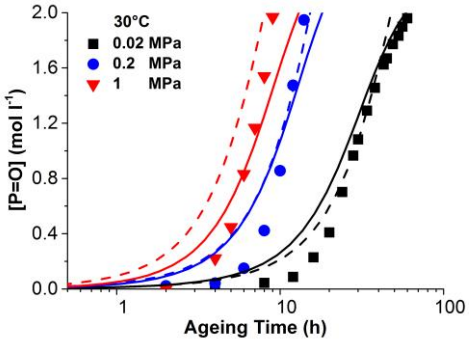

(b)

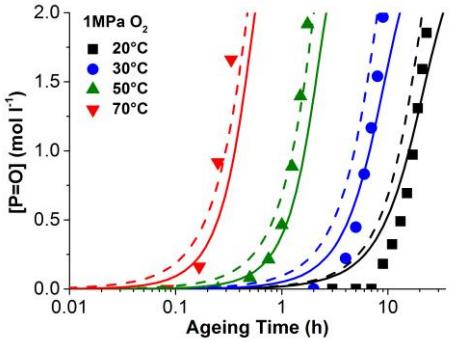

(c)

Figure 3.14: Variation of the carbonyl concentration as a function of the exposure time, for different ageing conditions of PDCPD: in air, at different temperatures (a); at 30 °C, under different oxygen pressures (b); under 1 MPa oxygen pressure, at different temperatures (c). NB: Dashed lines: simulation curves with the rate constants of set 1 (Table 3.4). Solid lines: simulation curves with the rate constants of set 2 (Table 3.4);

4.2 Formation of epoxides

FTIR spectra of thermo-oxidized PDCPD (Figure 3.15) display two bands at ca 852 cm^{-1} and 837 cm^{-1} that correspond to the symmetric ring deformation of epoxides. Such oxidation products are also involved in the thermo-oxidative behavior of polybutadiene [5]. The intensity of these absorption bands continuously increases during aging in air at 50 °C, but remains very weak. Consistently with NMR data (Figure 3.8), those species will not be taken into account as a stable product of thermal oxidation.

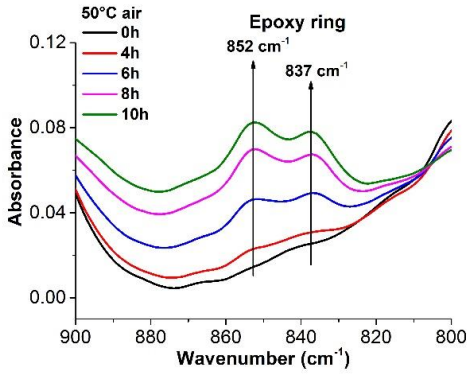

Figure 3.15: Changes in the FTIR spectra of M-PDCPD exposed at 50 °C in air.*

5. Stability of hydroperoxides

In polymers below 150°C, there are several reasons to ascribe the radical creations to defects in (very) small concentration and to hydroperoxide decomposition which becomes very fast the main source of radicals creation [17]. Hydroperoxides can hence be considered as the key products of oxidation, involved in both propagation step (POO°+PH → POOH+P°) and initiation step (δPOOH→αP°+ βPOO°). As previously written, they can decompose either by a unimolecular (POOH→PO°+°OH) or bimolecular ((POOH+POOH→PO°+POO°+H_2O) way and both processes may overlap.

The rate constants for bimolecular POOH decomposition can in principle be determined from the modeling (fitting) of induction period length under oxygen excess whereas the unimolecular one could be estimated from the oxidation kinetics under lower oxygen pressures [3]. However, such a method remains questionable since some other parameters (initial POOH concentration and propagation rate constants) must be somewhat arbitrarily fixed. Moreover, both uni-and bimolecular process can co-exist and assessing their rate constants from kinetic curves by fitting will lead to an infinity of rate constants.

Besides, the effect of high concentration catalyst in metathesis polymerization on the hydroperoxide decomposition remains open for us. This latter can be either uni- or bimolecular, the relative proposition of both reactions depending on temperature, oxygen pressure [3], conversion degree and possibly catalytic effects. The study of POOH stability and associated rate of decomposition is hence crucial to develop a reliable kinetic model for thermal oxidation.

To investigate those questions linked to hydroperoxide decomposition, we implemented here an alternative approach inspired from a paper by Billingham and al. [18]–[20] :

- selective thermolysis experiments with varying initial POOH concentration (being obtained from thermal oxidation experiments carried out at varying temperature and exposure times)

- comparison of PDCPD with varying Ruthenium amount, since it is actually known that metallic ions (originating either from the catalyst or sometimes fillers such clay) can be detrimental to the long term stability [21]–[23].

Thus, the PDCPD samples with different concentrations of catalysts were investigated: M*-PDCPD, L-PDCPD and H-PDCPD.

Firstly, M*-PDCPD, as a reference, were characterized experimentally. The changes in chemical structures of PDCPD exposed at 50°C under air were monitored by FTIR spectroscopy. An increase of the absorption band at ca 3400 cm^{-1}, corresponding to hydrogen-bonded hydroxyl groups, is observed in Figure 3.16. This broad band results from various species such as hydroperoxides, alcohols or carboxylic acids, all of which are oxidation products occurring in the thermal oxidation of other hydrocarbon polymers [24]. However, it is difficult to distinguish these different species, based on the FTIR data.

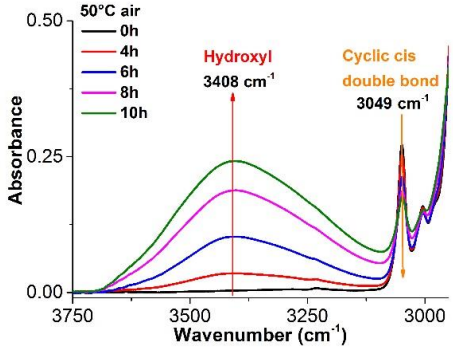

Figure 3.16: Changes in the FTIR spectra of M-PDCPD exposed at 50 °C in air.*

5.1 Hydroperoxides production

Hydroperoxides, which are the key species of the oxidation mechanism, can also be selectively

detected and quantified by other chemical or thermal methods, especially titration of hydroperoxides by DSC is already investigated in the literature [24]. The DSC traces of PDCDP samples oxidized, reported in Figure 3.17a, show an exothermic peak starting at about 50°C with a maximal heat release centered at 150°C. The heat released increases with the exposure time. Moreover, this signal is totally removed by SO_2 treatment (react with hydroperoxides) (Fig. 3.17a) or DMS (react with peracids and hydroperoxides) (Fig. 3.17b).

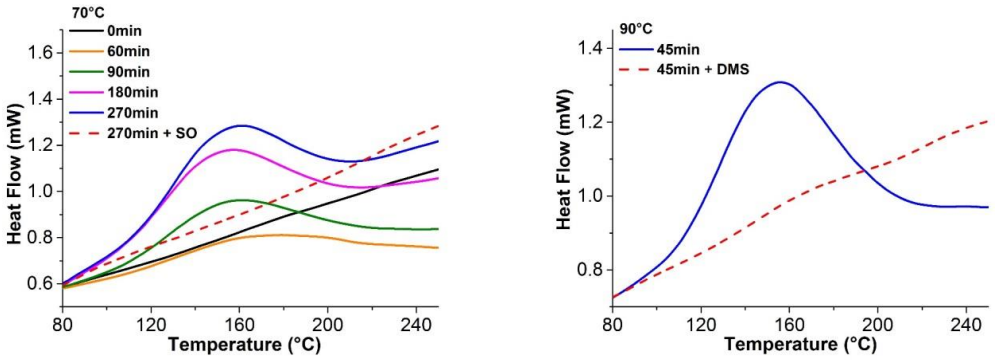

(a) **(b)**

Figure 3.17: DSC thermograms before (full line) and after (dashed line) SO_2 treatment for M-PDCPD exposed at 70°C under air (a); and before (full line) and after (dashed line) DMS treatment for M*-PDCPD exposed at 90°C 45min under air (b).*

It shows that the species responsible for the exotherm monitored by DSC are hydroperoxides (associated or not [25], [26]) resulting from the propagation step schematized in Figure 3.18. It should be noted that several kinds of hydroperoxides can actually be formed (Fig. 3.19). The relative probability of each kind of hydroperoxide (depending at least on bond dissociation of the C-H precursor, and hindrance) will not be discussed here.

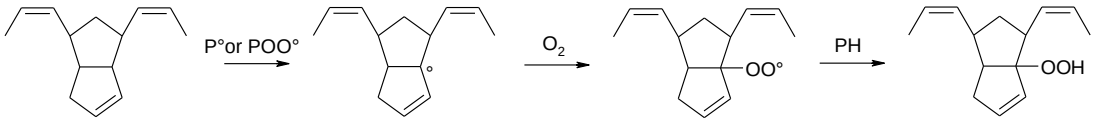

Figure 3.18: Propagation step: hydrogen abstraction.

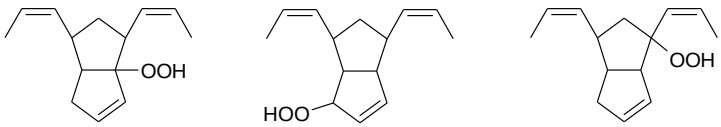

Figure 3.19: Possible structures of hydroperoxides formed within a thermally-oxidized PDCDP.

Thus, the POOH concentration was assessed from the value of the exotherm (Figure 3.7) and was calculated with the help of a molar enthalpy (440 kJ mol^{-1}) given by the previous study [2]. Results are plotted in Figure 3.20 for several temperatures together results of the kinetic model (see section 6 of this chapter). Figure 3.20 shows the growth curves of hydroperoxides as a function of the aging time, which has been confirmed experimentally by other authors [27]. For example, the POOH concentration at 50°C increases rapidly in the initial period to reach a value of about 1.5 mol l^{-1} after 10 h of exposure. A pseudo plateau was observed for each exposure condition under investigation (50-120°C under atmospheric air).

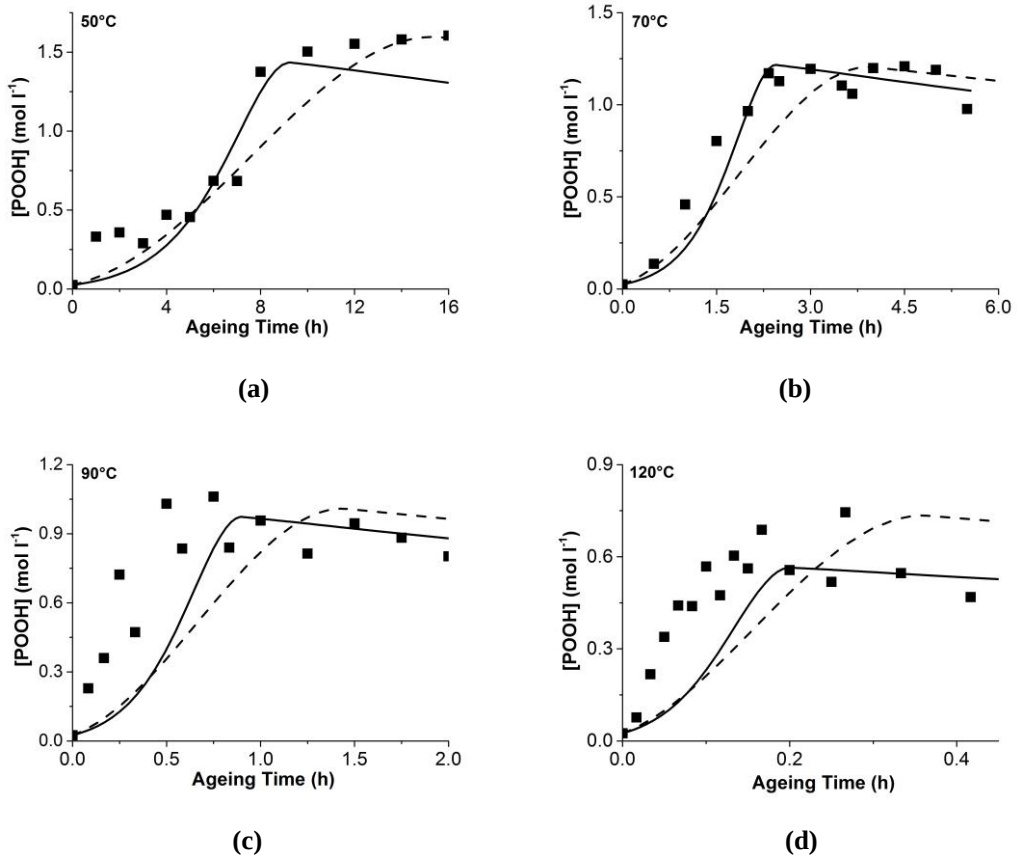

Figure 3.20: Changes in hydroperoxides (■) for thermal oxidation in M-PDCPD at 50°C (a), 70°C (b), 90°C (c), 120°C (d). NB: Dashed lines: simulation curves with the rate constants of set 1 (Table 3.4); Solid lines: simulation curves with the rate constants of set 2 (Table 3.4).*

5.2 Thermolysis of hydroperoxides

In order to consider the decomposition of hydroperoxides in PDCPD, thin samples of M*-PDCPD were oxidized firstly and then exposed in situ using DSC under nitrogen atmosphere.

After this thermolysis, residual hydroperoxides concentration was measured. Typical results are presented in Figure 3.21.

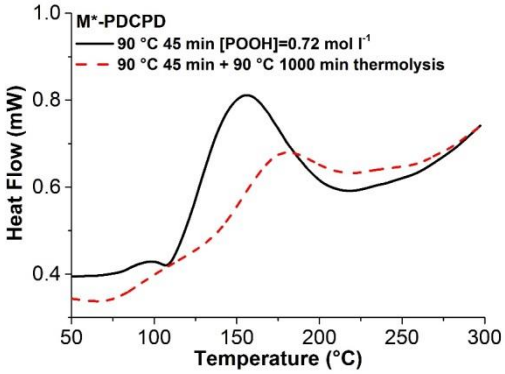

Figure 3.21: DSC thermograms before (full line) and after 1000 min thermolysis at 90°C (dashed line) for M-PDCPD exposed 45min at 90°C under air.*

Two kinds of samples have been considered in this study. First, samples with a high concentration of hydroperoxides (i.e. when the plateau in Figure 3.20 is reached), and secondly samples with a much lower hydroperoxide concentration (typically with [POOH] ~ 0.1 - 0.3 mol l^{-1}) to consider the early state of the degradation. All results are presented in Figure 3.22.

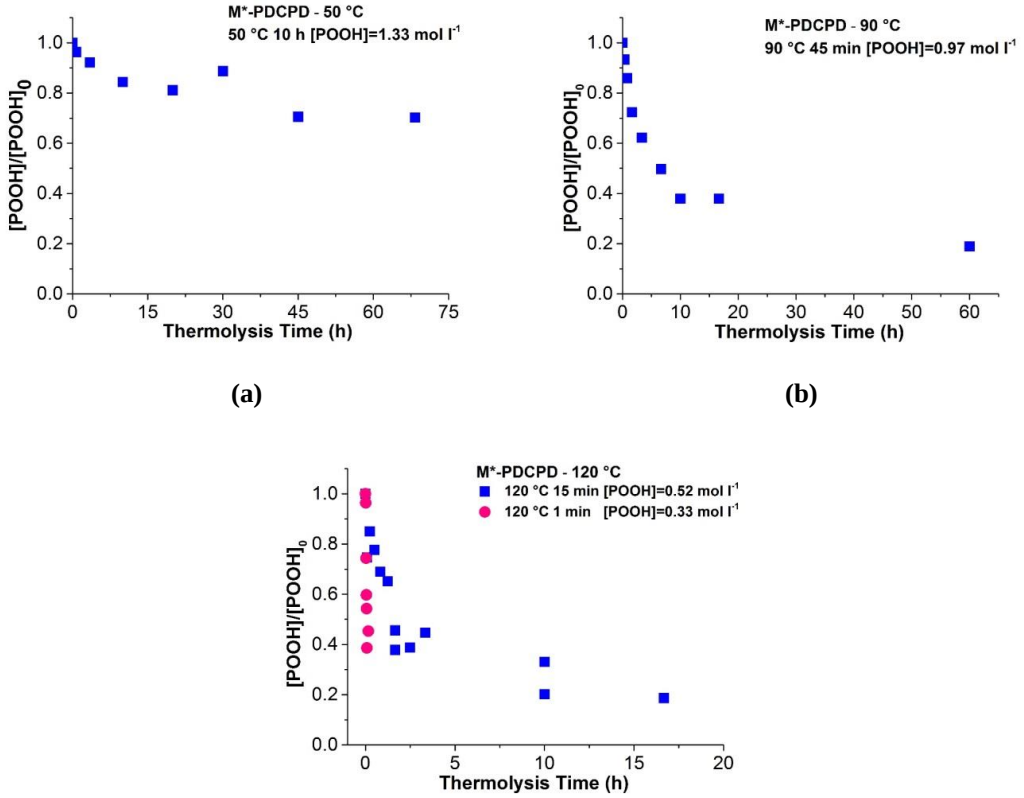

Figure 3.22: Changes in hydroperoxides for thermolysis of M-PDCPD at 50°C (a), 90°C (b) and 120°C (c). NB: time to totally destroy POOH at 50°C was too long so that thermolysis was interrupted after 70 h.*

The thermolysis curves are presented as changes in residual concentration (normalized by the initial concentration at the beginning of thermolysis) versus thermolysis time, for samples aged at 120°C, 90°C and 50°C with POOH have reached respectively 0.52 , 0.97 and 1.33 mol l^{-1} (i.e. at the plateau of POOH curves). They display an auto-decelerated shape. The time to reach for example $[POOH]/[POOH]_0 = 0.5$ clearly decreases with temperature (about 2 h at 120°C, 7 h at 90°C, more than 100 h at 50°C).

Those sets of experiments were completed by investigating the kinetics of thermolysis in the "low concentration domain" (i.e. for samples oxidized during low exposure times, such as 1 minute at 120°C under air, [POOH] = 0.33 mol l^{-1}). In this case, the time needed for $[POOH]/[POOH]_0 = 0.5$ is only 4 minutes showing that the thermolysis mechanism is different

in the “low concentration” and “high concentration” domains as it will be developed later.

The molecular changes observed by FTIR during those thermolysis experiments are shown in Fig. 3.23. According to these results, thermolysis always generates a decrease of hydroxyl band at 3400 cm^{-1} and an increase of carbonyl band centered at 1710 cm^{-1} independently of temperature suggesting that there is no difference between carbonyl functions generated from alkoxyl radical (coming from POOH→PO°+OH°) in the investigated temperature range.

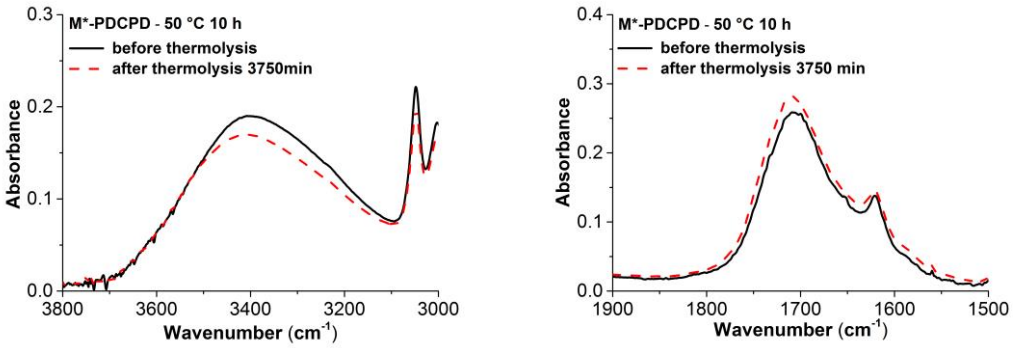

Figure 3.23: FTIR spectra for PDCPD before (full line) and after (dashed line) thermolysis at 50°C .

Using the difference of hydroperoxides concentration values from DSC measurement and the corresponding increase in carbonyl concentration from FTIR, the apparent carbonyl yield γ_1 from POOH decomposition can be obtained. It stays almost constant (close to 0.5) with temperature as shown in Figure 3.24. Another value based on the best fitting of C=O curves It was for example proposed to be 0.25 in polyisoprene [28]. It must be recalled that the γ_1 value from measurement (0.5) may be overestimated because the thermolysis process also generates some peroxy radicals likely to involve supplementary carbonyls for example from termination reactions (see the mechanistic scheme in section 6.1). Thus, the value of γ_1 may be lower than 0.5.

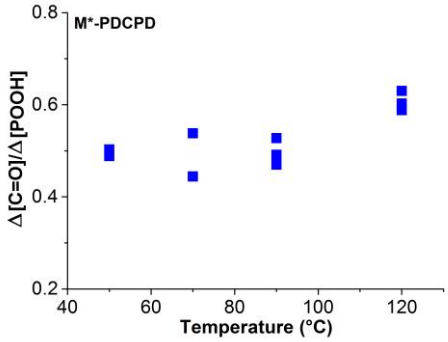

Figure 3.24: Apparent carbonyl yield as a function of temperature for M-PDCPD.*

5.3 Effect of catalyst

The oxidation kinetics of H-PDCPD and L-PDCPD were compared (NB: M*-PDCPD was not studied here because it was not polymerized in the same conditions and does not display the same concentration in double bonds as the H-PDCPD and the L-PDCPD).

Results are presented in Figure 3.25 for hydroperoxides and carbonyls. It shows that the presence of catalysts does not significantly change the level of POOH at the plateau whatever the temperature. In the meantime, results clearly show that the kinetics of carbonyl build-up (see section 5.2) are almost the same for the two catalyst levels considered here. This is particularly true in the steady state, i.e. when the rate for carbonyl build-up is maximal. In other words, the presence of catalyst permits to trigger the polymerization process with a minor incidence on polymer durability. As it will be seen in the next paragraph, those results offer us an opportunity to catch the predominant degradation mechanism in the “steady state”.

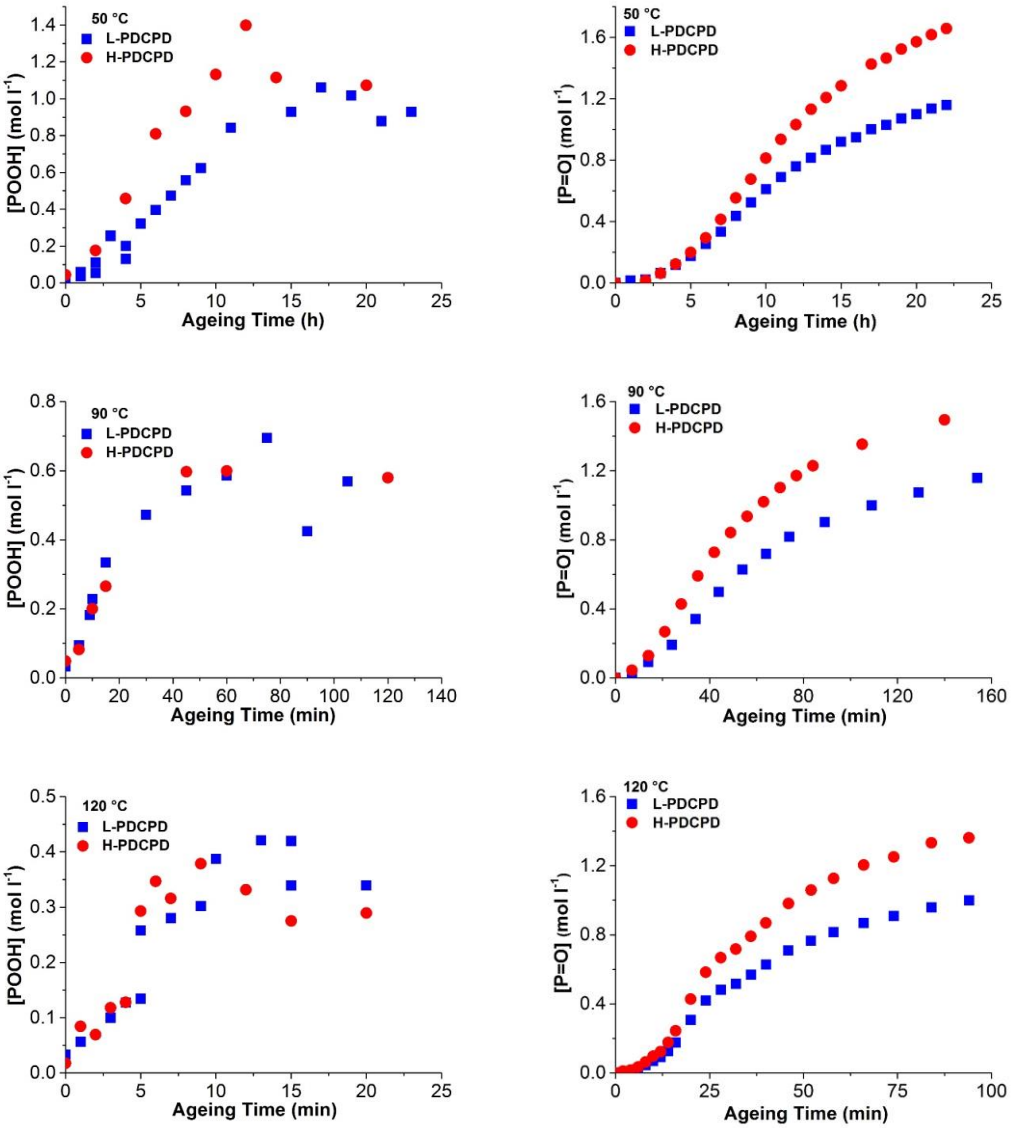

Figure 3.25: Changes in hydroperoxides and carbonyls concentration for L-PDCPD (■) and H-PDCPD samples (●) thermally oxidized at 50°C, 90°C and 120°C under air.

The molecular changes of L-PDCPD and H-PDCPD with ageing time (Figure 3.26) display the classic features of thermal oxidation i.e. an increase of hydroxyl band at about 3400 cm^{-1} corresponds to oxidation products (e.g. hydroperoxides, alcohols or carboxylic acids) and an increase of carbonyl band centered at about 1710 cm^{-1}.

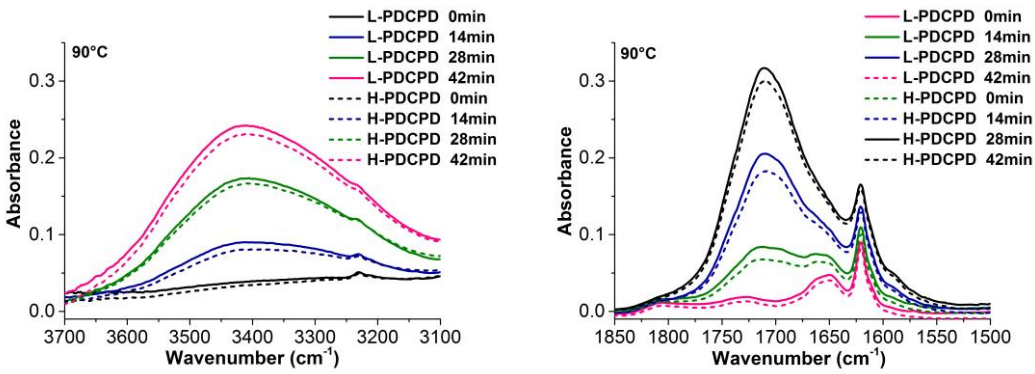

Figure 3.26: FTIR spectra of L-PDCPD (full line, 13.3 µm thickness) and H-PDCPD (dashed line, 12.8 µm thickness) exposed at 90°C under air.

As previously said, carbonyls are a key characteristic of thermal oxidation. The relevant formation mechanism was already detailed in the section of 4.1. Namely, the carbonyls come from:

① the initiation step of thermal oxidation (i.e. unimolecular and bimolecular decomposition of hydroperoxides).

② bimolecular POO° termination involving the dismutation of two alkoxys by a Russell mechanism [15], [29]: POO° + POO° → P=O

③ the decomposition of POOP°, which comes from the propagation step (i.e. addition reaction of POO° to double bonds), that rearrange into PO°.

Carbonyls formed from POOH decomposition are possibly aldehydes (and then carboxylic acids) or ketones whereas carbonyls formed from POO° are only ketones [2]. As will be seen later, only the unimolecular decomposition is influenced by catalyst residue. The fact that the carbonyl absorbance seems the same in L-PDCPD and H-PDCPD (Figure 3.26b) seems to indicate that the contribution of unimolecular POOH decomposition is negligible in a first approach compared to the two other carbonyl sources.

Figure 3.27 shows the thermolysis results of L-PDCPD and H-PDCPD.

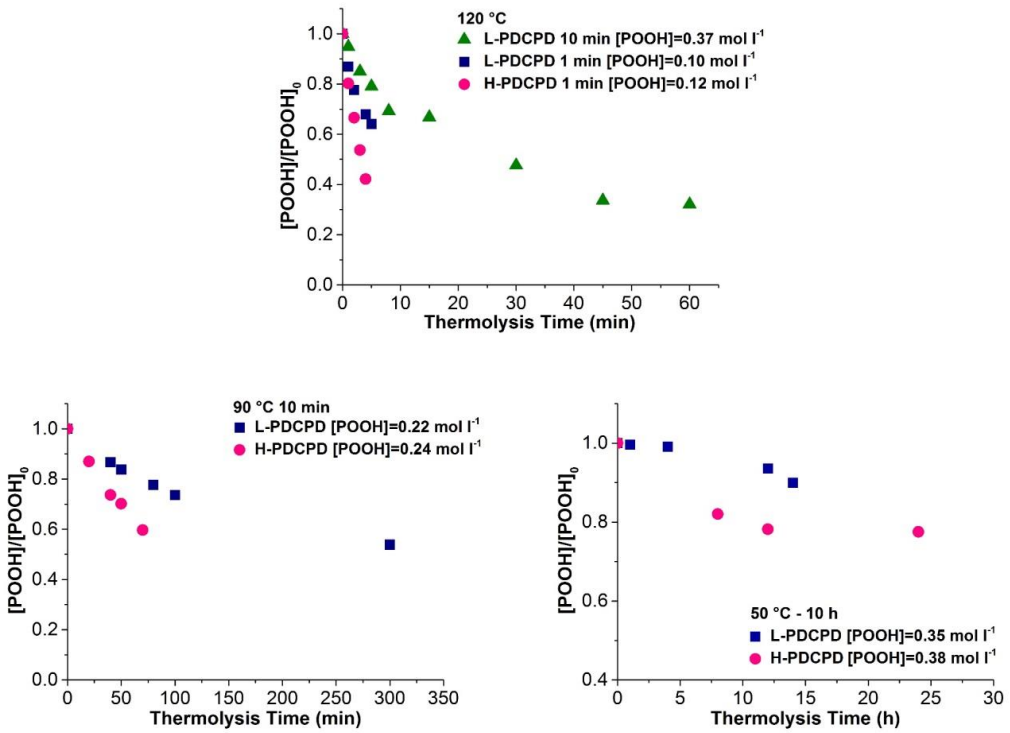

Figure 3.27: Changes in hydroperoxides for thermolysis of L-PDCPD (▲ or ■) and H-PDCPD (●) at 120°C, 90°C and 50°C.

It seems clear here that the presence of catalyst can influence the rate of POOH decomposition at least in the low concentration domain.

5.4 Estimation of rate constants for hydroperoxides decomposition

Gijsman and al. [30] showed the same curve shape of peroxides decomposition with an initially fast decomposition ascribed to peracids whereas the slow decomposing ones would be hydroperoxides. In fact, the SO_2 treatments suppress the exothermic signal whatever the oxidation time so that we will assume that POOH predominates independently the conversion degree.

5.4.1 Theoretical background

Firstly, in the frame of this work, it seems that there are three modes (from a kinetic point of view) for POOH decomposition:

Unimolecular uncatalyzed:	$POOH \rightarrow PO^{\circ} + HO^{\circ}$	k_{1u}
Bimolecular uncatalyzed:	$POOH + POOH \rightarrow POO^{\circ} + PO^{\circ} + H_2O$	k_{1b}
Unimolecular catalyzed:	$POOH + M^{n+} \rightarrow PO^{\circ} + HO^{-} + M^{(n+1)+}$	k_{c1}
	$POOH + M^{(n+1)+} \rightarrow POO^{\circ} + H^{+} + M^{n+}$	k_{c2}

The initiation step is composed of uni- and bimolecular decomposition of POOH which co-exist. The specific identification of both uni- and bimolecular rate constants is thus intricate (apart maybe in the case of oxidation under oxygen excess where bimolecular initiation predominates, but the identification of k_{1b} value remains somewhat dependent of the choice made for the other kinetic parameters in particular for propagation events).

It seems however that, depending on the level of hydroperoxide, reaction of radical creation from hydroperoxide decomposition are either predominantly uni- or bimolecular which makes it possible to selectively study each kind of initiation. The kinetic of decomposition can be written as below:

$$r_{uni0} = k_{1u0}[POOH] \qquad \textit{Equation 3.3}$$

$$r_{uni\ catal} = k_{1c}[M^{+}][POOH] \qquad \textit{Equation 3.4}$$

In other words, the unimolecular process is possibly described by an apparent rate constant:

$$\frac{d(POOH)}{dt} = r_{uni0} + r_{uni\ catal} = k_{1u}[POOH] \qquad \textit{Equation 3.5}$$

$$k_{1u} = k_{1u0} + k_{1c}[M^{+}] \qquad \textit{Equation 3.6}$$

whereas kinetics of bimolecular initiation is given by:

$$r_{bi} = -\frac{1}{2}\frac{d(POOH)}{dt} = k_{1b}[POOH]^2 \qquad \textit{Equation 3.7}$$

It means that

- If POOH decompose in an unimolecular process:

$$ln[POOH] = -k_{1u}t + ln[POOH]_0 \qquad \textit{Equation 3.8}$$

with time to destroy half of initially present hydroperoxides:

$$t_{\frac{1}{2}\ uni} = \frac{ln2}{k_{1u}} \qquad \textit{Equation 3.9}$$

- If they decompose in a bi molecular process:

$$\frac{1}{[POOH]} = 2k_{1b}t + \frac{1}{[POOH]_0} \qquad \textit{Equation 3.10}$$

with time to destroy half of initially present hydroperoxides:

$$t_{\frac{1}{2}\ bi} = \frac{1}{2k_{1b}[POOH]_0} \qquad \textit{Equation 3.11}$$

It is noted that in some cases, the situation is more intricate. For example, in PP, the decomposition takes place in two stages. A fast decomposition is first observed, and is followed by a slow decomposition [30] with a residual (persistent) concentration in POOH even at long thermolysis time. These two stages cannot be described by first- or second-order decay kinetics.

In the following, the discussions will be developed on the decomposition of POOH at high and low concentrations.

5.4.2 Decomposition of POOH in the high concentration domain

In our case, we considered separately thermolysis either in the "plateau" (Figure 3.8) or in the initial stage. Experimental data were plotted either in order 1 or order 2 diagrams (Figure 3.14). As it can be seen for experiments performed at 120°C, the mechanism (uni- or bimolecular) is

not the same since time to divide initial by 2 is not the same for samples in the plateau and in the low concentration domain (Figure 3.8c). The value of the regression coefficient will help us to decide which one of those two mechanisms was the most likely.

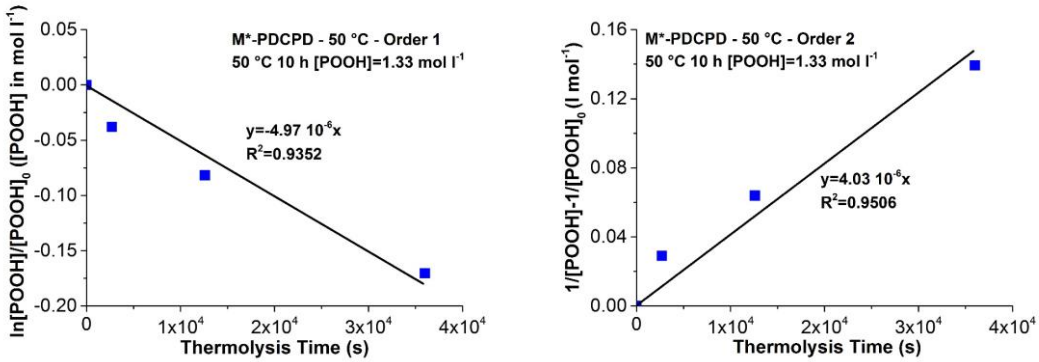

(a)

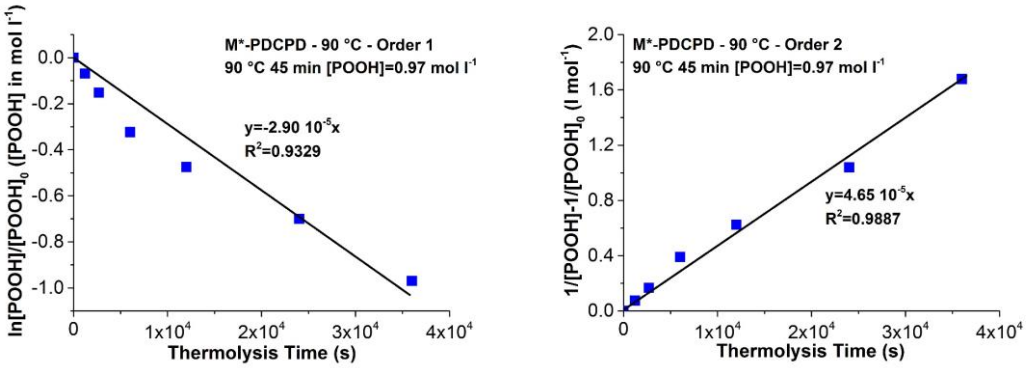

(b)

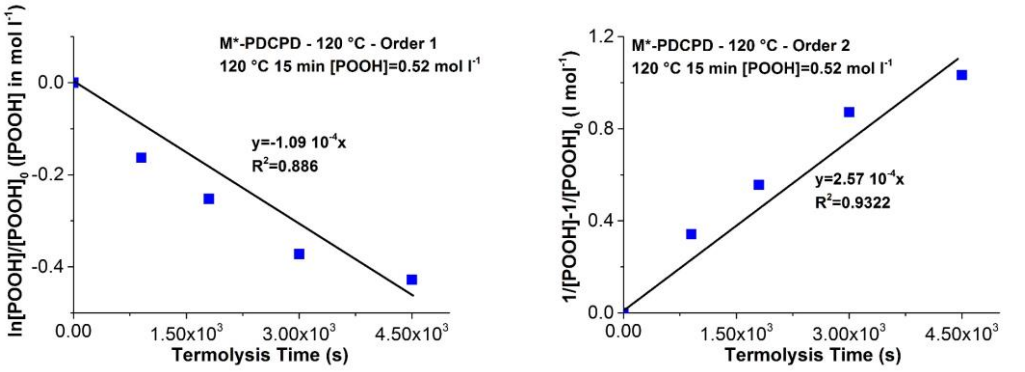

(c)

Figure 3.28: Linear equation of order 1 (left) and 2 (right) for M-PDCPD thermolysis at the pseudo plateau at 50°C (a), 90°C (b) and 120°C (c).*

Despite a certain scattering, it seems that POOH decomposition obeys rather a second order kinetics (i.e. POOH decompose in a bimolecular way). This is well in line with the FTIR observations showing the maxima of hydroxyl absorbance at 3400 cm^{-1} (Figure 7b) which is likely to be associated hydroperoxides [25], [26].

A supplementary argument militating in favor of the bimolecular process is that according to Figure 3.25, there is no significant effect of catalyst on the oxidation kinetics in particular in steady state (i.e. maximal POOH concentration and maximal carbonyl buildup rate). Let us recall that at steady state (under oxygen excess):

- in unimolecular mode

$$[POOH] = \frac{k_3^2[PH]^2}{k_{1u}k_6} \qquad \textit{Equation 3.12}$$

- in bimolecular mode

$$[POOH] = \frac{k_3[PH]}{2\sqrt{k_{1b}k_6}} \qquad \textit{Equation 3.13}$$

There are two possibilities for the same maximum level of POOH for H-PDCPD and L-PDCPD :

- either $k_{1u\,high} = k_{1u\,low}$ which seems in contradiction with other results presented in Figure 3.27 , and which will be developed in the next paragraph.

- or $k_{1b\,high} = k_{1b\,low}$ which seems more likely since the bimolecular process can be considered as an auto-assisted decomposition process.

Thus, the bimolecular process is favored when decomposing hydroperoxides with high concentration. k_{1b} values, which are half of slopes values for these linear equations of order 2, were hence plotted in an Arrhenius diagram (Figure 3.15) together with other values from other unsaturated substrates. There is no clear difference between polymers, consistently with the same nature of peroxides in α position of a double bond. Thus, k_{1b} values were identified by the thermolysis of hydroperoxides and will be used for further kinetic modeling (in section 6).

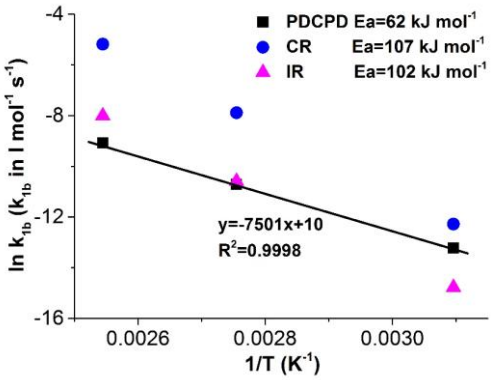

Figure 3.29: Arrhenius plot of k_{1b} values coming from thermolysis for PDCPD (■), CR (●) [6], IR (▲) [28].

5.4.3 Decomposition of POOH in the low concentration domain

The same theoretical treatment was applied for thermolysis experiments in the low concentration domain. An example of the results is presented in Figure 3.16. The results at 90°C and 50°C are presented in Appendix 1.

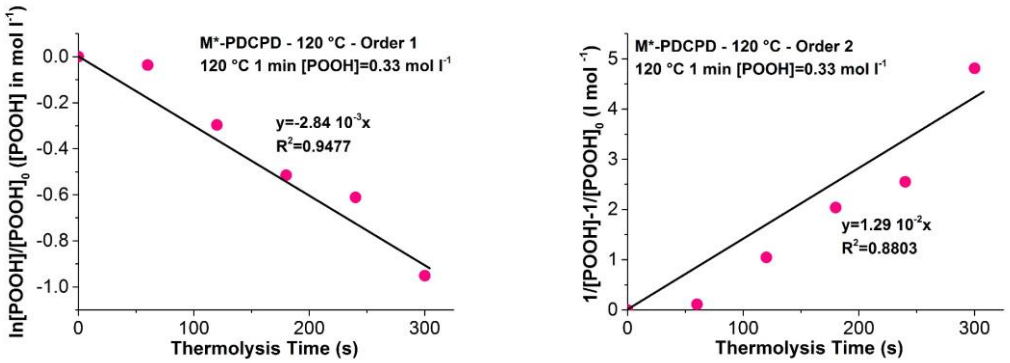

(a)

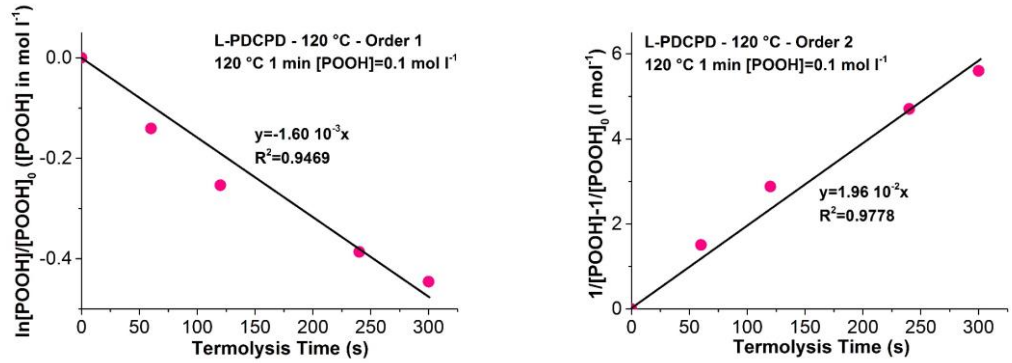

(b)

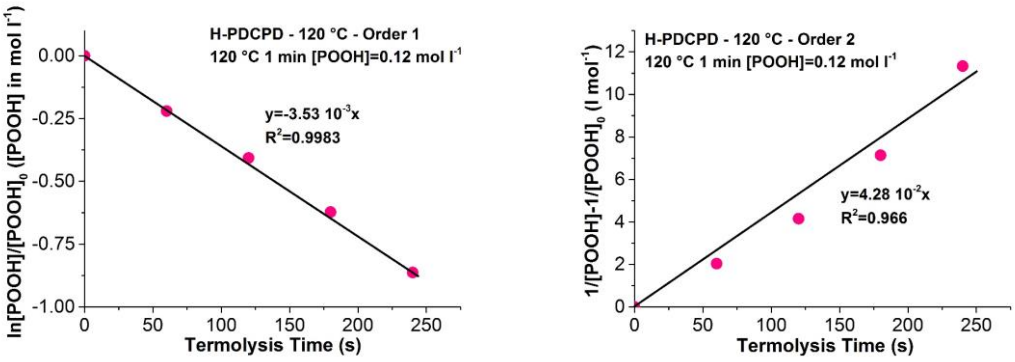

(c)

Figure 3.30: Linear equation of order 1 (left) and 2 (right) for M-PDCPD samples aged 1 minute at 120°C (a); for L-PDCPD samples aged 1 minute at 120°C (b); for H-PDCPD samples aged 1 minute at 120°C (c).*

In the domain of "low" POOH concentration (i.e. below 0.3 mol l^{-1}), POOH kinetics are clearly faster than those observed for initial POOH concentration (before thermolysis) at the plateau which can receive two interpretations. On the one hand, the POOH involved in reactions are not the same (POOH, POOP or peroxy acids) which seems contradictory with the experimental

results (POOH predominates according to the fact that SO_2 treatments destroy almost all peroxides); on the other hand, the order of the reaction relatively to POOH is not the same.

It seems however clear that the hypothesis of second order decomposition for low concentration is hard to support. The time to destroy half of initially present hydroperoxides in the case of thermolysis in the early period is faster than the one of thermolysis in the pseudo plateau. For example, $t_{1/2}$ for M*-PDCPD aged at 120°C for 15 minutes then thermolysis is 2 hours, whereas, $t_{1/2}$ for M*-PDCPD aged at 120°C for 1 minute then thermolysis is 4 minutes. According to the theoretical analysis ($t_{1/2\ uni} = \ln 2/k_{1u}$ and $t_{1/2\ bi} = ½[POOH]_0$), the "unimolecular" mechanism was thus envisaged. However, in some cases (high temperature and high catalysis content), the first order adjustment was not perfect. We thus envisaged the following scenario: in the "low concentration domain investigated here, both decomposition modes co-exist (but not in the same proportions), i.e.:

$$\frac{d(POOH)}{dt} = -k_{1u}[POOH] - 2k_{1b}[POOH]^2 \qquad \textit{Equation 3.14}$$

with k_{1b} determined from the decomposition in the high concentration region (see the previous paragraph) for the first time in PDCPD. The values of k_{1u} could be determined from the procedure illustrated in Figure 3.31.

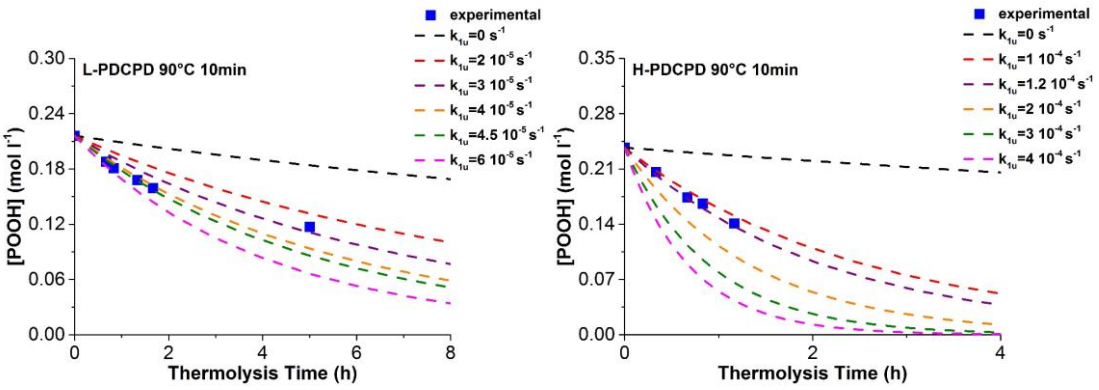

Figure 3.31: Numerical simulations for thermolysis of POOH with different value of k_{1u} at 90°C. NB: the dashed line with k_{1u} =0 corresponds to the contribution of k_{1b} in thermolysis at initially low POOH concentration.

From these modeling results in Figure 3.31, we can get access to k_{1u} values of which the values are summarized in Table 3.3 with a deviation range. Then the k_{1u} values are plotted versus

catalyst concentration and the ageing temperatures (Figure 3.32). The (apparent) rate constants identified from this procedure display two interesting characteristics:

- they increase with the catalyst content (Figure 3.32a). Such a feature is characteristic for us of a unimolecular process. According to Equation 3.6, a value characteristic for uncatalyzed unimolecular (denoted by k_{10}) could be determined. The hypothesis of linear changes of k_{1u} with catalyst content is, however, for us an oversimplification since ruthenium can exist in several ionic forms (Ru^{2+}, Ru^{3+} and Ru^{4+} and Eq. 3.3 are a simplified description). The change of k_{1u} with the catalyst content could be described as ln [k_{1u}] varies linearly with the ln [catalyst] (Fig. 3.32a). This characteristic leads to a new equation:

$$k_{1u} = k_{1u0} + k_{1c}[M^+]^x \qquad \textit{Equation 3.15}$$

with $x = 0.66$ (assuming that $k_{1u} \ll k_{1c}[M^+]^x$) which consistently with previous papers [31].

- they obey Arrhenius law with apparent activation energy close to 110 kJ mol^{-1} (Figure 3.32b) consistently which is the expected order of magnitude for first order rate constants for hydroperoxide decomposition [30].

Material	L, M, H-PDCPD	L-PDCPD	M*-PDCPD	H-PDCPD
Catalyst concentration (mol kg^{-1})		$1.18\ 10^{-4}$	$2.52\ 10^{-4}$	$3.53\ 10^{-4}$
Rate constants	k_{1b} ($l\ mol^{-1}\ s^{-1}$)	k_{1u} (s^{-1})		
Estimation method	Theoretical treatment of experimental data order 2 (Figure 3.14)	Simulation of thermolysis (Figure 3.17)	Simulation of thermolysis	Simulation of thermolysis (Figure 3.17)
T=50°C	$2.02\ 10^{-6}$	$1\ 10^{-6}$ - $1.6\ 10^{-6}$	/	$3.5\ 10^{-6}$ – $4\ 10^{-6}$
T=90°C	$2.33\ 10^{-5}$	$4\ 10^{-5}$ – $4.5\ 10^{-5}$	/	$1\ 10^{-4}$ – $1.2\ 10^{-4}$
T=120°C	$1.29\ 10^{-4}$	$1.6\ 10^{-3}$ – $1.8\ 10^{-3}$	$2.8\ 10^{-3}$ – $3\ 10^{-3}$	$3.3\ 10^{-3}$ – $3.6\ 10^{-3}$
E_a (kJ mol^{-1})	62	/	/	/
R^2	0.9999	/	/	/

Table 3.2: Summary of values of k_{1u} and k_{1b} measured by thermolysis experiments and by simulation.

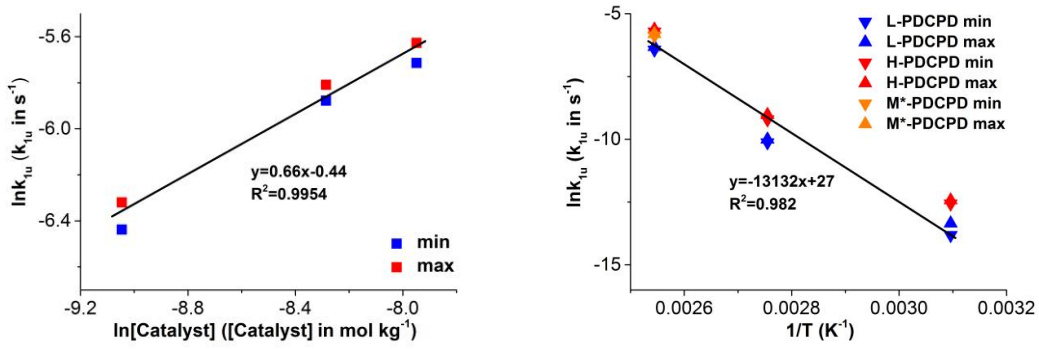

(a) **(b)**

Figure 3.32: Change of k_{1u} with catalyst concentration (a); Arrhenius plot of k_{1u} for different PDCPD system (b).

The simulation modeling of thermolysis curves seems to be a considerable method for determining the values of k_{1u} for L-PDCPD and H-PDCPD. As we can see, the value of k_{1u} for PDCPD "medium*" is between the k_{1u} of "low" and the one of "high" (Fig. 3.32b).

5.5 Conclusions

This section presents data related to the stability of hydroperoxides in PDCPD. Thermolysis experiments were performed to investigate the nature and kinetics aspects of the reaction of hydroperoxide decomposition (uni- or bimolecular). Even if POOH seem to decompose mostly by bimolecular process, an unimolecular seem to coexist in the earlier exposure times, and would be favored by the use of high ROMP catalyst amount for synthetizing materials. Nevertheless, it seems also possible that the metallic impurities progressively deactivate in contact with oxygen, water or any oxidation byproduct, inducing the decrease of the apparent unimolecular constant k_{1u} towards the uncatalyzed rate constant k_{1u0} (thus reducing even more the effect of catalyst on oxidation rate). In other words, the presence of catalyst permits to trigger the polymerization process with a minor incidence on polymer durability. Reversely, the possibility of POOH decomposition catalyzed by oxidation products (alcohols, carboxylic acids) occurring at high conversion degrees remains to be investigated.

The associated kinetic parameters were estimated and can be employed in a complete kinetic model for describing the whole oxidation process. The understanding of catalyst effect on thermal stability will be helpful to compound materials with the right tradeoff between fast polymerization and long term stability.

6. Kinetic modelling

The aim of this section is to derive a kinetic model based on the proposed chemical reactions and the reported chemical changes under several ageing conditions in relation to the changes in mechanical properties.

6.1 Proposal for a kinetic model

According to the experimental data describing chemical changes of thermo-oxidized PDCPD reported above, the following mechanistic scheme may be used for modeling the kinetic curves obtained during the ageing of additive-free PDCPD:

(1u)	$POOH \rightarrow 2P^{\circ} + \gamma_1 P=O$	k_{1u}
(1b)	$POOH + POOH \rightarrow P^{\circ} + POO^{\circ} + \gamma_1 P=O$	k_{1b}
(2)	$P^{\circ} + O_2 \rightarrow POO^{\circ}$	k_2
(3)	$POO^{\circ} + PH \rightarrow POOH + P^{\circ}$	k_3
(A1)	$P^{\circ} + C=C \rightarrow x + P^{\circ}$	k_{a1}
(A2)	$POO^{\circ} + C=C \rightarrow \gamma_1 P=O + P^{\circ}$	k_{a2}
(4)	$P^{\circ} + P^{\circ} \rightarrow \gamma_4 x + (1-\gamma_4)C=C + (1-\gamma_4)PH$	k_4
(5)	$P^{\circ} + POO^{\circ} \rightarrow \gamma_5 POOP + \gamma_5 x + (1-\gamma_5)POOH + (1-\gamma_5)C=C$	k_5
(6)	$POO^{\circ} + POO^{\circ} \rightarrow P=O + POH$	k_6

where x represents crosslinking concentration

It can be considered as an adaptation of the mechanistic scheme proposed by Tobolsky et al. [32] for the autoxidation of hydrocarbons (reactions 1u, 1b, 2, 3 and 6), together with some specific reactions for the reactivity of double bonds (reactions (a1) and (a2) [5], [6], [28]) and the effect of oxygen pressure (or concentration (reactions (4) and (5) [5]).

γ_1, γ_4 and γ_5 are the yields respectively for carbonyls from PO° decomposition, crosslinking from P° + P° and P° + POO° coupling. As previously explained, γ_1 is below the experimentally determined "apparent" yield value 0.5, and will be proposed to be 0.25 which accords with the value of polyisoprene [28]. γ_4 was fixed equal to 0, and it was checked that the numerical model was found to be insensitive to the value of γ_5 fixed equal to 0 since no POOP were detected in DSC.

In this work, the PDCPD films are thin enough (5-7 µm) to neglect the gradient of oxygen concentration through the thickness. $[O_2]$ can be calculated by the following equation: $[O_2]$ =

$S_{O2} \times P_{O2}$, S_{O2} is the solubility coefficient of oxygen in PDCPD: $S_{O2} = 10^{-7}$ mol l^{-1} Pa^{-1} [33] and is constant in the sample thickness during ageing.

The resulting system of differential equations can be derived from the kinetic scheme:

$$\frac{d[POOH]}{dt} = -k_{1u}[POOH] - 2k_{1b}[POOH]^2 + k_3[POO°][PH] + k_5(1-\gamma_5)[P°][POO°] \quad \textit{Equation 3.16}$$

$$\frac{d[P°]}{dt} = 2k_{1u}[POOH] + k_{1b}[POOH]^2 - k_2[P°][O_2] + k_3[POO°][PH] - 2k_4[P°]^2 - k_5[P°][POO°] + k_{a2}[POO°][C=C] \quad \textit{Equation 3.17}$$

$$\frac{d[POO°]}{dt} = k_{1b}[POOH]^2 + k_2[P°][O_2] - k_3[POO°][PH] - k_5[P°][POO°] - 2k_6[POO°]^2 - k_{a2}[POO°][C=C] \quad \textit{Equation 3.18}$$

$$\frac{d[P=O]}{dt} = \gamma_{1u}k_{1u}[POOH] + \gamma_{1b}k_{1b}[POOH]^2 + \gamma_1 k_{a2}[POO°][C=C] + k_6[POO°]^2 \quad \textit{Equation 3.19}$$

$$\frac{d[C=C]}{dt} = -k_{a1}[P°][C=C] - k_{a2}[POO°][C=C] + (1-\gamma_4)k_4[P°]^2 + (1-\gamma_5)k_5[P°][POO°] \quad \textit{Equation 3.20}$$

$$\frac{d[PH]}{dt} = -(2-\gamma_1)k_{1u}[POOH] - (1-\gamma_1)k_{1b}[POOH]^2 - k_3[POO°][PH] - 2k_{a1}[P°][C=C] - 2k_{a2}[POO°][C=C] + (1-\gamma_4)k_4[P°]^2 \quad \textit{Equation 3.21}$$

The resolution of this system of differential equations was carried out using the ODE23s solver of the Matlab software with the following boundary values at t = 0:

[C=C] = $[C=C]_0$ ~ 13 mol l^{-1} (adjusted from FTIR measurements).

[PH] = $[PH]_0$ = 2$[C=C]_0$ (since each double bond is surrounded by two allylic C-H likely to react in the oxidation process).

$[P°]_0$ = $[POO°]_0$ = 0.

[POOH] = $[POOH]_0$ = 2.5 10^{-2} mol l^{-1} (from the DSC measurements)

There are actually infinite sets of rate constants permitting an acceptable fit of experimental results presented in Figure 3.7 and 3.14. However, our aim is rather to propose a set of values allowing a reasonable fit but with a reasonable physical sense. For that purpose, an analytical resolution will be performed firstly to make a rough estimation of the order of magnitude of some rate constants and later the identification of the whole set.

6.2 Analytical solution and estimation of the rate constants

Let us for example focus on the "oxygen excess regime". It can be considered that:

- The initiation step is considered as being predominantly bimolecular in the steady state where POOH is maximal, with k_{1b} close (equal) to the value estimated in the previous part.

- The maximum carbonyl growth rate is considered to be closed to the theoretical steady-state rate, which may be calculated by assuming the substrate consumption to be negligible. Therefore, under this assumption, the steady state is considered to be reached at low conversion.

The steady-state regime implies that:

$$\frac{d[P^\circ]}{dt} + \frac{d[POO^\circ]}{dt} = 0 \qquad \textit{Equation 3.22}$$

$$\frac{d[POOH]}{dt} = 0 \qquad \textit{Equation 3.23}$$

Combined with equations 3.16, 3.17 and 3.18, these equations become:

$$2k_{1b}[POOH]^2 = 2k_4[P^\circ]^2 + 2k_5[P^\circ][POO^\circ] + 2k_6[POO^\circ]^2 \qquad \textit{Equation 3.24}$$

$$2k_{1b}[POOH]^2 = k_3[POO^\circ][PH] + k_5(1-\gamma_5)[P^\circ][POO^\circ] \qquad \textit{Equation 3.25}$$

In the oxygen-excess regime, the contributions of termination reactions (4), (5) and the addition reactions (A-1) can be neglected and the following expressions for the concentration of reactive

species can be derived:

$$[POO°]_\infty = \frac{k_3[PH]}{2k_6} \qquad \textit{Equation 3.26}$$

$$[POOH]_\infty = \frac{k_3[PH]}{2\sqrt{k_{1b}.k_6}} \qquad \textit{Equation 3.27}$$

Therefore, the rate of carbonyl production under oxygen excess can be given by the following equation:

$$r_{ox,s} = \frac{d[P{=}O]}{dt} = \gamma_1 k_{1b}[POOH]^2 + k_6[POO°]^2 + \gamma_1 k_{a2}[POO°][F]$$

$$= \frac{(\gamma_1+1){k_3}^2[PH]^2}{4k_6} + \frac{\gamma_1 k_{a2}k_3[C{=}C]^2}{k_6}$$

$$= \frac{(\gamma_1+1){k_3}^2[PH]^2}{4k_6} + \frac{\gamma_1 k_{a2}k_3[PH]^2}{4k_6} \qquad \textit{Equation 3.28}$$

Similarly, in the oxygen-excess regime, the consumption rate of double bonds is expressed as:

$$r_{C=C,s} = -\frac{d[C=C]}{dt} = k_{a2}[POO°][C=C] = \frac{k_{a2}k_3[PH][C=C]}{2k_6} = \frac{k_{a2}k_3[C=C]^2}{k_6}$$

Equation 3.29

Our strategy is the following: using k_2 and k_3 from literature [28], [5], and k_{1b} from the thermolysis of hydroperoxides (see section 5 – Table 3.3), k_{a2} and k_6 can be calculated according to the following equation:

$$k_6 = \frac{(\gamma_1+1){k_3}^2[PH]^2}{4(r_{ox,s}-\gamma_1 r_{C=C,s})} \qquad \textit{Equation 3.30}$$

$$k_{a2} = \frac{k_6 r_{C=C,s}}{k_3[C=C]^2} \qquad \textit{Equation 3.31}$$

The values of k_6 and k_{a2} deduced from this analytical calculation are compared with values obtained for rubbery polymers (polyisoprene [28], polychloroprene [6]) and model molecules (cyclopentene [34], indene [34]) as shown in Figure 3.33. The fact that they are several orders

of magnitude lower for PDCPD than for rubbery polymers and liquid compounds (Figure 3.33) can be discussed in terms of mobility-controlled reactions. To summarize and complete previously given explanations [1], [2] : POO° reactivity is lowered because of control by segmental relaxation which impacts very strongly POO° + POO° termination reactions.

Data from Figure 3.33b suggests that this effect is lower for POO° + C=C reaction consistently with the fact that in such reactions, C=C are in high concentration and their reactivity is not limited by diffusion compared to POO° + POO° where the reactivity of the two reactants is limited by diffusion.

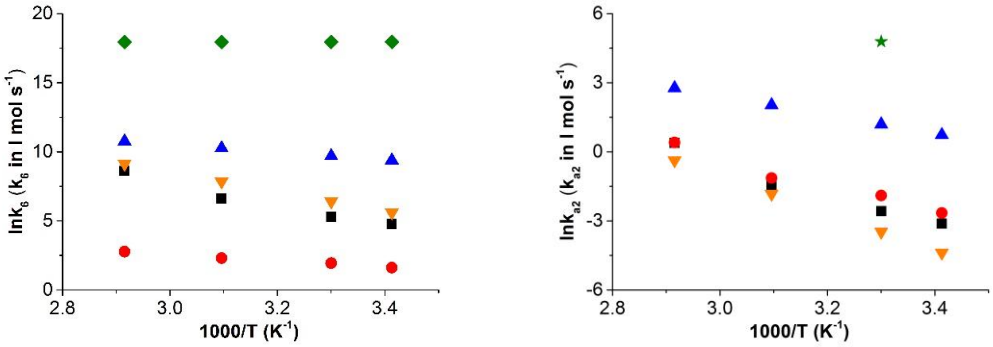

(a) **(b)**

Figure 3.33: Arrhenius plot for k_6 (a) and k_{a2} (b) for PDCPD (■, values deduced from the analytical approach; ●, values deduced from the numerical approach using model 2), polyisoprene (▲), polychloroprene (▼), cyclopentene (♦) and indene (★) for exposure at 50°C.

6.3 Numerical simulation

Following the analytical resolution of the system of equations from 3.22 to 3.31, a numerical resolution has been carried out without the assumptions used in the previous paragraph.

We firstly investigated the modeling in the oxygen-excess regime where only a few parameters play a role in the oxidation kinetics: k_{1b}, k_2, k_3, k_6 and k_{a2}:

- k_2 [28] and k_3 [5] are chosen from literature values.
- k_{1b} values are determined by the thermolysis of hydroperoxide at the pseudo plateau (see Table

3.3).

After focusing on the case of PDCPD oxidation under high oxygen pressure, the oxidation under low oxygen pressure is considered. In such conditions, the reaction of P° with C=C, and other terminations P° + P° and P° + POO° become prominent and their rate constants can be determined.

By respecting all the constraints (simulations under oxygen excess with rate constants estimated from analytical solutions), the first set of rate constants ("model 1") was obtained and lead to approximated simulations given by dashed lines (Fig. 3.7, Fig. 3.14 and Fig. 3.20).

The k_{1u} value we had to use was in particular unsatisfactory because it was almost 5 times higher than the one estimated by thermolysis, which was judged unacceptable. A second set was proposed in agreement with the estimation of thermolysis study, but a last reaction should be added to the mechanistic scheme:

(1b) $\mathrm{POOH} + \mathrm{HY} \rightarrow \mathrm{H_2O} + 2\mathrm{P}^\circ + \mathrm{HY}$ $\qquad k_{1c}$

where HY corresponds to the catalyst of POOH decomposition by oxidation stable products (carboxylic acids, alcohol…) as proposed by Denisov [34].

Its simulations ("model 2") are given in solid lines in Fig. 3.7, Fig. 3.14 and Fig. 3.20. Both two sets of rate constants are summarized in Table 3.4.

For two sets of rate constants, most of the "rules" expected for kinetic parameters for radicals processes seem to be verified: $k_4 > k_5 >> k_6$ [35], $E_4 \sim E_5 \sim 0$ kJ mol^{-1} [5], [6], [28], $k_{a1} >> k_{a2}$ [5], [6], [28]. The k_{1c} values obtained seem to be in the right order of magnitude [34]. Since the k_{1u} values in "model 2" are closer to the one estimated by thermolysis study, thus, the set 2 of "model 2" was adopted in our further study.

Set 1 - Model 1 (dashed lines in Fig. 3.7, Fig. 3.14 and Fig. 3.20)											
T (°C)	k_{1u} $\times 10^{6}$	k_{1b} $\times 10^{7}$	k_2 $\times 10^{-8}$	k_3 $\times 10^{3}$	k_4 $\times 10^{-8}$	k_5 $\times 10^{-8}$	k_6	$k_{6,a}$	k_{a1} $\times 10^{-3}$	k_{a2}	$k_{a2,a}$
20	1.5	1.7	1	3.6	5	1.0	5	117	6.0	0.035	0.04
30	3.8	3.9	1	9.1	5	1.3	7	199	7.0	0.1	0.08
50	12	18	1	48	5	1.7	10	758	9.0	0.37	0.24
70	60	70	1	210	5	2.4	16	5468	11	2.2	1.47
E_a	60	62	/	68	/	14	19	64	10	72	58
R^2	0.991	0.999	/	/	/	0.991	0.991	0.973	0.999	0.989	0.972
Set 2 - Model 2 (solid lines in Fig. 3.7, Fig. 3.14 and Fig. 3.20)											
T (°C)	k_{1u} $\times 10^{6}$	k_{1b} $\times 10^{7}$	k_{1c} $\times 10^{5}$	k_2 $\times 10^{-8}$	k_3 $\times 10^{3}$	k_4 $\times 10^{-8}$	k_5 $\times 10^{-8}$	k_6	k_{a1} $\times 10^{-3}$	k_{a2}	
20	0.6	1.7	1.7	1	3.6	5	2.5	5	5	0.07	
30	1.7	3.9	3	1	9.1	5	2.5	7	6.5	0.15	
50	5	18	12	1	48	5	2.5	10	11	0.32	
70	14	70	40	1	210	5	2.5	16	20	1.5	
E_a	51	62	53	/	68	/	/	19	23	49	
R^2	0.988	0.999	0.998	/	/	/	/	0.991	0.994	0.972	

Table 3.3: Rate constants (in l mol^{-1} s^{-1} except for k_{1u} in s^{-1}) used for simulations given in Figures 3.7, 3.14 and 3.20. NB: $k_{6,a}$ and $k_{a2,a}$ come from analytical calculations (Eq. 3.29 and 3.30) whereas k_6 and k_{a2} come from numerical solution (i.e. from curve fitting).

6.4 Conclusions

The thermal oxidation of PDCPD was studied under several temperatures and oxygen pressures. Beyond an induction period, the ageing was shown to induce a very strong decrease of the

double bond concentration together with a strong increase of the carbonyl concentration. These modifications at the chemical level are responsible for significant changes in some of the mechanical properties for thermal oxidation of PDCPD.

A kinetic model was developed on the basis of a reasonable mechanistic scheme so as to simulate and predict the chemical changes occurring in PDCPD during ageing. One of the main issues associated with such kinetic models is the high number of kinetic parameters to be determined. To overcome this concern, ageing of PDCPD under oxygen excess was used to "isolate" some of the key values among the kinetic parameters. The resulting kinetic model can simulate both carbonyl build-up and double bond consumption. Since hydroperoxides are key species of the oxidation process being quantifiable without the use of adjustable parameters (such as yields from a modeling point of view, or absorptivity values from an experimental point of view), the simulation of their formation and consumption was used for a better validation of the kinetic model.

The final kinetic model appears to be suitable at least in the domain of moderate degrees of conversion and allows the extent of PDCPD degradation to be predicted with time, temperature and external oxygen pressure as input parameters. The case of bulk material and of stabilized PDCPD should be addressed now to get closer to practical cases [1], [36], [37]. The DLO effects on the bulk PDCPD without stabilizers will be studied firstly in the following.

7. Diffusion Limited Oxidation

It is been shown that the diffusion limited oxidation effect exists in the case of PDCPD [1], [36], thus this phenomenon should be studied in our study to be taken into account in the prediction of the lifetime. The identification of the oxidation profile will be investigated experimentally by optical microscopy and by gravimetric study. Thus, the oxidation profile will be simulated with the created kinetic model.

7.1 Optical microscopy study of oxidation gradient

Thermal oxidation in air was performed on additive-free bulky samples (2 cm × 1 cm × 1 cm)

at 50°C, 70°C and 120°C for ageing times where the carbonyl concentration is maximum for corresponding thin samples. The microscopical pictures of the cross sections of the aged samples were obtained using an optical microscope, with a magnification of 20 in reflection mode. Figure 3.34 shows an example of micrographs obtained with the oxidized surface layers darker than the center of the samples. That confirmed that oxidation is controlled by the diffusion of oxygen (DLO effet) in the bulky PDCPD samples which have been observed by other authors [1]. The average oxidized layer thickness values were preliminarily determined from these micrographs for PDCPD aged in air at 50°C, 70°C and 120°C (Figure 3.34).

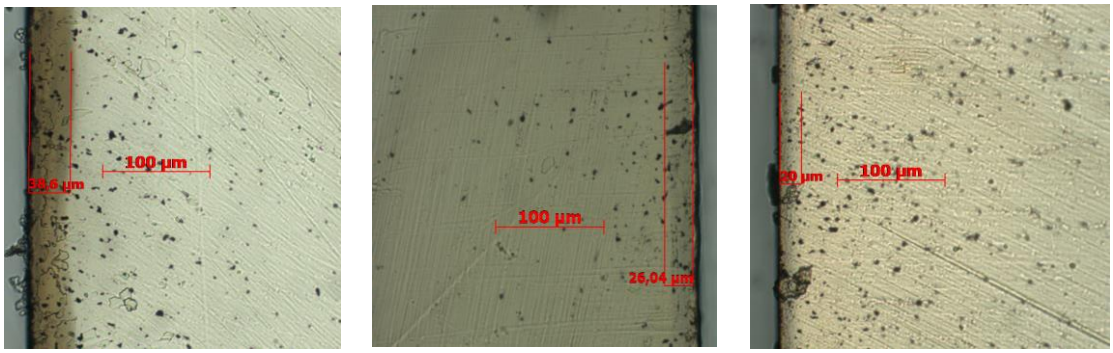

50°C 75h **70°C 16h** **120°C 8h**

Figure 3.34: Optical microscope observation (magnification × 20) of the oxidized layer of PDCPD after different exposure time in air.

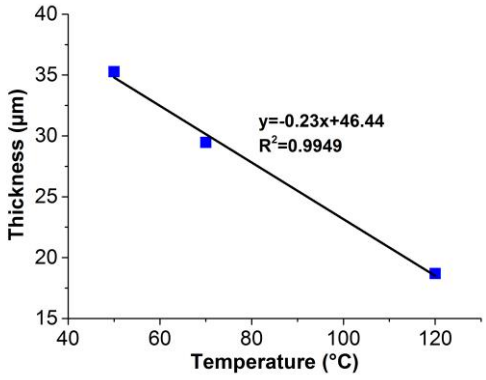

Figure 3.35: Thickness of the oxidized layer with ageing temperature for thermal ageing of PDCPD in air.

A linear decrease in the thickness of the oxidized layer as a function of ageing temperature is observed consistently with literature as recalled in the bibliographical study, which will be further confirmed by the gravimetric study.

The gravimetric study has been conducted for the purpose of confirming the thickness of the oxidized layer observed by the optical microscope. Samples with different thicknesses ranging from 10 to 100 µm were aged at 50°C in air so as to determine the maximal thickness below which oxidation is not controlled by oxygen diffusion. The mass changes have been plotted as a function of thermal ageing time in Fig. 3.36a and the rate of mass uptake (related to the oxidation rate r_{OX} [33]) reaches rapidly its maximal value (r_m). r_m depends on thickness in zone 1 of Fig.3.36b which corresponds that oxidation is controlled by the oxygen diffusion; whereas r_m is almost constant which means the sample thickness in this zone is less than TOL. Fig. 3.36b shows that the maximal rate seems almost constant for samples having a thickness lower than about 30 µm which corresponds here to twice the Thickness of Oxidized Layer (TOL). Thus, this TOL value (15 µm) at 50°C determined from the gravimetric seems to a little bit lower than the one from the microscope picture but his discrepancy is acceptable in a first approach. It should be noted that the observed TOL values are much higher for example in the case of unsaturated polyester (600 µm) [38] and epoxy resins (200 µm) [39].

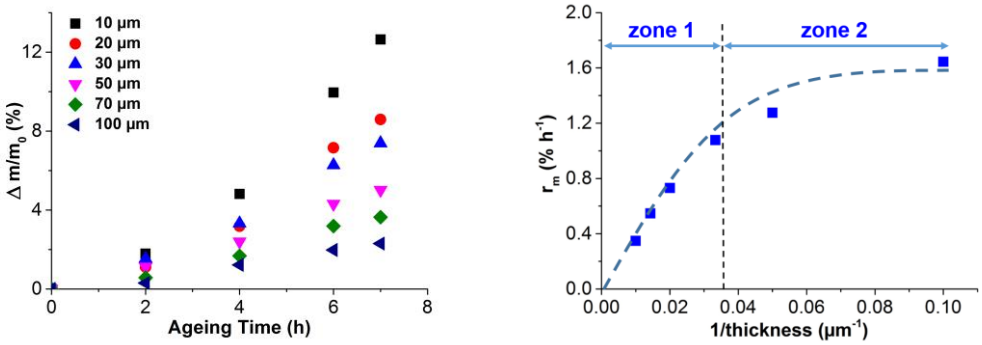

(a) **(b)**

Figure 3.36: Gravimetric curves (a) and maximal oxidation rate (rm) versus reciprocal thickness (b) for unstabilized PDCPD films aged at 50°C (NB: dashed lines guide the eyes, the vertical line indicate the reciprocal value of TOL).

7.2 Numerical simulation

The thickness TOL depends on both the oxidation rate r_{ox}, the diffusion coefficient of oxygen D_{O_2} and its equilibrium concentration $[O_2]$. The diffusion coefficients of PDCPD at different temperatures were estimated by Defauchy and al [33] (e.g. D_{O_2} = 1.19 10^{-11} at 50°C). In air, so the concentration of oxygen is calculated by $[O_2] = S_{O2} \times P_{O2}$ with $S_{O2} = 10^{-7}$ mol l^{-1} Pa^{-1} [33].

The numerical modeling of bulky sample is performed by solving the following equation:

$$\frac{d[O_2]}{dt} = D_{O_2}\frac{\partial^2[O_2]}{\partial x^2} - k_2[O_2][P^\circ] + k_6[POO^\circ]^2 \qquad \textit{Equation 3.32}$$

The other equations of the kinetic model and the boundary conditions remain unchanged. Thus, the oxidation profile, which evaluates the concentration of oxidation products (i.e. carbonyls) as a function of exposure time and thickness, is obtained by using the kinetic parameters of Table 3.4:

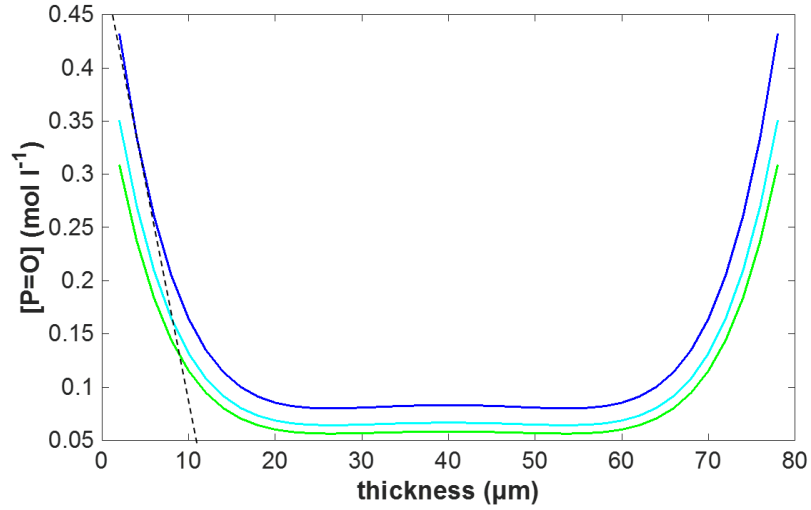

(a)

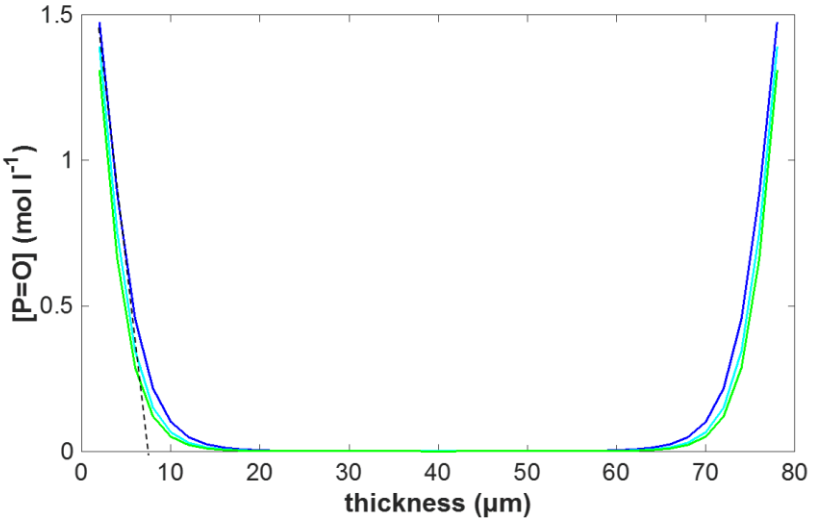

(b)

Figure 3.37: Modeling carbonyls concentration versus thickness for PDCPD aged at 50°C (a) and at 120°C (b).

The thickness oxidized layer is estimated as the intercept of the tangent line (dashed lines in Fig. 3.37) of the oxidation profile on the x axis. The results indicate that the thickness of the oxidized layer maximum at 50° C is about 12 μm, at 70°C is 10 μm and at 120°C is 8 μm. This difference between the experimental results based on micrographs and the simulation results can be the diffusion coefficients of oxygen may change with the oxidation time or inaccuracy of microscopy observations. However, at 50°C, the TOL obtained by simulation is closed to the one estimated by gravimetric study (TOL=15 μm). Generally, the simulated oxidation profile presents almost the same order of magnitude as the experimental results based on micrographs and gravimetric study. Thus, this kinetic model built for additive-free PDCPD makes it possible to predict the oxidation gradients due to DLO effects.

8. Conclusions

This chapter deals with the thermal oxidation of additive-free PDCPD. Firstly, the DSC titration is able to determine the concentration of hydroperoxides. That makes it possible to follow the change of POOH during thermal oxidation and estimate the rate constants of POOH decomposition (i.e. initiation step). The decomposition of POOH at which its corresponding concentration is maximum seems to decompose mostly by the bimolecular process. The associated kinetic parameters (k_{1b} and γ_1) were estimated and can be employed in a complete kinetic model for describing the whole oxidation process. It seems that the catalyst residues have a limit effect in uni-molecular decomposition of hydroperoxides.

Secondly, the FTIR was applied to follow the chemical changes in the PDCPD structure during thermal oxidation. The double bonds concentration of PDCPD was calculated by analyzing the FTIR results, which is confirmed by the ^{1}H NMR spectra. During thermal oxidation of PDCPD, beyond an induction period, the ageing was shown to induce a very strong decrease of the double bond concentration together with a strong increase of the carbonyl concentration. These modifications at the chemical level are responsible for significant changes in some of the mechanical properties of thermo-oxidized PDCPD.

Finally, based on the characterizations of DSC and FTIR, a reasonable mechanistic scheme was figured out to describe the mechanism of thermal oxidation of PDCPD. Then a kinetic model

was developed on the basis of this mechanistic scheme so as to simulate and predict the chemical changes occurring in PDCPD during ageing. The final kinetic model appears to be suitable at least in the domain of moderate degrees of conversion and allows the extent of PDCPD degradation to be predicted with time, temperature and external oxygen pressure as input parameters.

In the next chapter, the PDCPD with different stabilizers will be studied.

9. References

[1] P. Y. Le Gac, D. Choqueuse, M. Paris, G. Recher, C. Zimmer, and D. Melot, "Durability of polydicyclopentadiene under high temperature, high pressure and seawater (offshore oil production conditions)," *Polymer Degradation and Stability*, vol. 98, no. 3, pp. 809–817, Mar. 2013.

[2] E. Richaud, P. Y. Le Gac, and J. Verdu, "Thermooxidative aging of polydicyclopentadiene in glassy state," *Polymer Degradation and Stability*, vol. 102, pp. 95–104, Apr. 2014.

[3] E. Richaud, F. Farcas, P. Bartoloméo, B. Fayolle, L. Audouin, and J. Verdu, "Effect of oxygen pressure on the oxidation kinetics of unstabilised polypropylene," *Polymer Degradation and Stability*, vol. 91, no. 2, pp. 398–405, Feb. 2006.

[4] X. Colin, L. Audouin, and J. Verdu, "Determination of thermal oxidation rate constants by an inverse method. Application to polyethylene," *Polymer Degradation and Stability*, vol. 86, no. 2, pp. 309–321, Nov. 2004.

[5] M. Coquillat, J. Verdu, X. Colin, L. Audouin, and R. Nevière, "Thermal oxidation of polybutadiene. Part 2: Mechanistic and kinetic schemes for additive-free non-crosslinked polybutadiene," *Polymer Degradation and Stability*, vol. 92, no. 7, pp. 1334–1342, Jul. 2007.

[6] P. Y. Le Gac, G. Roux, J. Verdu, P. Davies, and B. Fayolle, "Oxidation of unvulcanized, unstabilized polychloroprene: A kinetic study," *Polymer Degradation and Stability*, vol. 109, pp. 175–183, Nov. 2014.

[7] M. J. Abadie, M. Dimonie, C. Couve, and V. Dragutan, "New catalysts for linear polydicyclopentadiene synthesis," *European Polymer Journal*, vol. 36, no. 6, pp. 1213–1219, Jun. 2000.

[8] J. Villarreal, J. Laane, S. Bush, and W. Harris, "Vibrational spectra and normal coordinate analysis for cyclopentene, cyclopentene-1-d1, cyclopentene-1, 2, 3, 3-d4 and cyclopentene-d8," *Spectrochimica Acta Part A: Molecular Spectroscopy*, vol. 35, no. 4, pp. 331–338, 1979.

[9] D. Nava, T. R. de Parada, E. González, N. Boscàn, and C. De La Cruz, "An infrared spectroscopic comparison of cis- and trans-CH=CH and vinyl CH=CH2 group frequencies of some hexenes, heptenes, and stereospecific and non-stereospecific polybutadienes," *Spectrochimica Acta Part A: Molecular and Biomolecular Spectroscopy*,

vol. 52, no. 10, pp. 1201–1210, Sep. 1996.

[10] D. Lin-Vien, N. B. Colthup, W. G. Fateley, and J. G. Grasselli, "CHAPTER 6 - Alkenes," in *The Handbook of Infrared and Raman Characteristic Frequencies of Organic Molecules*, San Diego: Academic Press, 1991, pp. 73–94.

[11] J. G. Calvert and J. N. Pitts, *Photochemistry*. New York, 1966.

[12] H. L. McMurry and V. Thornton, "Correlation of Infrared Spectra," *Anal. Chem.*, vol. 24, no. 2, pp. 318–334, Feb. 1952.

[13] R. M. Elder, J. W. Andzelm, and T. W. Sirk, "A molecular simulation study of the glass transition of cross-linked poly (dicyclopentadiene) networks," *Chemical Physics Letters*, vol. 637, pp. 103–109, 2015.

[14] D. B. Knorr Jr *et al.*, "Overcoming the structural versus energy dissipation trade-off in highly crosslinked polymer networks: ultrahigh strain rate response in polydicyclopentadiene," *Composites Science and Technology*, vol. 114, pp. 17–25, 2015.

[15] G. A. Russell, "Deuterium-isotope Effects in the Autoxidation of Aralkyl Hydrocarbons. Mechanism of the Interaction of PEroxy Radicals [1]," *Journal of the American Chemical Society*, vol. 79, no. 14, pp. 3871–3877, Jul. 1957.

[16] J. A. Howard and K. U. Ingold, "Self-reaction of sec-butylperoxy radicals. Confirmation of the Russell mechanism," *Journal of the American Chemical Society*, vol. 90, no. 4, pp. 1056–1058, Feb. 1968.

[17] L. Audouin, V. Gueguen, A. Tcharkhtchi, and J. Verdu, "'Close loop' mechanistic schemes for hydrocarbon polymer oxidation," *Journal of Polymer Science Part A: Polymer Chemistry*, vol. 33, no. 6, pp. 921–927, Apr. 1995.

[18] N. C. Billingham and M. N. Grigg, "The kinetic order of decomposition of polymer hydroperoxides assessed by chemiluminescence," *Polymer Degradation and Stability*, vol. 83, no. 3, pp. 441–451, Mar. 2004.

[19] N. C. Billingham, E. T. H. Then, and A. Kron, "Chemiluminescence from peroxides in polypropylene: II. Luminescence and kinetics of peroxide decomposition," *Polymer Degradation and Stability*, vol. 55, no. 3, pp. 339–346, Mar. 1997.

[20] L. Zlatkevich, "On the kinetic order of decomposition of polymeric hydroperoxides," *Polymer degradation and stability*, vol. 83, no. 2, pp. 369–371, 2004.

[21] G. Gutiérrez, F. Fayolle, G. Régnier, and J. Medina, "Thermal oxidation of clay-nanoreinforced polypropylene," *Polymer Degradation and Stability*, vol. 95, no. 9, pp.

1708–1715, 2010.

[22] E. M. Hoàng, N. S. Allen, C. M. Liauw, E. Fontán, and P. Lafuente, "The thermo-oxidative degradation of metallocene polyethylenes. Part 1: long-term thermal oxidation in the solid state," *Polymer degradation and stability*, vol. 91, no. 6, pp. 1356–1362, 2006.

[23] E. M. Hoàng, N. S. Allen, C. M. Liauw, E. Fontán, and P. Lafuente, "The thermo-oxidative degradation of metallocene polyethylenes: Part 2: Thermal oxidation in the melt state," *Polymer degradation and stability*, vol. 91, no. 6, pp. 1363–1372, 2006.

[24] E. Richaud, F. Farcas, B. Fayolle, L. Audouin, and J. Verdu, "Hydroperoxide titration by DSC in thermally oxidized polypropylene," *Polymer Testing*, vol. 25, no. 6, pp. 829–838, Sep. 2006.

[25] J. C. W. Chien, E. J. Vandenberg, and H. Jabloner, "Polymer reactions. III. Structure of polypropylene hydroperoxide," *Journal of Polymer Science Part A-1: Polymer Chemistry*, vol. 6, no. 2, pp. 381–392, 1968.

[26] J. C. W. Chien and H. Jabloner, "Polymer reactions. IV. Thermal decomposition of polypropylene hydroperoxides," *Journal of Polymer Science Part A-1: Polymer Chemistry*, vol. 6, no. 2, pp. 393–402, 1968.

[27] C. L. McGann *et al.*, "Air Activated Self-Decontaminating Polydicyclopentadiene PolyHIPE Foams for Rapid Decontamination of Chemical Warfare Agents," *Macromolecular rapid communications*, vol. 39, no. 12, p. 1800194, 2018.

[28] X. Colin, L. Audouin, and J. Verdu, "Kinetic modelling of the thermal oxidation of polyisoprene elastomers. Part 1: Unvulcanized unstabilized polyisoprene," *Polymer Degradation and Stability*, vol. 92, no. 5, pp. 886–897, May 2007.

[29] G. A. Russell, "The Rates of Oxidation of Aralkyl Hydrocarbons. Polar Effects in Free Radical Reactions1,2," *J. Am. Chem. Soc.*, vol. 78, no. 5, pp. 1047–1054, Mar. 1956.

[30] P. Gijsman, J. Hennekens, and J. Vincent, "The mechanism of the low-temperature oxidation of polypropylene," *Polymer Degradation and Stability*, vol. 42, no. 1, pp. 95–105, Jan. 1993.

[31] W. H. Richardson, "Metal Ion Decomposition of Hydroperoxides. IV. Kinetics and Products of Copper Salt Catalyzed Decomposition of t-Butyl Hydroperoxide," *J. Am. Chem. Soc.*, vol. 88, no. 5, pp. 975–979, Mar. 1966.

[32] A. V. Tobolsky, D. J. Metz, and R. B. Mesrobian, "Low Temperature Autoxidation of Hydrocarbons: the Phenomenon of Maximum Rates1,2," *J. Am. Chem. Soc.*, vol. 72, no.

5, pp. 1942–1952, May 1950.

[33] V. Defauchy *et al.*, “Kinetic analysis of polydicyclopentadiene oxidation,” *Polymer Degradation and Stability*, vol. 142, pp. 169–177, Aug. 2017.

[34] E. T. Denisov, *Polymer oxidation and antioxidant action*. 2000.

[35] K. T. Gillen, J. Wise, and R. L. Clough, “General solution for the basic autoxidation scheme,” *Polymer Degradation and Stability*, vol. 47, no. 1, pp. 149–161, Jan. 1995.

[36] Y. Hu, Y. Zhang, and S. Nutt, “Thermal oxidation aging of polydicyclopentadiene and composites,” *Polymer Composites*, vol. 39, no. 5, pp. 1742–1751, 2018.

[37] T. R. Long *et al.*, “Influence of molecular weight between crosslinks on the mechanical properties of polymers formed via ring-opening metathesis,” *Soft matter*, vol. 14, no. 17, pp. 3344–3360, 2018.

[38] J. S. Arrieta, E. Richaud, B. Fayolle, and F. Nizeyimana, “Thermal oxidation of vinyl ester and unsaturated polyester resins,” *Polymer degradation and stability*, vol. 129, pp. 142–155, 2016.

[39] E. Ernault, J. Dirrenberger, E. Richaud, and B. Fayolle, “Prediction of stress induced by heterogeneous oxidation: Case of epoxy/amine networks,” *Polymer Degradation and Stability*, vol. 162, pp. 112–121, Apr. 2019.

Chapter 4 Thermal stabilization of PDCPD

1. Introduction

The kinetic modeling is convenient for predicting the service lifetime of PDCPD provided that it is adapted to the specific nature of the materials used in practical applications. It is thus crucial to complete the scheme presented in the previous part by taking into account the effect of antioxidants aimed at increasing lifetime. Those latter can for example hold either phenols groups or hindered amine ones, which will be studied separately and then modeled in this chapter.

In this chapter, the thermal oxidation of PDCPD films (without Limited Oxidation effect) stabilized by butylated hydroxytoluene (BHT), Tinuvin 123 and Chimassorb 2020 will be firstly investigated at various temperatures (from 50°C to 120°C). The oxidation kinetics will be studied by IR spectroscopy by following carbonyl build-up. The previously established kinetic model will be completed to simulate the retarding effect of antioxidants on PDCPD oxidation. Finally, the oxidation profile for stabilized PDCPD will be investigated.

2. Initial characterizations of stabilized polymers

The addition of antioxidants bearing phenol groups is a conventional way to prevent polyolefins and rubbers from degradation [1]–[3]. Alternative antioxidants widely used to stabilize polymers are Hindered Amine Light Stabilizers (HALS) [1], [4]–[6]. To achieve long term stabilizing efficiency, high molecular weight antioxidants have gained much interest to overcome the physical loss and to enhance durability [7]. The most popular industrial approach to enhance physical persistence of stabilizers is to use oligomer stabilizers [8] [9].

Given the broad range of possible stabilizers packages for varying practical cases, our aim is test antioxidants with varying chemistry of the active groups (phenol group, N-O group and N-H group), molecular weight at several concentrations, and then illustrate the model capability to simulate their efficiency, adapt the model to other antioxidants than those investigated in this work and later improve the durability of PDCPD.

The chosen phenolic antioxidant was therefore butylated hydroxytoluene (BHT), and the

selected HALS were Tinuvin 123 and Chimassorb 2020, the structures of which are given in chapter 2 – Figure 2.2.

2.1 Compatibility study

The antioxidants must be compatible with the metathesis catalyst used to polymerize DCPD. In a first attempt, we decided to perform compatibility studies of these stabilizers with DCPD formulation based on a ruthenium metathesis catalyst (Ru2). The aim is to study in which extent antioxidants could interact with Ru catalyst and delay or inhibit the polymerization.

This kind of metathesis catalyst appeared to be only slightly affected by the presence of these three stabilizers as all samples reacted smoothly, reaching very high polymerization yields, expressed as the temperature increase between the initial and final temperature reached by the system (Figure 4.1). However, it must be noted that Tinuvin 123 and BHT present the results closed to the reference values (additive-free PDCPD) whereas Chimassorb 2020 showed the highest acceleration in this case. The reason for this accelerating effect is not clear. Let us recall that amines are known to be polar and have a basic behavior represented by a low pK_b value. Secondary amines present in Chimassorb 2020 have a lower pK_b than alkoxyamine present in Tinuvin 123 [10] but at the present stage, it is difficult to validate a scenario explaining results given in Figure 4.1.

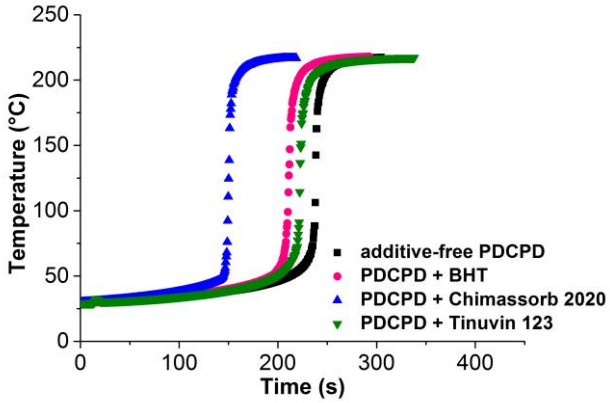

Figure 4.1: Thermographs of ROMP of DCPD catalyzed by ruthenium metathesis catalyst with and without antioxidants.

2.2 Calculation of stabilizers concentration

The concentrations of acting groups hold by antioxidants [AH] in PDCPD were deduced from the overall mass fraction x_{AH} by:

$$[AH] = \frac{f_{AH} \times d_{PDCPD} \times x_{AH}}{M_{AH}} = \frac{f_{AH} \times d_{PDCPD} \times (\frac{m_{AH}}{m_{PDCPD}})}{M_{AH}} = A \times x_{AH} \qquad \textit{Equation 4.1}$$

where :

- f_{AH} is the number of functionality. (i.e. 1 for BHT; 2 for Tinuvin 123; 8 to 11 for Chimassorb 2020 depend on its molar mass)
- d_{PDCPD} is the density of PDCPD (1 g cm^3).
- m_{AH} (g) and m_{PDCPD} (g) are the masses of antioxidants and PDCPD used to compound the sample, and x_{AH} is the corresponding weight fraction.
- M_{AH} (mol g^{-1}) is the molar mass of antioxidants. (220 g mol^{-1} for BHT; 737 g mol^{-1} for Tinuvin 123; 2600 – 3400 g mol^{-1} for Chimassorb 2020)

In the case of Chimassorb 2020, it can be verified that [NH] does not vary much with the incertitude on M_{AH}. For example, if M_{AH} = 2600, f_{AH} = 8.75 and if M_{AH} = 3400, f_{AH} = 12.2, but f_{AH}/M_{AH} remains almost constant.

5 concentrations of each stabilizer were studied for thermal oxidation in air, aim of comparing the efficiency of different antioxidants and better validate the model.

2.3 Characterization of double bonds in polymerized PDCPD

As described in chapter 3, the calculation of double bonds concentrations was done using Beer-Lambert law from the FTIR absorbance at 3050 cm^{-1}, 973 cm^{-1} and 733 cm^{-1}. The results are presented in Table 4.1. Interestingly, the double bond concentrations of stabilized PDCPD are a little bit lower than the one of additive-free PDCPD, which may be related to the interaction between antioxidant and catalyst after the polymerization. Besides, the catalyst used for additive-free PDCPD and stabilized PDCPD is not the same which may explain this difference.

The double bonds concentrations calculated will be used as imputs for the simulation part.

	[C=C] (mol l^{-1})
PDCPD + BHT	8 - 9
PDCPD + Tinuvin 123	9 - 10
PDCPD + Chimassorb 2020	8 - 9
Additive-free PDCPD	11 - 13

Table 4.1: Concentrations of double bonds for additive-free and stabilized PDCPD.

3. Thermal oxidation results

For stabilized PDCPD, the thermal oxidations were conducted in air at 50°C, 90°C and 120°C. In order to assess the stabilizing effect of antioxidants on PDCPD, the same measurements of carbonyl band by FTIR spectroscopy (see chapter 3) were conducted.

3.1 Effect of nature and concentration of stabilizers

For oxidation of PDCPD stabilized with BHT, Tinuvin 123 and Chimasorb 2020, some relevant results are shown in Figure 4.2.

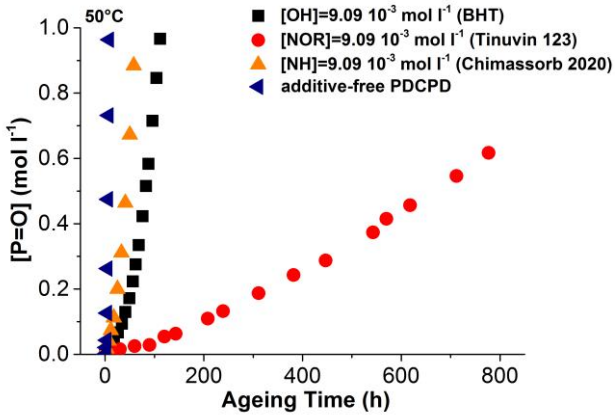

Figure 4.2: Carbonyls build-up for different stabilizers at 50°C under air.

These results justify that the different stabilizers display a stabilizing role in Ru based catalyst of PDCPD. Furthermore, the nature of the stabilizer has an apparent effect on the kinetics of

thermal oxidation: for example, using Tinuvin 123 is more beneficial for extension of the lifetime of PDCPD. The ranking of efficiency is that: Tinuvin 123 > BHT > Chimassorb 2020. Impressively, Chimassorb 2020, which is also the HALS stabilizer, displays a limited stabilizing performance. Figure 4.3 depicts the effect of concentration on functional groups of different antioxidants.

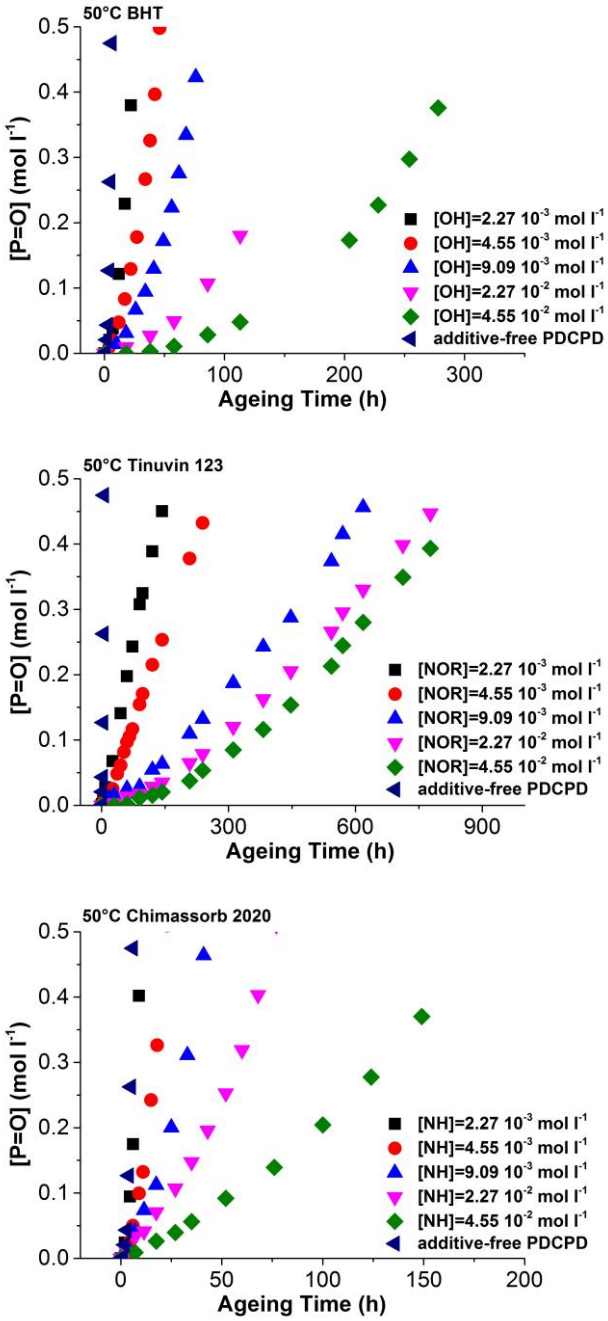

Figure 4.3: Changes of the carbonyl concentration as a function of the exposure time for PDCPD stabilized with 5 concentrations of functional group in BHT, Tinuvin 123 and Chimassorb 2020 and additive-free PDCPD at 50°C.

Several parameters can be obtained by analysis of these curves:

- the maximal oxidation rate,
- the induction time associated to lose of plasticity (see Figure 3.1 where [P=O] = 0.2 mol l^{-1} corresponds to the end-of-life criterion).

For better comparing the effect of increasing concentration of stabilizers, the changes of oxidation rate and lifetime versus concentration of stabilizers are summarized in Figure 4.4.

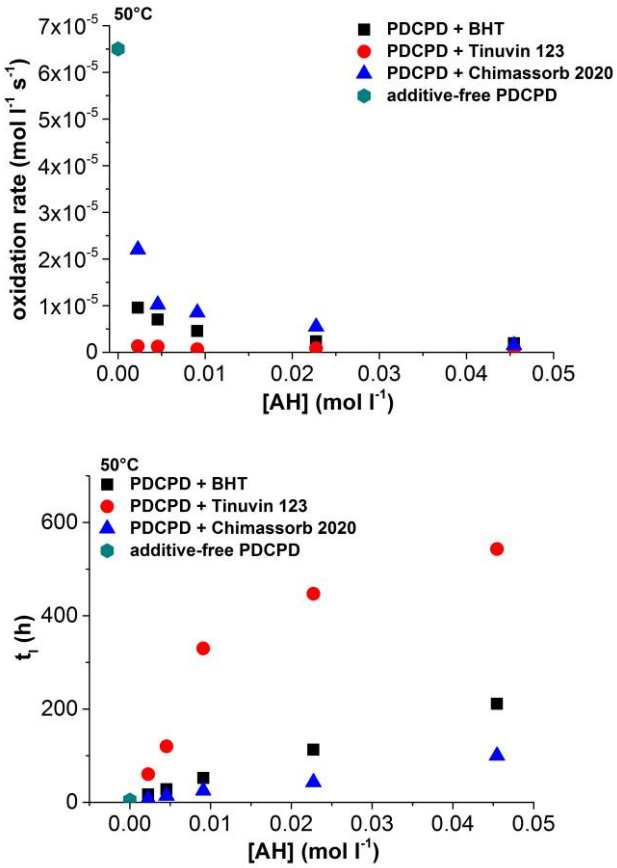

Figure 4.4: Changes of the oxidation rates and the lifetime with the concentration of stabilizers at 50°C.

These experimental results call for the following comments:

- In comparison with the additive-free PDCPD, BHT or Tinuvin 123 or Chimassorb 2020 antioxidants induce a decrease of oxidation rate and a significant increase of lifetime. This means all these antioxidants efficiently protect PDCPD in the temperature range under study.

- For these stabilizers, the corresponding oxidation rates decrease with the concentration of stabilizers then plateaus meanwhile the lifetimes increase also as a function of concentration of stabilizers. For BHT and Chimassorb 2020, the lifetime increases linearly with the concentration of stabilizers. However, for Tinuvin 123, the lifetime increases with the concentration of stabilizers but this increase becomes slower when the concentration of the functional group is beyond 9.09 10^{-3} mol l^{-1}. The possible explanation is linked to physical aspects of stabilization [8]: solubility and evaporation (due to its low molecular mass) occur when the concentration of stabilizer reaches high value. On the contrary, these physical problems seem to be absent in the case of Chimassorb 2020.

- As for efficiency, the ranking of these 3 different stabilizers is that: Tinuvin 123 > BHT > Chimassorb 2020. Tinuvin 123 displays the remarkable anti-oxidation performance (the slowest oxidation rate and the longest lifetime). Compared with Tinuvin 123, the phenolic stabilizer BHT is less efficient on PDCPD, because the phenol is irreversibly consumed by the reaction with radicals. HALS reacts in a regenerative way. Among the HALS stabilizers, Chimassorb 2020 shows less efficient performance, which will be discussed later in terms of reaction kinetic. It remains to explain why BHT is less efficient than Tinuvin 123 but more efficient than Chimassorb 2020. Several reasons can be envisaged: a part of Chimassorb 2020 is “destroyed” during polymerization by reaction with the co-catalyst, or high molar mass for Chimassorb 2020 limits its efficiency but this last explanation remains speculative since some authors observed either a decrease [8] or an increase of efficiency with stabilizer molar mass [11].

3.2 Effect of temperature

The thermal oxidation in air was performed at other temperatures (90°C and 120°C). The

influence of temperature is presented in terms of oxidation rate and lifetime for both BHT, Tinuvin 123 and Chimassorb 2020 (Figure 4.5).

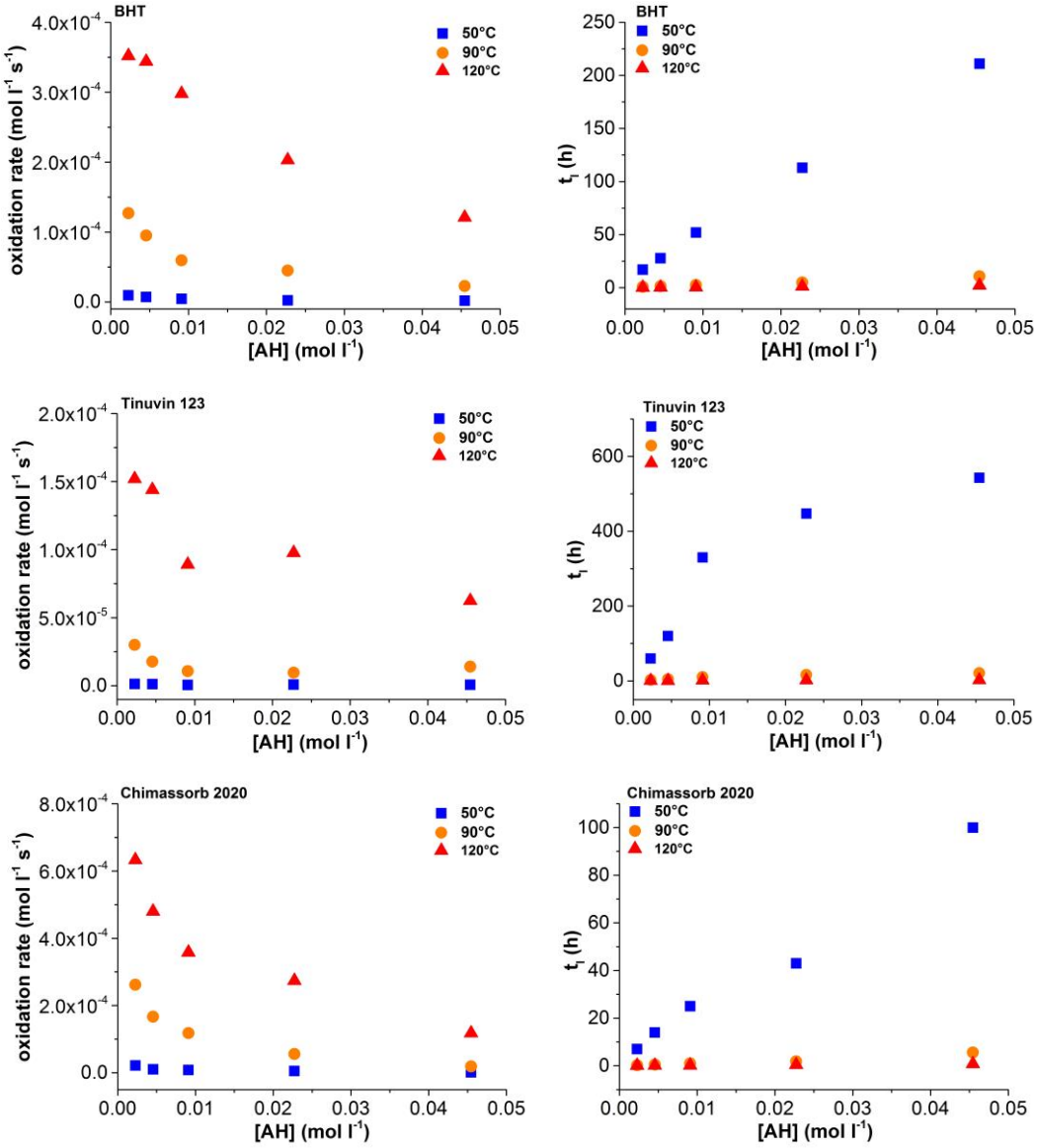

Figure 4.5: Changes of the oxidation rates and the lifetime with the concentration of stabilizers at 50°C, 90°C and 120°C.

Expectedly, the lifetime increases when ageing temperature decreases, meanwhile the oxidation rate decreases. The ranking of these 3 different stabilizers remains unchanged: Tinuvin 123 > BHT > Chimassorb 2020. For Tinuvin 123, the loss of stabilization efficiency (observed at 50°C) at elevated concentration is not obvious at higher temperatures. Since the solubility of antioxidants in polymers usually increases with temperature [12], the nonlinear shape of the

lifetime versus [AH] for Tinuvin 123 observed in Fig. 4.4 might be due to the low solubility of Tinuvin 123 in PDCPD.

Based on these complete experimental results, the modeling for each type of stabilizer will be developed in the next part.

4. Modeling of thin films oxidation

In this part, we will first propose the relevant mechanistic scheme together with some possible values of kinetic parameters and in a second step, we will propose some simulations and discuss the ability of the model to predict the lifetime of stabilized PDCPD.

4.1 Mechanistic scheme

4.1.1 Action of BHT

According to the literature [13], the action of BHT during thermal oxidation could be described by the following reactions:

(S1) $POO^{\circ} + AH \rightarrow POOH + A^{\circ}$ k_{s1}

(S2) $POO^{\circ} + A^{\circ} \rightarrow \text{inactive products}$ k_{s2}

Firstly, the labile hydrogen atom of phenolic antioxidants is captured by POO°, which competes with the reaction of

(3) $POO^{\circ} + PH \rightarrow POOH + P^{\circ}$ k_3

Then a radical recombination reaction takes place which is between POO° and A° to form inactive products.

The generated POOH during the reaction (3) decomposes like described in chapter 3: POOH $\rightarrow PO^{\circ} + {}^{\circ}OH$. Thus, reactions (S1) and (S2) consume 2 radicals (POO°) and create 2 radicals (PO° and $^{\circ}OH$). In the absence of phenols, one POO° radical gives a P° and a POOH i.e. 3

radicals in the end. This explains why phenols are efficient stabilizers.

As seen in chapter 3, there is no DLO effect in pure PDCPD films with a thickness below than 15 µm at 50°C. Thus, in principle, since

$$TOL^2 = D_{O2}\frac{[O_2]}{r_{ox}} \qquad \textit{Equation 4.2}$$

and $(\mathrm{D_{O2}})_{\mathrm{stablized}} = (\mathrm{D_{O2}})_{\mathrm{pure}}$, $[\mathrm{O_2}]_{\mathrm{stablized}} = [\mathrm{O_2}]_{\mathrm{pure}}$, *and* $(r_{ox})_{\mathrm{stablized}} < (r_{ox})_{\mathrm{pure}}$, we have:

$$\mathrm{TOL_{stablized}} > \mathrm{TOL_{pure}}$$

NB: pure corresponds to additive-free PDCPD. This reasoning will be justified later.

Therefore, the same as the additive-free PDCPD thermal oxidation study, thin films (15µm) were used in the stabilized PDCPD study. Their oxidation is supposed to be homogeneous in thickness. Based on the mechanistic scheme proposed in chapter 3, the equations related to POOH and POO° should be replaced by the following equations:

$$\frac{d[POOH]}{dt} = -k_{1u}[POOH] - 2k_{1b}[POOH]^2 + k_3[POO°][PH] + k_5(1-\gamma_5)[P°][POO°] - k_c[P=O][POOH] + k_{s1}[POO°][AH]$$

Equation 4.3

$$\frac{d[POO°]}{dt} = k_{1b}[POOH]^2 + k_2[P°][O_2] - k_3[POO°][PH] - k_5[P°][POO°] - 2k_6[POO°]^2 - k_{a2}[POO°][C=C] - k_{s1}[POO°][AH] - k_{s2}[POO°][A°]$$

Equation 4.4

Then, two new equations related to AH and A ° should be added in the case of thin samples:

$$\frac{d[AH]}{dt} = -k_{S1}[POO°][AH] \qquad \textit{Equation 4.5}$$

$$\frac{d[A°]}{dt} = k_{S1}[POO°][AH] - k_{s2}[POO°][A°] \qquad \textit{Equation 4.6}$$

It should be noted that the reaction (S2) is expected to be fast since it involves 2 radicals, thus $k_{s2} \geqslant 10^5$ l mol^{-1} s^{-1} [13] which is constant with ageing temperature. Some possible values of k_{s1} and k_{s2} are summarized in Table 4.2. Besides, according to data compiled by Denisov for PE [14], k_{s2} varies from 1.7 10^8 to 4.2 10^8 depending on the para substituent of antioxidant phenols (Table 4.2).

	PP [13]	PE [15]	PE [14]	PB [16]
k_{s1} (l mol^{-1} s^{-1})	40 (80°C)	4 10^4 (110°C)	/	3 (100°C)
E_{s1} (kJ mol^{-1})	70±10	80	/	/
k_{s1}/k_3	635 (80°C)	2 (110°C)	/	2 (100°C)
k_{s2} (l mol^{-1} s^{-1})	10^6	5 10^8 (110°C)	1.7 – 4.2 10^8	10^5 (100°C)
E_{s2}	0	0	/	0

Table 4.2: Kinetic parameters used in literature.

Besides, it is shown that for all the cases in $E_{s1} \geqslant E_3$ which is logic, because the O-H bond associated with the phenolic group is more stable than the C-H bond in PE or PP. In our case, the k_{s2} value was chosen equal to 10^7 whatever the ageing temperature. Then the k_{s1} values which are the only adjustable parameter will be determined by an inverse approach.

4.1.2 Action of Tinuvin 123

Tinuvin 123 bearing N-O groups belonging to HALS family where stabilization occurs by a conversion of active species (P° and POO°) into inactive ones. Based on the literature [17], [18], the following reactions are used to describe the action of Tinuvin 123:

(N1) $\mathrm{NO^\circ + P^\circ \rightarrow N - O - P}$ $\qquad k_{N1}$

(N2) $\mathrm{N - O - P + POO^\circ \rightarrow NO^\circ + C = C + POOH}$ $\qquad k_{N2}$

Therefore, these two reactions should be added to the mechanistic scheme describing thermal oxidation of additive-free PDCPD. Identically to BHT, some differential equations of the differential system must be modified:

$$\frac{d[P°]}{dt} = 2k_{1u}[POOH] + k_{1b}[POOH]^2 - k_2[P°][O_2]$$
$$+k_3[POO°][PH] - 2k_4[P°]^2 - k_5[P°][POO°] + k_{a2}[POO°][C=C]$$
$$+2k_c[P=O][POOH] - k_{N1}[NO°][P°] \qquad \textit{Equation 4.7}$$

$$\frac{d[POO°]}{dt} = k_{1b}[POOH]^2 + k_2[P°][O_2] - k_3[POO°][PH] - k_5[P°][POO°]$$
$$-2k_6[POO°]^2 - k_{a2}[POO°][C=C] - k_{N2}[N-O-P][POO°] \qquad \textit{Equation 4.8}$$

$$\frac{d[POOH]}{dt} = -k_{1u}[POOH] - 2k_{1b}[POOH]^2 + k_3[POO°][PH] + k_5(1-\gamma_5)[P°][POO°]$$
$$-k_c[P=O][POOH] + k_{N2}[N-O-P][POO°] \qquad \textit{Equation 4.9}$$

$$\frac{d[C=C]}{dt} = -k_{a1}[P°][C=C] - k_{a2}[POO°][C=C] + (1-\gamma_4)k_4[P°]^2$$
$$+(1-\gamma_5)k_5[P°][POO°] + k_{N2}[N-O-P][POO°] \qquad \textit{Equation 4.10}$$

Then two equations related to stabilizer active forms will be added:

$$\frac{d[NO°]}{dt} = -k_{N1}[NO°][P°] + k_{N2}[N-O-P][POO°] \qquad \textit{Equation 4.11}$$

$$\frac{d[N-O-P]}{dt} = k_{N1}[NO°][P°] - k_{N2}[N-O-P][POO°] \qquad \textit{Equation 4.12}$$

Some kinetic parameters from the literature are summarized in Table 4.3. It is noteworthy that k_{N1} (for reaction NO°+P°) value is reported to be very high for model compounds by Chateauneuf et al. [19] and Nicolas et al. [20]. Bauer and Gerlock [21] have also reported that k_{N1} and k_2 (rate constant for P°+O_2) are likely to have the same order of magnitude (about 10^8-10^9 l mol^{-1} s^{-1}), which means that k_{N1} have the higher order of magnitude than k_{N2} (rate constant for NOP+POO°).

	Model compounds [19]	Model compounds [20]	PE [17]
k_{N1} (l mol^{-1} s^{-1})	10^9 (20°C)	2 10^7 – 2 10^9 (18-24°C)	10^{10} (110°C)
	Model compounds [21]	/	PE [17]
k_{N2} (l mol^{-1} s^{-1})	2.3- 4.6 10^{-1} (25°C)	/	7 10^3 (110°C)
k_{N2}/k_3	/	/	4118 (110°C)

Table 4.3: Kinetic parameters used in literatures.

Based on these literature values, the new rate constants (k_{N1} and k_{N2}) for stabilization in PDCPD will be determined as follows: k_{N1} is fixed at 10^9 l mol^{-1} s^{-1} and k_{N2} will be adjusted by an inverse approach.

4.1.3 Action of Chimassorb 2020

Chimassorb 2020 does not contain directly the N-O groups. The N-H groups present in the structure will be converted into the N-O radicals, which leading the multi-step reactions during the process of action. According to the literature [17], [22], it seems that the following reactions could describe the mechanism of action:

(NH)	$NH + POO° \rightarrow POOH + N°$	k_{NH}
(O2)	$NH + O_2 \rightarrow N°$	k_{O2}
(N)	$N° + O_2 \rightarrow NOO°$	k_N
(NOO)	$NOO° + NOO° \rightarrow 2NO° + O_2$	k_{NOO}
(N1)	$NO° + P° \rightarrow N - O - P$	k_{N1}
(N2)	$N - O - P + POO° \rightarrow NO° + C = C + POOH$	k_{N2}

In this case, some differential equations should be changed:

$$\frac{d[POOH]}{dt} = -k_{1u}[POOH] - 2k_{1b}[POOH]^2 + k_3[POO°][PH] + k_5(1-\gamma_5)[P°][POO°]$$
$$-k_c[P=O][POOH] + k_{NH}[NH][POO°] + k_{N2}[N-O-P][POO°]$$

Equation 4.13

$$\frac{d[P°]}{dt} = 2k_{1u}[POOH] + k_{1b}[POOH]^2 - k_2[P°][O_2] + k_3[POO°][PH] - 2k_4[P°]^2$$
$$-k_5[P°][POO°] + k_{a2}[POO°][C=C] + k_c[P=O][POOH] - k_{N1}[NO°][P°]$$

Equation 4.14

$$\frac{d[POO°]}{dt} = k_{1b}[POOH]^2 + k_2[P°][O_2] - k_3[POO°][PH]$$
$$-k_5[P°][POO°] - 2k_6[POO°]^2 - k_{a2}[POO°][C=C]$$
$$-k_{NH}[NH][POO°] - k_{N2}[N-O-P][POO°]$$

Equation 4.15

$$\frac{d[C=C]}{dt} = -k_{a1}[P°][C=C] - k_{a2}[POO°][C=C] + (1-\gamma_4)k_4[P°]^2$$
$$+(1-\gamma_5)k_5[P°][POO°] + k_{N2}[N-O-P][POO°]$$

Equation 4.16

Then, a series of equations describing the changes of Chimassorb 2020 will be added:

$$\frac{d[NOO°]}{dt} = k_N[N°][O_2] - 2k_{NOO}[NOO°]^2$$

Equation 4.17

$$\frac{d[NO°]}{dt} = k_{NOO}[NOO°]^2 - k_{N1}[NO°][P°]$$
$$+k_{N2}[N-O-P][POO°]$$

Equation 4.18

$$\frac{d[NH]}{dt} = -k_{O2}[NH][O_2] - k_{NH}[NH][POO°]$$

Equation 4.19

$$\frac{d[N-O-P]}{dt} = k_{N1}[NO°][P°] - k_{N2}[N-O-P][POO°]$$

Equation 4.20

The k_{N1} and k_{N2} values reported in the literature have been mentioned above. It is been shown that the order of these new rate constants is likely to be [17]: $k_{O2} \ll k_{NH}$ and $k_{N2} \ll k_{NOO} < k_N < k_{N1}$. Bauer and Gerlock [21] have stated that the value of k_{NH} (rate constant for stabilizer + POO°) is higher than the one of k_3 (rate constant for PH + POO°). As reported in the literature [23], k_{O2} (rate constant for oxygen O_2 + labile hydrogen of NH) is very low. As the mechanistic scheme responsible for reaction (N1) and (N2) are the same for Tinuvin 123 and Chimassorb

2020, thus the k_{N1} and k_{N2} values are expected to be very close. So the simulation will be performed firstly for Tinuvin 123, then k_{N1} and k_{N2} values determined for Tinuvin 123 will be used in simulation for Chimassorb 2020. The other rate constants will be estimated by an inverse approach using these guidelines from literature.

4.2 Simulation results

The carbonyl accumulations for PDCPD stabilized with different types of antioxidants were simulated using rate constants given in chapter 3. The initial conditions remain the same as in chapter 3, and the initial conditions related to antioxidants are presented in Table 4.4. The corresponding results are presented in Figure 4.6 for 50°C, which shows acceptable simulation curves of carbonyl build-up for Tinuvin 123 and Chimassorb 2020. However, the one for BHT is less acceptable for different ageing temperatures (50°C, 90°C and 120°C).

	BHT	Tinuvin 123	Chimassorb 2020
$[POOH]_0$ (mol l^{-1})	$5\ 10^{-2} – 1.5\ 10^{-1}$	$5\ 10^{-2} – 1.5\ 10^{-1}$	$5\ 10^{-2} – 1.5\ 10^{-1}$
$[C=C]_0$ (mol l^{-1})	8 – 9	9 – 10	8 – 9
$[PH]_0$ (mol l^{-1})	16 – 18	18 – 20	16 – 18
$[NO°]_0$ (mol l^{-1})	/	0	0
$[O_2]_0$	$2.12\ 10^{-3}$	$2.12\ 10^{-3}$	$2.12\ 10^{-3}$
$[NOP]_0$ (mol l^{-1})	/	$2.27\ 10^{-3} – 4.55\ 10^{-2}$	0
$[NH]_0$ (mol l^{-1})	/	/	$2.27\ 10^{-3} – 4.55\ 10^{-2}$
$[N°]_0$ (mol l^{-1})	/	/	0
$[NOO°]_0$ (mol l^{-1})	/	/	0
$[NO°]_0$ (mol l^{-1})	/	/	0
$[AH]_0$ (mol l^{-1})	$2.27\ 10^{-3} – 4.55\ 10^{-2}$	/	/
$[A°]_0$ (mol l^{-1})	0	/	/

Table 4.4: Initial conditions used in simulation of stabilized PDCPD.

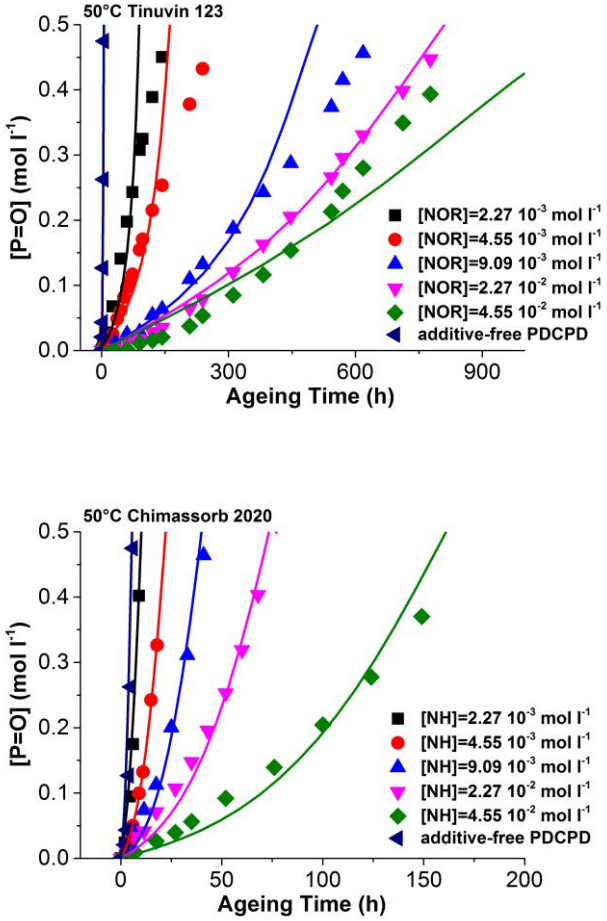

Figure 4.6: Simulation of variation of the carbonyl concentration as a function of the exposure time for PDCPD stabilized with 5 concentrations of functional group in Tinuvin 123 and Chimassorb 2020 and additive-free PDCPD at 50°C. Solid lines: simulation curves.

Since the oxidation rate and the lifetime are two key criteria for lifetime prediction of PDCPD, the relevant simulation results at different temperatures are summarized in Figure 4.7.

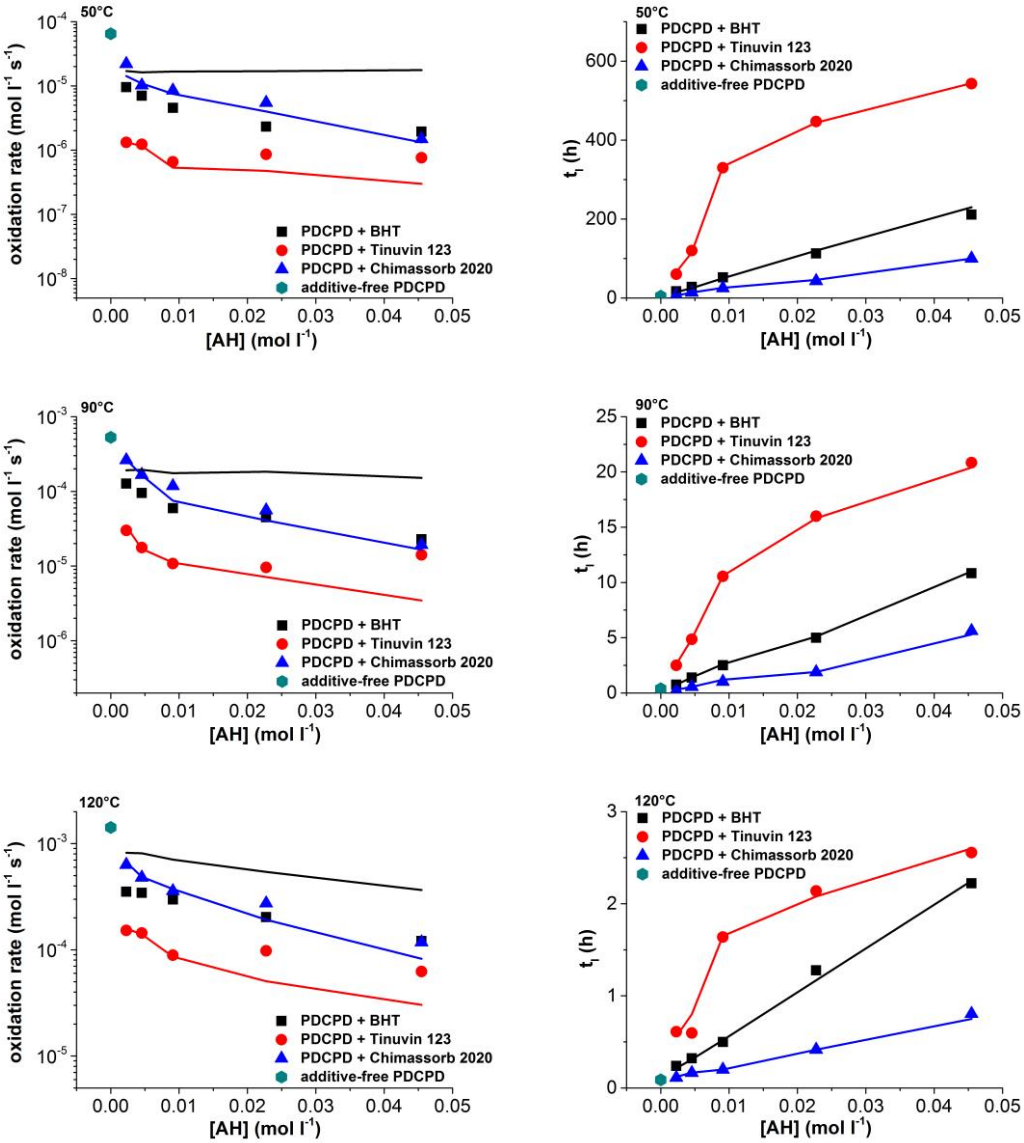

Figure 4.7: Changes of the oxidation rates and the lifetime with the concentration of stabilizers at 50°C, 90°C and 120°C. Solid lines: simulation curves.

These results call for the following comments:

- For PDCPD stabilized with Tinuvin 123 and Chimassorb 2020: the kinetic model simulates fairly the accumulation of carbonyl groups at 50°C, 90°C and 120°C for stabilizers HALS (i.e. Tinuvin 123 and Chimassorb 2020). Besides, the kinetic models can simulate the effect of concentration of stabilizers on lifetime at several temperatures together with the changes of oxidation rate.

Using the guidelines mentioned above, the relevant rate constants were determined and summarized in Table 4.4.

	BHT		Tinuvin 123			Chimassorb 2020					
	k_{s1}	k_{s2}	k_{N1}	k_{N2}	k_{N2}/k_3	k_{NH}	k_{O2}	k_N	k_{NOO}	k_{N1}	k_{N2}
50	25	10^7	$1\ 10^9$	1500	$3\ 10^4$	0.3	$1\ 10^{-5}$	$1\ 10^6$	$1\ 10^6$	$1\ 10^9$	1500
90	170	10^7	$1\ 10^9$	9000	$1\ 10^4$	6	$8\ 10^{-5}$	$1\ 10^6$	$1\ 10^6$	$1\ 10^9$	9000
120	750	10^7	$1\ 10^9$	20000	$5\ 10^3$	120	$2\ 10^{-4}$	$1\ 10^6$	$1\ 10^6$	$1\ 10^9$	20000
E_a	21	/	/	40	/	89	46	/	/	/	40
R^2	0.996	/	/	0.993	/	0.982	0.993	/	/	/	0.993

Table 4.5: Rate constants describing action of BHT, Tinuvin 123 and Chimassorb 2020.

The rate constants for Tinuvin 123 and Chimassorb 2020 display that the orders of magnitudes are well in line with the ones of PE [17] and of the literature shown in Table 4.3. Besides, the simulations are not very sensitive to the variation of k_N and k_{NOO}. We assume that the relevant reactions (N°+O_2 and NOO°+NOO°) are not decisive in stabilization. As expected, in the case of PDCPD, the k_{N1} values are very high because this reaction involves 2 very reactive radicals (P° and NO°) whereas the k_{N2} values are much lower than k_{N1} [21]; the k_{NH} values are higher than k_3 values [21]; the ratio between k_{N2} and k_{N3} is for example $3\ 10^4$ at 50°C; the k_{O2} values are very low [16], [23]; all of these properties accord with literatures.

For both these stabilizers, the precise orders of magnitude and ratio between rate constants may be different from other works as a result of discrepancies in the studied substrate and applied mechanistic scheme [17].

It is noteworthy that the values of k_{N1} and k_{N2} remain the same in both cases of Tinuvin 123 and Chimassorb 2020. Because these 2 rate constants describe the same reactions in Tinuvin 123 and Chimassorb 2020:

(N1) $\mathrm{NO^\circ + P^\circ \rightarrow N - O - P}$ k_{N1}

(N2) $\mathrm{N - O - P + POO^\circ \rightarrow NO^\circ + C = C + POOH}$ k_{N2}

Even if the chemical structures of these 2 stabilizes are different, such similarity further validates the mechanistic schemes used here to describe the oxidation kinetics.

- For PDCPD stabilized with BHT, the kinetic model is not able to simulate properly the changes of carbonyls as a function of time with the mechanistic scheme proposed above. On the basis of the reaction (S1) unchanged, several possible mechanistic schemes are proposed and tested:

Hypothesis 1 (S2)	$P° + A° \rightarrow$ inactive products	k_{s2}
Hypothesis 2 (S2)	$A° + A° \rightarrow AH$	k_{s2}
Hypothesis 3 (S2)	$POO° + A° \rightarrow POOA$	k_{s2}
(O2)	$AH + O_2 \rightarrow A° + HOO°$	k_{O2}
Hypothesis 4 (S2)	$A° + A° \rightarrow AH$	k_{s2}
(O2)	$AH + O_2 \rightarrow A° + HOO°$	k_{O2}

However, the simulations based on these hypothesizes and many sets of rate constants cannot fit the experimental curves. In further studies, the measurements of BHT residual concentration with ageing time should be conducted for better understanding the reason for this failure.

Furthermore, the kinetic model will help us to understand the efficiency of these different stabilizers: Tinuvin 123 > BHT > Chimassorb 2020. As described in the mechanistic scheme of BHT, the functional groups for stabilization (i.e. labile hydrogen atom of phenolic antioxidants) are irreversibly consumed. Thus, in comparaison with HALS stabilizers which can regenerate the functional group (NO°) during stabilization, BHT is less efficient. Tinuvin 123 is more efficient than Chimassorb 2020, because the functional groups for stabilization (i.e. NOP) are presented directly in the structure of Tinuvin 123. However, in the case of Chimassorb 2020, the N-H groups containing in the structure should be first converted into NO° as described by the corresponding mechanistic scheme. The simulation of POO° and NO° (Figure 4.8) will help us to explain the different effects between Tinuvin 123 and Chimassorb 2020.

Figure 4.8a shows that adding HALS stabilizers inhibits the significant increase of peroxy radicals POO° which is produced during propagation step of thermal oxidation ($P° + O_2 \rightarrow POO°$).

This inhibition is due to the reaction between N-O-P and POO° as described in the mechanistic scheme for both Tinuvin 123 and Chimassorb 2020. Figure 4.8b shows the NOP species exist in Tinuvin 123 from the beginning and are immediately available active. On the contrary, in the case of Chimassorb 2020, a delayed action of HALS is seen due to time for converting NH into NO° and NOP.

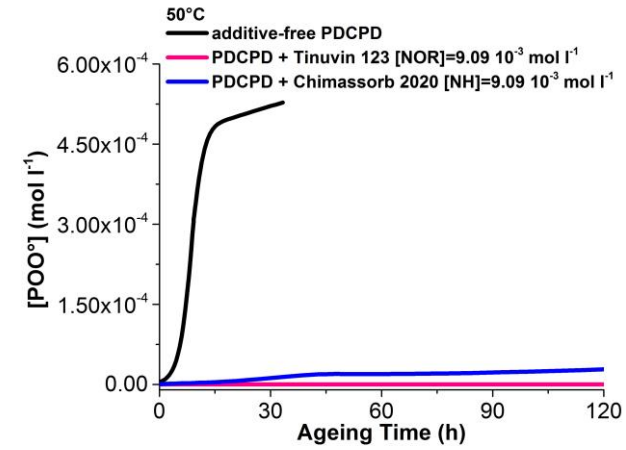

(a)

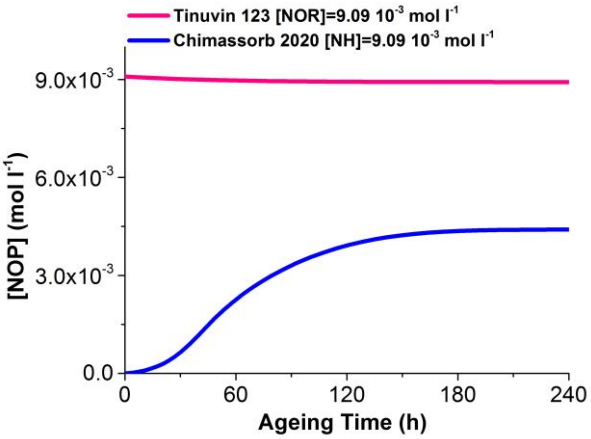

(b)

Figure 4.8: Simulation curves of POO° (a) and NOP (b).

In conclusion, the kinetic model used in this chapter gives acceptable simulations of experimental results, and simulates the effect of concentrations of functional groups for stabilization (at least in terms of lifetime and the effect of temperature) using physically reasonable orders of magnitude of the kinetic parameter values. Thus, this kinetic model is validated for additive-free PDCPD and now for stabilized PDCPD.

5. Diffusion Limited Oxidation in stabilized PDCPD

The effect of diffusion limited oxidation in the case of additive-free PDCPD has then been studied. Then this effect will be checked in the case of stabilized PDCPD. The identification of oxidation profile will be first investigated experimentally by optical microscopy.

Thermal oxidation in air was performed on bulky samples (2 cm × 1 cm × 1 cm) stabilized with Tinuvin 123 ([NOR]=2.27 10^{-3} mol l^{-1}) at 50°C for a long time where the carbonyl concentration is maximum for corresponding thin samples. The microscopical pictures of the cross sections of the aged samples were obtained using an optical microscope, with a magnification of 20 in reflection mode. An example result (Figure 4.9) shows that the oxidized surface layer is darker than the center of the sample. The corresponding thickness of oxidized layer is about 150 µm in the case of PDCPD stabilized Tinuvin 123, which confirms that oxidation is controlled by the diffusion of oxygen (DLO effet) in the bulky stabilized PDCPD. This result supports that DLO effects were neglected in the kinetic model by using thin stabilized PDCPD films (15 µm).

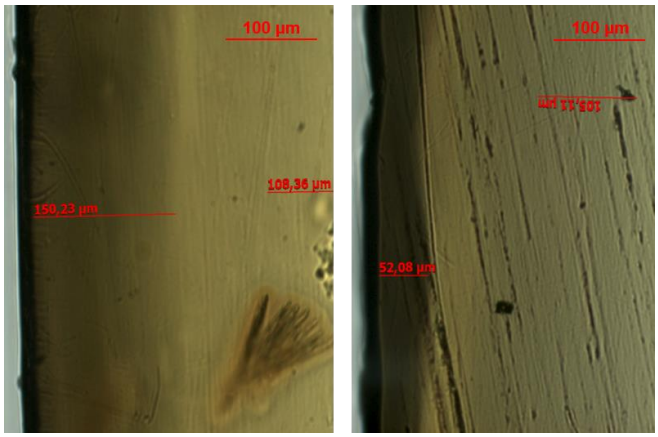

(a) **(b)**

Figure 4.9: Optical microscope observation (magnification × 20) of the oxidized layer for PDCPD stabilized by Tinuvin 123 ([NOR]=2.27 10^{-3} mol l^{-1}) (a) after exposure at 50°C for 200h.; for PDCPD stabilized by Chimassorb 2020 ([NH]=2.27 10^{-3} mol l^{-1}) after exposure at 50°C for 200h.

The numerical modeling of bulky sample is conducted by solving the following equation:

$$\frac{d[NO^{\circ}]}{dt} = -k_{N1}[NO^{\circ}][P^{\circ}] + k_{N2}[N-O-P][POO^{\circ}] + D_{NO^{\circ}}\frac{\partial^2[NO^{\circ}]}{\partial x^2}$$

Equation 4.11

$$\frac{d[N-O-P]}{dt} = k_{N1}[NO^{\circ}][P^{\circ}] - k_{N2}[N-O-P][POO^{\circ}] + D_{NOP}\frac{\partial^2[NOP]}{\partial x^2}$$

Equation 4.12

D_{NOP} is the coefficient diffusivity of "grafted" antioxidant and thus is equal to 0. $D_{NO^{\circ}}$ is a priori unknown in PDCPD. At first, the concentration in nitroxides remains very low so that most of Tinuvin 123 is expected to be grafted. So it can be considered that $D_{NO^{\circ}} = 0$. Using this first hypothesis, we can obtain the oxidation profile as shown in Figure 4.10a.

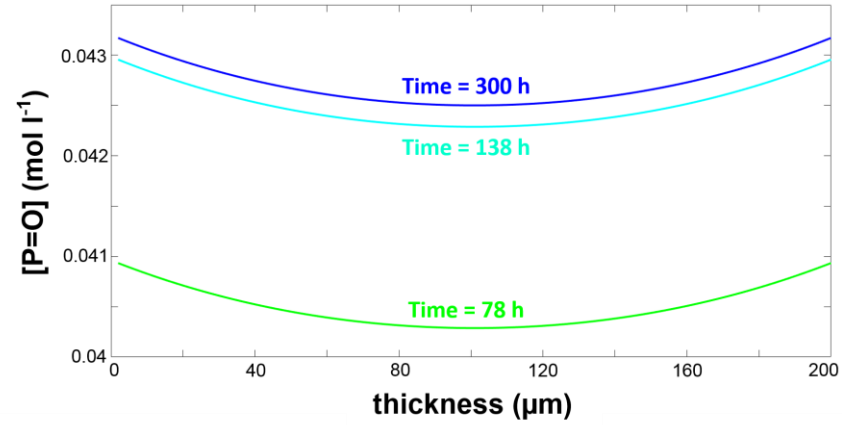

(a)

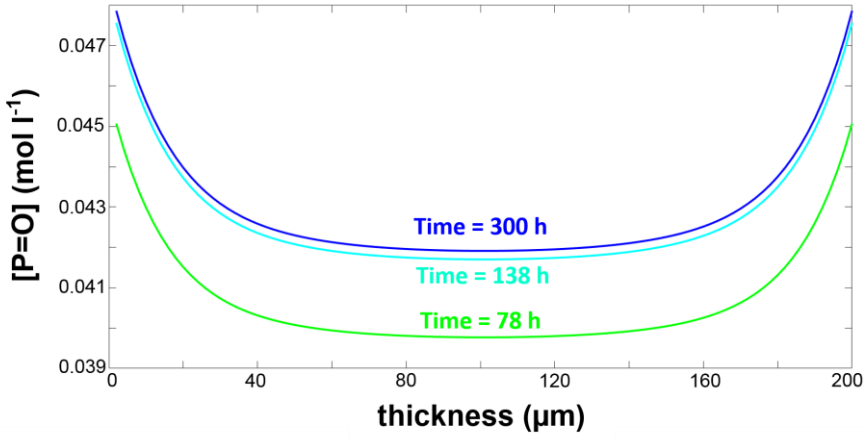

(b)

Figure 4.10: Modeling carbonyls concentration versus thickness for PDCPD stabilized by Tinuvin 123 ([NOR]=2.27 10^{-3} mol l^{-1}): (a) $D_{NO^{\circ}} = 0$; (b): $D_{NO^{\circ}} = 5\ 10^{-14}\ m^2\ s^{-1}$.

Let us consider now that a part of the antioxidant could be totally mobile. Using the diffusivity value D_{NO° = 5 10^{-14} m^2 s^{-1} inspired from [12], we obtained the simulation of the oxidation profile in Fig. 4.10b. It is clear that the thickness of the oxidized layer is always higher than the one of pure PDCPD. If the antioxidant is totally mobile, the oxidized layer would be about 30 µm thick (vs 15 µm for the unstabilized film see Chapter 3 Fig. 3.37a) and if stabilizer has any translational mobility, a 200 µm thick sample would be almost fully oxidized.

Those simulations are well in line with microscopic observations (Figure 4.9) and also with a recent work by Gijsman et al for polyamides [24]. In other words, adding antioxidants such as Hindered Amine stabilizers is an efficient way to slow down oxidation kinetics. However, in the case of thick materials, it could result in a thicker oxidized layer i.e. a stronger mechanical damage after the end of the induction period. The modeling of the embrittlement of thick stabilized samples [25] should help to decide what is the best solution for protecting such materials for long time exposures.

6. Conclusions

Based on the essential and thorough studies of kinetics about thermal oxidation of additive-free PDCPD, this chapter deals with the thermal oxidation of PDCPD stabilized with phenolic stabilizer and HALS for the first time.

Firstly, stabilized PDCPD displays the lower concentration of double bonds in the structure. The different stabilizers have an effective anti-oxidation function on Ru based catalyst PDCPD. The nature of stabilizer plays an important role in thermal oxidation kinetics. Tinuvin 123 shows a better protection performance compared with BHT and Chimassorb 2020. The inefficiency of BHT may be due to its sacrificial behavior. Tinuvin 123 allows a remarkable extension of the lifetime and a decrease in the oxidation rate. However, for Tinuvin 123, issue due to its solubility and physical loss have to be described for samples with “high” stabilizers concentration at low temperatures [26]. Even if both Tinuvin 123 and Chimassorb 2020 are regenerative stabilizers, Chimassorb 2020 displays a limited performance in terms of anti-oxidation due to conversion of N-H groups is needed in action mechanisms.

Last, it seems that stabilizers lead to an increase in the thickness of the oxidized layer. The effect on mechanical damage remains to be described but the use of kinetic model can help practitioners to make the best choice of stabilizers package.

7. References

[1] F. Gugumus, "Aspects of the stabilization mechanisms of phenolic antioxidants in polyolefins," *Die Angewandte Makromolekulare Chemie: Applied Macromolecular Chemistry and Physics*, vol. 137, no. 1, pp. 189–225, 1985.

[2] J. Pospíšil, "Chemical and photochemical behaviour of phenolic antioxidants in polymer stabilization: A state of the art report, part II," *Polymer Degradation and Stability*, vol. 39, no. 1, pp. 103–115, Jan. 1993.

[3] J. Pospíšil, "Chemical and photochemical behaviour of phenolic antioxidants in polymer stabilization—a state of the art report, Part I," *Polymer Degradation and Stability*, vol. 40, no. 2, pp. 217–232, Jan. 1993.

[4] F. Gugumus, "Current trends in mode of action of hindered amine light stabilizers," *Polymer Degradation and Stability*, vol. 40, no. 2, pp. 167–215, 1993.

[5] F. Gugumus and N. Lelli, "Light stabilization of metallocene polyolefins," *Polymer degradation and stability*, vol. 72, no. 3, pp. 407–421, 2001.

[6] N. Allen, K. Fatinikun, J.-L. Gardette, and J. Lemaire, "Thermal and photo-sensitised oxidation of polypropylene: Influence of hindered piperidine compounds," *Polymer Degradation and Stability*, vol. 3, no. 4, pp. 243–252, 1981.

[7] J. Malik, D. Tuan, and E. Špirk, "Lifetime prediction for HALS-stabilized LDPE and PP," *Polymer degradation and stability*, vol. 47, no. 1, pp. 1–8, 1995.

[8] P. Hrdlovič and Š. Chmela, "Oligomeric Stabilizers of HALS Type; Influence of Polarity and Molecular Mass on Efficiency," *International Journal of Polymeric Materials*, vol. 13, no. 1–4, pp. 245–254, 1990.

[9] J. Malík and G. Ligner, "Hindered amine light stabilizers: introduction," in *Plastics Additives*, Springer, 1998, pp. 353–359.

[10] K. Antoš and J. Sedlář, "Influence of brominated flame retardant thermal decomposition products on HALS," *Polymer Degradation and Stability*, vol. 90, no. 1, pp. 188–194, Oct. 2005.

[11] J. Malík, A. Hrivík, and D. Alexyová, "Physical loss of hindered amine light stabilizers from polyethylene," *Polymer Degradation and Stability*, vol. 35, no. 2, pp. 125–130, Jan. 1992.

[12] J. Malík, A. Hrivík, and E. Tomová, "Diffusion of hindered amine light stabilizers in low

density polyethylene and isotactic polypropylene," *Polymer Degradation and Stability*, vol. 35, no. 1, pp. 61–66, Jan. 1992.

[13] E. Richaud, B. Fayolle, and J. Verdu, "Polypropylene stabilization by hindered phenols – Kinetic aspects," *Polymer Degradation and Stability*, vol. 96, no. 1, pp. 1–11, Jan. 2011.

[14] E. Denisov and I. Afanas'ev, *Oxidation and Antioxidants in Organic Chemistry and Biology*. CRC Press, 2005.

[15] E. Richaud, "Kinetic modelling of phenols consumption during polyethylene thermal oxidation," *European Polymer Journal*, vol. 49, no. 8, pp. 2223–2232, 2013.

[16] M. Coquillat, "Vieillissement des propergols à matrice polybutadiène: modélisation cinétique de l'oxydation."

[17] E. Richaud, X. Colin, C. Monchy-Leroy, L. Audouin, and J. Verdu, "Polyethylene stabilization against thermal oxidation by a trimethylquinoleine oligomer," *Polymer Degradation and Stability*, vol. 94, no. 3, pp. 410–420, Mar. 2009.

[18] E. T. Denisov, "Mechanism of regeneration of hindered nitroxyl and aromatic amines," *Polymer Degradation and Stability*, vol. 25, no. 2–4, pp. 209–215, Jan. 1989.

[19] J. Chateauneuf, J. Lusztyk, and K. U. Ingold, "Absolute rate constants for the reactions of some carbon-centered radicals with 2,2,6,6-tetramethyl-1-piperidinoxyl," *The Journal of Organic Chemistry*, vol. 53, no. 8, pp. 1629–1632, Apr. 1988.

[20] J. Nicolas, Y. Guillaneuf, C. Lefay, D. Bertin, D. Gigmes, and B. Charleux, "Nitroxide-mediated polymerization," *Progress in Polymer Science*, vol. 38, no. 1, pp. 63–235, 2013.

[21] D. Bauer and J. Gerlock, "Photo-stabilisation and photo-degradation of organic coatings containing a hindered amine light stabiliser: Part III—Kinetics of stabilisation during free radical oxidation," *Polymer degradation and stability*, vol. 14, no. 2, pp. 97–112, 1986.

[22] A. Faucitano, A. Buttafava, F. Martinotti, and P. Bortolus, "First electron spin resonance identification of a nitrogen peroxy radical as intermediate in the photooxidation of 2,2,6,6-tetramethylpiperidine derivatives," *J. Phys. Chem.*, vol. 88, no. 6, pp. 1187–1190, Mar. 1984.

[23] E. T. Denisov and I. B. Afanas' ev, *Oxidation and antioxidants in organic chemistry and biology*. CRC press, 2005.

[24] P. Gijsman, W. Dong, A. Quintana, and M. Celina, "Influence of temperature and stabilization on oxygen diffusion limited oxidation profiles of polyamide 6," *Polymer Degradation and Stability*, vol. 130, pp. 83–96, Aug. 2016.

[25] E. Ernault, J. Dirrenberger, E. Richaud, and B. Fayolle, “Prediction of stress induced by heterogeneous oxidation: Case of epoxy/amine networks,” *Polymer Degradation and Stability*, vol. 162, pp. 112–121, Apr. 2019.

[26] F. Djouani, E. Richaud, B. Fayolle, and J. Verdu, “Modelling of thermal oxidation of phosphite stabilized polyethylene,” *Polymer Degradation and Stability*, vol. 96, no. 7, pp. 1349–1360, Jul. 2011.

Chapter 5 Effect of thermal oxidation of PDCPD on water absorption

1. Introduction

In this chapter, we will pay attention to the potential application of PDCPD as a field joint for offshore oil exploitation and more generally the ageing in water. Under service conditions, PDCPD material is subjected to seawater and a temperature profile through coating thickness. Thus, thermal oxidation of PDCPD will possibly further influence the water absorption behavior.

The objective of this chapter is to investigate the water transport properties in virgin and oxidized PDCPD (in particular the maximum concentration of absorbed water and the water diffusion coefficient). In the first part of this chapter, results obtained by DVS for unaged and oxidized PDCPD at one temperature (70°C) will be presented. A brief presentation of existing knowledge on the polymer-water interaction mechanisms will be recalled, and discussed in the case of PDCPD. Based on the mechanism chosen, the experimental results will be exploited terms of diffusion coefficient and interaction parameters. In the second part, experimental results will be presented and discussed at the other temperatures (50°C and 25°C). A mastercurve will be obtained to illustrate the whole water sorption behavior. Finally, a relation between water uptake and polar groups concentration will be proposed.

2. Experimental results and discussion

Water sorption experiments were carried out on thin films (about 7 μm) of additive-free PDCPD between 10 and 90% relative humidity (RH) at three temperatures using a DVS apparatus. PDCPD samples were aged firstly at 25°C, 50°C, 70°C for different ageing times. Then unaged samples and aged samples were taken to conduct water sorption experiments at corresponding temperatures (e.g. samples aged at 70°C were used in water sorption experiments at 70°C).

These tests made it possible to determine the maximum concentration of water absorbed, as well as diffusion of water in unaged and aged PDCPD.

2.1 Comparison of virgin and oxidized PDCPD

Firstly, a typical change in mass plot for unaged PDCPD is shown in Figure 5.1. It is clear that maximal water uptake in the unaged material is very low (typically below 0.3%), consistently with its apolar structure as already reported [1].

A clear difference appears for strongly oxidized PDCPD (160 minutes at 70°C under air as characterized in chapter 3) displaying a significant increase in maximal water uptake (higher than 3%).

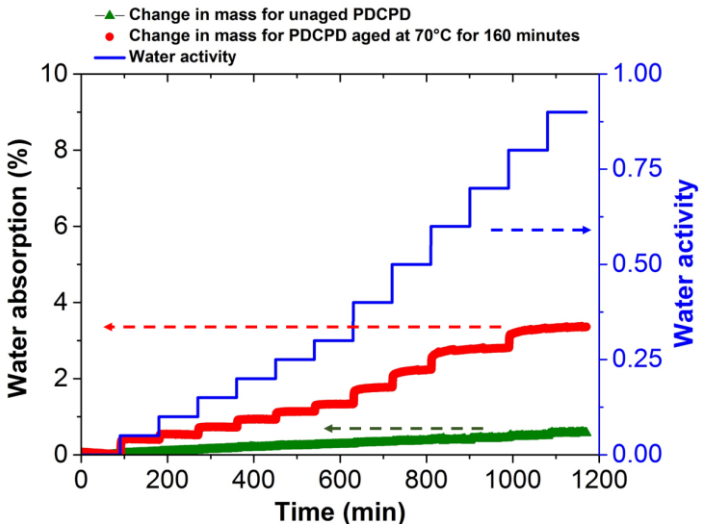

Figure 5.1: Sorption isotherms of time for unaged and aged PDCPD (70°C - 160 minutes).

Thin films of oxidized PDCPD with varying exposure levels were then tested in DVS at 70°C. The corresponding sorption isotherm (i.e. water uptake as a function of water activity) are presented in Figure 5.2. We can see that the water affinity of PDCPD largely increases with polymer oxidation level. For example, at a water activity 0.8, water content is almost 9 times higher in the oxidized sample (200 minutes at 70°C) compared to the unaged sample. As will be seen later, this result can be explained by the matter that the amount of absorbed water depends on the concentration in polar groups in polymers likely to bound with water [2]. For virgin PDCPD, sorption isotherm appears almost linear. This feature remains almost true for aged PDCPD at low water activity but a positive curvature seems to appear in the domain of high water activities (typically > 0.5). This feature indicates some changes in the polymer-water interaction mechanism, which will be investigated in the next paragraph.

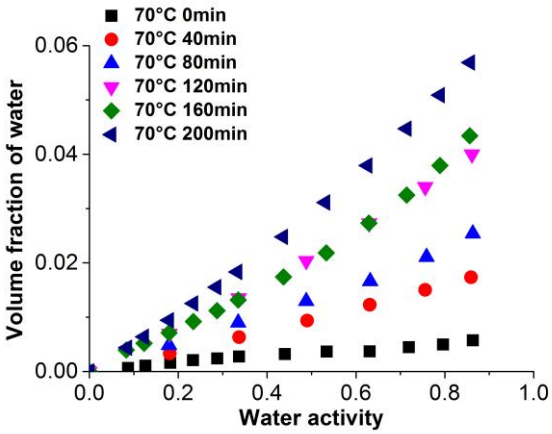

Figure 5.2: Volume fraction of water in PDCPD tested at 70°C as a function of water activity for PDCPD with different oxidation times at 70°C in oven.

2.2 Water sorption mechanism

We were thus interested in the sorption mechanisms responsible for the sorption isotherm presented in Figure 5.2. To our knowledge, there are three main mechanisms [3] which are shown schematically in Figure 5.3.

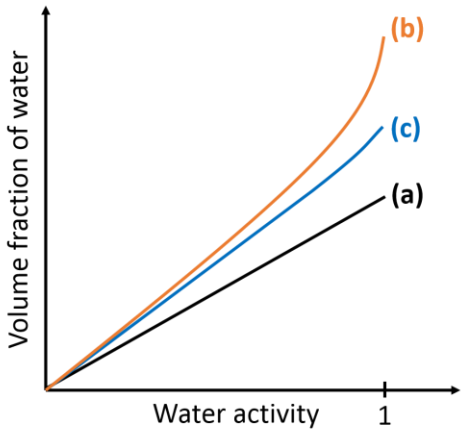

Figure 5.3: Different types of water sorption isotherms.

- Case (a): Water sorption isotherm is linear for all water activity, i.e. equilibrium water concentration increases linearly with water activity. The water absorption obeys Henry's law as described by equation 5.1:

$$v = H \times a \qquad \textit{Equation 5.1}$$

where v is the volume fraction of water, H is Henry's coefficient and a is the water activity or partial pressure.

This behavior is commonly observed for polymers with relative low hydrophilicity and with the physical properties unchanged after water absorption [3]. It seems however that Henry's law does not describe the experimental results for oxidized samples as shown in Figure 5.3 and in particular the positive concavity in the domain of high water activities.

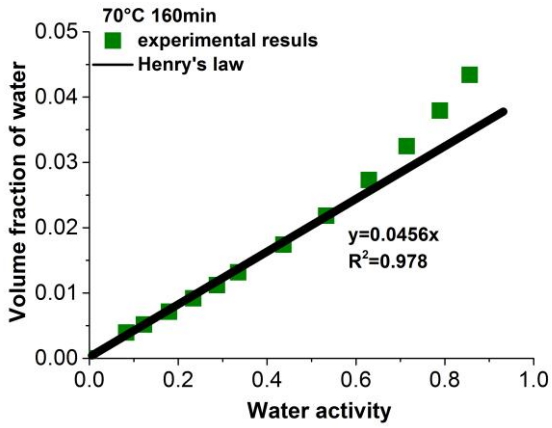

Figure 5.4: Water sorption isotherm for PDCPD aged at 70°C for 160 minutes. Solid line: Simulation by Henry's law.

Other mechanisms for polymer-water interaction must be investigated.

- Case (b): Water sorption isotherm can be described by the sum of Henry's law at low water activity and a supplementary contribution due to clusters at high water activity [4], [5]:

$$v = H \times a + B \times a^n \qquad \textit{Equation 5.2}$$

where B and n can be determined from experimental results.

The slight positive curvature in the DVS (Fig.5.3) might indicate presence of water clusters [6] (i.e. associated water molecules groups) within the oxidized PDCPD is possible. This later

means that water-water interactions are stronger than interactions between polymer-water [6]. In order to verify this assumption, the clustering function was calculated by the Zimm-Lundberg method [7], [8]:

$$f_{ZL} = -(1-v)\left[\frac{\partial a/v}{\partial a}\right]_{T,P} - 1 \qquad \textit{Equation 5.3}$$

Clusters occur when $f_{ZL} > -1$ and the mean cluster size (MCS) is given by:

$$MCS = 1 + v \times f_{zl} \qquad \textit{Equation 5.4}$$

The relevant mean cluster size were calculated and summarized in Table 5.1. It shows that the cluster size range from 1.4 to 1.8 at 0.9 water activity. MCS = 1 represents an isolated water molecule, MCS = 2 represents a cluster made of two water molecules [6], the maximum MCS in our cases is equal to 1.8, which verified that the formation of water cluster is very low even at high water activity. (NB: cluster size is for example higher than 7 in oxidized polychloroprene [9])

Aged at 70°C						
Ageing time (h)	unaged	0.67	1.33	2	1.33	3.33
MCS at 0.9 activity	1.8	1.4	1.5	1.6	1.6	1.7

Table 5.1: Mean cluster size for PDCPD tested at 70°C for different oxidation times at 70°C in oven.

A third mechanism was hence considered:

- Case (c): Water sorption isotherm is linear for low water activity, but have a positive concavity at high water activity. Then the water absorption obeys Flory-Huggins law [10]:

$$ln(a) = ln(v) + (1-v) + \chi(1-v)^2 \qquad \textit{Equation 5.5}$$

in which χ is the polymer-water interaction defined by the following expression:

$$\chi = \frac{V_m}{RT} \times (\delta_{polymer} - \delta_{water})^2 \qquad \textit{Equation 5.6}$$

where $\delta_{polymer}$ and δ_{water} are respectively the solubility parameters of polymer and water, V_m is the molar volume of water, R is the gas constant and T is the temperature. δ_{water} is close to 48 $MPa^{1/2}$ [11] and δ_{PDCPD} is about 17 ± 1 $MPa^{1/2}$ [12] as already observed for apolar polymers.

Figure 5.4 shows an example of experimental results obtained after 160 minutes of oxidation at 70°C compared with the Flory-Huggins equation curve fitting, which illustrates that that water content in the polymer can be described by Flory-Huggins equation.

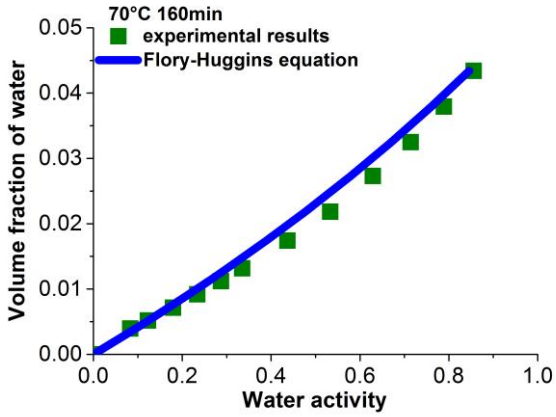

Figure 5.5: Determination of Flory-Huggins parameters for PDCPD samples aged 160 minutes at 70°C. Solid line: Simulation by Flory-Huggins equation.

Using Flory-Huggins equation [13] is interesting to focus on changes on interaction parameters as a function of oxidation level (i.e. the oxidation time at 70°C). Figure 5.6 displays that the interaction parameters, which are determined from the best fitting of sorption isotherms represented in Fig. 5.2, decreases with ageing time. Thermal oxidation of PDCPD actually forms oxidation products with polar groups (hydroxyls, carbonyls) which increases the solubility parameter of polymer thus decreasing the interaction parameter. The more polar groups generated, the smaller the value of the interaction parameter. In other words, the affinity with water increases with the ageing time.

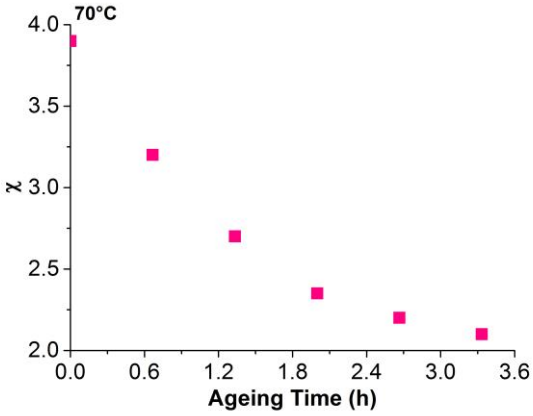

Figure 5.6: Changes on interaction parameters as a function of oxidation time for samples aged at 70°C in oven.

Basing on DVS results, it is also possible to focus on water diffusion mechanisms. Let us recall that two mechanisms exist for describing diffusivity in polymers:

- Fick's diffusion (Fig. 5.7a) characterized by a plateau at long ageing times and typical of diffusion of molecules at low concentration with weak or without interaction with polymer.

- Langmuir diffusion where plateau displays interaction with the hosting polymer (Fig. 5.7b).

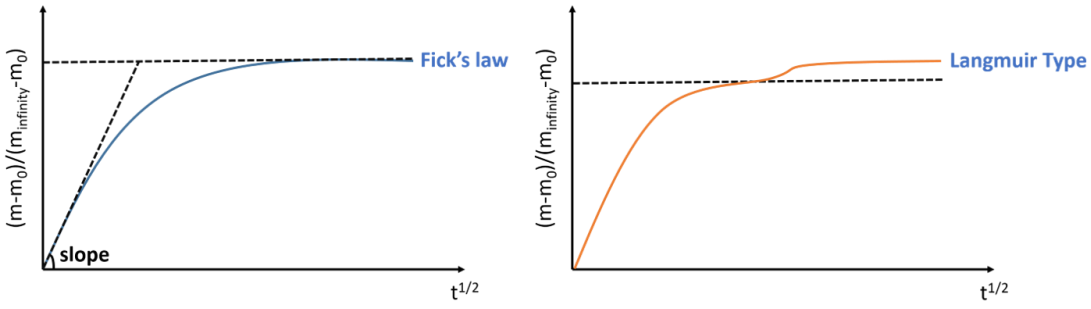

Figure 5.7: Water diffusion obeying Fick's law (a); Water diffusion appearing Langmuir mechanism (b).

In the case of Fickian diffusion, the equation for water transport is:

$$\frac{\partial C}{\partial t} = -D\frac{\partial^2 C}{\partial x^2} \qquad \textit{Equation 5.7}$$

where C (mol m^3) is the concentration of water absorbed at time t (s) at depth x (m) and D (m^2 s^{-1}) is the diffusion coefficient in the polymer matrix.

Fick's law is characterized by a linear increase in water concentration as a function of the square root of time, then a saturation plateau corresponding to the maximum concentration of water absorbed by the polymer. The diffusion coefficient can be determined from the slope represented in Figure 5.7a.

$$D = \frac{\pi}{16}e^2 \times slope \qquad \textit{Equation 5.8}$$

where e is the thickness of sample (7 µm in this case).

According to literature results, in the case of PEI and PEEK [14], the water diffusion coefficient in the PEI matrix decreases significantly with oxidation, because the diffusion of water would become essentially governed by the molecular interactions between water molecules and polar groups. In that case where the role of polymer-water interaction is important, Fick's law is not relevant to describe the relevant sorption kinetic, and it seemed to us that the Langmuir type of diffusion is better adapted to describe diffusivity.

Carter and Kibler [15] have developed the so-called Langmuir-type attributed to the presence of sites generating strong bonding with diffusion water [16] aimed at describing sorption curves given in Fig 5.7b. In this model, the first part of the kinetic curve is described by Fick's model where the mass increases linearly with the square root of time. They suggested a model involving bound and mobile water, which corresponds well to the water diffusion behavior in a polymer with polar groups (e.g. epoxy resins [17]) favoring polymer-water interaction. Later, Popineau et al. [17] confirmed the existence of those two types of water by NMR experiments, with a sorption mechanism represented in Figure 5.8.

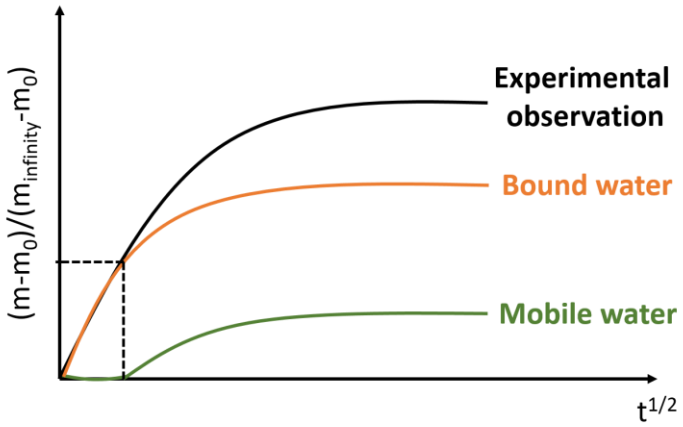

Figure 5.8: Schematic diagram of changes of mobile and bound water according to Popineau et al. [17].

The principle of diffusion of bound water could be tentatively schematized by the following steps [2]:

(1) $[P_1 \dots W] \rightarrow P_1 + W$

(2) $W \rightarrow$

(3) $W + P_2 \rightarrow [P_2 \dots W]$

At the beginning of absorption, the water molecules have strong interactions with the polymer. Then diffusion of bound water occurs. A water molecule jumps from a site P_1 to a site P_2. After a given time, the interaction sites for water molecules become saturated thus absorption reaches a quasi-equilibrium (Figure 5.8 - Bound water).

In the situation depicted in Fig. 5.8, the diffusivity of bound water can be estimated from the slope based on Fick's law [18], just as shown in Figure 5.9a. Therefore, the values of apparent diffusivity determined above are valuable for further discussion. We can observe that the diffusivity is a decrease function with water volume fraction namely the oxidation level (Fig 5.9b) which accords with literature results [2].

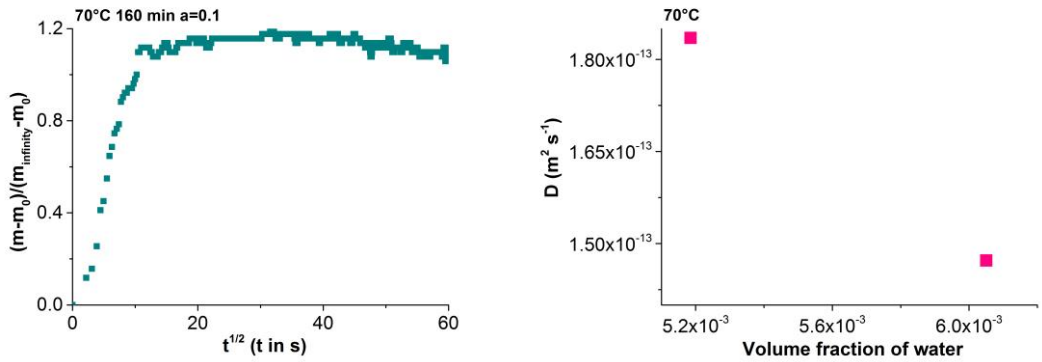

(a) **(b)**

Figure 5.9: Relative mass uptake curve for PDCPD aged at 70°C for 160 minutes (a); Diffusion coefficient for 0.1 activity as a function of oxidation time for samples aged at 70°C before characterization in DVS (b).

In conclusion, we can see that unaged PDCPD is a very apolar polymer that absorbs a very amount of water. When it undergoes oxidation, polar groups are created. The presence of these polar groups leads to a large increase in water content absorbed by the polymer. These conclusions are based on oxidation performed at one temperature (i.e. 70°C) for several durations. The remaining question is that can we generalize this behavior to any oxidation temperature in order to be able to connect water absorption behavior with the oxidation level in PDCPD.

2.3 Effect of temperature

Oxidation of PDCPD has been performed at 50°C and 25°C to verify if the results observed at 70°C depend on temperature. The results are presented in Figures 5.10a and b. For both ageing temperatures, there is a clear increase in water content after the thermal ageing of PDCPD, regardless of the water activity (Figures 5.10a and b). Moreover, for the same water activity, the water content increases as a function of the oxidation time.

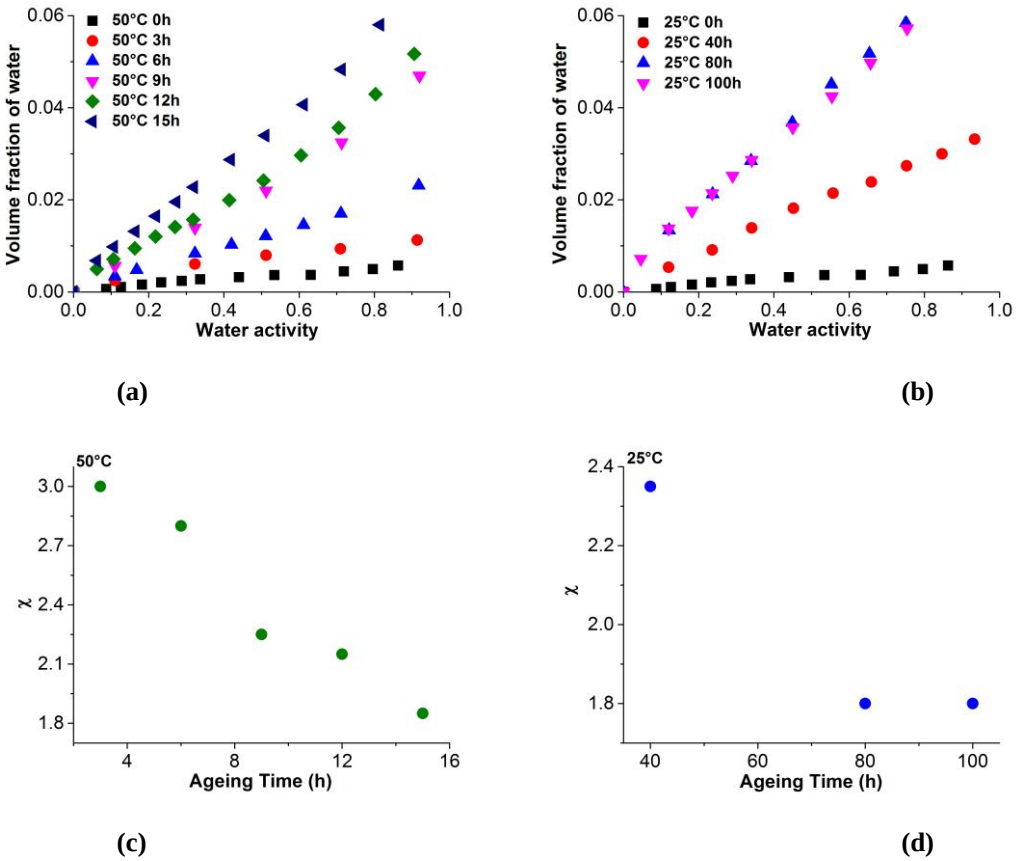

Figure 5.10: Water sorption isotherm for PDCPD tested at 50°C with different oxidation time at 50°C in oven (a); tested at 25°C with different oxidation time at 25°C (b); Changes on interaction parameters with oxidation time for samples aged at 50°C (c) and 25°C (d).

Here again, we focus first on water absorption mechanisms to see if there is an impact of testing temperature on this behavior. The three conclusions drawn for ageing at 70°C are verified. Firstly, the Henry's law is not able to describe correctly the water absorption behavior at high water activity. Secondly, the relevant cluster sizes were calculated. It shows that the mean cluster size for samples aged at 50°C and 25°C is in the range from 0 -1.4, meaning that the tendency to form water clusters is very slight. Finally, Flory-Huggins equation makes it possible to describe the corresponding water absorption behavior at 50°C and 25°C. Figures 10c and d display that the interaction parameters are decreasing functions with oxidation time for both ageing temperatures, which is in accord with the results obtained for samples aged at 70°C.

Chapter 3 has reported that the changes in the FTIR spectroscopy results. The band centered on the hydroxyl zone and carbonyl zone correspond to changes in concentrations of degradation

products during the thermal aging of PDCPD. The hydroxyls and carbonyls (ketones, aldehydes, and carboxylic acids), as the main oxidation products of PDCPD, also influence the water transport properties since they are the most polar products (containing OH groups and C=O groups). Their concentrations were calculated using Beer-Lambert law from the absorbance of the wide IR band centered at 3430 cm^{-1} and 1710 cm^{-1}.

Based on results obtained after ageing at 70, 50 and 25°C, it is possible to relate Flory-Huggins interaction parameter with the carbonyl C=O content in the material. As we can see, the parameter $\chi \times RT$ expressing the polarity difference between water and polymer $(\delta_{polymer} - \delta_{water})^2$ (Equation 5.6) decreases with the carbonyl concentration (Figure 5.13). Moreover, it appears that a mastercurve linking the water content in this material as a function of the oxidation level exists for all temperatures and ageing time considered here. These results further confirmed that the generated polar groups due to thermal oxidation increases the polymer solubility thus decrease the interaction parameter.

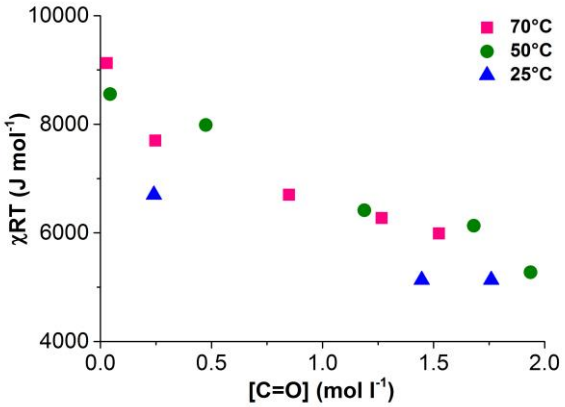

Figure 5.11: Changes on interaction parameters as a function of carbonyls concentration before characterization in DVS for samples aged at 70°, 50°C and 25°C.

The same "quasi-Fickian" behaviors are verified for low water activity (0.1 activity) for samples aged at 50°C and 25°C for long ageing time. Assessed diffusivity values were versus reciprocal of water volume fraction. As we can see, diffusivity is a decreasing function of the water volume fraction (Figure 5.14). This trend can be explained as follows: the appearance of polar species increases water solubility in polymer, but water becomes more and more bonded

with polymer oxidation products so that its diffusivity decreases during oxidation.

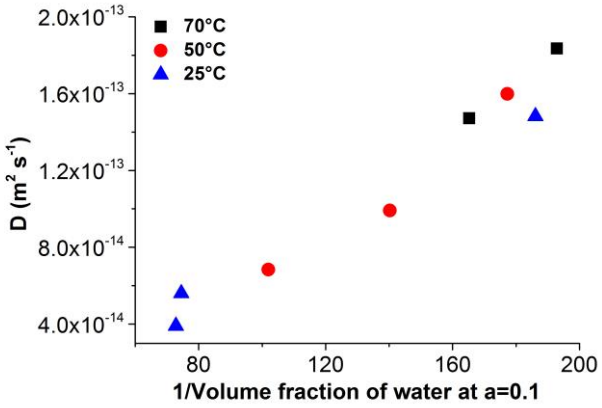

Figure 5.12: The diffusion coefficient for 0.1 activity as a function of reciprocal of water volume fraction.

2.4 Relation between water sorption and polar groups

In the last part of this chapter, a relation between water sorption and polar groups formed during thermal oxidation will be determined.

As we know, the absorbance of carbonyl at 1710 cm^{-1} results from ketones, aldehydes and carboxylic acids. The treatment of NH_3 enables us to identify carboxylic acid and estimate the relevant concentration, because ammonia can convert acid into ammonium carboxylates centered at 1550 cm^{-1} [19]. As a result, the presence of carboxylic acid is verified as shown in Figure 5.13, which is in line with literature results [20]. On the other hand, the wide peak at 3410 cm^{-1} corresponds to hydroxyls containing alcohols, carboxylic acids and hydroperoxides. The absorbances of carbonyls and hydroxyls were converted into concentrations using Beer-Lambert's law with $\varepsilon_{C=O}$ = 300 and ε_{OH} = 70 l mol^{-1} cm^{-1} [21]. The relation between the concentration of hydroxyls and carbonyls and the corresponding chemical substances can be summarized as:

$$[OH]\ (3410\ cm^{-1}) = [alcohols] + [hydroperoxids] + [carboxylic\ acids]$$

Equation 5.9

$$[C=O]\ (1710\ cm^{-1}) = [ketones] + [carboxylic\ acids]$$ *Equation 5.10*

The concentration of carboxylic acids can be calculated by the difference of absorbance before and after NH_3 treatment by using the equation 5.11.

$$[carboxilyc\ acids] = \frac{[C=O]}{1+\frac{\varepsilon_{carboxylic\ acids}}{\varepsilon_{ketones}}\times(1-\frac{A_{carboxylic\ acids}}{A_{ketones}})}$$ *Equation 5.11*

with $\varepsilon_{\text{carboxylic acids}}$ = 680 l mol^{-1} s^{-1} [22] and ε_{ketone} = 200 l mol^{-1} s^{-1} [23].

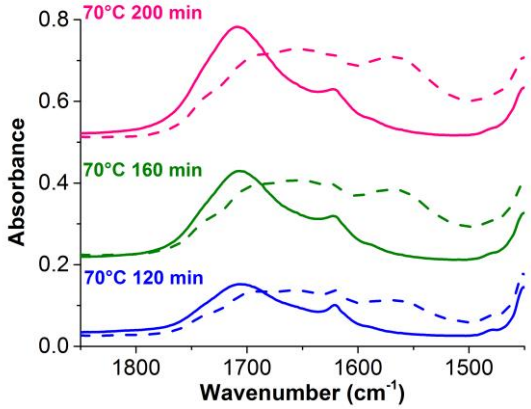

Figure 5.13: Effect of NH_3 treatment (full lines: before, dashed lines: after) for PDCPD exposed at 70°C under air.

By applying equation 5.9, 10 and 11, we can estimate the sum of the concentration of OH in alcohols and concentration of OH in hydroperoxides (i.e. $[\text{alcohols}] + [\text{hydroperoxids}]$), and the concentration of ketones (i.e. $[ketones]$). Table 5.2 shows the water volume fraction at 0.9 water activity and the relevant concentration of polar groups.

Therefore, a relation between water volume fraction and concentration of polar groups is determined by equation 5.12:

$$f_w = a[carboxylic\ acids] + b([alcohols] + [hydroperoxids]) + c[ketones]$$ *Equation 5.12*

with $a = 0.0889$, $b = 0.0028$ and $c = 0.001$.

We can see that carboxylic acids formed during thermal oxidation are more polar and create a stronger interaction with water compared to ketones and hydroxyls.

Temperature (°C)	70	70	70	50	50	50	25
Ageing Time (h)	2	2.67	3.33	9	12	15	100
fw at a=0.9	0.04	0.043	0.051	0..037	0.052	0.070	0.075
[OH] (mol l^{-1})	2.86	3.74	4.24	3.99	5.14	5.63	3.54
[C=O] (mol l^{-1})	0.85	1.27	1.52	1.191	1.68	1.94	1.76
[hydroperoxides] (mol l^{-1})	0.97	1.20	1.1	1.4	1.55	1.59	1.5
[carboxylic acids] (mol l^{-1})	0.23	0.39	0.49	0.35	0.54	0.64	0.60
[alcohols]+[hydroperoxides] (mol l^{-1})	2.63	3.35	3.74	3.64	4.60	5	2.94
[ketones] (mol l^{-1})	0.61	0.88	1.03	0.84	1.14	1.30	1.16

Table 5.2: Concentration of polar groups during ageing.

According to Table 5.2, some approximate ratios can be obtained:

$$[hydroperoxides] = 1/3[OH] \qquad \textit{Equation 5.13}$$

$$[ketons] = 2/3[C = O] = 2[carboxylic\ \ acids] \qquad \textit{Equation 5.14}$$

As we have seen in chapter 3, the kinetic model enables to predict the carbonyls concentration ([C=O]) and hyroperoxides concentration ([POOH]), with equation 5.13 and 14, we can directly estimate the concentration of ketones ([ketones]) and carboxylic acids ([carboxylic acids]). By applying equation 5.9, we can obtain the sum of concentration of alcohols and hydroproxides ([alcohols]+[hydroperoxides]). As a result, kinetic model can predict the water volume fraction thus the relevant diffusivity and interaction parameter using the mastercurves given in Figure 5.11 and 5.12. In other words, modeling approach can be used to predict PDCPD resistance in

presence of water.

3. Conclusions

This chapter deals with the water sorption behavior of virgin and aged PDCPD. Sample firstly aged at different temperatures (25°C- 70°C) in the oven then tested by DVS. According to DVS results, unaged PDCPD presents low water absorption ability within the temperature range considered here, whereas large water uptake can be observed when samples undergo thermal oxidation. For instance, the aged one (aged at 70°C for 160 minutes) presents 10 times higher water content than the virgin one. The water absorption mechanism has been studied. It was shown water sorption isotherm could not be described by Henry's law, and the mean cluster size estimated from the Zimm-Lundberg theory is low enough to be neglected whatever the water activity. Thus, the Flory-Huggins equation which shows a good fitting is selected to describe the water sorption behavior of PDCPD. The interaction parameter related to Flory-Huggins equation decrease with the oxidation level (i.e. ageing time). Since diffusivity of water decreases with water volume fraction, the interaction between water and polar sites of polymer plays an important role in water sorption and diffusion. The absorption kinetic can be described by Langmuir-type model involving bound water and mobile water. The fact that all these properties (volume fraction of water, interaction parameter and water diffusion coefficient) change with the oxidation level is closely related to polar groups (hydroxyls and carbonyls groups) created during thermal oxidation of PDCPD. A mastercurve showed that the interaction parameter is almost a linear function of carbonyl concentration. Since the kinetic model created for virgin PDCPD describes the carbonyls changes with ageing time, it is possible to predict water absorption in service conditions over time. If the effect of water on oxidation mechanism could be investigated (it is for example reported that water accelerates the decomposition of peroxides [24]). It remains in particular to address the effect of water uptake on mechanical properties of aged PDCPD.

4. References

[1] P. Y. Le Gac, D. Choqueuse, M. Paris, G. Recher, C. Zimmer, and D. Melot, "Durability of polydicyclopentadiene under high temperature, high pressure and seawater (offshore oil production conditions)," *Polymer Degradation and Stability*, vol. 98, no. 3, pp. 809–817, Mar. 2013.

[2] I. Merdas, F. Thominette, A. Tcharkhtchi, and J. Verdu, "Factors governing water absorption by composite matrices," *Composites Science and technology*, vol. 62, no. 4, pp. 487–492, 2002.

[3] B. Fayolle and J. Verdu, *Vieillissement physique des matériaux polymères*. Ed. Techniques Ingénieur, 2002.

[4] E. Gaudichet-Maurin, "Caractérisation et vieillissement d'une membrane d'ultrafiltration d'eau," 2005.

[5] B. Pomes, I. Derue, A. Lucas, J.-F. Nguyen, and E. Richaud, "Water ageing of urethane dimethacrylate networks," *Polymer degradation and stability*, vol. 154, pp. 195–202, 2018.

[6] E. M. Davis and Y. A. Elabd, "Water clustering in glassy polymers," *The Journal of Physical Chemistry B*, vol. 117, no. 36, pp. 10629–10640, 2013.

[7] B. H. Zimm and J. L. Lundberg, "Sorption of vapors by high polymers," *The Journal of Physical Chemistry*, vol. 60, no. 4, pp. 425–428, 1956.

[8] J. Lundberg, "Clustering theory and vapor sorption by high polymers," *Journal of Macromolecular Science, Part B: Physics*, vol. 3, no. 4, pp. 693–710, 1969.

[9] P. Y. Le Gac, G. Roux, P. Davies, B. Fayolle, and J. Verdu, "Water clustering in polychloroprene," *Polymer*, vol. 55, no. 12, pp. 2861–2866, Jun. 2014.

[10] M. Kurata, *Thermodynamics of Polymer Solutions*. CRC Press, 1982.

[11] J. Burke, "Solubility parameters: theory and application," *The Book and Paper Group Annual*, vol. 3, pp. 13–58, 1984.

[12] D. W. Van Krevelen and K. Te Nijenhuis, "Chapter 7 - Cohesive Properties and Solubility," in *Properties of Polymers (Fourth Edition)*, D. W. Van Krevelen and K. Te Nijenhuis, Eds. Amsterdam: Elsevier, 2009, pp. 189–227.

[13] J. Crank, *The mathematics of diffusion*. Oxford university press, 1979.

[14] E. Courvoisier, "Analyse et modélisation cinétique du vieillissement thermique des

matrices PEI et PEEK et ses conséquences sur l'absorption d'eau," Ecole nationale supérieure d'arts et métiers - ENSAM, 2017.

[15] H. G. Carter and K. G. Kibler, "Langmuir-type model for anomalous moisture diffusion in composite resins," *Journal of Composite Materials*, vol. 12, no. 2, pp. 118–131, 1978.

[16] A. Tcharkhtchi, P. Bronnec, and J. Verdu, "Water absorption characteristics of diglycidylether of butane diol–3, 5-diethyl-2, 4-diaminotoluene networks," *Polymer*, vol. 41, no. 15, pp. 5777–5785, 2000.

[17] S. Popineau, C. Rondeau-Mouro, C. Sulpice-Gaillet, and M. E. Shanahan, "Free/bound water absorption in an epoxy adhesive," *Polymer*, vol. 46, no. 24, pp. 10733–10740, 2005.

[18] P. Gilormini and J. Verdu, "On the role of hydrogen bonding on water absorption in polymers," *Polymer*, vol. 142, pp. 164–169, 2018.

[19] C. Wilhelm and J. Gardette, "Infrared identification of carboxylic acids formed in polymer photooxidation," *Journal of Applied Polymer Science*, vol. 51, no. 8, pp. 1411–1420, 1994.

[20] E. Richaud, P. Y. Le Gac, and J. Verdu, "Thermooxidative aging of polydicyclopentadiene in glassy state," *Polymer Degradation and Stability*, vol. 102, pp. 95–104, Apr. 2014.

[21] E. Richaud, F. Farcas, B. Fayolle, L. Audouin, and J. Verdu, "Hydroperoxide titration by DSC in thermally oxidized polypropylene," *Polymer Testing*, vol. 25, no. 6, pp. 829–838, Sep. 2006.

[22] F. M. Rugg, J. J. Smith, and R. C. Bacon, "Infrared spectrophotometric studies on polyethylene. II. Oxidation," *Journal of Polymer Science*, vol. 13, no. 72, pp. 535–547, 1954.

[23] M. Coquillat, J. Verdu, X. Colin, L. Audouin, and R. Nevière, "Thermal oxidation of polybutadiene. Part 2: Mechanistic and kinetic schemes for additive-free non-crosslinked polybutadiene," *Polymer Degradation and Stability*, vol. 92, no. 7, pp. 1334–1342, Jul. 2007.

[24] J. L. Henry, A. L. Ruaya, and A. Garton, "The kinetics of polyolefin oxidation in aqueous media," *Journal of Polymer Science Part A: Polymer Chemistry*, vol. 30, no. 8, pp. 1693–1703, 1992.

Conclusions and prospects

The aim of this thesis was to predict lifetime of polydicyclopentadiene (PDCPD) which is a thermoset synthesized by ROMP and considered in particular as a candidate for field-joint application in marine environment for oil-extraction application. In such conditions of use, PDCPD is subjected to moderate temperatures and water environment. It was already documented that unsaturated hydrocarbon polymers undergo thermal oxidation leading to the drop of their mechanical properties. However, PDCPD is an original case because it is the only (to our knowledge) hydrocarbon polymer oxidized in its glassy state with a high concentration in residual double bonds after polymerization, together with an elevated concentration in organometallic catalysts being somehow detrimental to its long term stability.

According to existing literature data, it was already documented that:

- the stress yield of PDCPD increases with ageing time, which is linked to increasing of crosslink density during thermal oxidation,

- the thermal oxidation of PDCPD is only confined on the surface due to the effect of diffusion limited oxidation.

It was however difficult to extrapolate the existing data to predict lifetime at a lower temperature. For that purpose, we have chosen to implement a kinetic modeling approach based on the rate of chemical processes involved in oxidation and stabilization of PDCPD.

The first step addressed the oxidation of additive-free PDCPD. In addition to the well-known stable trackers such as carbonyls, we paid particular attention to double bonds consumption. In fact, a multiscale study comparing changes in strain at break and yield stress measured from tensile tests with changes in concentration of remaining double bonds and formed carbonyls (from FTIR data) gave a “structure-properties” relationships linking changes at molecular scale with changes in mechanical properties. This indicates that a kinetic model able to predict chemical changes during oxidation would allow predicting the lifetime from a mechanical point of view. The kinetic model was derived from the Basic Autoxidation Scheme for hydrocarbons and involved several kinetic parameters which must be accurately estimated to perform a reliable lifetime prediction of PDCPD. For that purpose, the model has to simulate not only

changes in double bonds and carbonyls but also the changes in hydroperoxides, those latter being the key intermediates of radical oxidation and an excellent criterion to validate the model. This was however not sufficient since several sets of rate constants could actually lead to comparable and acceptable simulations. For determining the best set of rate constants, several "selective" experiments were conducted: ageing tests under varying oxygen pressures were performed to "isolate" the rate constants values for radical terminations and reactions between alkyl or peroxy radicals and double bonds. Some experiments of hydroperoxides thermolysis were also conducted. It was shown that hydroperoxides decompose mostly by a bimolecular process, with a unimolecular decomposition coexisting in the earlier exposure times. This latter would be favored by the use of high ROMP catalyst used for synthesizing materials but it has a limited influence on the overall oxidation rate. The kinetic model was able to simulate oxidation of PDPCD in particular in the 120 - 50°C temperature range and under 0.02 to 1.0 MPa oxygen pressures. Its rate constants can hence be extrapolated to lower temperatures corresponding to service conditions to perform a lifetime prediction.

The oxidation of thick samples was thus studied. It was shown that PDCPD oxidizes only in a very thin superficial layer (in comparison with many other thermosets) mainly because oxygen permeability is moderate and surface oxidation rate is very elevated. This specific feature of additive-free PDCPD was acceptably simulated by the kinetic model. For a better simulation of ageing in real conditions, it must now be checked if the permeability of oxygen in PDCPD changes with ageing time for example because free volume changes being induced by crosslinking.

In the second step, the thermal oxidation was carried out on stabilized PDCPD in order to get closer to "real materials". The challenge was to propose antioxidants that can be added to the reactive mixture without inhibiting polymerization and curing, together with displaying an efficient stabilizing role. We have thus compared a "classical" hindered phenol (BHT) and two Hindered Amines Stabilizers: Tinuvin 123 and Chimassorb 2020. The first one had the potential advantage of being an "activated" form (alkoxyamine) meanwhile the second one was expected to display a limited physical loss. Samples with iso-concentration in functional groups of antioxidants were compared in terms of carbonyl kinetic build-up. Tinuvin 123 presents the best anti oxidation performance compared with Chimassorb 2020 and BHT despite it was

shown that the solubility and evaporation problems could exist for Tinuvin 123 at higher concentrations. The stabilization mechanisms of these antioxidants were described as elementary reactions and the relevant kinetic parameters were obtained by an inverse approach (i.e. best curve fitting while respecting reasonable orders of magnitude). In particular, hindered amine light stabilizers were shown to be a promising candidate with good stabilizing properties and limited effect on the catalyzed ROMP. This stabilizing effect might be counterbalanced by an increase in the Thickness of Oxidized Layer but this remains to be fully described and modeled in the next works.

In the final step, in link with conditions of use, the impact of thermal oxidation on water absorption behavior was investigated. It was shown that virgin PDCPD displays very low water absorption because of its apolar structure. PDCPD hydrophilicity increases as the ageing time increases. This phenomenon was explained by the appearance of oxidation products creating stronger interactions with the water molecules. The possible effect on water diffusion was also addressed. The effect of water plastification on mechanical properties remains to be investigated in the future.

Finally, these successive steps enable a lifetime prediction of PDCPD by kinetic modeling from a fundamental point of view, the kinetic model was created for additive-free and stabilized PDCPD during thermal oxidation at 20°C to 120°C. It was in particular observed that the kinetic modeling approach can be implemented even in the case of glassy materials where mobility is considered as low. From a practical point of view, we hope its predictive capacities can help engineers for a better design of polymer structures subjected to severe conditions.

Appendix 1: Experimental results

The theoretical treatments were applied for thermolysis experiments in the low concentration domain: the results for L-PDCPD and H-PDCPD aged at 90°C and 50°C are presented in the figures below:

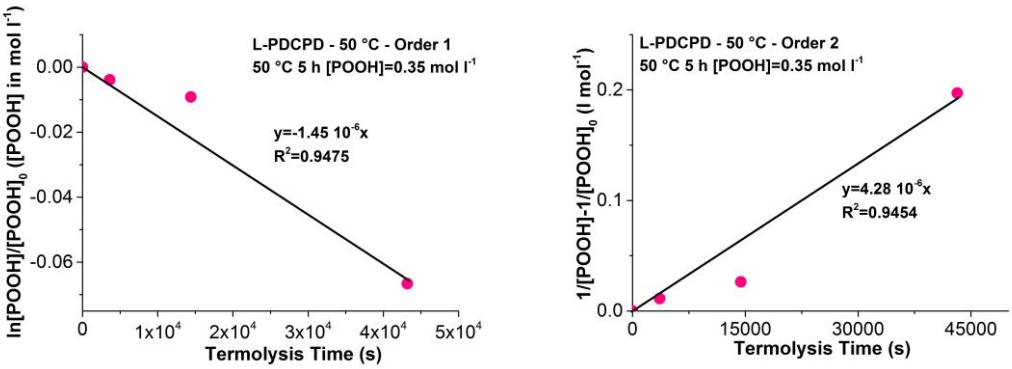

(a)

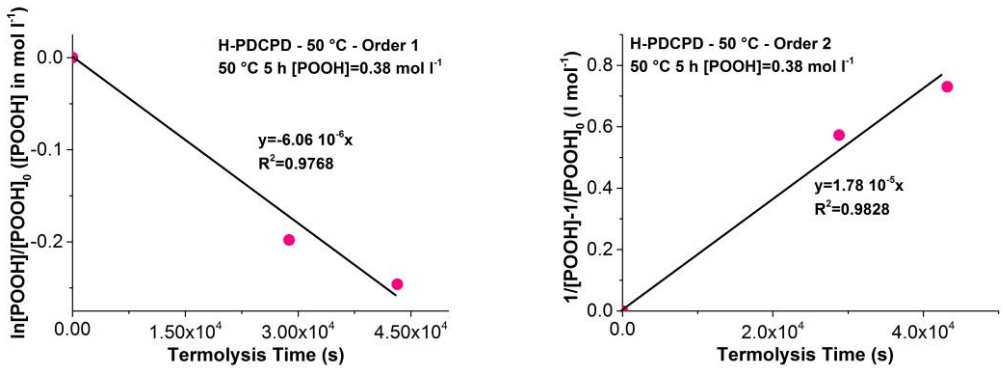

(b)

Figure A1.1: Linear equation of order 1 (left) and 2 (right) for L-PDCPD samples aged 5 hours at 50°C (a); for H-PDCPD samples aged 5 hours at 50°C (b).

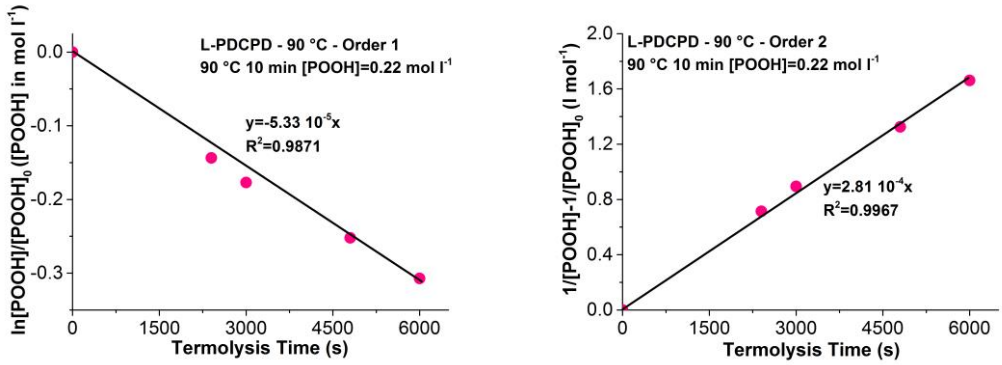

(a)

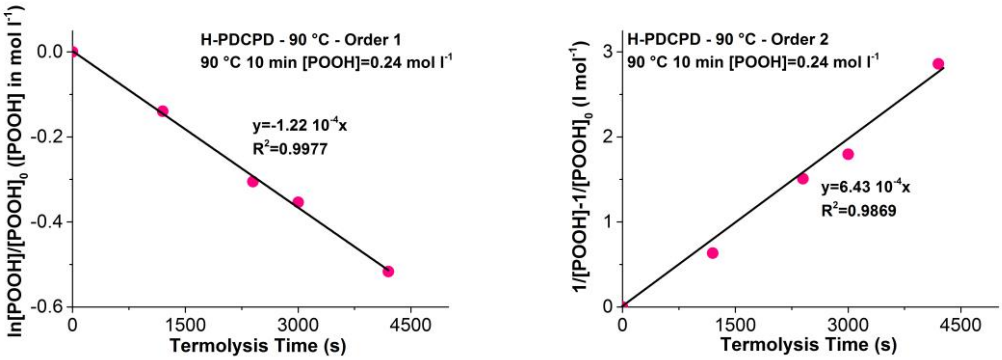

(b)

Figure A1.2: Linear equation of order 1 (left) and 2 (right) for L-PDCPD samples aged 10 minutes at 90°C (a); for H-PDCPD samples aged 10 minutes at 90°C (b).

Appendix 2: French summary

Introduction

Le prix Nobel de chimie 2005 a été attribué à Yves Chauvin, Robert H. Grubbs et Richard R. Schrock pour le développement de la réticulation par métathèse en synthèse organique. Après sa découverte dans les années 70, la réaction de métathèse d'oléfines a été largement développée et utilisée dans les industries pharmaceutiques et polymères. Le polydicyclopentadiène (PDCPD) est l'un des polymères les plus utilisés dans l'industrie, obtenu par polymérisation par métathèse par ouverture de cycle (ROMP). Il présente des propriétés particulièrement intéressantes d'un point de vue technique et économique : une ténacité élevée, une densité proche de 1, une bonne résistance chimique aux acides et aux bases en raison de sa structure hydrocarbonée, un temps de traitement court (moins de 5 minutes). La nouvelle génération de catalyseurs métalliques est insensible à l'oxygène et à l'eau et permet une polymérisation facile dans des conditions ambiantes.

Au vu de ses propriétés intrinsèques, ce polymère peut donc être envisagé pour une utilisation dans des environnements sévères, en particulier dans le milieu marin pour l'extraction de pétrole. Une potentielle utilisation de ce matériau pour les revêtements d'isolation de pipe est conditionnée (entre autres) par une forte durée de vie, typiquement 20 ans. Or la forte concentration en doubles liaisons dans le polymère et l'utilisation d'une concentration élevée de catalyseur pour la mise en œuvre par ROMP devraient renforcer l'instabilité chimique par rapport aux autres polymères hydrocarbonés, la question de la durabilité du PDCDP semble donc primordiale. D'autant plus qu'a notre connaissance, peu d'études ont portés sur la durée de vie de polymère thermodurcissable obtenue par ROMP.

Cette thèse a donc été réalisée dans le cadre du projet VRPOM « Vieillissement de Réseaux POlymérisés par Métathèse » accordé par l'ANR et associant l'Institut des Molécules et Matériaux du Mans (expert en métathèse), IFREMER (expert en vieillissement des polymères), société TELENE SAS (expert en fabrication de PDCPD) et Procédés et Ingénierie en Mécanique et Matériaux de Arts et Métiers ParisTech (expert en vieillissement des polymères et prévision de la durée de vie). La méthode de prévision de la durée de vie repose toujours sur des tests de vieillissement accéléré, qui doivent ensuite être extrapolés aux conditions de service. Compte tenu de la faible fiabilité des approches empiriques existantes, nous avons décidé

d’utiliser une approche plus moins empirique basée sur la compréhension des mécanismes et de la cinétique de dégradation.

Dans le premier chapitre de cette thèse, une présentation générale de ce polymère sera faite en termes de son mécanisme de polymérisation, des catalyseurs utilisés dans la ROMP et de son procédé de fabrication. Les études de vieillissement existantes de PDCPD seront présentées, y compris les modifications des propriétés mécaniques liées à la réticulation induite par l'oxydation thermique. En outre, les relations structure-propriété seront détaillées pour appuyer davantage cette explication. Le modèle cinétique non empirique adopté dans ce travail sera décrit dans ce chapitre, ainsi que l’étude mécanistique de l’oxydation thermique. L'approche permettant de décrire l'effet de la pression en oxygène, des antioxydants et de la diffusion de l'oxygène sera décrite afin d'établir une stratégie appropriée pour l'étude de la stabilité à l'oxydation de ce matériau en conditions de service.

Le deuxième chapitre présentera les matériaux et les méthodes expérimentales utilisés dans cette étude. Les différentes conditions d'exposition seront détaillées avec les méthodes de caractérisation des modifications chimiques et mécaniques au cours de l'oxydation thermique.

L’investigation du chapitre suivant (chapitre 3) part du cas le plus simple, à savoir PDCPD sans additif. L’objectif de cette partie est d’identifier les principaux produits d’oxydation, de proposer un mécanisme de dégradation et d’établir une relation structure-propriété permettant la prédiction de la fragilisation. Les résultats seront utilisés pour établir un modèle cinétique de PDCPD sans additif et déterminer certains paramètres cinétiques. Le modèle sera testé et validé par comparaison avec des expériences de vieillissement dans une large gamme de conditions expérimentales variant en fonction de la pression en oxygène (pour isoler certaines constantes de vitesse) et des températures (pour effectuer des extrapolations). La dernière partie de ce chapitre traitera de l'effet de la diffusion limitée de l'oxygène pour le PDCPD sans additif, qui sera étudié et modélisé par le modèle cinétique afin de prédire le comportement du matériau lorsqu’il est utilisé en forte épaisseur.

Ensuite, le chapitre 4 se concentrera sur le développement d’un modèle cinétique plus complet intégrant l’effet des antioxydants. Deux familles d’antioxydants seront considérées ici

(phénoliques et amines encombrées), elles se différencient par leurs mécanismes d'action (sacrificiel vs régénératif), l'impact de leur masse molaire (avec des effets sur les performances physiques telles que la limitation de l'évaporation) sera étudiée et leur efficacité pour ralentir la vitesse d'oxydation sera comparée. Les réactions de stabilisation seront décrites par de nouvelles constantes de vitesse, qui seront déterminées à partir des résultats expérimentaux et de la littérature. A partir des données expérimentales couplées au modèle cinétique, l'origine de la différence d'efficacité entre ces différents stabilisants sera discutée. Ces résultats nous aideront à choisir des stabilisants adaptés à la polymérisation de ROMP et à améliorer leur durée de vie.

Dans le dernier chapitre, l'effet de l'oxydation thermique du PDCPD sur le comportement de l'absorption d'eau sera étudié pour traiter le cas de l'oxydation thermique en milieu marin. Pour ce faire, nous comparerons les propriétés et les mécanismes de pénétration de l'eau (solubilité et diffusion) dans le PDCPD vierge (qui est par essence apolaire et donc hydrophobe) et dans celui vieilli thermiquement. Nous établirons provisoirement certaines relations décrivant le couplage entre le vieillissement thermique et le vieillissement de l'eau.

Une conclusion résumera les principaux résultats de cette thèse et proposera des travaux futurs possibles.

Résumé du chapitre 1 : Etude bibliographique

Ce premier chapitre est consacré à l'étude bibliographique du comportement du polydicyclopentadiène (PDCPD) et de l'oxydation thermique du polymère dans le but d'introduire la stratégie scientifique mise en œuvre dans cette étude. Tout d'abord, une présentation générale du contexte sera faite en considérant une description rapide du matériau, du processus de fabrication et des applications. Dans la seconde partie, les connaissances existantes sur l'oxydation thermique du PDCPD seront discutées, ainsi que la méthodologie de prédiction de la durée de vie; cette partie montrera comment l'approche mécanistique est utile pour une prédiction fiable. Ensuite, l'approche mécanistique sera détaillée en tenant compte de toutes les spécificités du PDCPD. Et enfin, nous proposerons une stratégie de travail pour modéliser l'oxydation thermique dans les PDCPD.

Contexte de l'étude

Le polydicyclopentadiène (PDCPD) est un polymère réticulé obtenu par polymérisation par métathèse par ouverture de cycle (ROMP) du monomère de dicyclopentadiène (DCPD). La ROMP, en tant qu'application de la métathèse des oléfines, est devenue une méthode efficace et puissante pour la synthèse de matériaux macromoléculaires. Une caractéristique majeure de cette réaction est que la double liaison insaturée dans le monomère peut encore rester dans le squelette carboné par rapport à toute autre forme de polymérisation. Le mécanisme de polymérisation du DCPD actuellement accepté, basé sur la proposition de Chauvin est décrit par la Figure A2.1 (voie a).

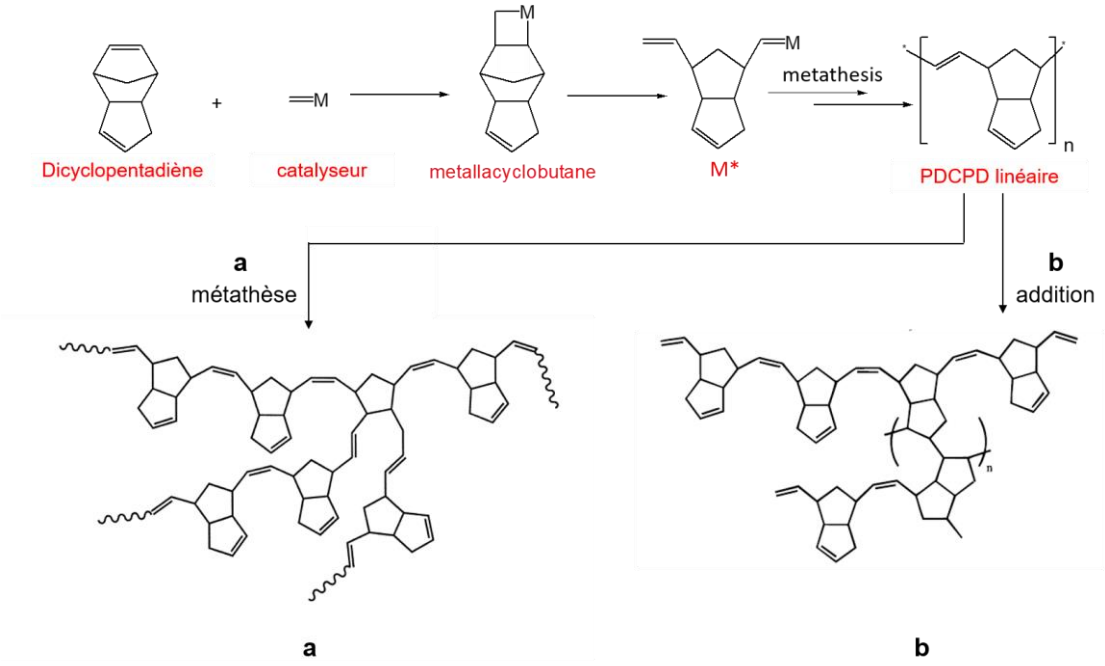

Figure A2.1: Deux mécanismes possibles pour la polymérisation du dicyclopentadiène.

Une autre possibilité concernant la polymérisation du DCPD a été proposé (voie b). Ces zones grises dans le mécanisme de réticulation compliquent la compréhension de la structure réticulée du PDCPD. La concentration restante en doubles liaisons (après polymérisation) doit donc être soigneusement déterminée avant de discuter du mécanisme de vieillissement.

Le catalyseur de ROMP est la clé de la préparation des matériaux PDCPD. Les catalyseurs les plus disponibles dans le commerce pour la méthathèse d'oléfines est les systèmes de catalyseurs alkylidènes métalliques. Tels systèmes catalytiques sont habituellement divisés en deux familles : les catalyseurs Schrock et les catalyseurs Grubbs. Les catalyseurs Schrock sont à base de Molybdène (Figure A2.2 a). Cependant, la manipulation des catalyseurs Schrock est plus exigeante, en raison de sa grande sensibilité à l'air et à l'humidité, par rapport aux catalyseurs Grubbs. Les catalyseurs de Grubbs sont des complexes d'alkylidènes à base de ruthénium (Figure A2.2 b,c,d). Avec plusieurs générations de développement, les catalyseurs Grubbs présentent de nombreux avantages dans les réactions ROMP : tolérance de nombreux groupes fonctionnels dans les substrats d'alcènes, stabilité à l'air et à l'humidité.

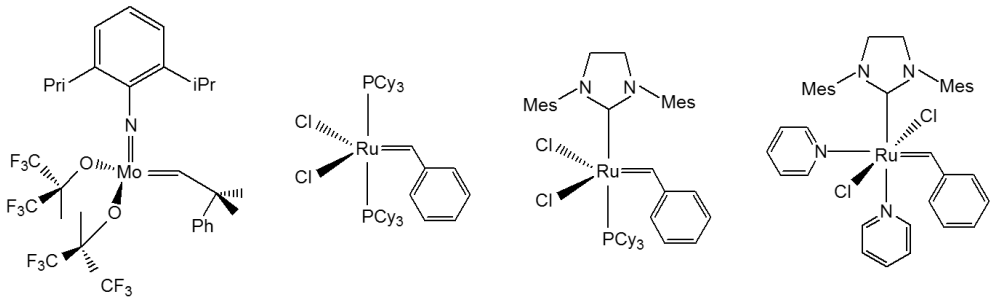

Figure A2.2: Différents catalyseurs pour la réaction ROMP.

La question de l'influence des catalyseurs et de leurs sous-produits sur la stabilité à long terme reste actuellement ouverte. En effet, on peut imaginer que le catalyseur peut potentiellement affecter la décomposition des hydroperoxydes selon un mécanisme qui sera détaillé dans la section suivante. Le choix des antioxydants est influencé par la nature catalyseur utilisé, car une interaction entre les antioxydants et le catalyseur peut se produire, ce qui peut entraîner des performances catalytiques plus faibles et une protection moins grande du polymère. Par conséquent, il est souhaitable d'étudier l'influence de différents systèmes de catalyseurs utilisés dans la polymérisation du DCPD.

Les résines PDCPD sont généralement traitées à l'aide du moulage par injection (RIM), car le ROMP du PDCPD répond généralement à la plupart des exigences d'un procédé RIM : faible viscosité du DCPD, polymérisation rapide avec un catalyseur approprié, aucun sous-produit gazeux. En utilisant un équipement RIM, deux composants constitués de DCPD et de catalyseur sont injectés simultanément dans un moule via une tête de mélange. La polymérisation démarre une fois que ces deux composants sont en contact. Par conséquent, à l'intérieur du moule, le mélange subit une réaction de ROMP pour produire du PDCPD. Ce processus libère de la chaleur et se termine en quelques minutes (généralement 5 min).

PDCPD présente des performances intéressantes : bonne performance d'impact, résistance chimique supérieure, très faible absorption. Dans cette thèse, PDCPD est considéré comme candidat à l'application sur Field-Joint dans l'industrie pétrolière offshore. La durée de vie requise pour ce Field Joint est de 20 ans. La question de la durabilité du PDCPD dans un

environnement offshore doit être évaluée.

Dégradation thermique du PDCPD à l'échelle macroscopique

Une étude précédente a montré une large modification des propriétés mécaniques dues à la réticulation lors du vieillissement thermo oxydatif du PDCPD. Par exemple, la contrainte au seuil d'écoulement augmente avec le temps de vieillissement. Autre que cela, l'oxydation induit une augmentation du module caoutchoutique. Ce phénomène peut s'expliquer par une forte augmentation de la densité du réseau due à la réaction sur la double liaison induite par l'oxydation du PDCPD (Figure A2.3).

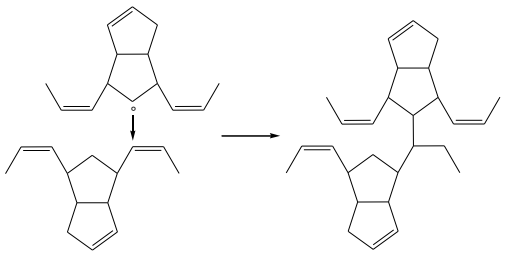

Figure A2.3: Réaction possible entre les radicaux et la double liaison pour former une réticulation.

En conclusion, la réticulation induite par l'oxydation induit une augmentation de la température de transition vitreuse, de la limite d'élasticité et du module caoutchoutique ainsi qu'une diminution de la ténacité. Ensuite, un modèle cinétique, qui sera détaillé dans la prochaine partie, pourrait prédire les changements dans la structure chimique et la densité de réticulation.

Cette étude a montré que l'oxydation thermique du PDCPD est confinée qu'à la surface, car l'oxygène diffusant à partir de l'environnement extérieur atteint à peine à l'intérieur de l'échantillon.

Il apparaît clairement que l'oxydation thermique est l'une des principales voies de dégradation de PDCPD. Mais la question est maintenant de savoir comment prévoir cette dégradation avec le temps et l'espace; c'est l'objectif de la section suivante.

Prédiction de la durée de vie

Dans des conditions de service, la dégradation des polymères d'hydrocarbures tels que le PDCPD est due (entre autres) à des réactions d'oxydation, qui produiront une perte de propriétés mécaniques. À une température donnée, la durée de vie t_F est définie par le temps d'exposition après lequel la propriété mécanique P atteint une valeur critique (P_F) appelée critère de fin de vie. Parmi les nombreuses méthodes existantes de prévision de la durée de vie, la méthode empirique et la moins empirique sont présentées et comparées ci-dessous. La loi d'Arrhenius (méthode empirique) est couramment utilisée dans l'industrie pour prédire la durée de vie de matériaux qui subit un vieillissement thermiquement. Néanmoins, de nombreux auteurs ont posé des questions sur la validité continue de la méthode « Arrhenius » et ont démontré un comportement non-arrhéniene en cas d'oxydation. Un tel écart entraîne une perte de fiabilité dans la prédiction de la durée de vie du polymère. C'est la raison pour laquelle une autre méthode de prédiction doit être développée.

Une approche non empirique est développée et prend en compte les changements structurels à plusieurs échelles (moléculaire, macromoléculaire, morphologique et macroscopique), permettant ainsi une prédiction fiable de la durée de vie des polymères. Cette approche multi-échelle repose sur la connaissance des mécanismes et de la cinétique de dégradation. Le principe de cette méthode est illustré ci-dessous :

L'oxydation thermique a d'abord lieu à l'échelle moléculaire : les mécanismes de dégradation chimiques doivent être compris et convertis en un schéma mécanistique de dégradation consistant en des réactions élémentaires obéissant à la loi d'Arrhénius. En appliquant une cinétique chimique, un modèle cinétique composé d'un système d'équations différentielles est établi. Sa solution numérique donne accès aux changements de composition chimique. Dans le cas de matériaux épais, l'utilisation d'un couplage réaction-diffusion dans ce modèle cinétique permet de prédire l'épaisseur des couches dégradées. Les changements à l'échelle moléculaire ont des conséquences sur l'échelle macromoléculaire à laquelle ce modèle cinétique permet également de prédire le nombre de scissions en chaîne et les actions de réticulation. Enfin, les modifications à l'échelle moléculaire du polymère manifestent sur les propriétés physiques à l'échelle macroscopique. Ainsi, la relation structure-propriétés permet de prédire les

changements de comportement mécanique lors de la dégradation du matériau.

Ce travail porte principalement sur la première étape de la méthode multi-échelle, à savoir l'étude de l'oxydation thermique à l'échelle moléculaire. Étant donné que le modèle cinétique est basé sur le schéma mécanistique de l'oxydation thermique du PDCPD, les aspects mécanistiques seront abordés en détail dans la section suivante.

Aspects mécanistiques de l'oxydation thermique du PDCPD

En raison de la complexité structurelle du PDCPD, il est nécessaire de comprendre le mécanisme d'oxydation thermique d'un polymère insaturé plus proche de notre cas. Ainsi, le mécanisme d'oxydation thermique des polymères insaturés (PB, PI et CR) est choisi comme référence pour les études sur les PDCPD. La présence de doubles liaisons doit être prise en compte, ce qui peut induire des réactions supplémentaires dans le mécanisme d'oxydation.

L'oxydation thermique est un processus en chaîne impliquant: les étapes d'initiation, de propagation et de terminaison. L'étape d'initiation contient la décomposition unimoléculaire et bimoléculaire d'hydroperoxydes. Propagation : L''oxydation a lieu principalement sur les carbones allyliques, car la liaison C-H d'un C-H allylique est la moins stable. Les doubles liaisons existant dans la structure induisent une étape supplémentaire de propagation, c'est-à-dire l'addition radicale aux doubles liaisons entraînant une réticulation :

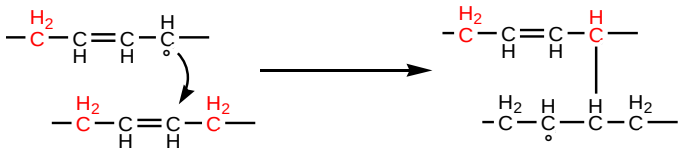

Figure A2.4: Réaction d'addition de P° aux doubles liaisons.

Les doubles liaisons peuvent aussi réagir avec peroxyle et former l'époxyde. Dans le cas de l'oxydation thermique du polymère, les réactions de terminaison impliquent à la fois P ° et POO ° en fonction de la pression d'oxygène externe.

Sur la base de la description des trois étapes d'oxydation (initiation, propagation, terminaison), il est possible d'établir un modèle cinétique d'oxydation. Un modèle cinétique a été proposé par une étude préliminaire. Mais plusieurs facteurs d'influence seront pris en compte : les effets de l'antioxydant, du catalyseur et de l'épaisseur, la concentration en oxygène, les températures variables et les différents ensembles de constantes de vitesse.

L'effets de la pression d'oxygène permet de déterminer les constants de vitesse de terminaison.

L'ajout de stabilisants joue un rôle important dans la prévention de la dégradation du polymère. Deux méthodes de stabilisation peuvent être proposées : Antioxydants phénoliques et Hindered Amine Light Stabilizers (HALS). Antioxydants phénoliques : Le mécanisme d'action est tel que l'atome d'hydrogène labile des antioxydants phénoliques est d'abord capturé par POO °, ce qui entre en compétition avec la réaction de POO ° en PH. HALS : L'action efficace du HALS est attribuée au cycle de régénération du nitroxyde qui maintient une concentration élevée des principales espèces actives pendant une longue période.

L'oxydation contrôlée par le phénomène de diffusion de l'oxygène (effet DLO) doit être prise en compte dans la prédiction de la durée de vie.

En raison du fait qu'un catalyseur est utilisé lors de la réaction de ROMP pour former PDCDP, la stabilité du polymère pourrait être modifiée par l'interaction entre les composés métalliques qui viennent de catalyseur et le polymère. L'accélérateur de décomposition de l'hydroperoxyde est l'un des principaux rôles d'un composé métallique. Ainsi, les résidus de catalyseurs devraient accélérer la décomposition thermique de POOH.

Conclusions et stratégie

En conclusion, il a été démontré que les méthodes empiriques ne permettent pas de prédire le comportement à long terme du PDCPD. Afin de prédire la durée de vie du PDCPD dans divers types de conditions de vieillissement (par exemple, dans des conditions sous-marines), la modélisation cinétique à multi-échelles est nécessaire, c'est l'objet de cette étude. Étant donné que PDCPD se trouve dans un environnement de dégradation complexe dans l'application

Field-joint en milieu marine, sa prévision de durée de vie sera divisée en deux parties à étudier: l'oxydation thermique et le lien avec les propriétés techniques (mécanique, interaction avec l'eau). Le mécanisme d'oxydation à l'échelle moléculaire est le but principal de cette thèse. Pour ce faire, notre stratégie est : 1. mise en place d'un modèle cinétique d'oxydation thermique pour non stabilisé PDCPD sans DLO ; 2. Etude de l'action des stabilisants sur PDCPD sans DLO ; 3. Etude du profil d'oxydation : 4. Etude de l'influence de l'oxydation thermique sur le comportement d'absorption de l'eau (sans additif, sans DLO).

Résumé du chapitre 2 : Matériaux et techniques expérimentales

Le chapitre 2 décrit les matériaux et techniques utilisés dans cette étude.

Matériaux

Cette étude est principalement réalisée sur du polydicyclopentadiène avec différentes formulations. On retiendra que :

- Le chapitre 3 porte sur le polydicyclopentadiène sans additif et le polydicyclopentadiène sans additif avec différentes concentrations de catalyseur.
- Le chapitre 4 porte sur le polydicyclopentadiène avec différent type de stabilisants.
- Le chapitre 5 est dédié à l'étude le comportement de l'absorption de l'eau de polydicyclopentadiène sans additif.

Techniques

Les techniques de caractérisation utilisées dans cette étude contiennent : FTIR, NMR, DSC, Microscopie optique, essai de traction, DVS. 2 type de échantillons ont porté dans cette étude : films fin et échantillon épais. En particulier, thermolyse d'échantillon vieilli a été fait en utilisant DSC.

Résumé du chapitre 3 : Oxydation thermique de PDCPD sans additif

L'étude de l'oxydation thermique se fait, dans un premier temps, sur le cas le plus simple, à savoir les échantillons minces de PDCPD sans additif. Ensuite, le modèle cinétique créé pour celui-ci sera adapté au PDCPD épais et stabilisé. Ce chapitre visera principalement à proposer un modèle plus complet, avec une meilleure validation de ses paramètres cinétiques. Pour cela, nous nous concentrerons sur la stabilité des hydroperoxydes pour estimer les constantes de vitesse d'initiation, sur la consommation de doubles liaisons (conformément au processus de réticulation) et sur la constitution de produits stables (principalement des carbonyles) sous plusieurs pressions d'oxygène pour accéder aux constantes de taux de terminaison. En amont, une brève étude des propriétés mécaniques sera proposée pour répondre partiellement aux relations questions relatives aux structure-propriétés associées au critère de fin de vie.

Propriétés mécaniques

Le comportement en traction de films de 60 µm d'épaisseur vieillis à 80°C est représenté dans la Figure A2.5 pour plusieurs concentrations de carbonyles et de doubles liaisons. Il apparaît clairement que l'oxydation conduit à une diminution de l'élongation à la rupture ainsi qu'à une augmentation de la contrainte au seuil. De plus, la diminution de la contrainte maximale peut être liée à la concentration des doubles liaisons restantes et des carbonyles formés. Cela signifie que l'utilisation d'un modèle cinétique permet de prédire les modifications chimiques au cours de l'oxydation, puis qu'un modèle cinétique permettrait de prédire la durée de vie d'un point de vue mécanique.

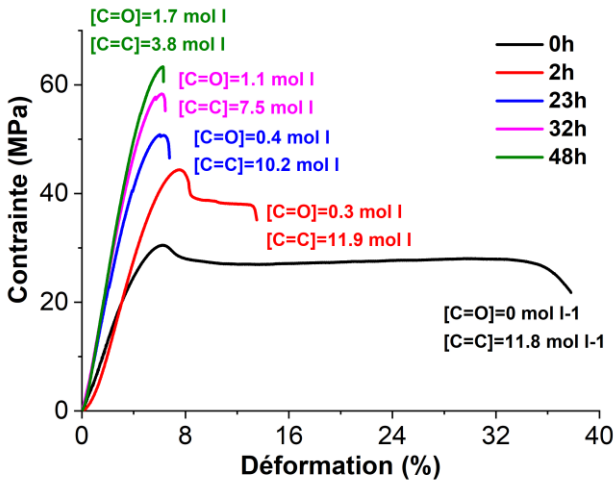

Figure A2.5: Courbes de traction pour les échantillons de PDPCD avec des temps d'exposition variables à 80°C sous air.

Consommation de doubles liaisons et terminaison

La détermination concentration en doubles liaisons dans le PDCPD est nécessaire pour proposer un modèle cinétique, les expériences FTIR ont d'abord été réalisés. L'attribution des bandes d'absorption caractéristiques pour les doubles liaisons a été vérifiée à l'aide de molécules modèles (cyclopentène et de polybutadiène) et s'est révélée en accord avec la littérature.

La concentration totale en doubles liaisons dans PDCPD est la somme de trois contributions correspondant à des liaisons cis -HC = CH- cycliques, des liaisons cis -HC = CH = cycliques et des liaisons trans -HC = CH- acycliques. En conséquence, la concentration en double liaison de PDCPD purifié, non vieilli, est d'environ 10-13 mol/l. D'après les résultats de RMN à l'état solide, la concentration en double liaison pour le PDCPD non traité a été estimée à 13 mol/l, ce qui est en bon accord avec la valeur déduite à partir des résultats de FTIR.

La comparaison des spectres IR obtenus sur des PDCPD vierges et des PDCPD oxydées sous air montre une diminution de la concentration de tous les types de doubles liaisons, ce qui indique des réactions entre doubles liaisons et radicaux. Des réactions d'addition de radicaux alkyles pourraient constituer un moyen possible de réticulation du PDCPD. Cette situation diffère de l'addition de radicaux peroxyle qui ne conduit pas à la réticulation, en raison de la

formation de produits époxydes :

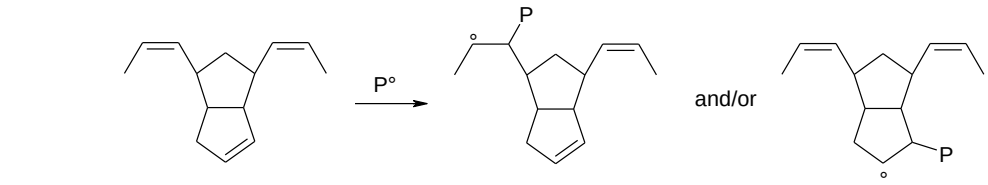

(a)

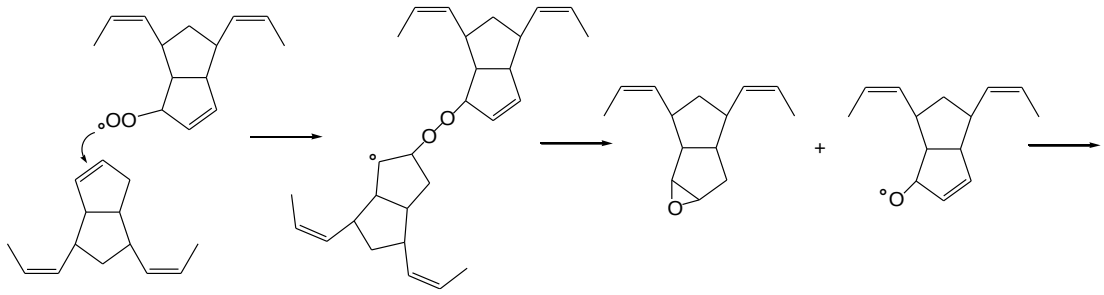

(b)

Figure A2.6: Etape de propagation: réaction d'addition de P° et POO° sur des doubles liaisons. NB1: les radicaux peuvent s'ajouter de chaque côté de la double liaison. NB2: l'addition intramoléculaire n'est pas prise en compte dans le cas du PDCPD en raison de son encombrement structurel.

Dans une première approche, nous avons considéré que les valeurs de chaque type de double liaison étaient presque identiques (NB: cette hypothèse permet également d'éviter les erreurs dues aux incertitudes dues à l'absorptivité molaire).

La Figure A2.7 indique les diminutions des doubles liaisons avec le temps de vieillissement pour PDCPD vieillis sous air.

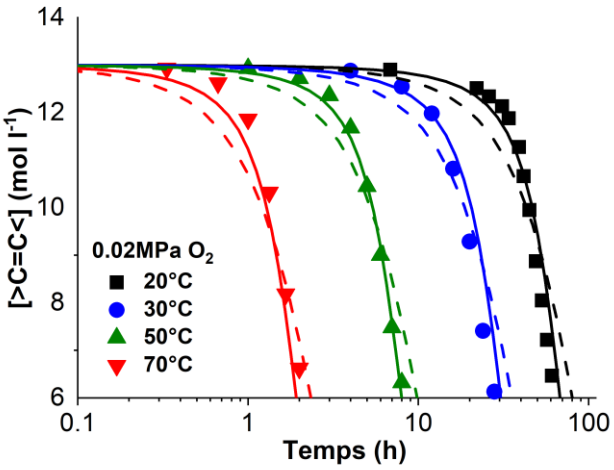

Figure A2.7: Consommation de double liaison pour les échantillons vieillis sous air à différentes températures.

Il est intéressant de noter que les méthodes RMN et FTIR donnent presque la même tendance pour les échantillons vieillis à temps court. Aux niveaux d'oxydation très élevés, ce qui n'est pas le but de la présente étude, une différence peut être observée entre la RMN et le FTIR.

Formation de produits d'oxydation

Les mesures FTIR montrent la formation d'une bande à environ 1710 cm^{-1} correspondant aux fonctions carbonyle. Ils proviennent de radicaux alkoxy formés au cours de : l'initiation, la terminaison et la décomposition de POOP°. La concentration en carbonyle augmente avec le temps de vieillissement après une période d'induction (Figure A2.8).

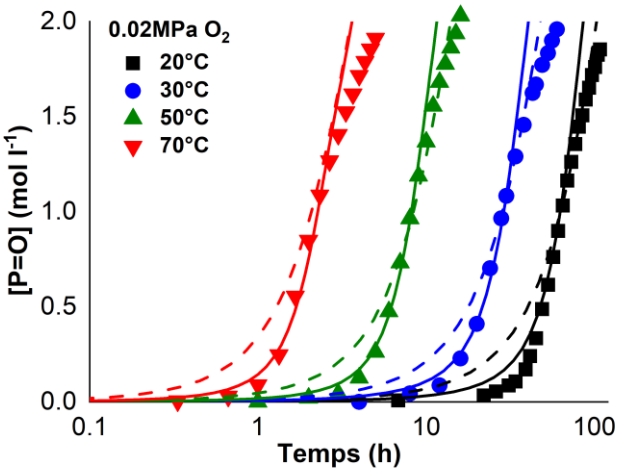

Figure A2.8: Formation de carbonyles pour les échantillons vieillis sous air à différentes températures.

Les spectres FTIR de PDCPD oxydé montrent deux bandes à environ 852 cm^{-1} et 837 cm^{-1} qui correspondent à la déformation de époxydes. L'intensité de ces bandes reste très faible. Ces espèces donc ne seront pas prises en compte en tant que produit stable de l'oxydation thermique.

Stabilité des hydroperoxydes

Les hydroperoxydes, qui sont les espèces clés du mécanisme d'oxydation, peuvent également être détectés et quantifiés de manière sélective par d'autres méthodes chimiques ou thermiques, notamment le titrage des hydroperoxydes par DSC. DSC résultat montre que les espèces responsables de pic exothermique mesuré par DSC sont les hydroperoxydes, dont la formation résulte de l'étape de propagation. Ainsi, la concentration en POOH a été évaluée à partir de la valeur de pic exothermique. La Figure A2.9 montre les courbes de croissance des hydroperoxydes en fonction du temps de vieillissement.

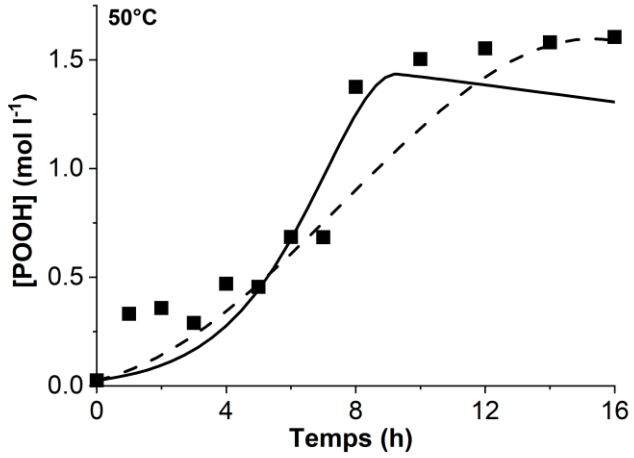

Figure A2.9: Changement de hydroperoxyde pour les échantillons vieillis sous air.

La concentration en POOH à 50°C augmente rapidement au cours de la période initiale pour atteindre une valeur d'environ 1,5 mol L^{-1} après 10 h d'exposition (un pseudo plateau) (Figure A2.9).

Afin de prendre en compte la décomposition des hydroperoxydes dans le PDCPD, des échantillons minces M*-PDCPD ont été oxydés dans un premier temps, puis exposés in situ à l'aide de DSC sous atmosphère d'azote. Après cette thermolyse, la concentration résiduelle en hydroperoxydes a été mesurée. Deux types d'échantillons ont été pris en compte dans cette étude, le premier avec une concentration élevée d'hydoperoxydes (c'est-à-dire lorsque le plateau est atteint) et le second avec une concentration d'hydroperoxydes beaucoup plus faible (typiquement avec [POOH] ~ 0,1 - 0,3 mol l-1) considérer l'état initiale de la dégradation. Les courbes de thermolyse (Figure A2.10) sont présentées en tant que variations de la concentration résiduelle (normalisées par la concentration initiale au début de la thermolyse) en fonction du temps de thermolyse.

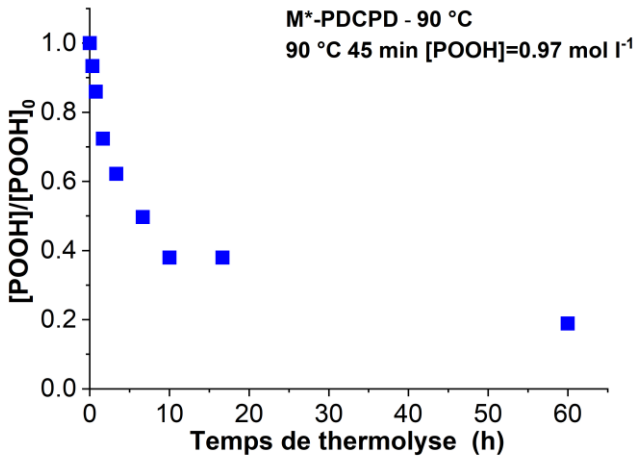

(a)

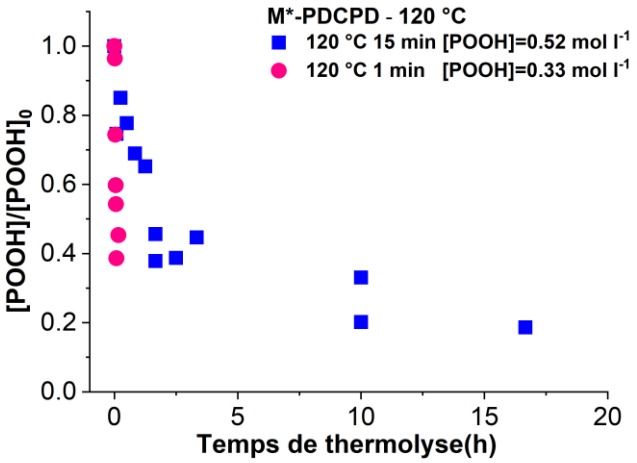

(b)

Figure A2.10: Changements de la concentration en hydroperoxydes au cours de la thermolyse.

Pour étudier l'effet de la concentration en catalyseur, la cinétique d'oxydation de H-PDCPD et de L-PDCPD a été comparée. Les résultats montrent que la présence de catalyseurs ne modifie pas de manière significative le niveau de POOH au plateau quel que soit la température de vieillissement (Figure A2.11a). En outre, les résultats on observe clairement que la cinétique de formation du carbonyle est très similaire pour les deux niveaux de catalyseur considérés ici (Figure A2.11b).

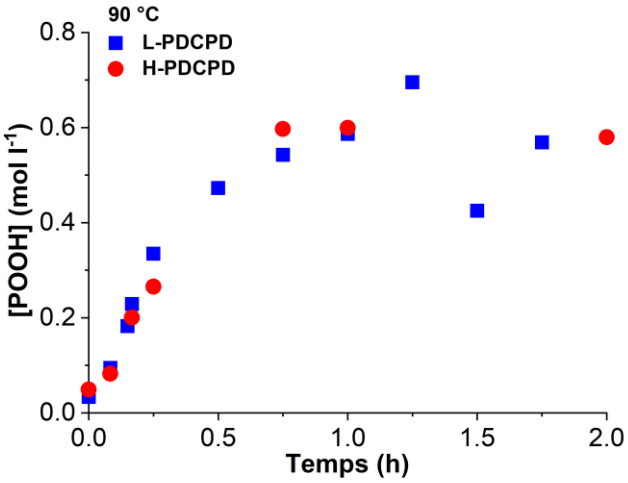

(a)

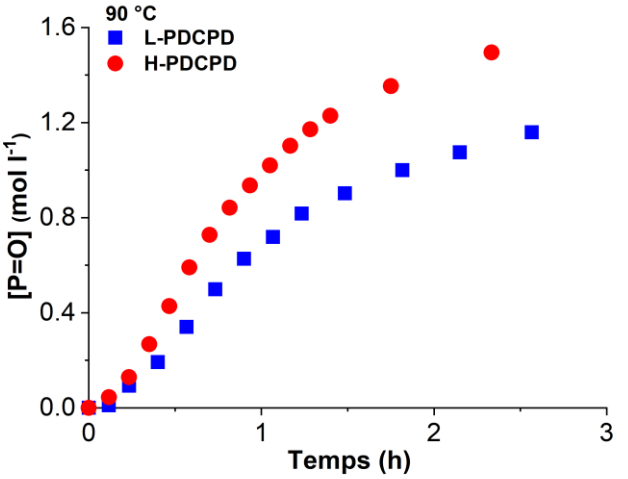

(b)

Figure A2.11: Évolution de la concentration en hydroperoxydes pour les échantillons de L-PDCPD et H-PDCPD.

Figure A2.12 montre les résultats de thermolyse de L-PDCPD et de H-PDCPD.

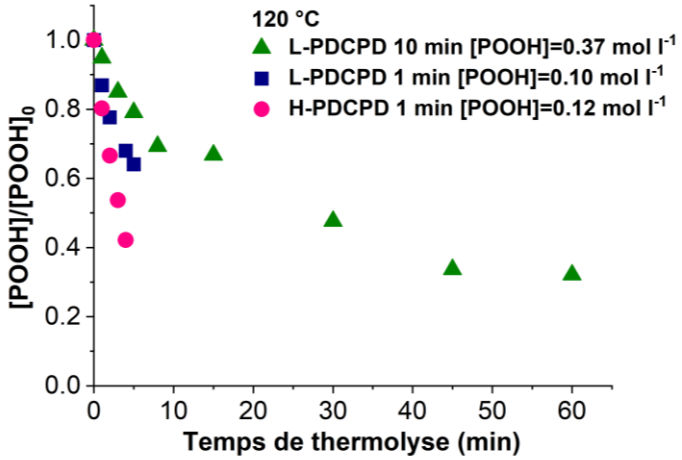

(a)

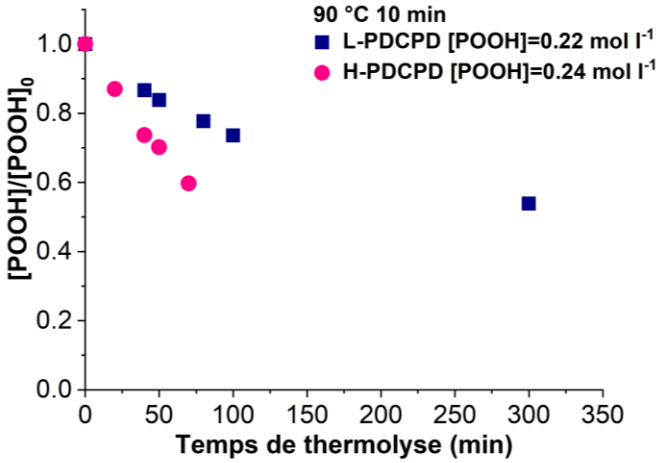

(b)

Figure A2.12 : Évolution de la concentration en hydroperoxydes pour la thermolyse de L-PDCPD et de H-PDCPD.

Dans notre cas, nous avons considéré séparément la thermolyse soit au niveau du « plateau » (i.e. pour des fortes concentration) soit à la période initiale de la dégradation (i.e. pour des faibles concentrations). Les données expérimentales ont été tracées dans des diagrammes d'ordre 1 ou d'ordre 2 (Figure A2.13). Il semble que la décomposition de POOH obéisse plutôt à une cinétique du second ordre (c'est-à-dire que POOH se décompose de manière bimoléculaire). Les valeurs de k_{1b}, qui représentent la moitié des valeurs de pente pour ces équations linéaires d'ordre 2, ont donc été obtenus. Le même traitement théorique a été appliqué

aux expériences de thermolyse dans le domaine des faibles concentrations.

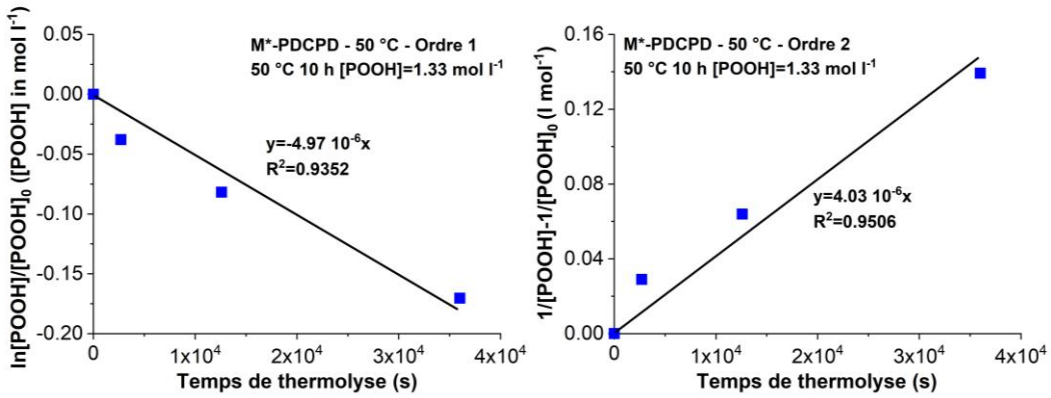

Figure A2.13: Équation linéaire d'ordre 1 (gauche) et 2 (droite) pour la thermolyse du M -PDCPD sous pseudo plateau.*

Dans le domaine de la concentration « basse » en POOH (c'est-à-dire inférieure à 0,3 mol l^{-1}), la cinétique de la POOH est nettement plus rapide que celle observée pour la concentration initiale en POOH (avant la thermolyse) au niveau du plateau (Fig. A2.10b), deux interprétations sont possibles. Il semble toutefois évident que l'hypothèse d'une décomposition de second ordre pour une faible concentration est difficile à soutenir (Figure A2.14).

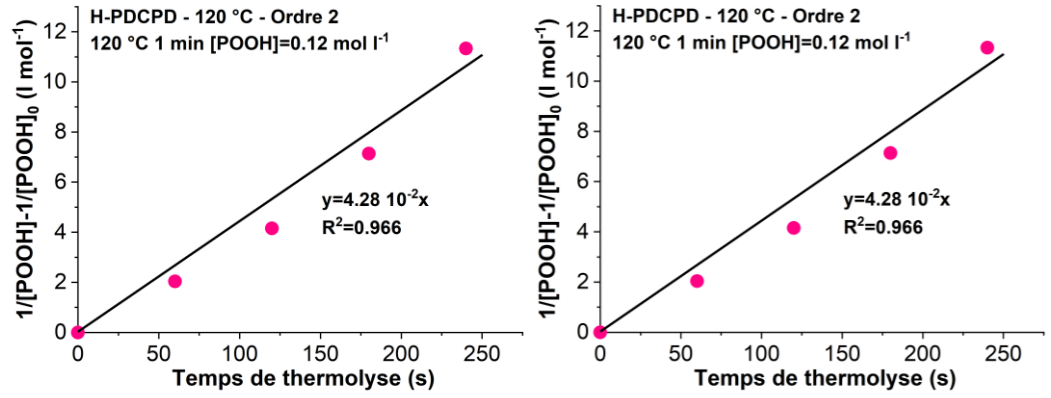

Figure A2.14: Équation linéaire d'ordre 1 (gauche) et 2 (droite) pour les échantillons de H-PDCPD vieillis à 120°C pour 1 minutes.

Nous avons donc envisagé le scénario suivant: dans le domaine de faible concentration en POOH étudié ici, les deux modes de décomposition coexistent (mais pas dans les mêmes

proportions), à savoir :

$$\frac{d(POOH)}{dt} = -k_{1u}[POOH] - 2k_{1b}[POOH]^2$$

avec k_{1b} déterminé à partir de la décomposition dans la région à haute concentration. Les valeurs de k_{1u} peuvent être déterminées à partir de la procédure illustrée dans Figure A2.15 :

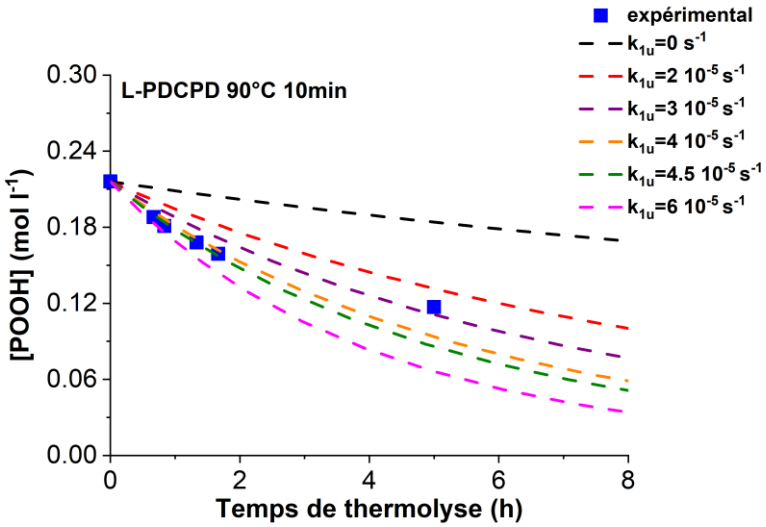

Figure A2.15: Simulations numériques pour la thermolyse de POOH avec différentes valeurs de k_{1u}.

À partir de ces résultats de modélisation, nous pouvons accéder aux valeurs de k_{1u}. Les constantes de vitesse (apparentes) identifiées à partir de cette procédure présentent une caractéristique intéressante : ils augmentent avec la concentration en catalyseur (Figure A2.16). Un tel comportement est caractéristique pour nous d'un processus unimoléculaire. Même si les POOH semblent se décomposer principalement par un processus bimoléculaire, un unimoléculaire semble coexister pour le temps d'exposition court, et serait favorisé par l'utilisation d'une quantité élevée de catalyseur ROMP pour la synthèse de matériaux. De plus, il semble possible que les impuretés métalliques se désactivent progressivement au contact de l'oxygène, de l'eau ou de tout sous-produit d'oxydation, induisant la diminution de la constante unimoléculaire apparente k_{1u} vers la constante de vitesse non catalysée k_{1u0} (réduisant ainsi davantage l'effet du catalyseur sur la vitesse d'oxydation).

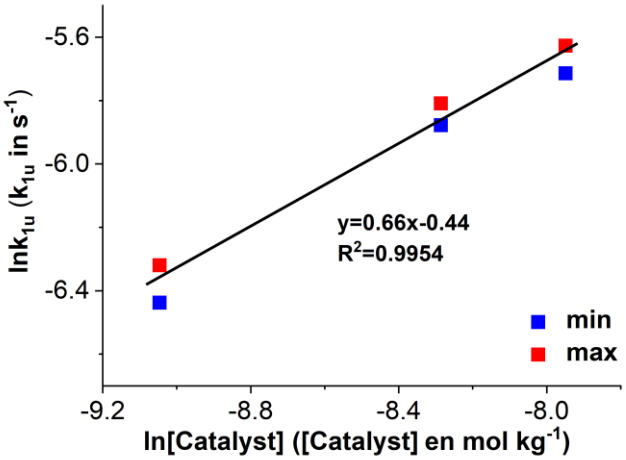

Figure A2.16: Changement de k_{1u} avec la concentration de catalyseur.

La modélisation par simulation des courbes de thermolyse semble être une méthode intéressante pour déterminer les valeurs de k_{1u} pour L-PDCPD et H-PDCPD. Comme on peut le constater, la valeur de k_{1u} pour M*-PDCPD est comprise entre le k_{1u} de L-PDCPD et celui de H-PDCPD (Figure A2.17).

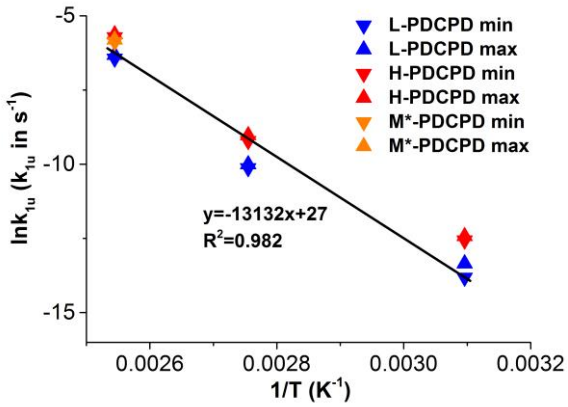

Figure A2.17: Loi d'Arrhenius de k_{1u} pour différents systèmes de PDCPD.

Modélisation cinétique

Selon les données expérimentales décrivant les modifications chimiques du PDCPD thermo-oxydé décrites ci-dessus, un schéma mécanistique a été proposé pour modéliser les courbes cinétiques obtenues lors du vieillissement de PDCPD sans additif.

Il existe en fait une infinité d'ensembles de constantes de vitesse permettant un ajustement acceptable des résultats expérimentaux. Cependant, notre objectif est plutôt de proposer un ensemble de valeurs permettant un ajustement raisonnable mais avec un sens physique. Pour ce faire, une résolution analytique sera effectuée dans un premier temps pour estimer approximativement l'ordre de grandeur de certaines constantes de vitesse, puis l'identification de l'ensemble.

En respectant toutes les contraintes (simulations sous excès d'oxygène avec des constantes de vitesse estimées à partir de solutions analytiques), un premier ensemble de constantes de vitesse (« modèle 1 ») a été obtenu et a conduit à des simulations approximatives données en traits pointillés dans les figures ci-dessus (Consommation de double liaison, formation de carbonyles et changement de hydroperoxyde - Figures A2.7,8 et 9).

La valeur de k_{1u} que nous devions utiliser était particulièrement insatisfaisante car elle était presque 5 fois plus élevée que celle estimée par thermolyse, qui a été jugée moins inacceptable. Un second modèle a été proposé en accord avec valeur de k_{1u} estimé par l'étude de thermolyse, mais une dernière réaction devrait être ajoutée au schéma mécanistique :

(1b) $\mathrm{POOH} + \mathrm{HY} \rightarrow \mathrm{H_2O} + 2\mathrm{P}^\circ + \mathrm{HY}$ $\qquad k_{1c}$

où HY correspond au catalyseur de décomposition de la POOH par des produits stables à l'oxydation (acides carboxyliques, alcool…).

Ses simulations « modèle 2 » sont indiquées en traits pleins dans les Figures A2.7, 8 et 9 (Consommation de double liaison, formation de carbonyles et changement de hydroperoxyde). Le modèle cinétique final semble convenir au moins dans le domaine des degrés de conversion modérés et permet de prévoir la dégradation du PDCPD en fonction du temps, de la température et de la pression d'oxygène externe.

Effets DLO

L'identification du profil d'oxydation sera réalisée expérimentalement par microscopie optique puis confirmée par une étude gravimétrique. Les valeurs moyennes d'épaisseur de couche oxydée (pour le PDCPD vieilli sous air à 50°C, 70°C et 120°C) déterminées par microscopie optique micrographies est présenté sur Figure A2.18. Ainsi, le profil d'oxydation sera simulé avec le modèle cinétique créé. Les résultats de simulation indiquent que l'épaisseur maximale de la couche oxydée à 50°C est d'environ 12 µm (Figure A2.19), à 70°C de 10 µm et à 120°C de 8 µm. Cette différence entre les résultats expérimentaux basés sur des micrographies et les résultats de la simulation peut correspondre aux coefficients de diffusion de l'oxygène susceptibles d'évoluer avec le temps d'oxydation ou l'inexactitude des observations de microscopie. Cependant, à 50°C, le TOL obtenu par simulation est proche de celui estimé par étude gravimétrique (TOL = 15 µm). En règle générale, le profil d'oxydation simulé présente presque le même ordre de grandeur que les résultats expérimentaux basés sur des micrographies et des études gravimétriques. Ainsi, ce modèle cinétique construit pour la PDCPD sans additif permet de prédire les gradients d'oxydation dus aux effets DLO.

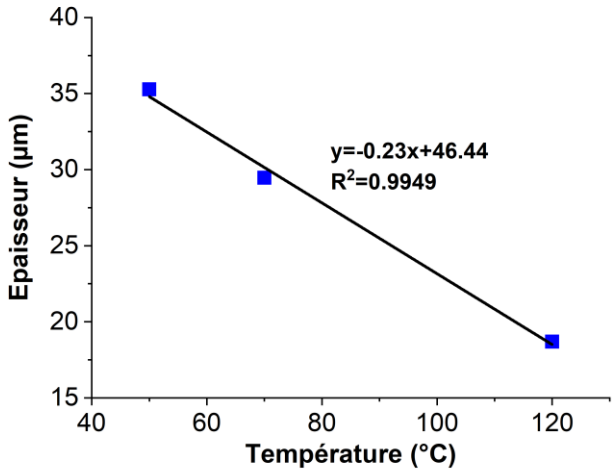

Figure A2.18: Evolution de l'épaisseur de la couche oxydée avec la température de vieillissement pour le vieillissement thermique de PDCPD sous air.

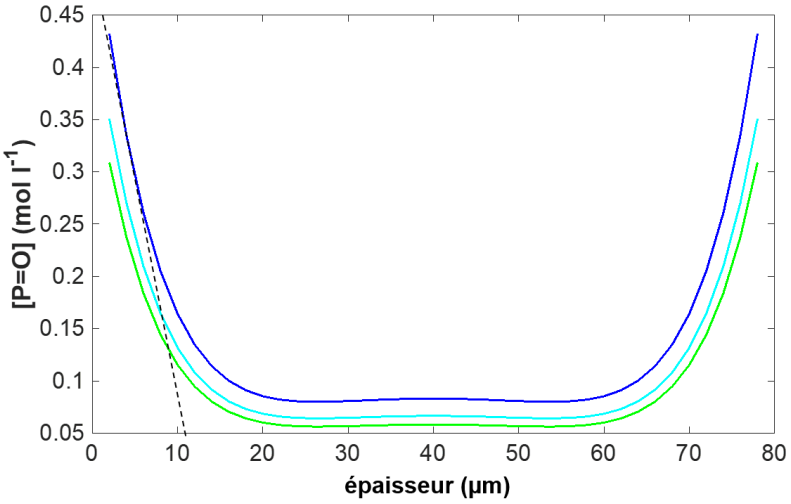

Figure A2.19: Modélisation de la concentration en carbonyles en fonction de l'épaisseur de PDCPD vieilli à 50°C.

Résumé du chapitre 4 : Oxydation thermique du PDCPD stabilisé

Dans ce chapitre, l'oxydation thermique de films de PDCPD (sans effet DLO) stabilisée par l'hydroxytoluène butylé (BHT), Tinuvin 123 et Chimassorb 2020 sera tout d'abord étudiée à différentes températures (de 50°C à 120°C). La cinétique d'oxydation sera caractérisée par spectroscopie IR en suivant l'accumulation de carbonyle. Le modèle cinétique précédemment établi sera complété pour simuler l'effet d'inhibition des antioxydants sur l'oxydation du PDCPD. Enfin, le profil d'oxydation du PDCPD stabilisé sera étudié.

Caractérisations initiales de polymères stabilisés

Les antioxydants doivent être compatibles avec le catalyseur de métathèse utilisé pour polymériser le DCPD. Lors d'une première étape, nous avons décidé de réaliser des études de compatibilité de ces stabilisants avec la formulation de DCPD à base d'un catalyseur de métathèse du ruthénium (Ru2). L'objectif est d'étudier dans quelle mesure les antioxydants pourraient interagir avec le catalyseur de Ru et retarder ou inhiber la polymérisation.

Il apparait que ce type de catalyseur de métathèse n'est pas (ou très peu) affecté par la présence de ces trois stabilisants, car tous les échantillons ont réagi sans à-coups, atteignant des rendements de polymérisation très élevés, exprimés en élévation de température entre la température initiale et finale atteinte par le système (Figure A2.20). Cependant, il convient de noter que Tinuvin 123 et BHT présentent les résultats proches des valeurs de référence (PDCPD sans additif), tandis que Chimassorb 2020 a montré la plus forte accélération dans ce cas. La raison de cet effet d'accélération n'est pas évidente. Rappelons-nous que les amines sont connues pour être polaires et ont un comportement de base représenté par une faible valeur de pK_b. Les amines secondaires présentes dans Chimassorb 2020 ont un pK_b inférieur à celui de l'alcoxyamine présent dans Tinuvin 123, mais au stade actuel, il est difficile de valider un scénario expliquant les résultats présentés à la Figure A2.20.

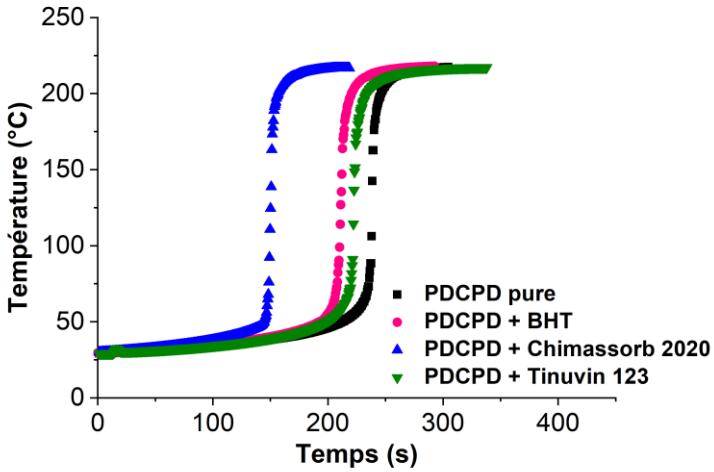

Figure A2.20: Thermographes de ROMP de DCPD catalysés par un catalyseur de métathèse du ruthénium avec et sans antioxydants.

Cinq concentrations en groupement fonctionnel de chaque stabilisant ont été étudiées pour l'oxydation thermique sous air, dans le but de comparer l'efficacité de différents antioxydants et de mieux valider le modèle cinétique.

Il est intéressant de noter que la concentration en double liaison de PDCPD stabilisé est plus faible que celui de pur. Cette différence peut être liée à l'interaction entre l'antioxydant et le catalyseur après la polymérisation. En outre, le catalyseur utilisé pour le PDCPD pur et le PDCPD stabilisé n'est pas le même. Les concentrations en doubles liaisons calculées seront utilisées comme paramètres initiaux pour la partie simulation.

Résultats d'oxydation thermique

Pour le PDCPD stabilisé, l'oxydation thermique a été effectuée sous air à 50°C, 90°C et 120°C. Afin d'évaluer l'effet stabilisant des antioxydants sur le PDCPD, les mêmes mesures de la bande carbonyle par spectroscopie FTIR (voir le chapitre 3) ont été effectuées.

Les résultats (Fig. A2.21) justifient que les différentes stabilisant assurent une fonction anti-oxydation sur le PDCPD. De plus, la nature du stabilisant a un effet apparent sur la cinétique de l'oxydation thermique. Le classement d'efficacité est celui suivant : Tinuvin 123 > BHT >

Chimassorb 2020.

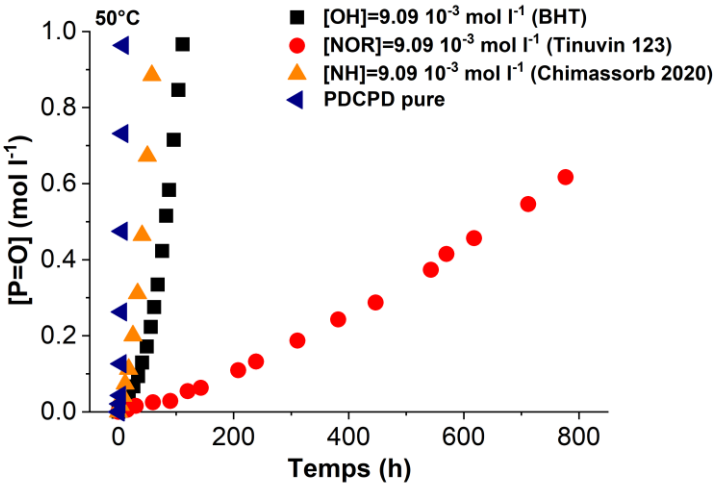

Figure A2.21: Accumulation de carbonyles pour PDCPD stabilisés avec différents stabilisants vieillis à 50°C.

La Figure A2.22 illustre l'effet de la concentration en groupement fonctionnel de différents antioxydants.

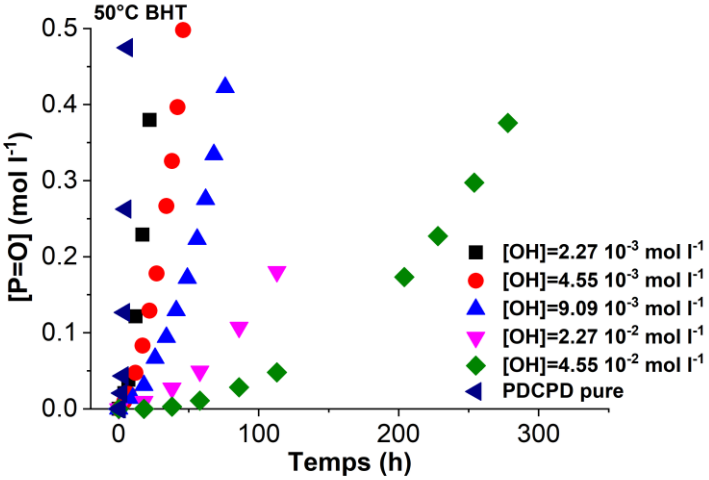

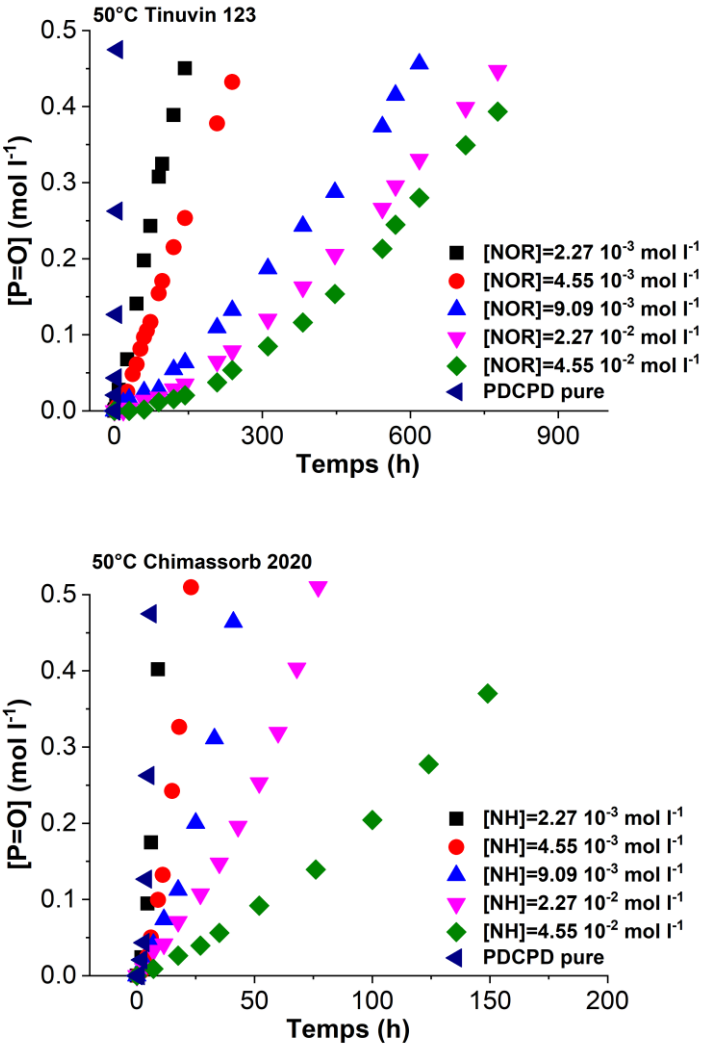

Figure A2.22: Variation de la concentration en carbonyle en fonction du temps d'exposition pour le PDCPD stabilisé avec 5 concentrations de groupement fonctionnel dans BHT, Tinuvin 123 et Chimassorb 2020 et PDCPD sans additif à 50°C.

Plusieurs paramètres peuvent être obtenus en analysant ces courbes :

- le taux d'oxydation maximal.
- le temps d'induction associé à la perte de plasticité (Figure A2.5: par exemple, [P = O] = 0,2 mol l^{-1} correspond au critère de fin de vie).

Pour mieux mettre en évidence l'impact de la concentration de stabilisants, les évolutions du

taux d'oxydation et de la durée de vie en fonction de la concentration en groupement fonctionnel de stabilisants sont résumées dans la Figure A2.23.

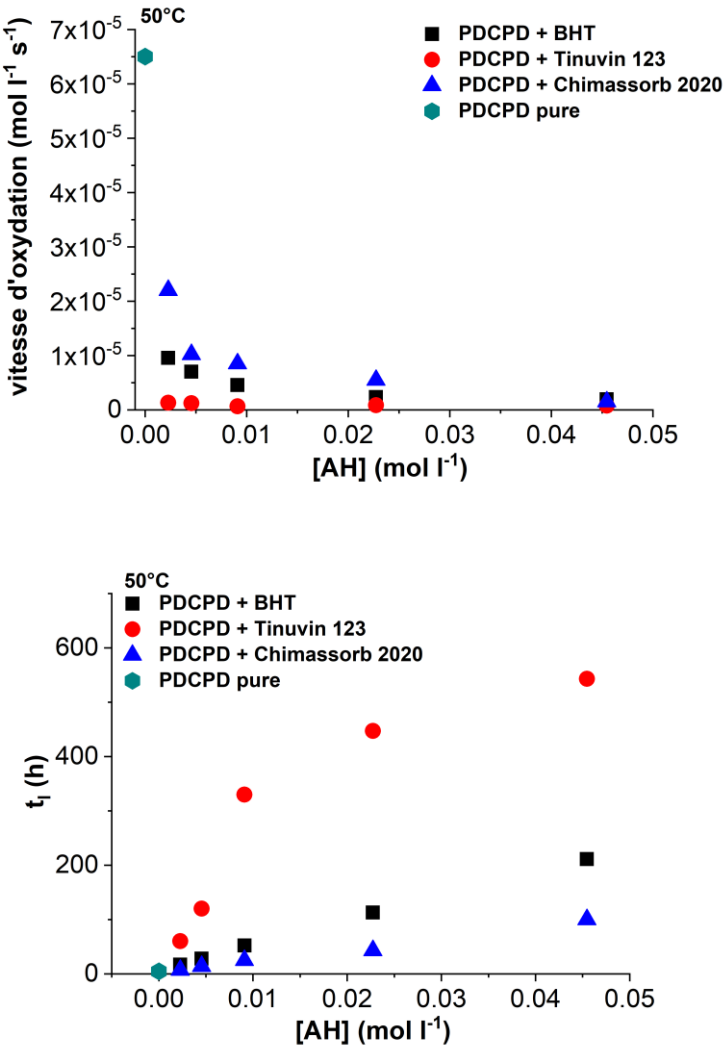

Figure A2.23: Changements de la vitesse d'oxydation et de la durée de vie avec concentration en groupement fonctionnel des stabilisants à 50°C.

Ces résultats expérimentaux appellent les commentaires suivants :

- Les vitesses d'oxydation diminuent avec la concentration en stabilisants, tandis que les durées de vie augmentent en fonction de la concentration en stabilisants. Pour Tinuvin 123, la durée de vie augmente avec la concentration en stabilisants, mais cette augmentation devient plus lente lorsque la concentration du groupe fonctionnel est supérieure à 9,09 10^{-3} mol l^{-1}.

L'explication possible est liée aux aspects physiques de la stabilisation : la solubilité et l'évaporation (dues à sa faible masse moléculaire) se produisent lorsque la concentration en stabilisant atteint une valeur élevée.

En ce qui concerne l'efficacité, le classement de ces 3 différents stabilisants est le suivant: Tinuvin 123> BHT> Chimassorb 2020. Tinuvin 123 présente une remarquable performance anti-oxydante. Le stabilisant phénolique BHT est moins efficace sur PDCPD, car le phénol est consommé de manière irréversible, alors que le HALS réagit de manière régénératrice. Parmi les stabilisants HALS, Chimassorb 2020 affiche des performances moins efficaces, ce qui sera discuté ultérieurement en termes de cinétique de réaction. Il reste à expliquer pourquoi le BHT est moins efficace que Tinuvin 123 mais plus efficace que Chimassorb 2020. Plusieurs raisons peuvent être envisagées : une partie de Chimassorb 2020 est « détruite » au cours de la polymérisation par réaction avec le co-catalyseur, ou une masse molaire élevée pour Chimassorb 2020 limite son efficacité.

L'oxydation thermique sous air a été réalisée à autres températures (90°C et 120°C). L'influence de la température est présentée en termes de vitesse d'oxydation et de durée de vie (Figure A2.24).

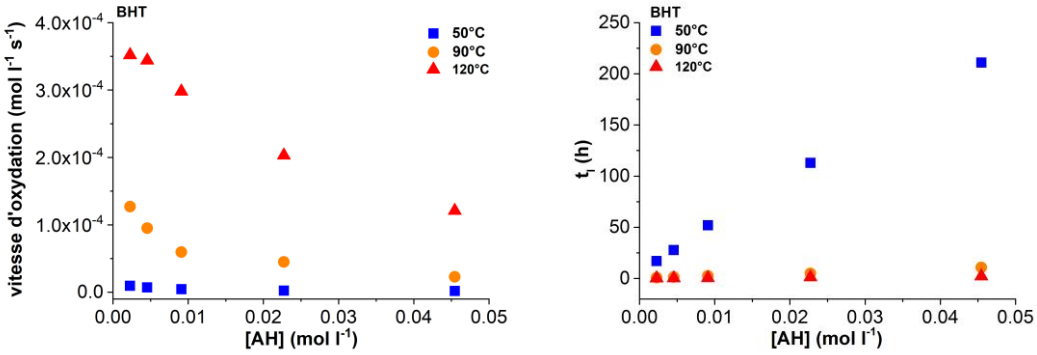

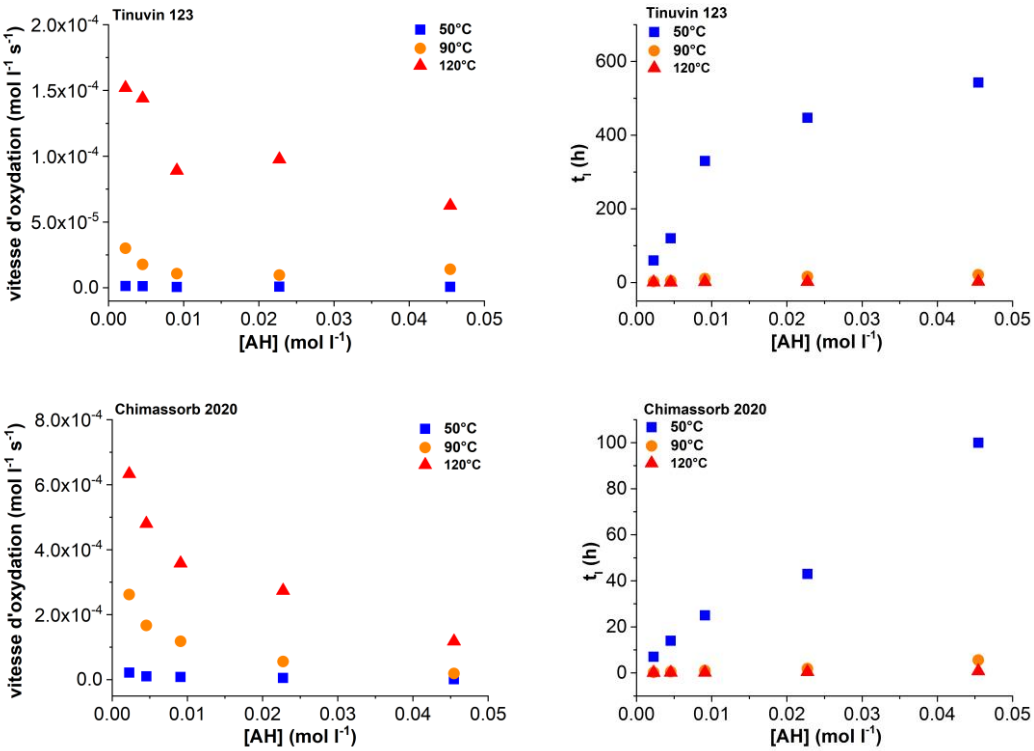

Figure A2.24: Variations de la vitesse d'oxydation et de la durée de vie avec la concentration en groupement fonctionnel des stabilisants.

Comme on pouvait s'y attendre, la durée de vie augmente lorsque la température de vieillissement diminue, tandis que la vitesse d'oxydation diminue. Le classement de ces 3 différents stabilisants reste inchangé. Pour Tinuvin 123, la perte d'efficacité de la stabilisation (observée à 50 ° C) à une concentration élevée n'est pas évidente à des températures plus élevées. Comme la solubilité des antioxydants dans les polymères augmente généralement avec la température, la forme non linéaire de la durée de vie versus [AH] pour Tinuvin 123 observée sur la Figure A2.23 pourrait être due à la faible solubilité de Tinuvin 123 dans PDCPD.

Modélisation de l'oxydation des films minces

Dans cette partie, nous proposerons d'abord les schémas mécanistiques pertinents ainsi que des valeurs possibles de paramètres cinétiques, puis nous présenterons les résultats des simulations et discuterons de la capacité du modèle à prédire la durée de vie de PDCPD stabilisé.

Les accumulations de carbonyles pour PDCPD stabilisés avec différents types d'antioxydants ont été simulées à l'aide des constantes de vitesse indiquées au chapitre 3. Les conditions initiales restent identiques à celles du chapitre 3. Les résultats correspondants sont présentés aux Figures A2.25 et A2.26 pour 50°C, qui montre les courbes de simulation acceptables de l'accumulation de carbonyle pour Tinuvin 123 et Chimassorb 2020. Cependant, celle pour le BHT est moins acceptable pour différentes températures de vieillissement (50°C, 90°C et 120°C).

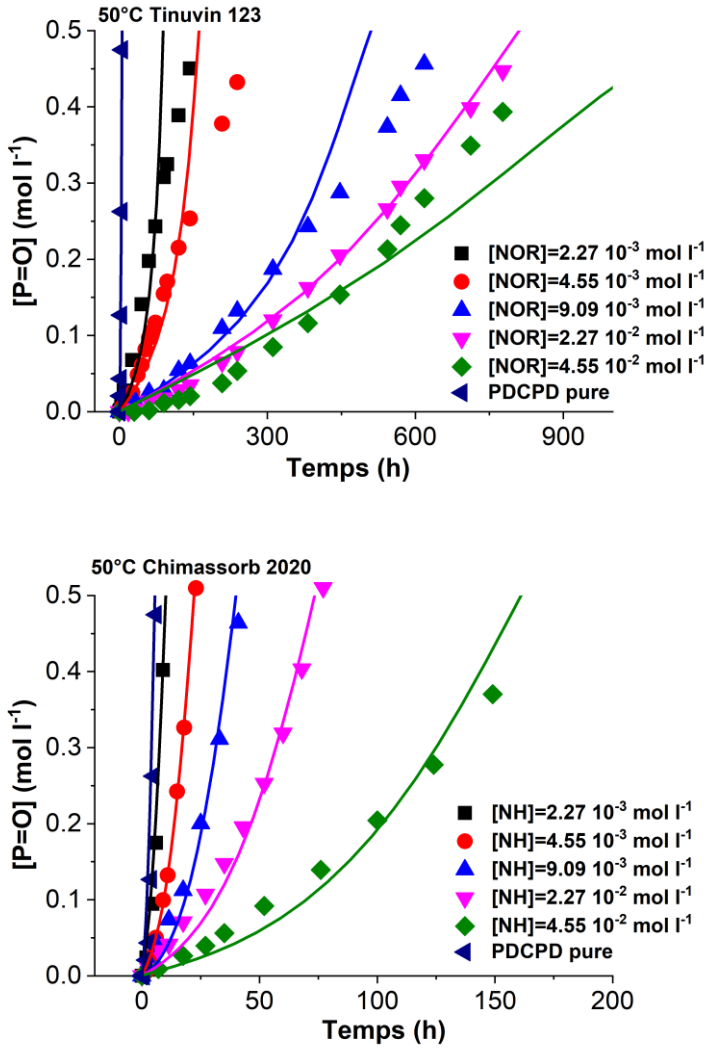

Figure A2.25: Simulation de la variation de la concentration en carbonyle en fonction du temps d'exposition pour le PDCPD stabilisé avec 5 concentrations du groupe fonctionnel dans Tinuvin 123, Chimassorb 2020 et le pur PDCPD à 50°C. Lignes pleines: courbes de simulation.

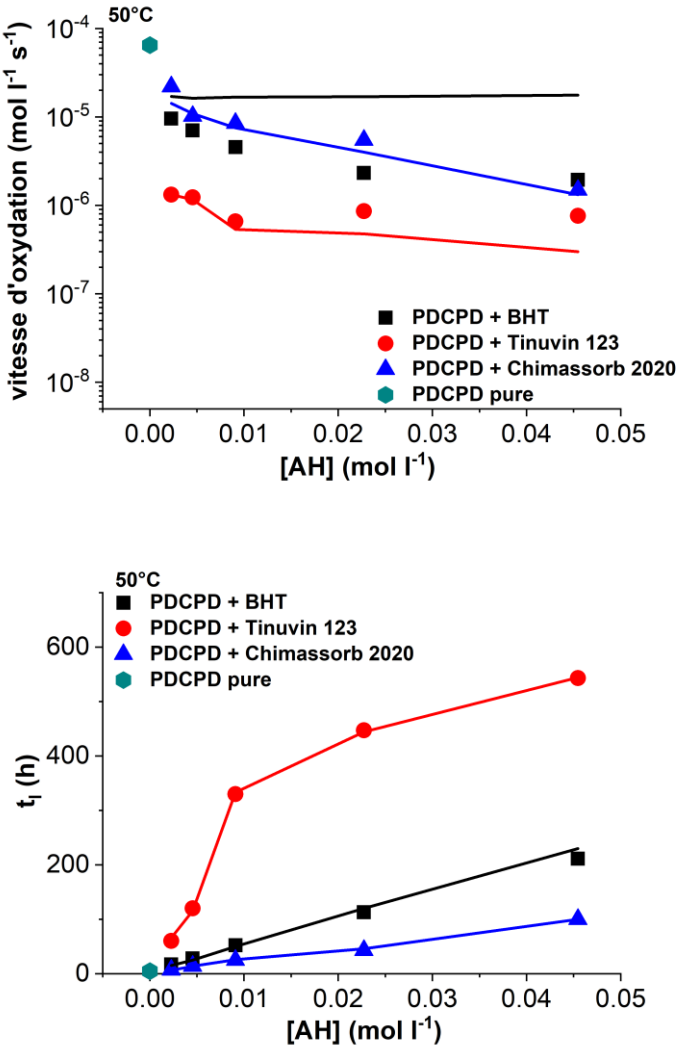

Figure A2.26: Changements de la vitesse l'oxydation et de la durée de vie avec la concentration en stabilisants à 50°C. Lignes pleines: courbes de simulation.

Pour le PDCPD stabilisé avec Tinuvin 123 et Chimassorb 2020 : le modèle cinétique simule l'accumulation de groupes carbonyles à 50°C, 90°C et 120°C. En outre, les modèles cinétiques peuvent simuler l'effet de la concentration de stabilisants sur la durée de vie ainsi que les variations de la vitesse d'oxydation. Les constantes de vitesse pour Tinuvin 123 et Chimassorb 2020 montrent que les ordres de grandeur conforment aux valeurs de littérature.

Pour le PDCPD stabilisé avec du BHT, le modèle cinétique n'est pas capable de simuler correctement les changements de carbonyles en fonction du temps avec le schéma mécanistique

proposé ci-dessus. Sur la base de la réaction (S1) inchangée, plusieurs schémas mécanistes possibles ont été proposés et testés. Cependant, les simulations basées sur ces hypothèses ne peuvent pas simuler les courbes expérimentales. Dans des études ultérieures, les mesures de la concentration résiduelle en BHT avec le temps de vieillissement devraient être effectuées pour mieux comprendre la raison de cet échec.

En conclusion, le modèle cinétique utilisé dans ce chapitre donne des simulations acceptables de résultats expérimentaux et simule l'effet des concentrations de groupes fonctionnels des stabilisants sur la stabilisation (au moins en termes de durée de vie et d'effet de la température) en utilisant des ordres de grandeur physiquement raisonnables des paramètres cinétiques. Ainsi, ce modèle cinétique est validé pour le PDCPD pur et maintenant pour le PDCPD stabilisé.

Effet DLO dans PDCPD stabilisé

D'après les observations de microscope optique et les résultats de simulation (Figure A2.27), il semble que les stabilisants entraînent une augmentation de l'épaisseur de la couche oxydée. Il est clair que l'épaisseur de la couche oxydée est toujours supérieure à celle du PDCPD pur. Si l'antioxydant est totalement mobile, la couche oxydée aura une épaisseur d'environ 30 µm (contre 15 µm pour le film non stabilisé, voir Fig. A2.19) et si le stabilisant présente une mobilité de translation, un échantillon de 200 µm d'épaisseur sera presque entièrement oxydé. En d'autres termes, l'ajout d'antioxydants tels que les HALS est un moyen efficace de ralentir la cinétique d'oxydation.

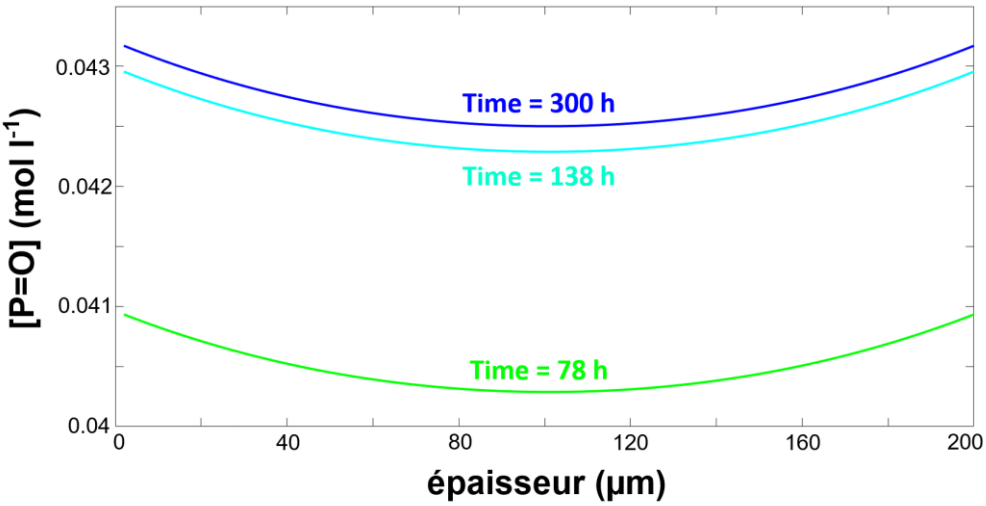

(a)

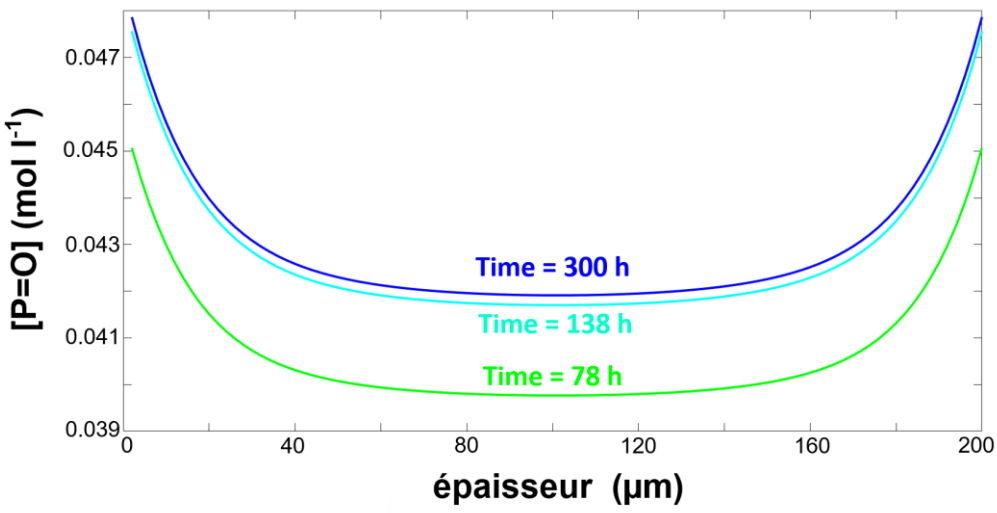

(b)

Figure A2.27: Modélisation de la concentration en carbonyle en fonction de l'épaisseur pour le PDCPD stabilisé par Tinuvin 123 ([NOR] = 2,27 10^{-3} mol l^{-1}): (a) $D_{NO^\circ} = 0$; (b): $D_{NO^\circ} = 5\ 10^{-14}$ m^2 s^{-1}.

Résumé du chapitre 5 : Effet de l'oxydation thermique du PDCPD sur l'absorption d'eau

Dans ce chapitre, nous nous focaliserons sur l'application potentielle du PDCPD en tant que « Field Joint » pour l'exploitation pétrolière en mer et plus généralement pour le vieillissement dans l'eau. En service, le matériau PDCPD est soumis à de l'eau de mer et à un profil de température en fonction de l'épaisseur du revêtement. Ainsi, l'oxydation thermique du PDCPD influencera potentiellement le comportement d'absorption d'eau. L'objectif de ce chapitre est d'étudier les propriétés de transport de l'eau dans les PDCPD vierges et oxydées.

Résultats expérimentaux et discussion

Des expériences de sorption d'eau ont été réalisées sur des films minces (environ 7 µm) de PDCPD sans stabilisants, présentant une humidité relative (HR) comprise entre 10 et 90% à trois températures, à l'aide d'un appareil DVS. Les échantillons de PDCPD ont tout d'abord été oxydés à 25°C, 50°C et 70°C pour différentes durées de vieillissement. Ensuite, des échantillons non vieillis et des échantillons oxydés ont été prélevés pour mener des expériences de sorption d'eau à des températures correspondantes (par exemple, des échantillons vieillis à 70°C ont été utilisés dans des expériences de sorption d'eau à 70°C).

La Figure A2.28 présente la courbe typique de changement de masse pour le PDCPD non vieilli. Il est clair que l'absorption maximale d'eau dans le matériau non vieilli est très faible (généralement inférieure à 0,3%) à cause de sa structure apolaire. Une différence apparaît pour les PDCPD fortement oxydés (160 minutes à 70°C sous air, comme décrit au chapitre 3), présentant une augmentation significative de l'absorption maximale d'eau (supérieure à 3%).

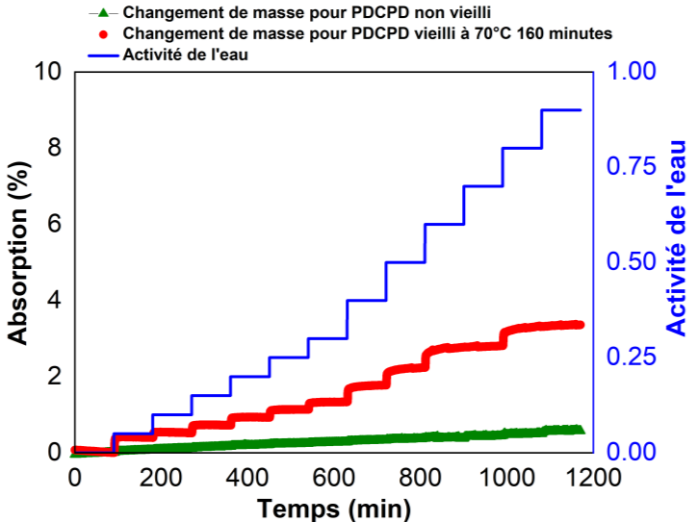

Figure A2.28: Courbes des changements de mass pour les PDCPD non vieillis et vieillis (70°C - 160 minutes).

Des films minces de PDCPD oxydé avec des niveaux d'exposition variables ont ensuite été testés dans du DVS à 70°C. Les isothermes de sorption correspondants (i.e. l'absorption d'eau en fonction de l'activité de l'eau) sont présentés à la Figure A2.29. Nous pouvons voir que l'affinité de PDCPD pour l'eau augmente considérablement avec le niveau d'oxydation du polymère. Pour le PDCPD vierge, l'isotherme de sorption apparaît presque linéaire. Cette caractéristique reste vraie pour les PDCPD vieillis mais uniquement pour des faibles valeur d'activité de l'eau. Pour des fortes valeurs d'activité de l'eau, une sortie de linéarité est observée. Cette caractéristique indique des modifications du mécanisme d'interaction polymère-eau, qui seront examinées dans le paragraphe suivant.

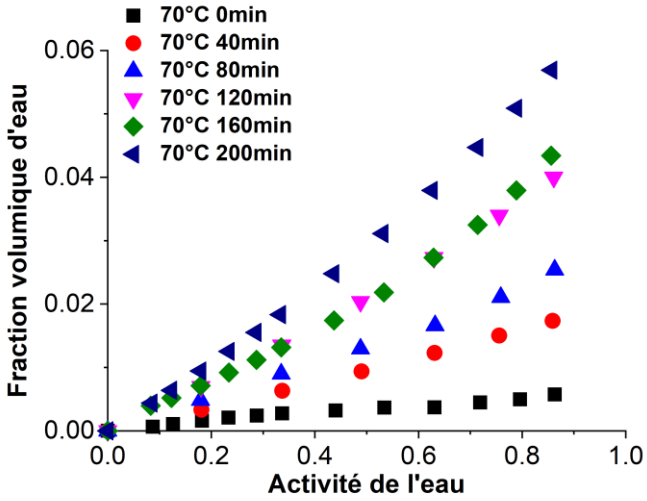

Figure A2.29: Fraction volumique de l'eau dans le PDCPD testée à 70°C en fonction de l'activité de l'eau pour le PDCPD avec différents temps d'oxydation à 70°C dans l'étuve.

Nous nous sommes donc intéressés aux mécanismes de sorption responsables de l'isotherme de sorption présenté à la Figure A2.30. À notre connaissance, il existe trois mécanismes principaux :

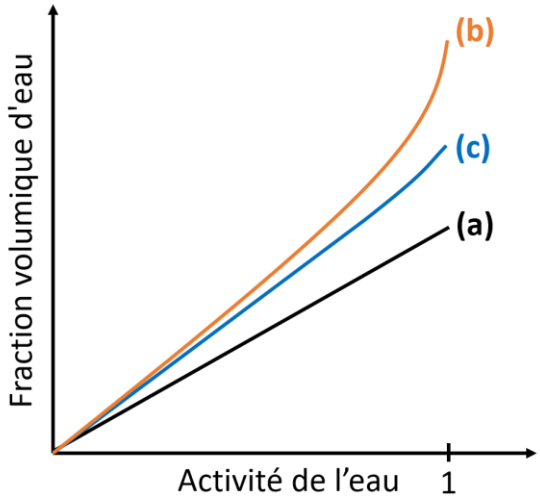

Figure A2.30: Différents types d'isothermes de sorption d'eau.

- (a) : L'absorption d'eau obéit à la loi de Henry.

- (b) : L'isotherme de sorption d'eau peut être décrit par la somme de la loi de Henry à faible activité de l'eau et d'une contribution supplémentaire due aux cluster d'eau à forte activité de

l'eau.

- (c) : L'absorption d'eau obéit à la loi de Flory-Huggins.

La Figure A2.31 montre un exemple de résultats expérimentaux obtenus après 160 minutes d'oxydation à 70°C par rapport à l'ajustement de la courbe d'équation de Flory-Huggins. Il apparait donc que l'absorption de l'eau dans le PDCPD vieillis peut être décrite par l'équation de Flory-Huggins.

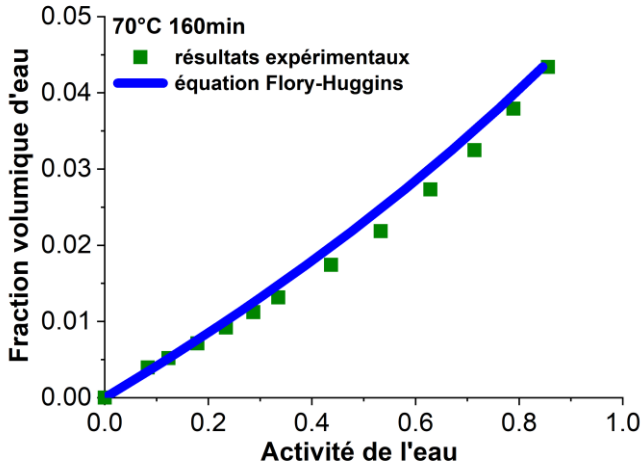

Figure A2.31: Détermination des paramètres de Flory-Huggins pour PDCPD vieillis 160 minutes à 70°C. Lignes pleines: Simulation par l'équation de Flory-Huggins.

L'utilisation de l'équation de Flory-Huggins est intéressante pour se concentrer sur les modifications des paramètres d'interaction en fonction du niveau d'oxydation (c'est-à-dire le temps d'oxydation à 70°C). La Figure A2.32 montre que les paramètres d'interaction, déterminés à partir du meilleur ajustement des isothermes de sorption représenté à la Figure A2.31, diminuent avec le temps de vieillissement. L'oxydation thermique du PDCPD forme en fait des produits d'oxydation avec des groupements polaires (hydroxyles, carbonyles), ce qui augmente le paramètre de solubilité du polymère, diminuant ainsi le paramètre d'interaction. Plus les groupes générés sont polaires, plus la valeur du paramètre d'interaction est petite. En d'autres termes, l'affinité avec l'eau augmente avec le temps de vieillissement.

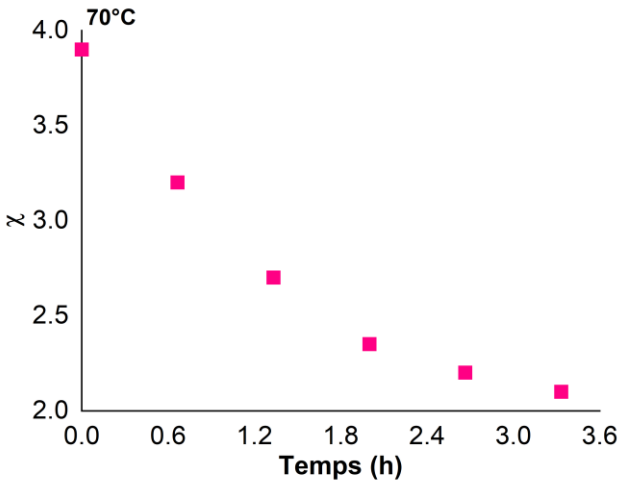

Figure A2.32: Modification des paramètres d'interaction en fonction du temps d'oxydation pour les échantillons vieillis à 70°C.

Basé sur les résultats du DVS, il est également possible de se concentrer sur les mécanismes de diffusion de l'eau.

La loi de Fick est caractérisée par une augmentation linéaire de la concentration de l'eau en fonction de la racine carrée du temps, puis par un plateau de saturation correspondant à la concentration maximale en eau absorbée par le polymère. Le coefficient de diffusion peut être déterminé à partir de la pente représentée à la Figure A2.33a.

Carter et Kibler ont mis au point le modèle de Langmuir attribué à la présence de sites générant une forte liaison avec de l'eau. Dans ce modèle, la première partie de la courbe cinétique est décrite par le modèle de Fick où la masse augmente de façon linéaire avec la racine carrée du temps (Figure A2.33b). Ils ont suggéré un modèle impliquant de l'eau liée et de l'eau mobile (Figure A2.34).

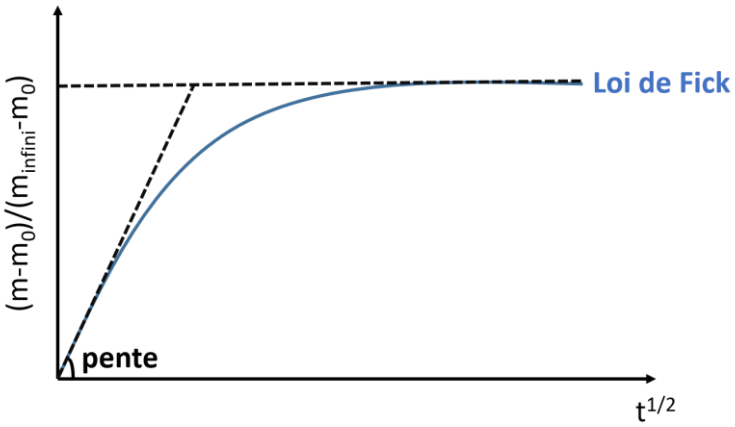

(a)

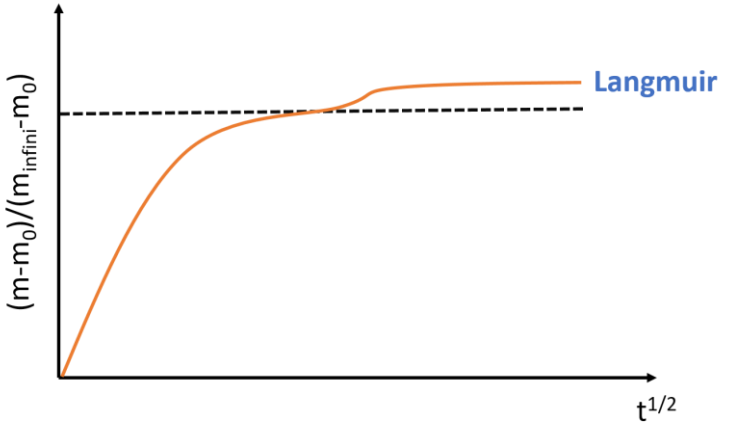

(b)

Figure A2.33: Diffusion d'eau obéit à la loi de Fick (a); Diffusion d'eau obéit au mécanisme de Langmuir (b).

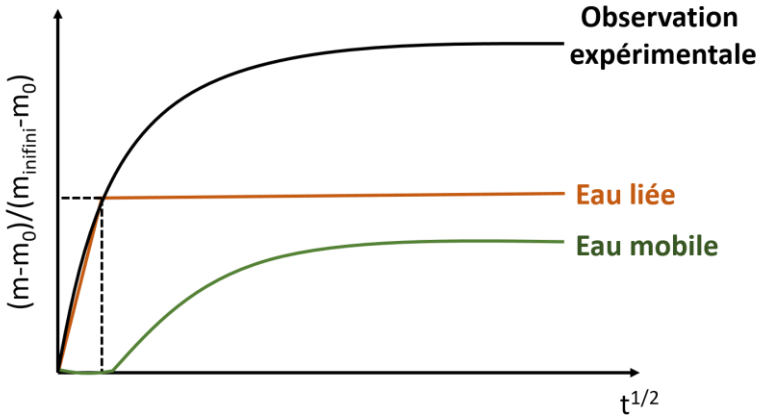

Figure A2.34: Diagramme schématique des changements d'eau mobile et liée.

Dans la situation décrite à la Fig. A2.34, la diffusivité de l'eau liée peut-être estimée à partir de la pente basée sur la loi de Fick, comme illustré à la Figure A2.35a. Par conséquent, les valeurs de diffusivité apparente déterminées ci-dessus sont intéressantes pour une discussion ultérieure. Nous pouvons observer que la diffusivité diminue avec la fraction de volume d'eau, à savoir le niveau d'oxydation (Figure A2.35b).

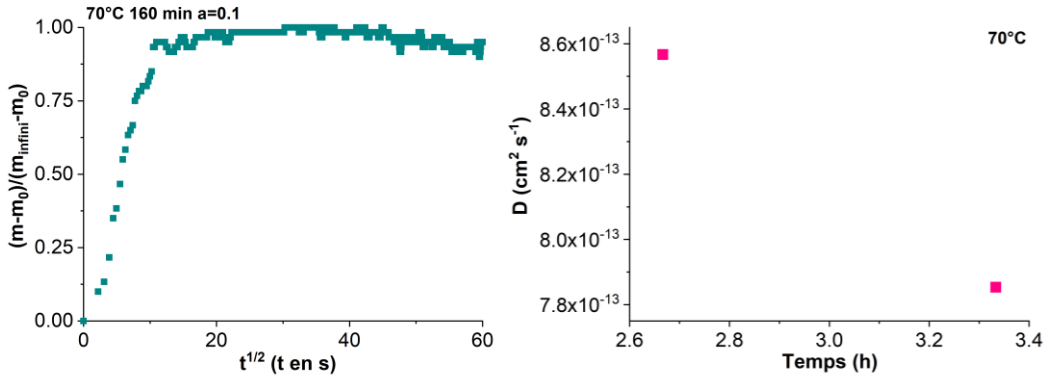

(a) **(b)**

Figure A2.35: Courbe d'absorption de masse relative pour le PDCPD vieilli à 70°C pour 160 minutes (a); Coefficient de diffusion pour 0,1 activité en fonction du temps d'oxydation pour le PDCPD vieilli à 70°C avant caractérisation dans le DVS (b).

L'oxydation du PDCPD a été réalisée à 50°C et à 25°C pour vérifier si les résultats observés à 70°C étaient ou non dépendent de la température. Les résultats sont présentés aux Figure A2.36. Pour les deux températures de vieillissement, il y a une augmentation de la teneur en eau après le vieillissement thermique du PDCPD, quelle que soit l'activité de l'eau (Figure A2.36a et b). De plus, pour une même activité de l'eau, la teneur en eau augmente en fonction du temps d'oxydation.

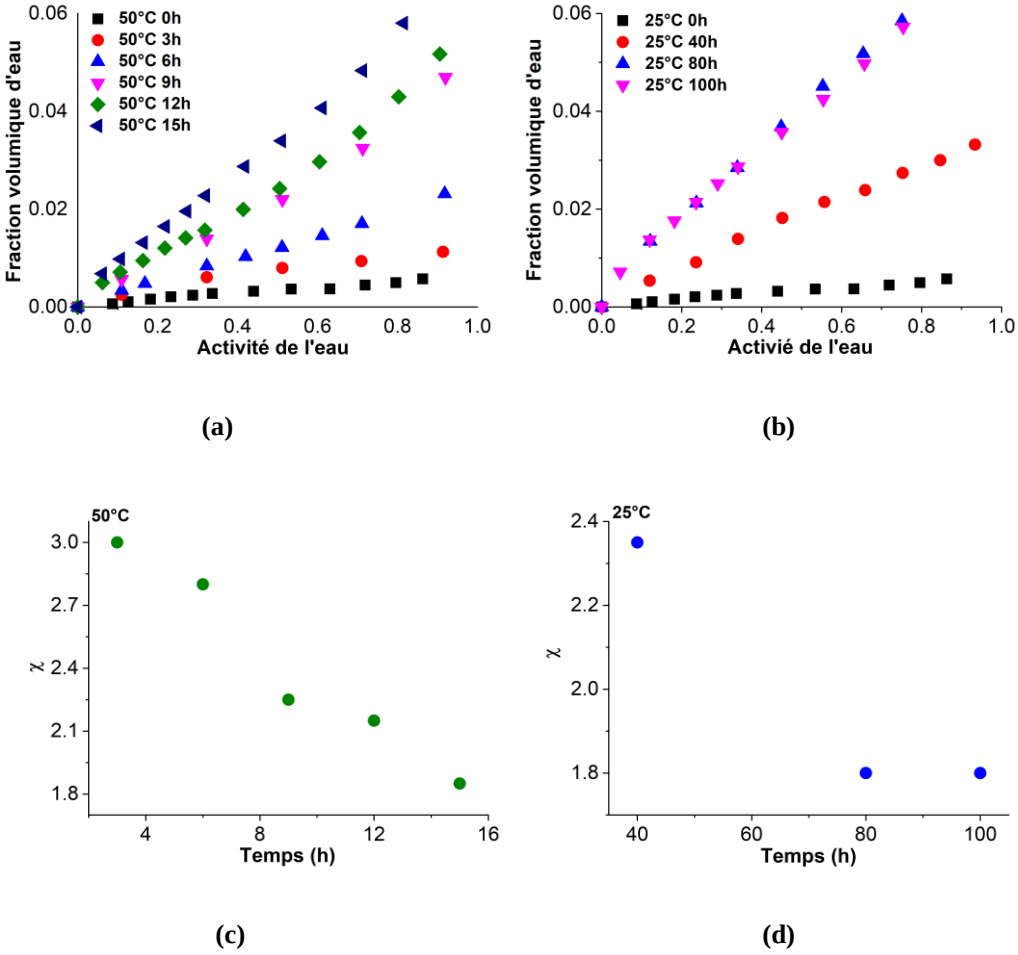

Figure A2.36: Isotherme de sorption d'eau pour PDCPD testé à 50°C avec différents temps d'oxydation à 50°C (a); testé à 25°C avec différents temps d'oxydation à 25°C (b); Changements des paramètres d'interaction avec le temps d'oxydation pour les échantillons vieillis à 50°C (c) et 25°C (d).

Là encore, nous nous intéressons tout d'abord aux mécanismes d'absorption d'eau pour déterminer si les températures de vieillissement ont un impact sur ce comportement. Les trois conclusions tirées pour le vieillissement à 70°C sont vérifiées. Tout d'abord, la loi de Henry n'est pas capable de décrire correctement le comportement d'absorption d'eau en cas de forte activité de l'eau. Deuxièmement, les tailles de cluster pertinentes ont été calculées. Il montre que la taille moyenne des clusters pour les échantillons vieillis à 50°C ou 25°C est comprise entre 0 et 1,4, ce qui signifie que la tendance à la formation de cluster d'eau est très faible. Enfin, l'équation de Flory-Huggins permet de décrire le comportement d'absorption d'eau correspondant à 50°C et à 25°C. Les Figures A2.36 c et d montrent que les paramètres d'interaction sont des fonctions décroissantes avec le temps d'oxydation pour les deux

températures de vieillissement, ce qui est conforme aux résultats obtenus pour des échantillons vieillis à 70°C.

Selon les résultats obtenus après un vieillissement à 70, 50 et 25 ° C, il est possible de relier le paramètre d'interaction Flory-Huggins à la concentration en carbonyle (C = O) dans le matériau. Comme on peut le constater, le paramètre $\chi \times RT$ exprimant la différence de polarité entre l'eau et le polymère $(\delta_{polymer} - \delta_{water})^2$ diminue avec la concentration en carbonyle (Figure A2.37). De plus, il semble qu'il existe une courbe maîtresse liant la teneur en eau de ce matériau en fonction du niveau d'oxydation pour toutes les températures et la durée de vieillissement considérées ici. Ces résultats ont en outre confirmé que les groupes polaires générés en raison de l'oxydation thermique augmentent la solubilité du polymère, diminuent ainsi le paramètre d'interaction.

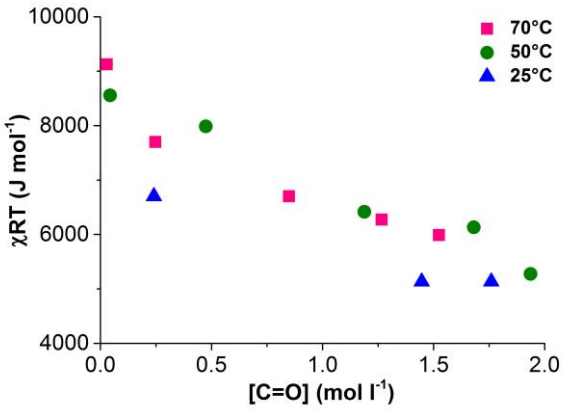

Figure A2.37: Changement des paramètres d'interaction en fonction de la concentration en carbonyles avant caractérisation dans le DVS pour les échantillons vieillis à 70°C, 50°C et 25°C.

Les mêmes comportements « quasi-fickiens » sont vérifiés pour une faible activité de l'eau (0,1 activité) pour des échantillons vieillis à 50°C et à 25°C pour une longue durée de vieillissement. Les valeurs de diffusivité évaluées étaient en fonction de l'inverse de la fraction volumique de l'eau. Comme on peut le constater, la diffusivité est une fonction décroissante de la fraction volumique de l'eau (Figure A2.38). Cette tendance peut s'expliquer comme suit: l'apparition d'espèces polaires augmente la solubilité de l'eau dans le polymère, mais l'eau devient de plus en plus liée aux produits d'oxydation du polymère, de sorte que sa diffusivité diminue lors de l'oxydation.

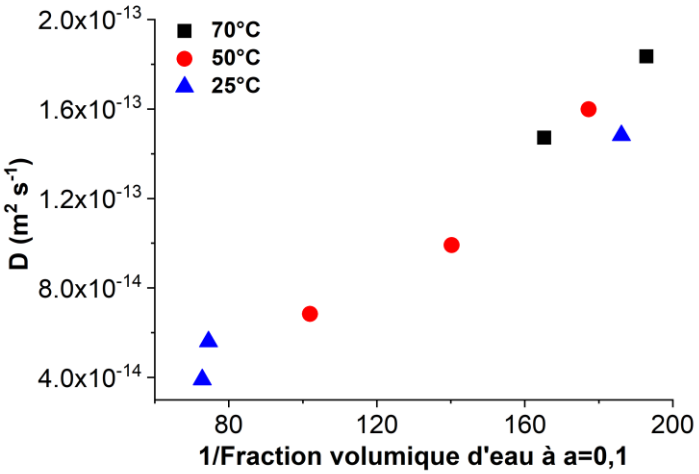

Figure A2.38: Le coefficient de diffusion pour 0,1 activité en fonction de l'inverse de la fraction volumique de l'eau.

Dans la dernière partie de ce chapitre, une relation entre la sorption d'eau et les groupes polaires formés lors de l'oxydation thermique est déterminée par l'équation suivante :

$$f_w = a[acide\ \ carboxyliques] + b([alcools] + [hydroperoxyds]) + c[cétones]$$

avec $a = 0.0889,\ b = 0.0028$ and $c = 0.001$.

Nous pouvons observer que les acides carboxyliques formés lors de l'oxydation thermique sont plus polaires et créent une interaction plus forte avec l'eau par rapport aux cétones et aux hydroxyles.

Conclusions et perspectives

Le but de cette thèse était de prédire la durée de vie du polydicyclopentadiène (PDCPD), un polymère thermodurcissable synthétisé par ROMP et considéré notamment comme candidat à une application « Field Joint » en milieu marin. Dans de telles conditions d'utilisation, le PDCPD est soumis à des températures modérées et à un environnement aqueux. Il a déjà été démontré que les polymères d'hydrocarbures insaturés subissent une oxydation thermique, ce qui entraîne une chute de leurs propriétés mécaniques. Cependant, PDCPD est un cas original car c'est le seul (à notre connaissance) polymère oxydé à l'état vitreux avec une concentration élevée en doubles liaisons résiduelles après polymérisation, ainsi qu'une concentration élevée en catalyseurs organométalliques est en quelque sorte préjudiciable à sa stabilité à long terme.

Selon les données existantes dans la littérature, il était déjà documenté que:

- le contrainte au seuil d'écoulement du PDCPD augmente avec le temps de vieillissement, ce qui est lié à l'augmentation de la densité de réticulation lors de l'oxydation thermique ;

- l'oxydation thermique du PDCPD n'est confinée qu'en surface en raison de l'effet d'oxydation limitée par la diffusion.

Il était toutefois difficile d'extrapoler les données existantes pour prédire la durée de vie à une température plus basse. Pour ce faire, nous avons choisi de mettre en œuvre une approche de modélisation cinétique basée sur la vitesse des processus chimiques impliqués dans l'oxydation et la stabilisation du PDCPD.

La première étape a concerné l'oxydation du PDCPD sans additif. En plus des traceurs stables bien connus tels que les carbonyles, nous avons porté une attention particulière à la consommation de doubles liaisons. En fait, une étude multi-échelles comparant les modifications de la déformation à la rupture et de la contrainte limite mesurées à partir d'essais de traction avec les modifications de la concentration des doubles liaisons restantes et des carbonyles formés (à partir des données FTIR) a donné une relation « structure-propriétés » reliant les modifications à l'échelle moléculaire aux modifications des propriétés mécaniques.

Cela indique qu'un modèle cinétique capable de prédire les changements chimiques au cours de l'oxydation permettrait de prédire la durée de vie d'un point de vue mécanique. Le modèle cinétique est dérivé du schéma de base de l'autoxydation pour les hydrocarbures et fait intervenir plusieurs paramètres cinétiques qui doivent être estimés avec précision pour permettre une prédiction fiable de la durée de vie du PDCPD. Pour ce faire, le modèle doit simuler non seulement les modifications des doubles liaisons et des carbonyles, mais également les modifications des hydroperoxydes, ces derniers étant les intermédiaires clés de l'oxydation radicalaire et un excellent critère de validation du modèle. Cela n'était cependant pas suffisant, car plusieurs ensembles de constantes de vitesse pouvaient en réalité conduire à des simulations comparables et acceptables. Pour déterminer le meilleur ensemble de constantes de vitesse, plusieurs expériences « sélectives » ont été réalisées : des tests de vieillissement sous différentes pressions d'oxygène ont été réalisés pour « isoler » les valeurs des constantes de vitesse pour les terminaisons radicalaires et les réactions entre radicaux alkyles ou peroxy et les doubles liaisons. Certaines expériences de thermolyse d'hydroperoxydes ont également été menées. Il a été montré que les hydroperoxydes se décomposaient principalement par un processus bimoléculaire, avec une décomposition unimoléculaire coexistant dans les temps d'exposition initiaux. Ce dernier serait favorisé par l'utilisation d'un catalyseur ROMP élevé utilisé pour la synthèse de matériaux, mais son influence sur le taux d'oxydation global est limitée. Le modèle cinétique a permis de simuler l'oxydation du PDPCD, en particulier dans la plage de température allant de 50°C à 120°C et sous des pressions d'oxygène de 0,02 à 1,0 MPa. Ses constantes de vitesse peuvent donc être extrapolées à des températures plus basses correspondant aux conditions de service pour effectuer une prévision de durée de vie.

L'oxydation d'échantillons épais a donc été étudiée. Il a été démontré que le PDCPD ne s'oxyde que dans une très fine couche superficielle (comparativement à de nombreux autres résines thermodurcissables), principalement parce que la perméabilité à l'oxygène est modérée et que le taux d'oxydation de surface est très élevé. Cette caractéristique spécifique du PDCPD sans additif a été simulée de manière acceptable par le modèle cinétique. Pour une meilleure simulation du vieillissement en conditions réelles, il faut maintenant vérifier si la perméabilité de l'oxygène dans le PDCPD change au cours du vieillissement, par exemple parce que les changements de volume libre sont induits par la réticulation.

Dans un deuxième temps, l'oxydation thermique a été réalisée sur PDCPD stabilisé afin de se rapprocher des « matériaux réels ». Le défi consistait à proposer des antioxydants pouvant être ajoutés au mélange réactif sans inhiber la polymérisation, tout en affichant un rôle stabilisant efficace. Nous avons donc comparé un phénol encombré « classique » (BHT) et deux stabilisants à base d'amines encombrées: Tinuvin 123 et Chimassorb 2020. Le premier avait l'avantage potentiel d'être une forme « activée » (alcoxyamine), tandis que le second devait présenter une perte physique limitée. Les échantillons présentant une iso-concentration dans des groupes fonctionnels d'antioxydants ont été comparés en termes d'accumulation cinétique de carbonyle. Tinuvin 123 présente les meilleures performances anti-oxydation comparées à Chimassorb 2020 et au BHT, bien qu'il ait été démontré que des problèmes de solubilité et d'évaporation pouvaient exister pour Tinuvin 123 à des concentrations plus élevées. Les mécanismes de stabilisation de ces antioxydants ont été décrits comme des réactions élémentaires et les paramètres cinétiques pertinents ont été obtenus par une approche inverse (c'est-à-dire le meilleur ajustement de courbe tout en respectant des ordres de grandeur raisonnables). En particulier, les stabilisants HALS se sont révélés être un candidat prometteur avec de bonnes propriétés stabilisantes et un effet limité sur la ROMP catalysée. Cet effet stabilisant pourrait être contrebalancé par une augmentation de l'épaisseur de la couche oxydée, mais cela reste à décrire et à modéliser de manière complète dans les travaux suivants.

Lors de la dernière étape, en lien avec les conditions d'utilisation, l'impact de l'oxydation thermique sur le comportement d'absorption de l'eau a été étudié. Il a été démontré que le PDCPD vierge présente une très faible absorption d'eau en raison de sa structure apolaire. L'hydrophilie du PDCPD augmente à mesure que le temps de vieillissement augmente. Ce phénomène s'explique par l'apparition de produits d'oxydation créant des interactions plus fortes avec les molécules d'eau. L'effet possible sur la diffusion de l'eau a également été abordé. L'effet de la plastification à l'eau sur les propriétés mécaniques reste à étudier dans le futur.

Enfin, ces étapes successives permettent de prédire la durée de vie du PDCPD par modélisation cinétique d'un point de vue fondamental. Le modèle cinétique a été créé pour le PDCPD stabilisé et sans additif au cours de l'oxydation thermique à une température comprise entre 20 ° C et 120 ° C. Il a notamment été observé que l'approche de modélisation cinétique peut être mise en œuvre même dans le cas de matériaux vitreux où la mobilité est considérée comme

faible. D'un point de vue pratique, nous espérons que ses capacités prédictives pourront aider les ingénieurs à mieux concevoir les structures en polymères soumises à des conditions extrêmes.

Vieillissement thermique du polydicyclopentadiène

RESUME : Le polydicyclopentadiène (PDCPD) est un polymère thermodurcissable synthétisé à partir de la polymérisation par métathèse par ouverture de cycle, qui présente l'avantage d'un temps de polymérisation court du fait de la présence de doubles liaisons et de l'utilisation de catalyseurs organométalliques. Dans cette thèse, PDCPD est considéré comme un candidat pour des applications en milieu marin, pour lesquelles la question de la durabilité doit être évaluée. L'objectif de ce travail est d'établir un modèle cinétique non empirique pour la prédiction de la durée de vie du PDCPD au cours de l'oxydation thermique. Tout d'abord, la caractérisation par spectroscopie Infrarouge et dosages des peroxydes au cours de l'oxydation a été réalisée afin de mettre en place un modèle cinétique pour le PDCPD sans stabilisant. En particulier, les constantes de vitesse d'initiation ont été identifiées par une étude de la thermolyse des hydroperoxydes; les constantes de vitesse de terminaison ont été obtenues par des expériences spécifiques sous différentes pressions d'oxygène. L'effet du catalyseur sur la cinétique d'oxydation a également été étudié dans ce travail. La consommation de doubles liaisons du polymère entraîne une augmentation significative de la concentration de nœuds de réticulation, puis une augmentation de la contrainte de rupture de PDCPD. Le modèle cinétique créé prédit ces tendances ainsi que l'épaisseur de la couche oxydée. L'effet des stabilisants visant à ralentir la vitesse d'oxydation a également étudié expérimentalement puis modélisé. En particulier, les amines encombrées (HALS) se sont révélées très efficaces et compatibles avec les catalyseurs de la ROMP. Dans la dernière partie, l'effet de l'oxydation thermique du PDCPD sur le comportement de sorption de l'eau a été étudié. Le PDCPD vierge présente une très faible absorption d'eau à cause de sa structure apolaire, alors que le PDCPD vieilli est plus hydrophile en raison de la formation de groupes polaires ce qui peut avoir une influence sur sa durée de vie en milieu marin.

Mots clés : Polydicyclopentadiène, Vieillissement thermique, Cinétique, Prédiction

Thermal ageing of polydicyclopentadiene

ABSTRACT : Polydicyclopentadiene (PDCPD) is a thermoset polymer synthesized from ring opening metathesis polymerization with the advantage of short processing time due to the presence of double bonds and the use of organometallic catalysts. In this thesis, PDCPD is for example considered as a candidate for the field-joint in a marine environment. The question of the durability of PDCPD has to be assessed. The objective of this work is to establish a non-empirical kinetic model for the lifetime prediction of PDCPD during thermal oxidation. Firstly, the characterization by Infrared spectroscopy and peroxide titration of PDCPD during its thermal oxidation was conducted to set up a kinetic model for additive-free PDCPD. In particular, the initiation rate constants have been identified especially through hydroperoxide decomposition rates; the termination rate constants have been obtained by specific experiments under various oxygen pressures. The consumption of double bonds in the polymer causes a significant increase in crosslink concentration then increasing yield stress of PDCPD. The kinetic model predicts those trends as well as the thickness of the oxidized layer. The effect of stabilizer aimed at slowing down the oxidation rate was also experimentally studied and modeled. In particular, hindered amine stabilizers were shown to be promising candidates with good stabilizing properties and compatible with ROMP catalysts. Lastly, the effect of thermal oxidation of PDCPD on water sorption was investigated. Virgin PDCPD presents very low water absorption due to its apolar groups. Whereas, aged PDCPD shows increased hydrophilicity associated with polar groups build-up (which can probably impact its lifetime in marine conditions.

Keywords : Polydicyclopentadiene, Thermal ageing, Kinetic, Prediction

Arts et Métiers Sciences et Technologies

HESAM UNIVERSITÉ